UNIVERSITÀ DEGLI STUDI DI TRIESTE

XXIX CICLO DEL DOTTORATO DI RICERCA IN CHIMICA

DESIGN, SYNTHESIS AND CHARACTERIZATION OF GSK-3β AND CK-1δ INHIBITORS

Settore scientifico-disciplinare: **CHIM/08**

DOTTORANDO / A
SARA REDENTI

COORDINATORE
PROF. MAURO STENER

SUPERVISORE DI TESI
PROF. GIAMPIERO SPALLUTO

ANNO ACCADEMICO 2015/2016

The work described in this dissertation was carried out at the University of Trieste, under the supervision of Prof. Giampiero Spalluto.

I wish to thank the Erasmus+ Program for the scholarship which allowed me to spend three months in the research group of Prof. Ana Martinez at the Centro de Investigaciones Biologicas in Madrid (Spain).

Ai miei genitori

Abstract

Protein Kinases (PKs) are one of the largest protein families encoded by the human genome. PKs catalyze phosphorylation reactions on serine, threonin or tyrosin residues, thus regulating numerous cell functions and signalling pathways, and their deregulation, usually hyperactivation, is often cause/consequence of diseases. In fact, nowadays PKs represent one of the most important and still emerging class of therapeutic targets.

The glycogen synthase kinase 3 (GSK-3) is a highly conserved serine/threonine protein kinase encoded by two genes that yield two related proteins termed GSK-3α and β. Phosphorylating more than one hundred different substrates, GSK-3 is involved in a great number of cellular pathways, including Wnt and Hedgehog, and aberrant activity of the kinase is reported in various prevalent pathological diseases, such as diabetes, central nervous system (CNS) diseases and cancer. Similarly, recent evidences have suggested the involvement of another protein kinase, the casein kinase 1 (CK-1), in neurodegenerative disorders, sleeping disorders, parasites infections and cancer. CK-1 is a monomeric serine/threonine kinase present in all eukaryotes; specifically, in mammalians, seven genetically distinct isoforms are known, and two of them, CK-1δ and CK-1ε, are expressed predominantly in brain.

Taking into account all these considerations, the main purpose of this project is the synthesis of new chemical entities such as GSK-3β and/or CK-1δ inhibitors as potential therapeutic agents, particularly focusing on neuroinflammation-related disorders.

Since all kinases present an ATP-binding site, we can deduce that adenine-like nuclei could be suitable scaffolds to design novel ATP-competitive inhibitors. In particular, we focused our attention on fused 5 and 6 membered rings: [1,2,4]triazolo[1,5-*a*][1,3,5]triazines (TT) and [1,2,4]triazolo[1,5-*c*]pyrimidines (TP), two classes of heterocyclic derivatives well known in literature. Both TT and TP scaffolds were obtained following the synthetic pathways reported in literature, modifying the TT nucleus at 2, 5 and 7 positions and the TP one at 2, 5, 7 and 8. All new compounds were evaluated for GSK-3β and/or CK-1δ inhibitory activity, with promising inhibitors being subjected to more comprehensive studies, including kinetic assays, docking simulations and PAMPA assay for blood-brain barrier (BBB) permeability prediction.

The results obtained in this work are reported and discussed in three distinct chapters:

Synthesis and characterization of GSK-3β inhibitors

In the first chapter, GSK-3β inhibitors have been developed inserting on the TT scaffold different functional groups, some of them are present in Roscovitine (**I**), a purine inhibitor of several kinases currently undergoing clinical trials, and its analogues reported in literature. After chemical characterization, all the newly synthetized derivatives were evaluated against GSK-3β, and many of them presented inhibitory activities against the enzyme in the micromolar range. Structure-activity relationship (SAR) studies on the TT series revealed that substitutions at the 2-position of the scaffold is detrimental in terms of potency, while substitutions at both the 5- and 7-positions are essential to retain good affinity to the kinase. At the 7-position, aromatic groups (in particular, 3-pyridylmethylamino, IC_{50}=0.63 μM) are well tolerated, while at the 5-position the (R)-2-aminobutan-1-ol chain (IC_{50}=2.2 μM) and *N*-Boc-3-aminocyclohexylamino group (IC_{50}=0.80 μM) have allowed to create positive interactions with the kinase pocket. On two representative derivatives of this series, kinetic experiments were performed, confirming an ATP-competitive behavior of our TTs towards

GSK-3β (**Figure I**). Furthermore, some of the most active derivatives (IC_{50} < 10 μM) resulted to be able to pass the blood-brain barrier (BBB) according to the PAMPA assay, an essential feature for all those drugs that target CNS diseases.

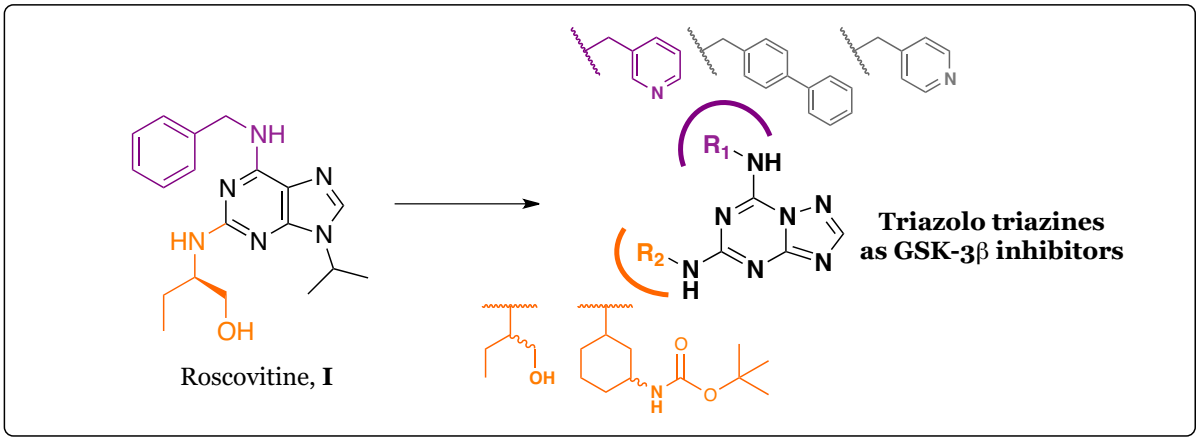

Figure I – TTs as GSK-3β inhibitors

Synthesis and characterization of CK-1δ inhibitors

In this chapter, are described the synthesis and characterization of novel CK-1δ ATP-competitive inhibitors. The pyrimidine derivative Meridianin E (**II**) and a TT derivative (SF46, **III**) were used as starting point and structural modifications at the TP and TT scaffolds were then considered in order to investigate the binding affinity and potency of the novel CK-1δ inhibitors. The most promising results were obtained introducing at the 2-position variously substituted phenyl groups: in particular, *m*-hydroxy (IC_{50} = 0.30 μM) and *m,m*-dihydroxyphenyl (IC_{50} = 0.18 μM) moieties have proven to be the ideal pharmacophore to obtain CK-1-inhibitory activity in the submicromolar range. Other modifications on the two scaffolds, such as the introduction of small amide groups at 8-position of TP core or a benzylamino one at 7(TP)/5(TT)-positions, contributed to increase the affinity towards this kinase (**Figure II**). Notably, benzylamino derivatives also showed enhanced BBB permeability. Moreover, molecular docking simulations allowed us to identify some important interactions between our derivatives and the ATP-binding site of CK-1δ, which could be useful to optimize the substitutions on the TT and TP scaffolds.

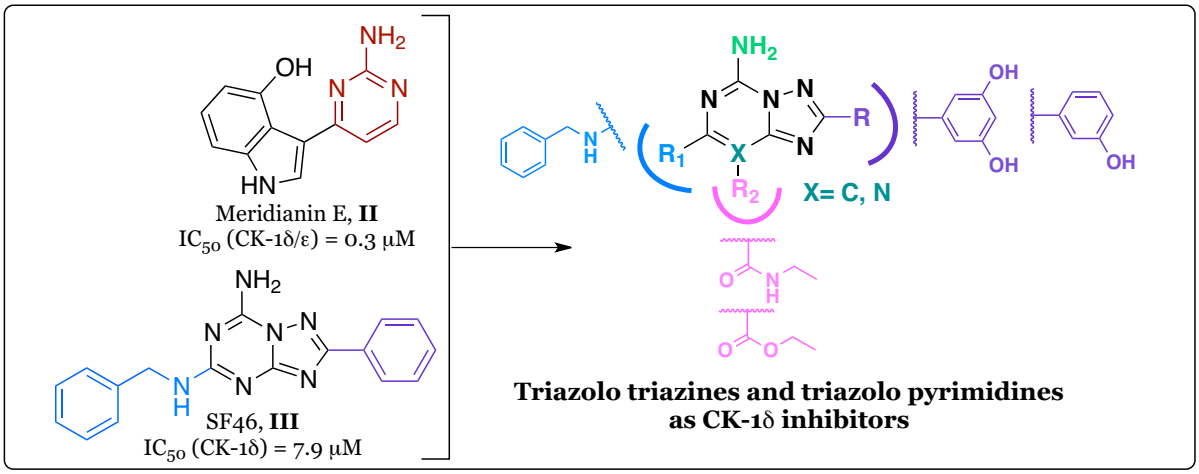

Figure II – TTs and TPs as CK-1δ inhibitors

Synthesis and characterization of dual GSK-3β/CK-1δ inhibitors

Due to the involvement of both kinases in Wnt and Hedgehog signaling pathways, which recently emerged to be linked to neuroinflammatory cascades, and in the formation of hyperphosphorylated protein *tau*, dual GSK-3β/CK-1δ inhibitors could be interesting to assess a synergistic effect in the treatment of neurodegenerative diseases. So, in the present part of the work, we decided to modify the TT scaffold in order to achieve a covalent inhibition of GSK-3β, by selectively targeting the cysteine 199 (Cys199), a key residue located in the active site of this kinase, and at the same time to reversibly inhibit CK-1δ. In particular, we inserted at the 2-position of the TT core a cyanoacrylamide moiety, a Michael-acceptor group that can react with cysteine thiol of C199 under physiological conditions in a manner that is energetically favorable but reversible, thus minimizing the chance of irreversible modification of off-target peptides and proteins (e.g. glutathione). Moreover, it bears an amide moiety, already present in the CK-1δ inhibitor D4476 (**IV**). The newly synthetized derivative **V** resulted a potent GSK-3β inhibitor (IC_{50}=0.17 μM) that inhibited also CK-1δ in an ATP competitive manner with an IC_{50} value of 0.68 μM. Its reactivity in front of thiols was evaluated through UV-spectrometry and HPLC-MS methodology and its binding mode to GSK-3β has been investigated, both theoretically and experimentally. In fact, kinetic assays on compound **V** were performed and showed a mixed ATP-competitive/non-ATP-competitive behaviour; on the other hand, time-dependent experiments confirmed that a covalent interaction with GSK-3β took place (**Figure III**). Interestingly, despite compound **V** has not shown an optimal BBB-permeability, it resulted able to increase the survival of cells treated with 6-OHDA or MPTP, two models of Parkinson's disease (PD), and also enhance β-catenin expression.

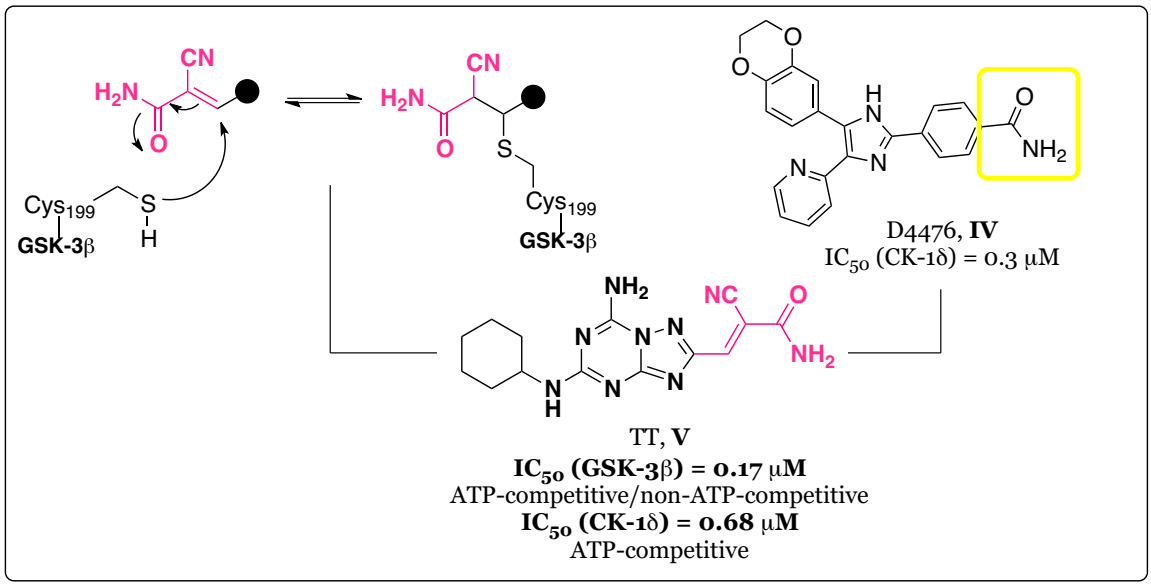

Figure III – Dual GSK-3β/CK-1δ inhibitor

In conclusion, in this work, new adenine-like derivatives have been developed as GSK-3β and CK-1δ inhibitors. Notably, for some compounds submicromolar-range inhibition values were achieved and many of them resulted able to cross the blood-brain barrier (BBB), thus representing valuable tools to further investigate the role of both kinases in neuroinflammation and neurodegenerative disease models.

Riassunto

Le protein-chinasi (PKs) costituiscono una delle più grandi famiglie di proteine codificate dal genoma umano; esse catalizzano reazioni di fosforilazione su residui serinici, treoninici o tirosinici di diversi substrati proteici, regolando in questo modo numerose funzioni cellulari. Le chinasi sono tra le proteine maggiormente coinvolte nei processi di trasduzione dei segnali intracellulari e di conseguenza appare chiaro che la loro deregolazione (spesso iper-attivazione) può esser causa di diverse patologie umane. Le chinasi rappresentano, infatti, uno dei più importanti gruppi di proteine bersaglio da parte dei farmaci ad uso clinico. La glicogeno sintasi chinasi 3 (GSK-3) è una serin/treonin chinasi altamente conservata, di cui esistono due isoforme: α e β. GSK-3 è un enzima cruciale nella regolazione di numerose funzioni fisiologiche cellulari, che vanno dall'apoptosi al controllo dell'espressione genica, ed è in grado di fosforilare più di cento substrati proteici diversi. In particolare, un'alterazione dell'attivita dell'isoforma β è stata riscontrata in diverse malattie degenerative del sistema nervoso centrale, oltre che nel diabete di tipo II e in alcune forme di cancro. Crescenti evidenze dimostrano il coinvolgimento anche di un'altra proteina chinasi, la caseina chinasi 1 (CK-1), in malattie neurodegenerative, disturbi del sonno, infezioni parassitarie e cancro. CK-1 è una serin/treonin chinasi monomerica espressa in tutti i sistemi eucariotici; in particolare, nei mammiferi, sono note sette isoforme e due di queste, CK-1δ e CK-1ε, sono espresse prevalentemente nel sistema nervoso centrale.

Lo scopo principale di questo lavoro di tesi è stato la sintesi di nuovi inibitori di GSK-3β e/o di CK-1δ come potenziali agenti per contrastare la neuroinfiammazione e patologie neurodegenerative ad essa correlate. In particolare, ci siamo focalizzati sulla sintesi di derivati a struttura [1,2,4]triazolo[1,5-*a*][1,3,5]triazinica (TT) e [1,2,4]triazolo[1,5-*c*]pirimidinica (TP), due sistemi eterociclici ampiamente descritti in letteratura. Tali nuclei sono correlabili alla porzione adeninica dell'ATP e pertanto sono stati progettati per inibire le due chinasi tramite competizione con l'ATP stesso nel suo sito di legame dell'enzima.

Entrambi i nuclei triazolo-triazinici e triazolo-pirimidinici sono stati ottenuti seguendo le vie di sintesi riportate in letteratura, modificando nelle posizioni 2, 5 e 7 il nucleo TT e 2, 5, 7 e 8 quello TP. Tutti i nuovi composti sono stati valutati per la loro attività inibitoria su GSK-3β e/o CK-1δ, e i derivati più promettenti sono stati sottoposti a saggi di cinetica enzimatica, studi di docking molecolare e studi *in vitro* per predirne la capacità di permeare la barriera ematoencefalica (BEE).

In particolare, i risultati ottenuti in questo lavoro di tesi sono riportati e discussi in tre distinti capitoli:

Sintesi e caratterizzazione di inibitori di GSK-3β

Nel primo capitolo, sono stati sviluppati nuovi inibitori di GSK-3β a struttura triazolo-triazinica (TT), variamente sostituita con diversi gruppi funzionali, alcuni dei quali presenti nella Roscovitina (**I**), un inibitore purinico di diverse chinasi attualmente in fase pre-clinica, e in alcuni dei suoi analoghi riportati in letteratura. Tutti i nuovi composti sintetizzati sono stati testati su GSK-3β e molti hanno dimostrato efficacia nell'inibire l'enzima a concentrazioni nel *range* micromolare. Una prima valutazione in termini di relazione struttura-attività sulla serie triazolo-triazinica rivela che sostituzioni in posizione 2 del nucleo TT portano ad una perdita di potenza inibitoria, mentre sostituzioni in entrambe le posizioni 5 e 7 sono importanti per mantenere una buona affinità verso la chinasi. In posizione 7 sono risultati ben tollerati gruppi aromatici (in particolare, il gruppo 3-piridilmetilammino, IC_{50} =

0.63 μM), mentre in posizione 5 la catena (R)-2-amminobutan-1-olica (IC_{50} = 2.2 μM) e il gruppo *N*-Boc-3-amminocicloesilamminico (IC_{50} = 0.80 μM) permettono di instaurare interazioni positive con la tasca per l'ATP della chinasi. Due derivati rappresentativi di questa serie sono stati sottoposti a saggi di cinetica enzimatica, confermando un comportamento ATP-competitivo dei nostri derivati triazolo-triazinici nei confronti di GSK-3β (**Figura I**). Inoltre, alcuni dei derivati più attivi (IC_{50} <10 μM) sono in grado di superare la barriera emato-encefalica (BEE) secondo il saggio *in vitro* PAMPA, una caratteristica essenziale per tutti quei farmaci che hanno come bersaglio malattie del sistema nervoso centrale.

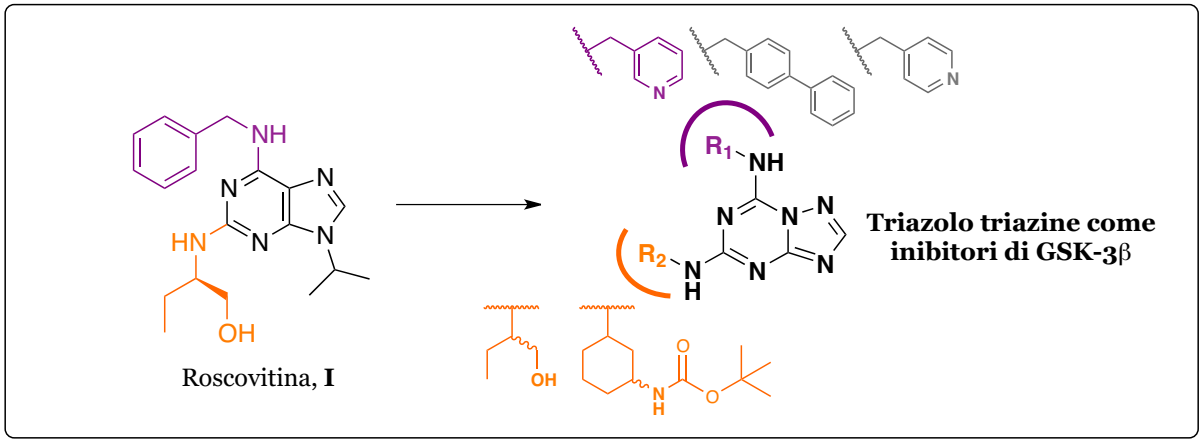

Figura I – Nuovi inibitori di GSK-3β a struttura triazolo-triazinica

Sintesi e caratterizzazione di inibitori CK-1δ

In questo capitolo, sono state descritte la sintesi e la caratterizzazione di nuovi inibitori ATP-competitivi di CK-1δ. I punti di partenza per la progettazione di questa serie di composti sono stati il derivato pirimidinico Meridianina E (**II**) e un derivato TT (SF46, **III**) in precedenza ottenuto nel nostro gruppo di ricerca. Sono state quindi apportate alcune modifiche strutturali ad entrambi i nuclei TP e TT, con il fine di esaminare l'affinità di legame e la potenza dei nuovi inibitori di CK-1δ. I risultati più promettenti sono stati ottenuti introducendo nella posizione 2 di entrambi i nuclei gruppi fenilici variamente sostituiti: in particolare, i gruppi *m*-idrossifenil (IC_{50} = 0.30 μM) e *m,m*-diidrossifenil (IC_{50} = 0.18 μM) sono risultati il farmacoforo ideale per ottenere un'attività inibitoria di CK-1δ nell'ordine submicromolare. Altre modificazioni dei due eterociclici, come l'introduzione di piccoli gruppi ammidici in posizione 8 del nucleo TP o di un gruppo benzilamminico nelle posizioni 7(TP) o 5(TT), hanno contributo ad aumentare l'affinità verso questa chinasi (**Figura II**).

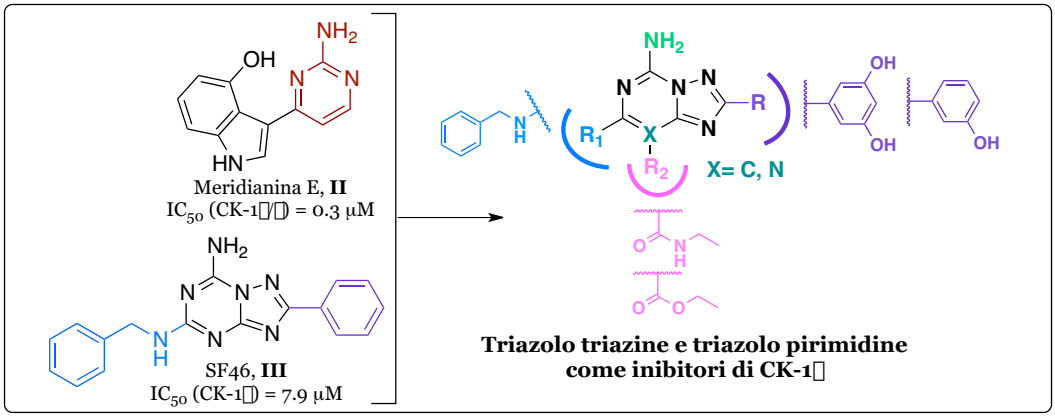

Figura II – Nuovi inibitori di CK-1δ a struttura triazolo-triazinica e triazolo-pirimidinica.

Inoltre, i derivati benzilamminici hanno anche dimostrato una miglior capacità di attraversare la BEE. Infine, simulazioni di *docking* molecolare hanno permesso di individuare alcune importanti interazioni tra i nostri derivati e il sito di legame per l'ATP di CK-1δ, che potrebbero essere utili per un'ulteriore ottimizzazione strutturale dei sistemi TT e TP.

Sintesi e caratterizzazione di inibitori duali di GSK-3β e CK-1δ

Considerato il coinvolgimento di entrambe le chinasi nelle vie di segnale di Wnt e Hedgehog, recentemente correlate alla cascata della neuroinfiammazione, e nell'iperfosforilazione della proteina *tau*, inibitori duali di GSK-3β e CK-1δ potrebbero essere uno strumento utile per valutare l'effetto dell'inibizione di entrambe le chinasi per il trattamento di malattie neurodegenerative. In questa parte del lavoro, abbiamo quindi deciso di modificare il nucleo TT per ottenere un'inibizione covalente di GSK-3β a livello del residuo cisteina 199 (Cis199), e allo stesso tempo inibire reversibilmente CK-1δ. In particolare, abbiamo inserito in posizione 2 della triazolo-triazina una cianoacrilamide, un gruppo accettore di Michael in grado, in condizioni fisiologiche, di reagire con il tiolo della Cis199 in modo rapido ma reversibile, minimizzando così il rischio di interazioni irreversibili non desiderate con peptidi e proteine (ad esempio il glutatione). Inoltre, il residuo ammidico, già presente nell'inibitore D4476 (**IV**), può conferire affinità verso CK-1δ. Il derivato **V** è risultato infatti un potente inibitore sia di GSK-3β (IC_{50}=0.17 μM) che di CK-1δ (IC_{50}=0.68 μM, ATP-competitivo), confermando quindi la validità del razionale. La reattività di **V** di fronte a gruppi tiolici è stata valutata attraverso spettroscopia UV e HPLC-MS, e il suo legame con GSK-3β è stato studiato sia teoricamente che sperimentalmente. Saggi di cinetica enzimatica hanno difatti mostrato un comportamento misto ATP-competitivo/non-ATP-competitivo di **V**, mentre studi effettuati variando il tempo di incubazione con la chinasi confermano l'instaurarsi di un'interazione covalente tra il ligando e GSK-3β (**Figura III**). Inoltre, nonostante non abbia mostrato una spiccata permeabilità alla BEE, **V** è in grado di aumentare la sopravvivenza di cellule trattate con 6-OHDA o MPTP, due modelli *in vitro* per lo studio della malattia di Parkinson (PD), e anche di aumentare l'espressione della β-catenina.

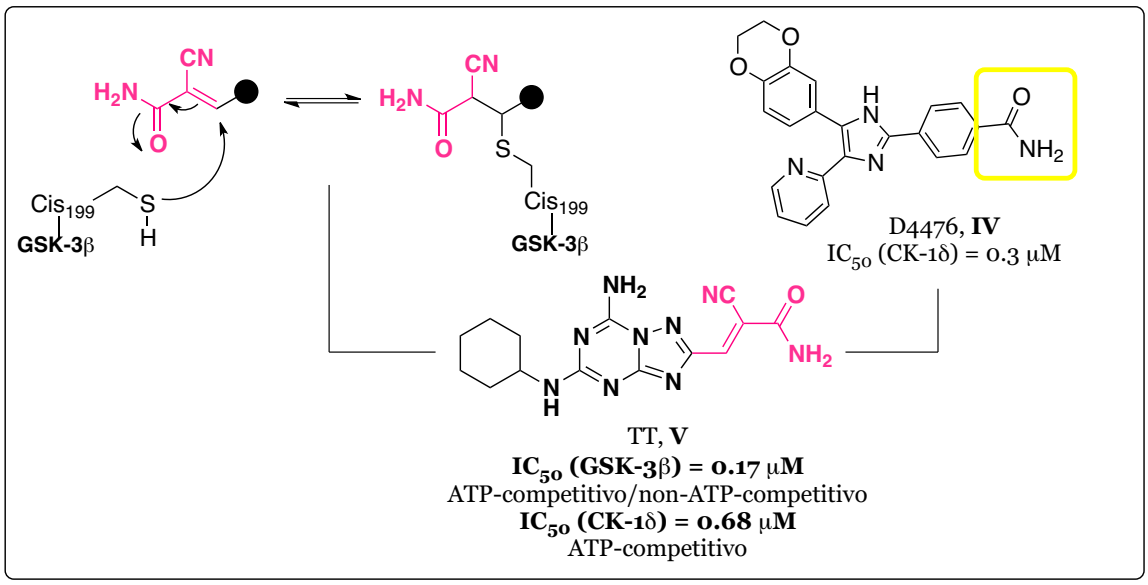

Figura III – Inibitore duale di GSK-3β e di CK-1δ a struttura triazolo-triazinica.

In conclusione, in questo lavoro di tesi, nuovi derivati a struttura simil-adeninica sono stati sviluppati come inibitori di GSK-3β e CK-1δ. In particolare, per alcuni composti sono stati raggiunti valori d'inibizione nell'ordine submicromolare e molti di loro si sono dimostrati in grado di attraversare la barriera emato-encefalica (BEE), rappresentando quindi un prezioso strumento per approfondire ulteriormente il ruolo di queste due chinasi in modelli di neuroinfiammazione e malattie neurodegenerative.

Table of Contents

List of Abbreviations

#	6-OHDA	6-Hydroxydopamine
A	Abl	Ableson Leukemia Oncogene Cellular Homolog
	AD	Alzheimer's Disease
	ADAM	A Disintegrin and Metalloproteinase
	ADP	Adenosine Diphosphate
	AGC	Protein Kinase A, G And C Family
	AIH	Amphetamine-Induced Hyperlocomotion
	AKAP	A-Kinase Anchor Proteins
	ALS	Amiotrophic Lateral Sclerosis
	AML	Acute Myeloid Leukemia
	APC	Adenomatous Polyposis Coli
	APE	Alanine/ Proline/Glutamic Acid
	APP	Amyloid Precursor Protein
	ATP	Adenosine Triphosphate
	AXL	from the greek word "Anexelekto"
	Aβ	β-Amyloid
B	BACE-1	β-Site APP-Cleaving Enzyme 1
	BBB	Blood-Brain Barrier
	BCL	B Cell Leukemia Protein
	BD	Bipolar Disorder
	BMAL	Brain and Muscle ARNT (Arylhydrocarbon Receptor Nuclear Translocator)-Like Protein
	Boc	*tert*-Butyloxycarbonyl
	bp	boiling point
	bs	broad singlet
	BSA	*N,O*-Bis(trimethylsilyl)acetamide
	BTK	Bruton's Tyrosine Kinase
	β-ME	β-Mercaptoethanol
	β-TrCP	β-Transducin Repeat-Containing Protein
C	c-Myc	Avian Myelocytomatosis Virus Oncogene Cellular Homolog
	CaMK	Calcium/Calmodulin-Dependent Kinase
	CARMA-1	Caspase Recruitment Domain-Containing Membrane-Associated Guanylate Kinase Protein-1
	CBP	CREB-Binding Protein
	CDK	Cyclin-Dependent Kinase
	cGMP	Cyclic Guanosine Monophosphate
	ChK	Checkpoint Kinase 1
	Ci	Cubitus Interruptus
	CK	Casein Kinase
	CLK	Cdc (Cell Division Control Protein)-Like Kinase
	CLL	Chronic Lymphoid Leukemia
	CLOCK	Circadian Rythms of Locomotor Activity Kaput
	CMGC	Cyclin-Dependent Kinase, Mitogen-Activated Protein Kinase, Glycogen Synthase Kinase, Cdc-Like kinase family
	CNS	Central Nervous System
	COX	Cyclooxygenase

	CRMP-2	Collapsin Response Mediator Protein 2
	CRY	Cryptochrome Protein
D	d	doublet
	DBU	1,5-Diazabiciclo[5.4.0]undec-5-ene
	DC50	Half-Maximal Displacement Concentration
	DCM	Dichloromethane
	dd	doublet of doublets
	DMF	Dimethylformamide
	DMP	Dess-Martin Periodinane
	DMSO	Dimethylsulfoxide
	DNA	Deoxyribonucleic Acid
	dt	doublet of triplets
	DTT	Dithiothreitol
	DVL	Segment Polarity Protein Dishevelled Homolog
	DYRK	Dual Specificity Tyrosine-Phosphorylation-Regulated Kinase
E	EDTA	Ethylenediaminetetraacetic acid
	EGF	Epidermal Growth Factor
	EGRF	Epidermal Growth Factor Receptor
	EGTA	Ethylene glycol-bis(β-aminoethyl ether)-*N,N,N',N'*-tetraacetic acid
	EPSC	Excitatory Postsynaptic Currents
	ERK	Extracellular Signal-Regulated Kinase
	ES-MS	Electrospray Mass Spectrometry
	ESC	Embryonic Stem Cells
	EtOAc	Ethyl Acetate
F	FDA	Food and Drug Administation
	FGFR	Fibroblast Growth Factor Receptors
	FOXL-2	Forkhead Box Protein L2
	FOXO	Forkhead Box O
	FRAT/GBP	Frequently Rearranged in Advanced T-Cell Lymphomas / GSK-3 Binding Protein
	FST	Forced Swimming Test
	FTLD	Frontotemporal Lobar Degeneration
G	GAPDH	Glyceraldehyde 3-Phosphate Dehydrogenase
	Gli	Glioma-Associated Oncogene Protein
	GLUT	Glucose Transporters
	GMP	Guanosine Monophosphate
	GS	Glycogen Synthase
	GSK-3	Glycogen Synthase Kinase 3
	GTP	Guanosine Triphosphate
H	HD	Huntington's Disease
	HEPES	4-(2-Hydroxyethyl)-1-piperazineethanesulfonic acid
	HER-2	Human Epidermal Growth Factor Receptor 2
	HH	Hedgehog pathway
	HIF	Hypoxia-Inducible Factors
	HMDSO	Hexamethyldisiloxane
	HPLC-MS	High Performance Liquid Chromatography-Mass Spectrometry
	HR-I/II	Hydrophobic Region II And II
	HSTF-1	Heat Shock Transcription Factor-1

I	I-κB	Inhibitor of NF-κB
	IC50	Half-Maximal Inhibitory Concentration
	IKK	IκB Kinase
	IL	Interleukin
	IRAK	Interleukin-1 Receptor-Associated Kinase
	IRS	Insulin Receptor Substrate
J	*J*	Couplings constant
	JAK	Janus Kinase
	KHD	Kinesin Homology Domain
L	LATS	Large Tumor Suppressor Kinase
	LB	Lewy Bodies
	LEF	Lymphoid Enhancer-Binding Factor
	LPS	Lipopolysaccharide
	LRP	LDL-Receptor-Related Protein
	LTD	Long Term Depression
	LTP	Long Term Potentiation
M	m	multiplet
	m-CPBA	*meta*-Chloroperoxybenzoic acid
	MAP	Mitogen-Activated Protein
	MAPK/STE	Mitogen-Activated Protein Kinase
	MAPKAP	MAP Kinase Activated Protein Kinase
	MCL	Mantle Cell Lymphoma
	MCP-1	Monocyte Chemoattractant Protein-1
	MDD	Major Depressive Disorder
	MDM2	Mouse Double Minute 2 Homolog
	MIP-1	Macrophage Inflammatory Proteins
	MLCK	Myosin Light-Chain Kinase
	mp	melting point
	MPTP	1-Methyl-4-phenyl-1,2,3,6-tetrahydropyridine
	mRNA	Messenger Ribonucleic Acid
	mTOR	Mammalian Target of Rapamycin
	MTT	3-(4,5-Dimethylthiazol-2-yl)-2,5-diphenyltetrazolium
N	NF-κB	Nuclear Factor κB
	NFAT	Nuclear Factor of Activated T Cells
	NFT	Neurofibrillary Tangles
	NMDA	N-Methyl-D-Aspartate
	NMR	Nuclear Magnetic Resonance
	PAMPA	Parallel Artificial Membrane Permeability Assay
P	PBS	Phosphate-Buffered Saline
	PD	Parkinson's Disease
	PDB	Protein Data Bank
	PER	"Period" Protein
	Ph	Phenyl
	PHF	Paired Helical Filaments
	PI-3K	Phosphoinositide 3-Kinase
	PIP-2	Phosphatidylinositol 3,4-Bisphosphate
	PK	Protein Kinase
	PKA	Protein Kinase A
	PKB/AKT	Protein Kinase B

	PKC	Protein Kinase C
	PPSE	Polyphosphoric Acid Trimethylsilyl Ester
	PS-1/2	Presenilin 1/2
	PSC	Pluripotent Stem Cells
	Ptch	Patched
Q	q	quartet
R	r.t.	room temperature
	RGC	Retinal Ganglion Cells
S	s	singlet
	SAR	Structure-Activity Relationship
	SD	Standard Deviation
	SLK	Sterile20-Like Kinase
	SMA	Spinal Muscular Atrophy
	SMN	Survival Motor Neuron
	Smo	Smoothened
	SOD	Superoxide Dismutase
	Src	Rous Sarcoma Oncogene Cellular Homolog
	STE	Homologs of Yeast Sterile7, Sterile11 and Sterile20 Kinase Family
	Syk	Spleen Tyrosine Kinase
T	t	triplet
	TAZ	Tafazzin
	TBST	Tris-Buffered Saline and Tween 20
	TCF	T Cell Factor
	TCI	Targeted Covalent Inhibitors
	td	triplet of doublets
	TEA	Triethylamine
	TEF	Thyrotroph Embryonic Factor
	TFA	Trifluoroacetic Acid
	THF	Tetrahydrofurane
	TK	Tyrosin Kinase
	TKL	Tyrosine Kinase-Like
	TLC	Thin-Layer Chromatography
	TLR	Toll-Like Receptor
	TNF-α	Tumor Necrosis Factor-α
	TP	[1,2,4]Triazolo[1,5-*c*]Pyrimidine
	TR-FRET	Time-Resolved Fluorescence Energy Transfer
	TSC	Tuberous Sclerosis Complex
	TT	[1,2,4]Triazolo[1,5-*a*][1,3,5]Triazine
U	UB	Ubiquitin
	UV	Ultraviolet Radiation
W	Wnt	Wingless and Int
Y	YAP	Yes-Associated Protein 1
Z	ZDF	Zucker Diabetic Fatty

Abbreviations of Amino Acids

Ala	Alanine	A
Arg	Arginine	R
Asn	Asparagine	N
Asp	Aspartic acid	D
Cys	Cysteine	C
Gln	Glutamine	Q
Glu	Glutamic acid	E
Gly	Glycine	G
His	Histidine	H
Ile	Isoleucine	I
Leu	Leucine	L
Lys	Lysine	K
Met	Methionine	M
Phe	Phenylalanine	F
Pro	Proline	P
Ser	Serine	S
Thr	Threonine	T
Trp	Tryptophan	W
Tyr	Tyrosine	Y
Val	Valine	V

1 Background

1.1 PROTEIN KINASES

This PhD project focuses its attention on the largest group of enzymes found in nature: the protein kinases (PKs). PKs catalyze the transfer of the γ-phosphoryl group of high-energy donor molecules, adenosine-5'-triphosphate (ATP) or more rarely guanosine-5'-triphosphate (GTP), to a hydroxyl group of an amino acid side chain in a protein substrate, and this process is defined phosphorylation (**Figure 1**).[1] This transfer is facilitated by magnesium (Mg^{2+}), which chelates the γ- and β-phosphate groups to lower the threshold for phosphoryl transfer to the nucleophilic hydroxyl group.[2]

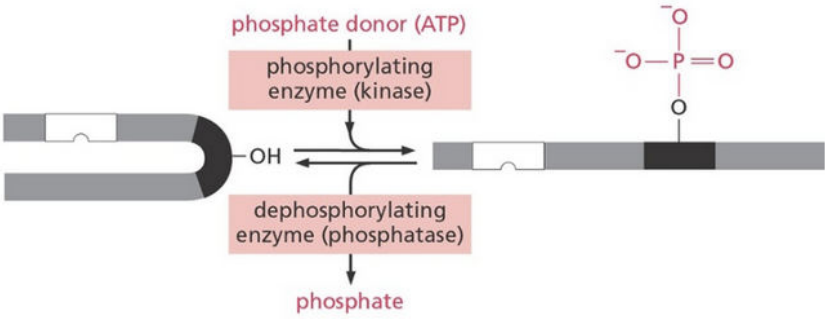

Figure 1. Protein phosphorylation and dephosphorylation.[3]

At physiological pH, the introduction of the dianionic, double-negative charged phosphoryl group causes conformational modifications of the protein structure, which may lead to an increase or a decrease in their intrinsic activity.[4] Thereby kinases are able to activate or inhibit single proteins to play a specific role, turn on or off entire cellular pathways, lead to the formation or destabilization of protein complexes, and sequester protein for their ubiquitination.[1] The phosphorylation process plays thus a central role in the regulation of several cellular functions common to all eukaryotes such as, for example, DNA replication, gene transcription, cell cycle control, intracellular transport of proteins, cytoskeleton rearrangement, cell motility and metabolism.[5] Given the enormous importance of its role, it is clear that phosphorylation itself requires a regulation; in fact, it can be reversed by protein phosphatases, enzymes that can remove the phosphate covalently bound to the protein substrates bringing them back to their initial state. The life of the cell is thus dependent on a fine balance between kinases and phosphatases activity.

Since protein phosphorylation is essential for a wide range of biological mechanisms, a deregulation of this process can lead to dysfunctions in cellular signaling and these, in turn, can lead to different pathological conditions, such as cancer, diabetes, arthritis, neurological and metabolic disorders. [6,7]

The reversible phosphorylation of proteins, catalyzed by protein kinases and phosphatases, was first identified as a regulatory mechanism in the 1950s, however, it was only in the late 1980s that developing inhibitors of PKs started to be one of the fastest emerging fields in pharmaceutical research.[8] The first two drugs shown to target these classes of enzyme were staurosporin, a nanomolar inhibitor of protein kinase C (PKC) and rapamycin, an inhibitor of the protein kinase mTOR (mammalian target of rapamycin), both immunosuppressants that were developed and approved for clinical use before their mechanism of action was identified.[8] The first protein kinase inhibitor to reach the market was Fasudil, an inhibitor of several protein kinases with relatively low potency approved in Japan in 1995 for the treatment of cerebral vasospasm. However, the breakthrough came with the discovery of Imatinib (Gleevec®, Novartis), the first drug to be developed by

targeting a specific protein kinase (the protein tyrosine kinase c-Abl) and approved for clinical use in the United States in 2001. The success obtained by Imatinib helped to dispel the myth which it is not possible to obtain at the same time potent and selective PK inhibitors, and PKs have now become the second most important group of drug targets, after G-protein-coupled receptors (**Figure 2**).[9]

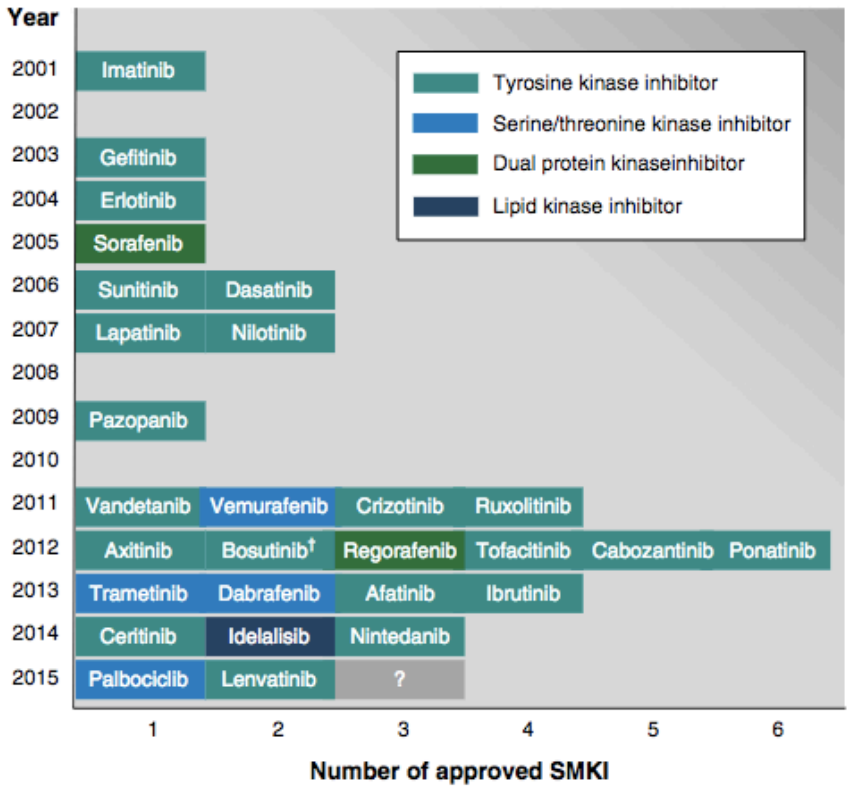

Figure 2. Approved small-molecules kinase inhibitors (SMKI) from 2001 to June 2015.[10]

1.1.1 Protein kinases classification

The developing of molecular cloning strategies and sequencing techniques dramatically accelerated the identification of protein kinases, which at the end of the 1990s were expected to be more than a thousand, according to extrapolations from yeast and nematode genomes. It is now known that the human genome encodes 518 protein kinases, grouped into over 57 families, which represent 1.7% of all human genes, and 20 lipid-modifying kinases. Among the 518 kinases, 478 present an eukaryotic protein kinase (ePK) catalytic domain, while the remaining 40 kinases, lacking sequence similarity to the ePK domain, are referred to as the atypical protein kinases (aPKs) (**Figure 3**).[1]

Kinases can be classified on the basis of structural and functional similarities. So, it is possible from this point of view to divide them into eight main families:[2]

I. **AGC (Cyclic nucleotide regulated protein kinase family)**: this group mainly includes Ser/Thr-specific protein kinases as PKA (cAMP-dependent protein kinase), PKB (protein kinase B or AKT), PKG (cGMP-dependent protein kinase) and PKC (calcium dependent protein kinase).
II. **CaMK (Kinases regulated by Ca^{2+}/CaM and close relative family)**: this group includes the family of protein kinases regulated by Ca^{2+} and calmodulin

(CaMK), the MLCK (Myosin light-chain kinase) and five MAPKAPKs (MAP kinase activated protein kinase).

III. **CGMC (CDK, GSK-3, MAPK, CK2)**: a heterogeneous group of kinases including ten CDKs (cyclin dependent kinase), ERK (extracellular signal–regulated kinase), CK-2 (casein kinase 2) and GSK-3α/β (glycogen synthase kinase 3), one of the two targets of this project.

IV. **STE (related to yeast non-mating or sterile genes)**: the family that includes STE7 or MAP2K (MAP kinase kinase), STE11 or MAP3K (MAP kinase kinase kinase), STE20 or MAP4K (MAP kinase kinase kinase kinase).

V. **CK-1 (casein kinase 1 family)**: in this group are included all the isoforms of casein kinase 1, including the isoform δ, object of our studies together with GSK-3β.

VI. **TK (tyrosine kinase):** this group consists of receptor TKs (RTKs) and non-receptor (cytosolic) TKs, including Src kinase, Abl (Abelson tyrosine kinase), and JAK (Janus kinase) kinases. RTKs are transmembrane proteins as the human epidermal growth factor receptor (HER/EGFR) family and the insulin receptor (IR).

VII. **TKL (tyrosine kinase-like):** members of the TKL group are mostly serine/threonine kinases but have sequences resembling those of the TK group. The group includes the interleukin-1 (IL-1) receptor-associated kinase (IRAK) and the transforming growth factor beta (TGF-β) receptors.

VIII. **RGC (receptor guanylyl cyclase):** it consists of pseudokinases that convert GTP to cyclic GMP (guanylyl cyclases).

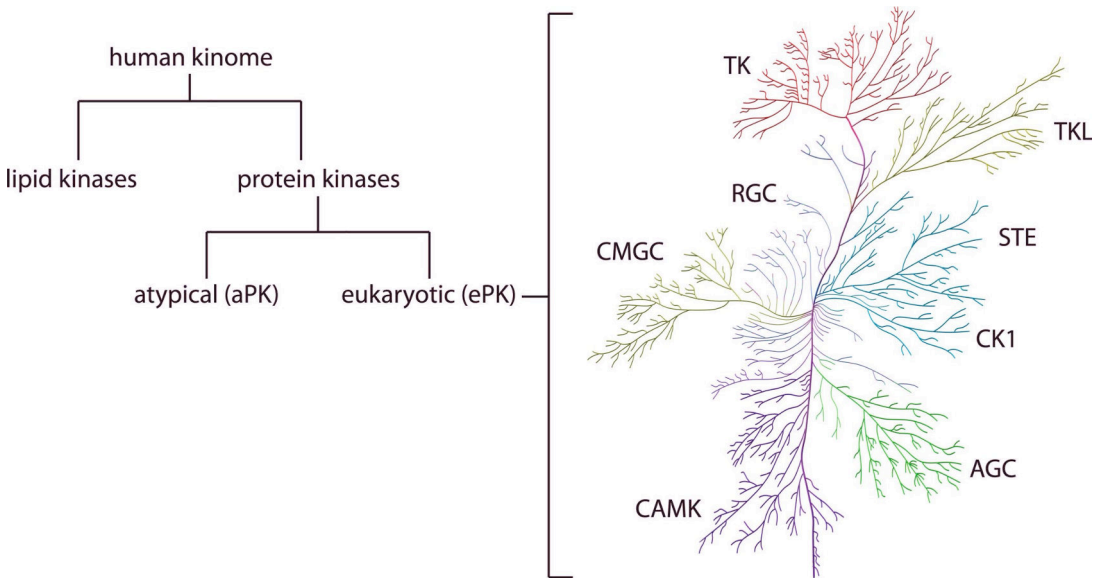

Figure 3. The human kinome and phylogenetic classification of human ePKs.[2]

PKs can be also classified on the basis of the amino acid residue that can accept the phosphate group and comprises three main families:[11]

I. **Ser/Thr-specific protein kinases:** utilize the alcoholic group of a serine and/or a threonine as acceptor of the phosphate group.

II. **Tyr-specific protein kinases:** catalyze the phosphorylation of the phenolic group of the tyrosine.

III. **Dual-specificity protein kinases**: able to phosphorylate both Ser/Thr and Tyr residues.

1.1.2 Protein kinases structure

In recent years, the crystallographic structures of various protein kinases have become available in the Protein Data Bank (PDB), co-crystallized with their cofactors (e.g. metal ions), their protein substrate or with inhibitors, which allowed to clarify the functional role of some amino acid residues identified as crucial for the catalytic activity of the corresponding kinase.[5] In general, a protein kinase is constituted by two lobes: the N-terminal lobe, smaller in size, rich in β sheet structures and involved in the ATP binding, and the C-terminal lobe, rich in α-helix structures and involved in the interactions with the peptide substrate.[12] The two lobes are linked by a hinge region, a short sequence of conserved residues that form hydrogen bonds with the adenine moiety of the ATP. Between the two lobes, a deep cleft is formed, that constitutes the recognition site of the ATP. The N-terminal residue of the hinge region is named the gatekeeper residue: it is located in the back wall of the ATP binding site and controls the access to a hydrophobic pocket that lies behind the adenine-binding pocket.[13] The size and hydrophobicity of the gatekeeper residue determine the accessibility of the hydrophobic pocket by kinase inhibitors. Ser/Thr kinases usually present large, hydrophobic gatekeeper residues, such as Phe or Met, whereas Tyr kinases often have a smaller residue, such as Thr or Val. As far as we are concerned, Leu132 is the gatekeeper residue of GSK-3β,[14] while Met82 is for CK-1δ.[15] As reported before, divalent metal ions are essential to coordinate ATP for γ-phosphate transfer. GSK-3β has a peculiar requirement for two divalent magnesium ions[16] and structural characterization indicates these divalent magnesium ions bind at the interface of the two lobes.[17]

Some structural features have been found to be critical for catalysis and for protein kinase control:[18]

- **The ATP-binding loop (N-terminal lobe):** contains the motif GXGXXGV, also called the glycin rich loop, highly conserved in almost all eukaryotic protein kinases. It has the function of anchoring the ATP to the protein. In GSK-3β the sequence is GNGSFGV (residues 63-69),[19] while in CK-1δ is GEGSFGV (residues 19-25).[20]
- **The C-helix of the N-terminal lobe:** forms a salt-bridge between nearly invariant Glu (Glu97 in GSK-3β), to an invariant Lys within the N-terminal lobe (Lys85 in GSK-3β)[21], which has been recognized as being essential for maximal enzyme activity, allowing optimal positioning of the ATP phosphate; in the CK-1δ structures this particular interaction is not reported.[20,22]
- **The catalytic loop**: it is characterized by the HRD motif (histidine-arginine-aspartic acid), which contains a conserved Asp, presumed to act as the catalytic base during the transfer of the phosphoryl group. In the case of GSK-3β the Asp involved is Asp181 (HRD, 179-181)[21], while in CK-1δ is Asp128 (HRD, 126-128)[22].
- **The activation loop**: it is located on the C-lobe and is one of the most important control elements of protein kinase activity; it is flanked by the highly conserved DFG triplet (aspartic acid-phenylalanine-glycine) and the consensus APE motif (alanine-proline-glutamic acid), whose function has not been well characterized yet.[5,23] In particular, the Asp of the DFG motif chelates the metal ion(s) that bridges the β- and γ-phosphates of the ATP, thus orientating the γ-phosphate for transfer. In these conditions, the Asp side chain points towards the ATP binding site and so the active state is named *DGF-in* conformation. The activation loop often contains a

phosphorylation site that upon phosphorylation induces a conformational change on the loop, allowing the peptide substrate to bind.[24]

In GSK-3β, the activation loop contains a conserved tyrosine residue, Tyr216, which, when phosphorylated, seems to confer activity to the kinase promoting substrate accessibility.[25] However, even when non-phosphorylated, the activation loop of GSK-3β presents a conformation very similar to that seen in active state kinases. This suggests that this is the explanation for the constitutive activity of GSK-3β.[26] The mechanism of this phosphorylation is still unclear: several kinases are reported to mediate Tyr216 phosphorylation, but in recent years evidences suggest an autophosphorylation process, which exploits an intramolecular tyrosine kinase activity.[27]

In CK-1δ, the activation loop is called L-9D and the conserved APE motif is here substituted by the SIN sequence.[20] It is longer than comparable loops in other kinases and contains three possible phosphorylatable amino acids: Tyr161, Thr166 and Ser179.[20] However, in the structure of the unphosphorylated fully active CK-1δ, the loop L-9D is in the open conformation, thus leaving the active site accessible to the peptide substrate. This means that phosphorylation at the L-9D loop is not essential for the activity of the kinase.[22] In addition, the L-9D loop contains a kinesin homology domain (KHD), that is thought to be involved in the interaction of CK-1δ with components of the cytoskeleton.[28]

- **Autoinhibitory sequence elements**: these elements promote the inactivation of the kinases by occupying the substrate peptide-binding site like the real substrate.[1] For example, GSK-3β is inhibited as consequence of phosphorylation of the residue Ser9, found near the N-terminus. In fact, phosphorylated Ser9 simulates the pre-phosphorylation of substrates and, therefore, the N-terminal tail can function as a pseudo-substrate that precludes the access of substrates to the catalytic site.[29] Several kinases have been found to phosphorylate GSK-3β at Ser9, including PKB, in response to insulin stimuli, MAPKAP kinase-1, after epidermal growth factor stimulation, certain isoforms of PKC and PKA.[30] On the other hand, CK-1δ presents in its catalytic domain a dimerization domain (DD), containing various amino acids that can occupy the adenine-binding site when CK-1δ is in the dimeric form. As a consequence, ATP cannot reach the active centre of the kinase and the formation of homodimers have an autoinhibitory effect on CK-1δ.[31] Moreover, as it happens with Ser9 phosphorylation in GSK-3β, even CK-1δ activity can be regulated by reversible phosphorylation through autophosphorylation. In fact, the residues Ser318, Thr323, Ser328, Thr329, Ser331 and Thr-337 in the C-terminal domain resulted to be involved in autophosphorylation events, causing the block of the catalytic core of the kinase.[28]

1.2 GLYCOGEN SYNTHASE KINASE 3 (GSK-3)

Within the CMGC group of protein kinases, of special interest for our project there is glycogen synthase kinase 3 (GSK-3), a constitutively active multi-potent serine/threonine kinase, that is ubiquitously present in all mammalian cells, and its homologues have been identified in all eukaryotes. GSK-3 was first discovered in 1978 by Sir Philip Cohen from the University of Dundee, Scotland, and recognized as a key mediator of the insulin pathway, mainly by phosphorylating the key enzyme glycogen synthase (GS) and blocking the incorporation of glucose into glycogen.[32] It phosphorylates GS at multiple serine residues within a proline-rich sequence of amino acids, thus defining GSK-3 as a proline-directed

Ser/Thr kinase.[33] Further studies revealed that, in addition to glucose metabolism, GSK-3 was a crucial regulator of multiple signaling pathways involving glycogen metabolism, cell cycle, gene expression, protein synthesis, cellular metabolism, motility, apoptosis, neuroprotection, proliferation, and survival through interactions with multiple pathways including Wnt, MAP-kinase (MAPK), or PI3K/Akt signal transduction pathways.[34]

Two mammalian isoforms of GSK-3, encoded by distinct genes, were identified: GSK-3α (mapped to chromosome 19q13.2) and GSK-3β (mapped to chromosome 3q13.3). These two isoforms are structurally identical to 98% within their kinase domains, but differ in C- and N-terminal residues. GSK-3α, in fact presents an extra N-terminal glycine rich region, which results in molecular weight difference between the two isoforms: GSK-3α is 51kD while GSK-3β is 47kD (**Figure 4**).[35,36]

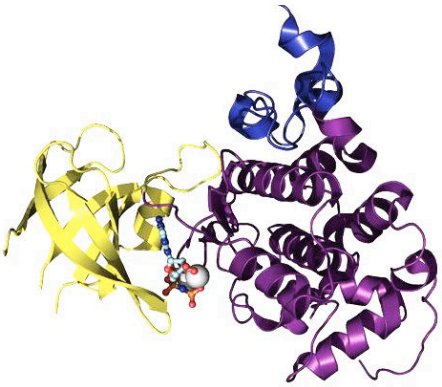

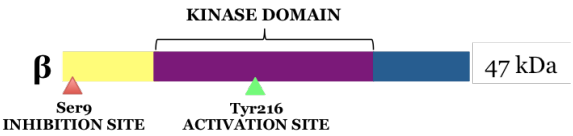

Figure 4: Glycogen synthase kinase-3β (GSK-3β) structure (PDB structure 1UV5). In yellow the N-terminal domain, in magenta the α-helical kinase domain and the C-terminal domain in blue. In the strand diagram of GSK-3β are reported the site of regulation: phosphorylation of Ser-9 inactivates the enzyme, while phosphorylation of Tyr-216 exerts a positive regulation of the enzyme. [36]

Moreover, an alternative splicing variant of GSK-3β has been reported; it was termed GSK-3β2 and contains the splice insert of exon 8b, which encodes an extra 13 amino acid sequence in the catalytic domain. GSK-3β2 has been found in human and rodent species and seems to present an altered kinase activity.[37]

Despite their homology, GSK-3 isoforms undergo distinct regulatory mechanisms and exhibit different activities in certain situations. The functions of both GSK-3 isoforms have been examined in transgenic mice. Deletion of both alleles of GSK-3β in mice resulted lethal in embryogenesis, while mice that lacked both alleles of GSK-3α were viable, but displayed sensitivity to insulin and glucose.[38]

Moreover, despite detectable mRNA levels in nearly all tissue, high levels of the α isoform are observed in human testis while GSK-3β is especially abundant in human brain.[39] This is one of the reasons why, for the aim of our work, we focused our attention on the β isoform of GSK-3.

1.2.1 GSK-3β regulation and its substrates

The determination of crystalline structure of GSK-3 allowed the identification of the different mechanisms of enzyme control and function.[26,29] As previously described in Chapter 1.1.2, when fully active, GSK-3β is phosphorylated at Tyr 216 through a mechanism still not well clarified. Active GSK-3β phosphorylates most of its substrates through a unique mechanism, which requires priming of the substrates by another protein kinase. The amino acid sequence recognized is Ser/Thr-X-X-X-Ser-P/Thr-P, where the first Ser or Thr residue represents the target of GSK-3β phosphorylation, X represents a generic residue (often a Proline) and the phosphorylated residue (Ser-P/Thr-P) is the priming phosphorylation site.[40]

For example, GS requires priming phosphorylation by CK-2 before being phosphorylated at different sequential sites by GSK-3.[35] However, some substrates such as Axin do not require previous phosphorylation by other protein kinases prior to being phosphorylated at Thr609 and Ser614 by GSK-3β.[41] The explanation of GSK-3β mechanism of primed substrate recognition is found in the presence of a triad of basic residues (Arg96, Arg180, Lys205), of which the side chains provide a positively charged area suitable for the negatively charged phosphate group on the primed residue.[26]

On the other hand, GSK-3β activity is inhibited physiologically in at least two different ways: through direct phosphorylation (Ser9) by other kinases (e.g. PKB, in the case of insulin stimulation,[42] or MAPKAP-1β, in the case of EGF[43])[26] or through formation and disruption of protein complexes involved in different pathways, as it happens for example in the canonical Wnt (Wingless and Int) pathway.[35,44]

The Wnt proteins are glycoproteins rich in cystein residues that regulate cellular growth, differentiation, migration and fate.[45] GSK-3β is known to form the so called "destruction complex" with Axin, APC (*Adenomatous Polyposis Coli* protein) and β-catenin. Without a Wnt signal, GSK-3 is activated and can phosphorylate the primed β-catenin on different serine residues (Ser33, Ser37, Ser41), thus targeting it for ubiquitination and consequent degradation *via* proteasome.[46,47] The phosphorylation of β-catenin by GSK-3 is facilitated by Axin, which binds and supports the different components of the complex. The binding of secreted Wnt ligands to the co-receptor Frizzled and LRP5/LRP6 (low-density lipoprotein receptor-related proteins 5 or 6) activates the protein FRAT/GBP (Frequently Rearranged in advanced T-cell lymphomas/GSK-3 Binding Protein) that, with DVL (disheveled protein), binds the site of GSK-3 usually occupied by Axin. In this way, it is prevented the formation of the complex GSK-3/Axin/APC/β-catenin, thus β-catenin is not phosphorylated by GSK-3 and subsequently is not degraded by the ubiquitin-proteasome system.[48] Therefore β-catenin can accumulate in the cytoplasm and translocate to the nucleus, where it binds to transcription factors of TCF/LEF (T-cell factor/ lymphoid enhancer-binding factor-1) family and activates the transcription of target genes (e.g. the proto-oncogene *c*-Myc and cyclin D1).[49]

Recently, other regulatory mechanisms of GSK-3β were reported, including N-terminal proteolysis. The proteolytic enzyme calpain is, in fact, able to remove the regulatory N-terminal domain of GSK-3β *in vitro*, generating fragments of about 30-40 kDa. Interestingly, this truncation augments the kinase activity, due to the loss of the regulatory domain containing the inhibitory Ser9. Calpain acts preferentially on the isoform β and its activation is triggered by intracellular Ca^{2+} levels increase, which may be caused, for example, by stimulation of ionotropic NMDA receptors.[50]

Finally, GSK-3 is regulated through its intracellular distribution.[51] GSK-3β is mainly localized in the cytoplasm, but is also present in the nucleus and mitochondria. The GSK-3β nuclear activity is generally greater than the cytoplasmic one and further increases during apoptosis, in response to p53 stimulation or through interaction with FRAT.[52] The export of GSK-3β from the nucleus to the cytoplasm, and vice versa, can prevent interaction with its substrates, thus regulating the activity.[51]

1.3 CASEIN KINASE 1 (CK-1)

The first casein kinase activity was identified in 1954 by Burnett and Kennedy through experiments conducted on rat liver using casein as phosphorylatable substrate.[53] Later in 1969, two distinct enzymes were reported to be responsible of this activity and they were called casein kinase 1 (CK-1) and casein kinase 2 (CK-2).[54] They share the ability of readily phosphorylate casein *in vitro*, however casein is the physiological substrate only of one of the members of casein kinases family, the so-called genuine casein kinase (G-CK), responsible for the phosphorylation of casein within the lactating mammary gland. [55]

The CK-1 family represents a small group within the family of Ser/Thr-protein kinases and is found in all eukaryotic organisms, from yeast to human, in all tissues and cellular compartments and localized both in nucleus and in cytoplasm. So far, seven CK-1 isoforms (α, β, γ_1, γ_2, γ_3, δ, and ε) have been characterized in mammals, and their molecular weight varies from 37 kD to 51 kD. In addition, alternate splicing generates several variants of their coding genes.[56] They have been described to act as monomeric, constitutively active enzymes, which exclusively recognize ATP as phosphate donor and are generally co-factor independent.[57] The family members have the highest homology in their kinase domains (53–98% identical), while outside CK-1 isoforms show little homology to each other and differ in length and amino acid sequence of their N- and C-terminal segments. At the moment, crystal structures of human CK-1 isoforms γ_1, γ_2, γ_3, δ and ε have been resolved.[15]

In this work, we will focus on the isoform δ of CK-1, due to its superior relevance and its involvement in several pathologies, such as neurodegenerative disorders, including Alzheimer's disease (AD), sleeping disorders and cancer.[15,58]

CK-1δ isoform weighs 49100 Da and its gene has been mapped in locus 19pl3.3. It appears to be very similar to CK-1ε, with which it forms the so-called δ/ε subfamily. Both isoforms have a long C- terminal tail (ca. 100 residues), responsible for regulating enzyme activity through inhibitory autophosphorylation (**Figure 5**).[59]

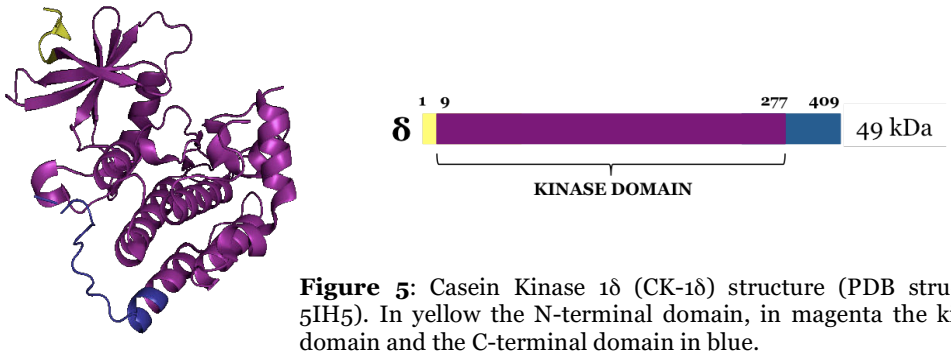

Figure 5: Casein Kinase 1δ (CK-1δ) structure (PDB structure 5IH5). In yellow the N-terminal domain, in magenta the kinase domain and the C-terminal domain in blue.

1.3.1 CK-1δ regulation and its substrates

Although more than 140 *in vitro* and *in vivo* substrates for CK-1 isoforms have been reported, features underlying its substrate specificity are still a matter of investigation.[15] CK-1δ belongs to the group of acidotropic protein kinases; in fact it mainly recognizes substrates containing acidic or phosphorylated amino acid residues. Preferably, CK-1δ phosphorylates Ser/Thr residues found within the sequence pSer/Thr-X-X-(X)-Ser/Thr, where pSer/Thr are pre-phosphorylated serine or threonine residue. [15] However, CK-1 not necessarily requires a primed substrate, rather acts as a priming kinase, which generates the consensus sequence

for phosphate directed kinases as, for example, GSK-3.[60] In fact, it was demonstrated that the phosphorylated amino acid could be replaced by a strain of negatively charged acidic amino acids.[61] In addition, CK-1 family members also recognize non-canonical motives such as the sequence S*LS, in which S* is the target serine, found in the transcription factors family NFAT (nuclear factor of activated T-cells), β-catenin and adenomatous polyposis coli (APC).[60]

CK-1 expression and activity is modulated by different effectors: stimulation of cells with insulin or gastrin, as well as treatment with topoisomerase inhibitors or γ-irradiation, lead to elevated CK-1 activity and/or protein levels. On the contrary, increased membrane concentration of phosphatidylinositol-4,5-biphosphate (PIP2) reduces CK-1 activity.[15]

At the protein level, autophosphorylation of different Ser and Thr residues in the C-terminal tail of the CK-1δ isoform results in inhibition of the kinase activity (see Chapter 1.1.2).[28] In fact, the cleavage of the C-terminal domain by endoproteases, as well as the dephosphorylation of autophosphorylation sites, lead to elevated kinase activity, as it happens to the N-terminal domain of GSK-3β.[62] In addition, CK-1δ is also phosphorylated by other kinases, including PKA, PKB, CLK2 (CDC-like kinase 2), PKC-α, and Chk-1 (Checkpoint kinase 1).[28,62] In addition to post-translational modifications, subcellular localization and compartmentalization are essential for CK-1 function, maintaining kinase and substrate into close proximity.[28] In the case of CK-1δ, it has been shown that the subcellular localization depends on the enzymatic activity of the kinase: actually, CK-1δ in mammalian cells is mainly cytoplasmic and also enriched at the centrosomes in interphase cells; on the other hand, two inactive mutants of the kinase were detected almost exclusively in the nucleus, suggesting that protein kinase activity is required for the cytosolic localization of CK-1 and prevention of nuclear accumulation.[63] Finally, CK-1 activity can furthermore be regulated by interaction with other proteins, for example A-kinase anchoring protein 450 (AKAP450).[64] AKAP450 has an established role in anchoring different signaling molecules to the centrosome and Golgi, including CK-1δ and ε. This association, indeed, addresses CK-1δ/ε activity towards the regulation of molecular events occurring within these organelles.[65]

1.4 CELLULAR SIGNALING and PATHOLOGICAL IMPLICATIONS

On the basis of the substrates identified along the years, GSK-3β and CK-1δ regulate over 100 proteins involved in metabolic and signaling pathways, as well as structural proteins and transcription factors. Recent studies indicate that the signaling pathways triggered by these molecules are very often deregulated in pathological conditions. A brief overview of GSK-3β and CK-1δ functions is presented hereafter.

1.4.1 Metabolic pathways

As early as 1979, GSK-3 was suggested to be a negative regulator of glycogen synthesis in the PI3K/insulin signaling pathway. In fact, GSK-3β was shown to phosphorylate different serine residues of glycogen synthase (GS), reducing its activity (**Figure 6**).[32] After stimulation with insulin, the insulin receptor substrates 1 and 2 (IRS1 and IRS2) recruit PI3K, which activates AKT by phosphorylation at Thr308 and Ser473. AKT subsequently phosphorylates GSK-3β at its inhibitory Ser9 residue, which is no longer able to phosphorylate and inhibit glycogen synthase, resulting in increased glucose storage through glycogen synthesis.[30] Moreover, Buller *et al.* reported that GSK-3 is a negative regulator of

basal glucose uptake through down regulation of glucose transporter 1 (GLUT1) expression. GLUT1 expression can be activated by mammalian target of rapamycin (mTOR) signaling pathway and, in this case, GSK-3β seems to exert its inhibitory activity through phosphorylation of the tumor suppressor tuberous sclerosis complex subunit 2 (TSC2).[66] For its extensive and central role in glucose metabolism, GSK-3 is considered a highly targetable molecule for the treatment of type II diabetes. Moreover, the inhibition of GSK-3β, together with the inhibition of dual specificity tyrosine-phosphorylation-regulated kinase 1A (DYRK1A), is capable of inducing β-cells proliferation, thus offering an opportunity for therapeutic intervention in diabetes.[67]

Also CK-1 is involved in the regulation of glycogen metabolism. In fact, in the cytosol, CK-1 acts in synergism with PKA[68] to phosphorylate and negatively regulate the activity of glycogen synthase at Ser10 residue (**Figure 6**).[69]

Figure 6: "Hierarchical phosphorylation" of GS by GSK-3, CK-1, PKA, AMPK and CK-2.[3]

1.4.2 Wnt pathway

The signaling of the Wnt family of secreted lipoproteins has central roles in embryogenesis, in adult tissue homeostasis and also in human tumorigenesis.[45] In fact, mutation of several intracellular components of the Wnt pathway is thought to be critical in many forms of cancer.[70] Moreover, recent studies show that the Wnt pathway also has an important role in some aspects of neuronal circuit development, such as neuronal migration, synaptic differentiation, mature synapse modulation and synaptic plasticity.[71] Moreover, it may have potential in the prevention of neurodegenerative diseases that involve synaptic impairment.[72]

GSK-3β participation in the Wnt signaling pathway is of fundamental importance, as previously described (Chapter 1.2.1). Although it was considered for a long time to exert only a negative role in this pathway, by phosphorylating and targeting β-catenin for ubiquitination and degradation, recent advances indicate that it also participates in the phosphorylation and activation of the Wnt co-receptor LRP6, thus providing a new mechanism for the suppression of its own activity and β-catenin stabilization (**Figure 7**).[73]

Abnormal β-catenin levels have been highlighted in different types of cancer, principally in the colorectal one,[70] therefore the idea of a therapeutic GSK-3 inhibition should be considered with concern due to the possibility of malignancy development.

In the canonical Wnt/β-catenin signaling pathway, all CK-1 isoforms seem to be involved, rendering the comprehension of their involvement quite complex. Moreover, CK-1 holds a role both in negative and in positive regulation of Wnt signaling and often discrepant results concerning CK-1 isoforms functions are reported, since highly affected by the experimental conditions and physiological settings used in each study (**Figure 7**).[15,46] Focusing on the isoform δ, its negative roles on Wnt signaling include phosphorylation of β-catenin at Ser45 together with CK-1ε and α isoforms, with the latter considered the main effector; as consequence, β-catenin is primed for GSK-3β-mediated phosphorylation and thus

downregulated.[46,56] Furthermore, a second level of negative regulation of Wnt signaling is the phosphorylation by CK-1δ/ε of LEF-1, which leads to the disruption of the transcriptional activity of the LEF-1/β-catenin complex. CK-1δ/ε isoforms have been shown to phosphorylate other members of the Wnt pathways, including axin and APC.[56] In particular, phosphorylated APC has increased β-catenin interactions and competes with axin for binding to β-catenin.[56] This phosphorylation is believed to occur by the concerted action of CK-1 and GSK-3;[74] Ferrarese *et al.* showed that the process is initiated by CK-1, able to phosphorylate S1510 and S1505, and phosphorylation of S1505 primes subsequent phosphorylation of S1501 by GSK-3. Then, pS1501 triggers the hierarchical phosphorylation of S1504 and S1507 by CK-1. Finally, pS1507 primes the phosphorylation of both S1510 and S1503 by CK-1 and GSK-3, respectively, thus completing all six phosphorylation steps.[74] On contrary, CK-1 (in particular δ and ε isoforms) stabilizes β-catenin interacting with Dvl, a key intermediate linking Frizzled receptors and downstream components in the Wnt pathway. Phosphorylation of Dvl at multiple sites can induce a conformational change in the β-catenin destruction complex, thereby preventing β-catenin from being phosphorylated and degraded.[28,64]

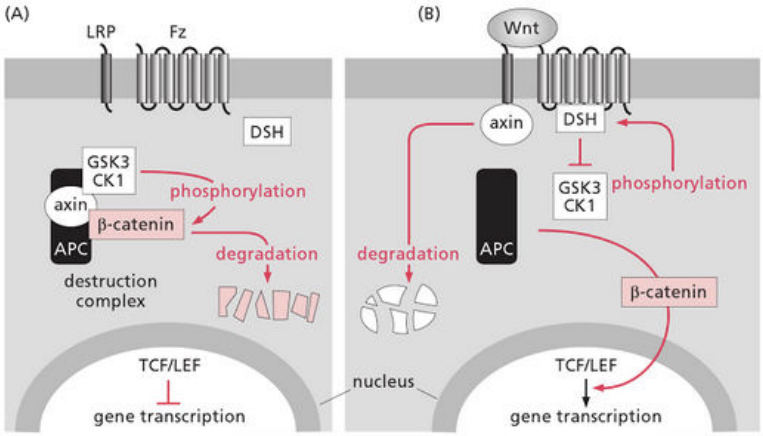

Figure 7: The Wnt signaling pathway. A) In the absence of Wnt stimuli. B) Response to Wnt stimuli.[3]

1.4.3 Hedgehog pathway

Hedgehog signaling is an essential pathway in embryonic development, as well as adult stem cell maintenance. Aberrant activation of the Hedgehog (Hh) pathway has been associated with numerous malignancies including basal cell carcinoma, medulloblastoma, and pancreatic cancer.[75] On the other hand, several reports also suggest that positive regulators of the Hh pathway could be used in the treatment of neurodegenerative diseases. In fact, activation of the Hh pathway seems to be neuroprotective and regenerative in models of Parkinson's Disease (PD), stroke and diabetes neuropathy, and increases the proliferation and neural differentiation of endogenous precursor cells in adult brain.[76] Nevertheless, the role of Hh signaling in the adult brain is still poorly investigated.

In the absence of ligand, the Hh ligand receptor Patched (Ptch), which is located on the plasma membrane, represses the activity of the transmembrane protein Smoothened (Smo), through a mechanism that is still not clearly understood (**Figure 8**). In this way, the multi-protein complex, composed of PKA, GSK-3β and CK-1δ, can interact and phosphorylate the Gli (Glioma-associated oncogene) transcription factors, that are partially degraded along the ubiquitin pathway (UB), yielding their repressor N-terminal truncated forms (GliR).[15] Finally, GliR acts as a repressor of Hh target genes. In the mammalians, there are three

known Gli transcription factors, Gli1, Gli2 and Gli3, while the homologue in *Drosophila* is the transcription factor *Cubitus interruptus* (Ci).[77]

Signaling in this pathway is triggered when the Hh ligands [Sonic hedgehog (Shh), Indian hedgehog (Ihh), or Desert hedgehog (Dhh)] binds to Patched. Binding of Hh inhibits Patched resulting in Smo activation. Active Smo triggers the release of Gli transcription factors from the protein complex and their consequent translocation to the nucleus, where they induce Hh genes transcription (**Figure 8**).[77]

So, as it happens in Wnt, both GSK-3β and CK-1δ play a negative role in Hh signaling. In 2002, Price and Kalderon demonstrated in fact that CK-1δ and GSK-3β mediated the phosphorylation of full length Ci, thereby preventing Hh target gene transcription.[56,78]

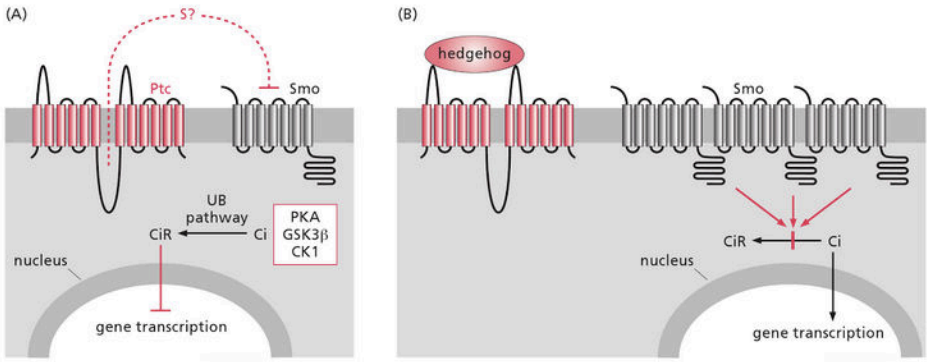

Figure 8: The Hh signaling pathway. A) In the absence of Hh stimuli. B) Response to Hh stimuli. Ci/CiR are the homologues Gli/GliR in mammalians.[3]

1.4.4 Hippo pathway

Hippo pathway is a conserved pathway that controls organ development by regulating cell proliferation, apoptosis and stem cell self-renewal and its deregulation contributes to tumorigenesis.[79]

In human, the pathway includes a serine-threonine kinases cascade [STE20-like protein kinases 1/2 (SLK1/2), large tumor suppressor kinase 1/2 (LATS1/2)] and downstream transcriptional effectors that regulate cell proliferation and cell death in response to contact inhibition. In response to high cell densities, activated LATS1/2 phosphorylates the transcriptional coactivators YAP and TAZ, promoting their cytoplasmic localization, leading to cell apoptosis and restricting organ size overgrowth. When the Hippo pathway is inactivated at low cell density, both YAP and TAZ translocate into the nucleus to bind to the transcription enhancer factor (TEAD/TEF) family of transcriptional factors to promote cell growth and proliferation.[28] In 2010, Zhao *et al.* reported CK-1δ/ε as a regulator of Hippo pathway. In fact, phosphorylation on YAP (Ser381) by LATS acts as priming signal for subsequent phosphorylation of YAP by CK-1δ/ε, which in turn recruit cellular ubiquitin ligase β-TrCP and lead YAP to ubiquitination and degradation.[79] Other studies have demonstrated also the involvement of GSK-3β in this pathway. In fact, the phosphorylation of TAZ (Ser-58/62) by GSK-3β creates a binding site for β-TrCP, thus resulting in TAZ ubiquitination and degradation. The YAP/TAZ complex also interacts with other transcriptional factors or signaling molecules, by which Hippo pathway-mediated processes are interconnected (e.g. Wnt growth factors).[80] For example, TAZ can be considered a downstream component of Wnt/β-catenin signaling cascade. In the absence of Wnt activity, the β-catenin destruction

complex (APC, Axin, and GSK-3) also keeps TAZ at low levels. Phosphorylated β-catenin in fact bridges TAZ to its ubiquitin ligase β-TrCP.[81]

1.4.5 p53 pathway and DNA-damage

DNA damage response pathways, mediated through the tumor suppressor p53, play an important role in the cell intrinsic responses to genome instability such as apoptosis. Modifications of p53 function are among the most frequent alterations in human cancers.[36]

Both CK-1δ and GSK-3β are involved in the regulation of p53 in response to DNA damage. GSK-3β presents both pro- and anti-apoptotic roles, depending on cell type, transformation status, and the signaling pathways activated. While GSK-3 mostly promotes cell death stimulating the mitochondrial intrinsic apoptotic pathway, it also inhibits the death receptor-mediated extrinsic apoptotic signaling pathway. It is widely known that GSK-3β forms a complex directly with nuclear p53 to promote p53-induced apoptosis and also phosphorylates it at Ser33.[36,82] However, during endoplasmic reticulum (ER) stress, GSK-3β phosphorylates p53 on different residues (Ser315 ad Ser376), inducing its cytoplasmic localization and preventing its stabilization.[83] Moreover, GSK-3 also phosphorylates the p53-specific E3 ubiquitin ligase MDM2.[36] As MDM2 becomes more stable with this post-translational modification, degradation of p53 is consequently enhanced. Both p53 and MDM2 are also substrates of CK-1 isoforms. Three CK-1 isoforms (α, δ and ε) are able to phosphorylate the p53 *in vitro* and *in vivo* resulting in its activation and apoptosis induction. Moreover, CK-1δ can phosphorylate MDM2, thus stabilizing and activating p53.[15,84]

In addition to GSK-3β and CK-1δ regulating p53, GSK-3β and CK-1δ themselves are regulated by p53. In fact, the binding to p53 mutually activates GSK-3 through an unknown mechanism that does not involve phosphorylation, indicating the co-dependence of both the factors to induce intrinsic apoptosis.[82] Similarly, CK-1δ expression is influenced by the level of p53 and by DNA damage, suggesting a functional interaction between the two molecules.[84]

1.4.6 Inflammation and Neuroinflammation

Inflammation is considered a non-specific and innate response of the organism able to counteract harmful stimuli and maintaining tissue homeostasis but, when uncontrolled, can lead to exacerbation of pathological conditions, such as neurodegenerative diseases, diabetes and cancer. The inflammatory response involves a fine balance between innate system, considered the first line of defense and responsible of the recruitment of immune cells to sites of infection and inflammation through the production of cytokines, and the adaptive immunity (lymphocytes T and B).[85] Inflammatory activation of astrocytes and microglia (neuroinflammation) is considered a pathological hallmark and important mechanism in neurodegenerative diseases, such as Alzheimer's disease (AD), amyotrophic lateral sclerosis (ALS), and Parkinson's disease (PD)[86]. However, the signaling mechanisms underlying these neuroinflammatory events are not fully understood and there is evidence that these inflammatory responses can serve both neuroprotective and neurotoxic roles.[87]

GSK-3 is implicated in the modulation of NF-κB signal pathway, the primary pathway involved in the activation of pro-inflammatory genes and modulation of the survival, proliferation, differentiation of B and T lymphocytes and cytokine production (**Figure 9**).[88,89] The NF-κB proteins are a family of inducible cytoplasmic transcription factors, activated by Toll-like receptors (TLRs) and are regulated by inhibitory protein IκB. NF-κB is a heterodimer composed by two proteins, RelA/p65 and p50. In its inactive state, NF-κB is

bound to IκB protein and its nuclear localization signal blocked.[90] Several stimuli, such as TNF-α, IL-1, bacterial lipopolysaccharide (LPS), viral proteins, ultra violet radiations (UV) and free radicals, induce the degradation of IκB protein, through phosphorylation on two Ser residues in the N- terminal domain by the kinase complex of IkB (IKK). The consequent degradation of IκB releases the heterodimers NF-κB RelA/p65 and p50 and exposes the nuclear localization signal present in RelA/p65, promoting the translocation to the nucleus of NF-κB, where, interacting with other transcriptional factors, induces the expression of the target genes.[90] It is widely reported that GSK-3 has a fundamental role in NF-κB gene-specific transcription. GSK-3β in fact directly phosphorylates RelA/p65, facilitating the access of NF-κB to specific pro-inflammatory genes.[91,92]

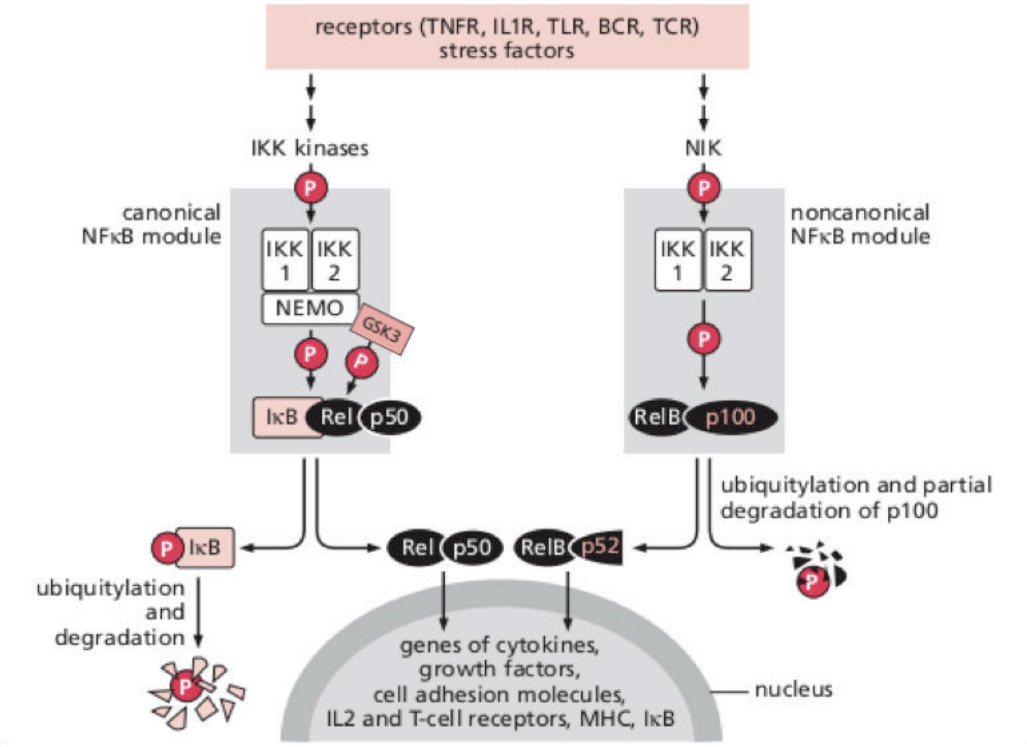

Figure 9: GSK-3β in the NF-κB canonical pathway.[3]

In addition, the optimal RelA/p65 transcriptional activity is mediated by the association with the nuclear co-activator CBP (CREB Binding Protein). For the interaction with CBP, phosphorylated RelA/p65 competes with CREB and when CREB is bound to CBP, NF-κB activity is inhibited. The activation of GSK-3β leads to the translocation of NF-kB in the nucleus (where it complexes with CBP for the transcription of pro-inflammatory cytokines) and the simultaneous phosphorylation-dependent down-regulation of CREB that is responsible of the production of anti-inflammatory cytokines (e.g. IL-10).[93] Thus, inhibitors of GSK-3β act on both sides of the inflammatory response, reducing inflammatory cytokines (NF-κB inhibited) and increasing anti-inflammatory cytokines (CREB activated). Inhibition of pro-inflammatory actions of GSK-3β have been reported to produce beneficial effects in animal models of multiple inflammatory diseases including endotoxic shock, arthritis, peritonitis and colitis, while increasing evidences suggest that GSK-3β inhibitors also may counteract inflammation in CNS diseases.[89]

In response to foreign or endogenous signals, both astrocytes and microglia adopt an activated phenotype resulting in the release of pro-inflammatory mediators (cytokines as

TNF-α, interleukins as IL-1β and IL-6, chemokines MCP-1 and MIP-1).[94] Although the molecular events that mediate the release of cytokines from activated microglia are not fully understood, glial inflammatory activation seems to be regulated by several different pathways including mitogen-activated protein kinases (MAPK) and NF-κB.[86] Green *et al.* supported GSK-3β involvement showing that, in cultures of rat glial cells stimulated with LPS, the inhibition of GSK-3 promotes an anti-inflammatory effect due to the reduction of pro-inflammatory cytokines IL-1β and TNF-α and increased levels of anti-inflammatory cytokine IL-10.[95] Furthermore, lithium, considered the first inhibitor of GSK-3β,[96] seems able to reduce the production of pro-inflammatory modulators such as IL-2, IL-6 and TNF-α in human monocytes.[93]

The potential role for CK-1 isoforms in inflammatory diseases such as arthritis or asthma remains largely unknown. The most involved isoform in regulating lymphocyte activation and granulocyte physiology seems to be the α one. Different studies reported that CK-1 (mostly CK-1α) inhibits the activity of nuclear factor of activated T cells (NFAT)[15], a known regulator of lymphocyte activation also phosphorylated by GSK-3β (**Figure 10**). But CK-1 negatively regulates also tumor necrosis factor signaling by phosphorylating the p75 TNF receptor, and these observations tend to suggest that activation of CK-1 may result in anti-inflammatory effects.[15,97] Moreover, CK-1α was found to be a bi-functional regulator of NF-κB signaling: in fact, it terminates the receptor-induced NF-κB activation, through CARMA1, while its association to the CBM (CARMA/BCL10/MALT1) complex has been shown to lead to NF-κB activation.[15] Recently, also CK-1γ1 has been demonstrated to be a negative regulator by directly phosphorylating the NF-κB subunit RelA/p65. Concerning CK-1δ, it blocks the transcription induced by HIF-1 (Hypoxia-inducible factor), which promotes the survival of granulocytes, but also of cancer cells. CK-1δ is able to phosphorylate the Ser-247 residue present in the regulatory domain of HIF-1α, thus leading to a loss of its transcriptional properties.[15]

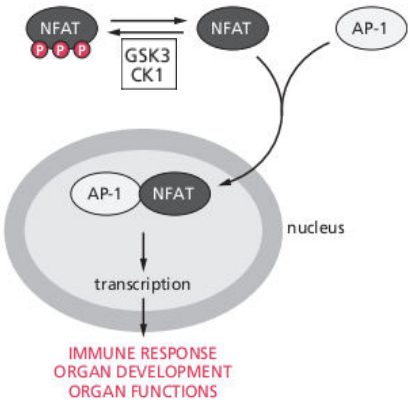

Figure 10: GSK-3β and CK-1 in the NFAT pathway. Dephosphorylated NFAT translocates in the nucleus to stimulate numerous genes transcription, in cooperation with other transcription factors as AP-1 (activator protein 1). NFAT is inactivated by phosphorylation catalyzed by different kinases, including GSK-3β and CK-1. [3]

1.4.7 Mood disorders

Links between GSK-3β and mood disorders have been shown in both animal models and humans, even though the mechanisms underlying this connection remain unclear.[98] The first evidence in support of this claim is that lithium, used for decades as a mood stabilizer in the treatment of bipolar disorder (BD), was identified in 1996 as a reversible inhibitor of GSK-3 with an *in vitro* IC_{50} of around 1-2 mM.[99] Moreover, the administration of selective GSK-3β inhibitors to mice has been reported to causes antidepressant-like behavioral effects, while

GSK-3β knockin mice, where GSK-3β cannot be regulated by inhibitory phosphorylation on Ser9, are more inclined to have depressive-like behaviors compared to wild-type mice.[100] The administration of currently used anti-depressant (fluoxetine or imipramine), anti-convulsant (valproate) or anti-psychotic (risperidone, olanzapine, clozapine) drugs showed increased levels of pSer9-GSK-3β.[101]

Typically, mood disorders such as BD, schizophrenia and major depressive disorder (MDD) correlate with disturbances of the circadian rhythms.[102] Circadian rhythms are cyclic changes in physiology and biochemistry with a ~24 hour period that, depending on an autonomous oscillator system, controls the transcription/translation of different genes. These genes encode and are activated by the circadian transcription factor CLOCK/BMAL1.[103] CLOCK/BMAL1 actions can be repressed by PER and CRY, protein substrates of both CK-1δ and GSK-3β. PER and CRY phosphorylation leads to changes in their stability, association and nuclear translocation where they can repress CLOCK/BMAL1, thus creating a negative feedback loop.[104]

1.4.8 Neurodegenerative Diseases

Protein kinases have been mostly exploited so far in therapeutic areas that concern oncology and inflammation. However, different PKs, including GSK-3β and CK-1δ, are widely accepted as key components of molecular mechanisms underlying neurodegeneration and neuroprotection.

1.4.8.1 Alzheimer's Disease (AD)

Alzheimer's disease (AD) is the most common form of dementia and the most prevalent of the tauopathies. It is defined by the appearance of two typical pathological hallmarks within specific areas of the brain, in particular multiple deposits of senile plaques, composed of extracellular amyloid beta (Aβ) peptide, and neurofibrillary tangles (NFTs), composed of intracellular aggregates of the microtubule-associated protein (MAP) *tau*.[105] In AD, mutated *tau* dissociates from microtubules, destabilizing them and interfering with their cellular mechanisms and transport, and forms paired helical filaments (PHF), which tend to clump together in rigid and insoluble neurofibrillary tangles (NFTs). Abnormal phosphorylation of *tau* is considered one of the earliest signs of neuronal degeneration and appears to precede *tau* aggregation or amyloid formation. As reported by Hanger *et al.*, both GSK-3β and CK-1δ can phosphorylate *tau*, covering the three-quarters of the Ser/Thr phosphorylation sites identified in *tau* and sharing at last 16 phosphorylation sites (**Table 1**).[106] Moreover, CK-1δ can act as priming kinase for GSK-3β on *tau*.[107] Interestingly, the overexpression of *tau* in turn increases GSK-3β activity, thus perpetuating the phosphorylation of *tau*.

Aβ protein derives from the amyloid precursor protein APP, a trans-membrane protein whose fate can follow two different routes: the first is the non-amyloidogenic pathway in which APP undergoes the action of the α- and γ-secretase. The α-secretase is part of the ADAM family (a disintegrin and metalloprotease domain), whose activity seems to be negatively regulated by GSK-3β.[108] In addition, GSK-3β interferes with the γ-secretase complex, in particular phosphorylating presenilin 1 (PS1). In the amyloidogenic pathway, APP is degraded by β-site APP cleaving enzyme 1 (BACE1), an aspartyl-protease highly expressed in Alzheimer's patients, and this leads to the release of Aβ protein, which aggregates into insoluble plaques and oligomers.[108] GSK-3β contributes to the proteolytic

cleavage of APP by BACE1 through a NF-κB-mediated mechanism. The NF-κB transcription factor, regulated by GSK-3β (as described in Chapter 1.4.5) is, in fact, related to the expression of BACE1.[108] GSK-3β is thus considered one of the most important links between the two pathological hallmarks of AD. GSK-3β not only hyperphosphorylates *tau*, but it is also positively regulated by Aβ, which increases GSK-3 catalytic activity, thus promoting *tau* phosphorylation.[108]

Table 1: Phosphorylation sites identified in Alzheimer *tau* and targeted by GSK-3β and/or CK-1δ. [a]Where phosphorylation occurs at one of two or one of four closely-spaced residues on *tau* is reported.[109]

Site in *tau*	Alzheimer *tau*	GSK-3β	CK-1δ	Site in *tau*	Alzheimer *tau*	GSK-3β	CK-1δ
S68	*			S237	*	*	*
T69	*	*		S238	*		
T71	*			S258	*	*	*
S113	*			S262	*	*	*
T175	*	*		S289	*	*	*
T181	*	*		S356	*	*	*
S184	*	*	*	Y394	*		
S185	*			S396	*	*	*
S191	*			S400	*	*	
Y197	*			S403	*		
S198	*	*	*	S404	*	*	*
S199	*	*		S409	*	*	
S202	*	*		S412	*	1/4[a]	*
S208	*			S413	*	1/4[a]	1/2[a]
S210	*	*	1/2[a]	T414	1/2[a]	1/4[a]	1/2[a]
T212	*	*	1/2[a]	S416	1/2[a]	1/4[a]	*
S214	*	*	*	S422	*		
T217	*	*		T427	*		
T231	*	*		S433	*		*
S253	*	*		S435	*		*

Concerning APP, only the isoform ε of CK-1 contributes to the accumulation of Aβ, and in turn this promotes an increase in kinase activity.[15]

In addition to hyperphosphorylation of *tau* and the increased production of Aβ, GSK-3β is highly involved in AD memory impairment, inflammatory responses, cholinergic deficit and neuronal loss through activation of the intrinsic apoptotic signaling pathway.[110] In particular, the dysfunction of synaptic plasticity is one of the earliest signs of AD, and the long-term potentiation (LTP) process directly correlates with memory and learning. GSK-3β plays a key role in maintaining balanced the equilibrium between LTP and LTD (long-term depression). Suppression of Wnt or PI3K signaling, with a consequent increase of GSK-3β activity, impairs LTP. Thus the inhibition of GSK-3β promotes the induction of LTP and the inactivation of the LTD, strengthening the synaptic efficiency and therefore improving learning and memory. [110]

1.4.8.2 Parkinson's Disease (PD)

PD is the second most common neurodegenerative disorder after AD. It is characterized by motor symptoms, such as tremor, rigidity, postural instability and bradykinesia. The main pathological hallmarks of PD are the loss of dopaminergic neurons and the presence of eosinophilic inclusions rich in α-synuclein, called Lewy bodies (LB), in the *substantia nigra pars compacta* in the midbrain.[111] These abnormalities are the result of a complex pathological process that includes oxidative stress, mitochondrial dysfunction, protein

aggregation and neuroinflammation.

In recent years, many authors reported that inhibition of GSK-3β can protect against MPTP (1-methyl-4-phenyl-1,2,3,6-tetrahydropyridine), 6-OHDA (6-hydroxydopamine) and LPS-induced neurotoxicity.[112–114] GSK-3β is in fact implicated in microglial-mediated inflammation and GSK-3β inhibitors may have neuroprotective effects.[112] L'Episcopo *et al.* highlighted a cross talk between inflammatory and Wnt/β-catenin signaling pathways in a MPTP-induced model of PD. In particular during the early degeneration phase of MPTP toxicity, hyper-activated microglia led to activation of signaling pathways critically involved in the physiological control of cells homeostasis, at least in part through Wnt signaling downregulation. As already discussed, this led to GSK-3β activation and consequent β-catenin degradation, contributing to neurogenic impairment in PD.[115]

GSK-3β is responsible of phosphorylation of both *tau* and α-synuclein proteins. As α-synuclein, also *tau* has already been observed to be incorporated into the LBs. α-Synuclein interacts directly with *tau*, promoting its phosphorylation by PKA and mutual aggregation into fibrils, and GSK-3β seems the link between the two proteins. α-Synuclein in turn modulates the activation of GSK-3β, enhancing Tyr216 phosphorylation.[116] Also CK-1δ is localized within LBs and is responsible of α-synuclein phosphorylation in the C-terminal domain (Ser129). It was also demonstrated that the enzyme is able to phosphorylate, in collaboration with the kinase CDK5, the parkin protein, an E3 ubiquitin ligase, which mutations have been associated to the early onset of autosomal recessive Parkinsonism.[58]

1.4.8.3 Amyotrophic Lateral Sclerosis (ALS)

ALS is a lethal progressive neurodegenerative disorder that specifically affects the upper and lower motor neurons in the adult, leading to atrophy of skeletal muscles, spasticity and paresis. Familial ALS is characterized by mutations in the gene for the free radical-scavenging metalloenzyme Cu,Zn-superoxide dismutase (SOD1) and in the Tar DNA binding protein 43 (TDP-43).[117,118] High levels of GSK-3β expression were detected in the spinal cord and in the frontal and temporal cortex of ALS patients. Treatment of ALS models *in vitro* and *in vivo* with GSK-3β inhibitors appears to slow down the death of motor neurons and the advancement of the degeneration, probably through increase of cell survival signals that normally are blocked by GSK-3β (eg. HSTF-1, heat shock transcription factor-1) or suppression of pro-apoptotic and inflammatory signals (eg. release of cytochrome c from mitochondria).[119]

Regarding CK-1, the δ isoform is responsible for the phosphorylation of the TDP-43 protein, the main component of inclusion bodies in amyotrophic lateral sclerosis (ALS) and frontotemporal lobar degeneration (FTLD). CK-1δ was the first kinase reported to phosphorylate TDP-43 directly and has been determined to phosphorylate many different sites on TDP-43 *in vitro*.[117] Also GSK-3β occurs in TDP-43 aggregates and its inhibition reduces their cytosolic accumulation; moreover GSK-3β seems to have a role in TDP-43 nuclear translocation.[120]

1.5 PROTEIN KINASE INHIBITORS

Targeting protein kinases with small inhibitors is one of the most challenging fields in pharmacology and drug discovery. Different classifications of kinase inhibitors could be formulated: at first, they can be divided into covalent (or irreversible) inhibitors and non-

covalent (or reversible) inhibitors, and the latter have received most of the attention over the years; otherwise, it can be taken into consideration the binding site of the inhibitor on the PK target. In the light of these considerations, different types of inhibitors could be thus distinguished:

Type I: This group of kinase inhibitors are the classical ATP-competitive inhibitors that target the *DFG-in* conformation of the enzyme. Most of them possess a heterocyclic scaffold that orients itself in the adenine-binding region of the ATP pocket, thus establishing one to three hydrogen bonds with amino acids of the hinge region, and functional groups added to the heterocyclic core to occupy regions not exploited by ATP in order to improve selectivity and potency.[121]

The ATP-binding site, occupied by type I inhibitors, is highly conserved throughout the kinome and we can distinguish different regions as illustrated in **Figure 11**:

1. Adenine region: it is a generally hydrophobic pocket; the N1 and N6 nitrogen atoms of adenine are able to establish hydrogen bonds with amino acids in the hinge region. Most of the inhibitors are able to establish one to three of these bonds.[122]
2. Sugar pocket: a hydrophilic pocket, barely exploited by type I inhibitors.[122]
3. Hydrophobic region I: this space in the backside of the pocket is often unused by ATP, and so it deserves particular interest for the synthesis of selective PKs inhibitors. Its size depends on the gatekeeper residue; in fact, when it presents a sterically hindered side chain, the HR-I will be small, while when a small size residue represents it, HR-I will be wider.[122]
4. Hydrophobic region II: as it happens with HR-I, ATP neither exploits HR-II. It is exposed to the solvent and can be useful for increasing the binding affinity of the inhibitors towards the kinase.[122]
5. Phosphate binding site: it is very exposed to the solvent and could be exploited to increase the selectivity of the inhibitors, due to the presence of not conserved amino acids. On the other hand, it is less important regarding the binding affinity.[122]

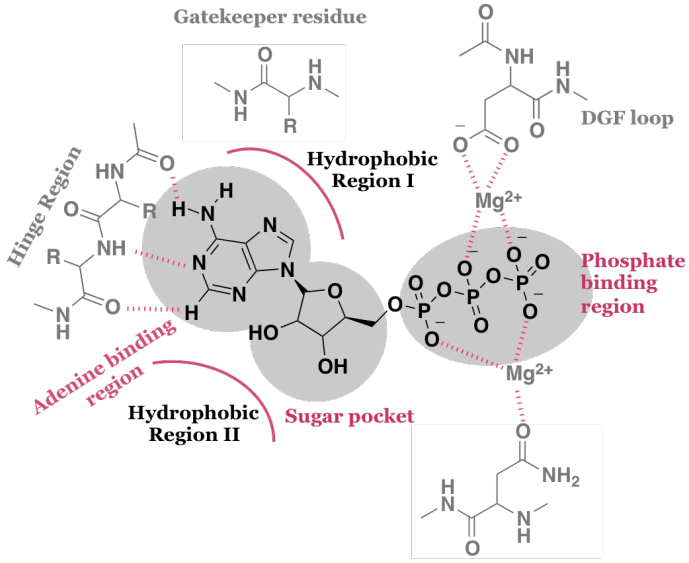

Figure 11: Sub-regions of the APT-binding site.

Precisely because the ATP-binding site is highly conserved among kinases, the obtaining of selectivity is challenging aim. In addition, when designing ATP-competitive inhibitors, potency needs to be high for the inhibitors to compete with ATP in the cell ([ATP] = 1-5 mM).[123]

Type II: type II inhibitors are compounds, which target the *DFG-out* conformation (inactive conformation) of the kinase. They partially occupy the ATP binding site and extend past the gatekeeper into an adjacent allosteric site, created after the rearrangement of the activation loop that results in a movement of a phenyl ring, from the phenylalanine in the DFG loop, out of a hydrophobic pocket and into the ATP binding site. Type II inhibitors have shown advantageous pharmacological properties, including improved target specificity compared to type I inhibitors. The most famous example of type II inhibitor is imatinib (c-ABL inhibitor).[121]

Type III: these inhibitors bind to an allosteric hydrophobic region in the catalytic domain of the kinase near the ATP-binding pocket but do not interact with the hinge region.[124] These inhibitors are characterized by high selectivity, as they exploit binding sites and regulatory mechanisms that are unique to a particular kinase.

Type IV: these are truly allosteric inhibitors that target kinases outside the catalytic domain, for instance by interfering with the binding of an interacting protein. Even in this case the interaction interests peculiar sequences of the target enzyme, thus enhancing the selectivity of the inhibitor.[125]

Type V: to this group belong bisubstrate or bivalent inhibitors, which consist of two conjugated fragments, each targeted to a different binding site of the enzyme. These compounds have the potential to combine the high affinity and potency of traditional active site binding inhibitors with the selectivity of inhibitors that target the protein kinase surface outside the ATP-binding pocket.[126]

Type VI: this group of kinase inhibitors is represented by covalent inhibitors that mostly bind to the ATP-binding site.[127] The covalent bond irreversibly prevent the interaction of ATP with the kinase and is characterized by a long half-life, thus maximizing the effectiveness of the inhibitor while reducing the exposure to the drug.[128] Despite the great interest in developing this kind of inhibitors, there is a great concern about the potential toxicity and off-target activity (reactivity towards proteins, DNA and glutathione). But covalent kinase inhibitors with well-balanced molecular recognition and reactivity should provide efficacy, selectivity and the safety margins required for regulatory approval.[129] Nowadays, the common approach is the design of targeted covalent inhibitors (TCIs), small molecules addressed to bind covalently a specific molecular target. The TCIs recently described in literature show common features, in particular a heterocyclic core structure (driving portion), generally resembling that of reversible ATP-competitive inhibitors, carrying at a proper position an electrophilic "warhead", such as Michael acceptors, epoxides or acetylenes, that covalently interact with a specific cysteine or lysine residue in the target protein (**Figure 12**).[130]

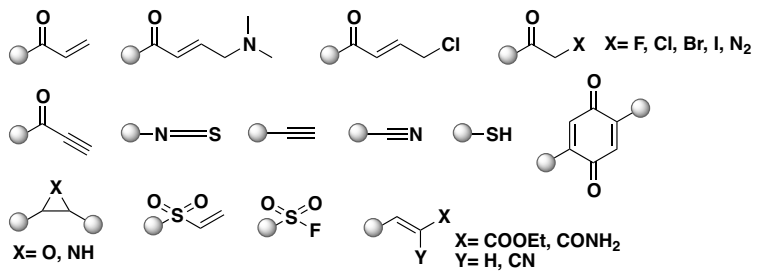

Figure 12. Examples of TCIs warheads.[130]

This approach led in recent years to the approval of several covalent kinase inhibitors, especially in the oncology field. Examples are afatinib, an EGFR inhibitor approved by the FDA in 2013 for the treatment of metastatic non-small cell lung cancer (NSCLC),[131] and ibrutinib, a covalent inhibitor of BTK (Bruton's tyrosine kinase) approved for the treatment of mantle cell lymphoma (MCL) and chronic lymphocytic leukaemia (CLL).[132][131]

The general mechanism of action of TCIs (**Equation 1**) presupposes a non-covalent interaction between the molecule and the enzyme, driven by the affinity for the protein, which arranges its electrophile moiety near the specific nucleophile to be targeted (k_i). The warhead of the inhibitor then undergoes nucleophilic attack creating a covalent bond between the protein and the molecule (k_1). In the case of an irreversible inhibitor, the covalent bond cannot normally be cleaved ($k_2 = 0$). The non-covalent binding (k_i) needs to be long enough to allow nucleophilic attack (k_1) to take place, and in turn the nucleophilic attack (k_1) needs to be fast enough to occur while the drug is bound non-covalently to the kinase (k_i).[129]

Equation 1

$$E + I \underset{k_i}{\rightleftharpoons} E \cdot I \overset{k_1}{\underset{k_2}{\dashrightarrow}} E\text{-}I$$

To date, only lysine and cysteine have been reported to react with kinase inhibitors thus creating a covalent bond, and there is no report about nucleophilic attack from a serine or threonine residues on a kinase inhibitor yet.[128] Cysteines, with their thiol group (pKa = 8.5), are the most commonly targeted residues and have been classified into five groups according to their positions in the kinase (**Figure 13**).[128] In detail, group 1 cysteines are located in the P-loop (dark blue) as in FGFR (fibroblast growth factor receptor) tyrosine kinase, while the bordering group 2 cysteines are situated in the "roof" of the ATP binding pocket (pink, e.g. ribosomal S6 kinase Cys463); cysteines located in hinge region belong to group 3, (yellow, e.g. EGFR Cys797), while in group 4 there are DFG-motif neighboring cysteines (light blue).[7] Group 5 (in red) represents the cluster of cysteines that lies on the activation loop, as Cys312 in CDK7.[133]

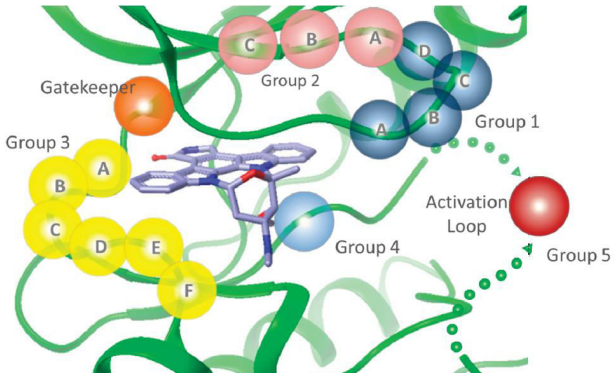

Figure 13 - Schematic representation of targetable cysteines in or near the ATP binding pocket of kinases in the active conformation (based on the crystal structure of interleukin 2 tyrosine kinase, PDB code 1SM2).[128]

Even though the kinome is composed of more than 500 kinases, irreversible inhibitors have targeted only 20 of them, and one of these is GSK-3β. In fact, it presents a not conserved cysteine (Cys199) classified in the Group 4, adjacent to the DFG-motif and near the bottom of the ATP binding pocket.[128] At the moment, no CK-1δ covalent inhibitors have been reported.

Substrate competitive: these inhibitors characteristically target the substrate-binding region of protein kinases; the substrate-binding pockets of kinases are, in general, less conserved than the ATP-binding pockets of protein kinases. Thus, it is hypothesized that small peptides or proteins, designed to compete with the substrate for the binding with the kinase, would present an attenuated potency but a very high selectivity.[9]

1.5.1 GSK-3 Inhibitors

The discovery that GSK-3 plays a key role in the regulation of several functions focused the interest of both academic and industrial environments on this kinase and on development of pharmacologic inhibitors to verify its putative role as therapeutic target. Among the conspicuous numbers of small molecules targeting GSK-3 reported in these years, only three of them have reached clinical trials: AZD1080 (**1**), Tideglusib (NP-031112, **2**) and LY2090314 (**3**) (**Figure 14**).[134]

The indolyl derivative AZD1080 (**1**), synthesized by AstraZeneca, is a potent inhibitor of GSK-3α/β [K_i(GSK-3α)=6.9 nM, K_i(GSK-3β)=31 nM], that shows >14-fold selectivity towards CDK2, CDK5, CDK1 and ERK2. It is bioavailable after oral administration and able to pass the blood-brain barrier (BBB).[135] *In vitro*, AZ1080 (**1**) is able to inhibit the phosphorylation of *tau* in human cells expressing the protein and in intact rat brain. Interestingly, sub-chronic but not acute administration with AZD1080 (**1**) reverses the block of LTP caused by MK-801, a non-competitive NMDA receptor antagonist, demonstrating that a prolonged GSK-3 inhibition is required to restore synaptic plasticity.[135] In 2006, **1** has entered clinical Phase I: oral administration of AZD1080 (**1**) in ascending doses to healthy volunteers confirmed the preclinical data. However, clinical trials have been abandoned due to a poor therapeutic window and nephrotoxicity.[134,136]

Tideglusib (NP-031112, **2**) is an orally available, BBB permeable, small-molecule drug of the thiadiazolidinone class, developed by Neuropharma. It is a non ATP-competitive GSK-3β inhibitor with IC_{50} of 60 nM, whose mechanism of action has been investigated only recently.[134] Dominguez *et al.* demonstrated an irreversible behavior, reporting the lack of recovery in enzyme function after the unbound drug has been removed from the reaction medium and a dissociation rate constant not-significantly different from zero. Moreover, Tideglusib (**2**) failed to inhibit other kinase containing a residue homologous to Cys199 in their active site, which means that it acts through a specific inhibition mechanism. Nevertheless a covalent modification of GSK-3β by Tideglusib (**2**) is not confirmed, but the irreversible inhibition and the slow turnover of GSK-3β in neuronal cells can prolong the duration of the pharmacological effect and can be exploited to maximize its therapeutic potential.[137] *In vitro*, Tideglusib (**2**) reduces *tau* phosphorylation and prevents apoptotic death in human neuroblastoma cells and murine primary neurons. Moreover, it exerts a potent neuroprotective effect from glutamate-induced toxicity on rat primary astrocytes, or microglial cultures (decrease of TNF-α and COX-2 expression and apoptotic cells). In adult male rats, Tideglusib (**2**) injected into the hippocampus dramatically reduces kainic acid-induced inflammation, while in APP/*tau* double transgenic mice, lowers the levels of *tau* phosphorylation, decreases amyloid deposition and plaque-associated astrocytic proliferation and prevents memory deficits.[136,138] It reached clinical trials phase II for cognitive disorders, such as AD and progressive supranuclear palsy (PSP), and it is also currently being assayed in adolescents with autism spectrum disorders and in adolescents and adults presenting myotonic dystrophy.[134]

More recently, LY2090314 (**3**) reached clinical trials for cancer treatment. LY2090314 (**3**), developed by Eli Lilly, is a potent inhibitor with IC_{50} values of 1.5 nM and 0.9 nM for GSK-3α and GSK-3β, respectively, which, *in vitro*, is able to stabilize β-catenin. A phase I/II study has been conducted to test LY2090314 (**3**) in combination with different chemotherapies in metastatic pancreatic cancer patients, while a phase II trial on acute leukemia revealed a weak action of **3** as a single agent.[139–141]

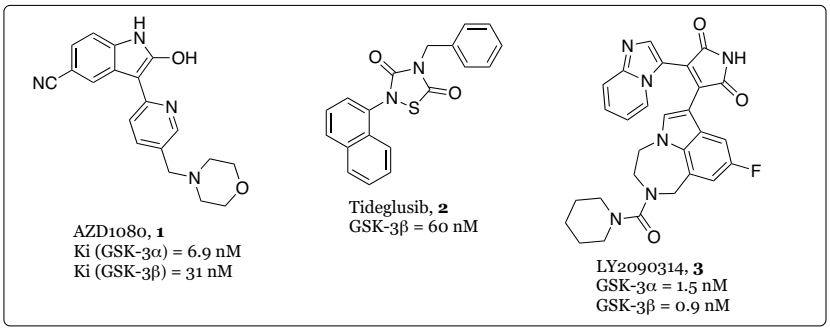

Figure 14 – GSK-3β inhibitors that reached clinical trials (**1-3**).[134]

1.5.1.1 ATP-competitive inhibitors

In recent years, the marine environment has been shown to be source of organic structures with promising biological activities for CNS diseases and in fact also different GSK-3 inhibitors were isolated from marine organisms (**Figure 15**, panel A).

The bis-indole indirubin (**4**), a purple dye used in traditional Chinese medicine, is an inhibitor of cyclin-dependent protein kinases (CDKs) and GSK-3β at nanomolar levels. In the years, several analogues were synthesized, all able to inhibit both GSK-3β and the CDKs in ATP-competitive manner. Among all, the most interesting analogue is 6-bromoindirubin-3'-oxime (6-BIO, **5**), which has demonstrated higher selectivity for GSK-3β than for CDKs (16-fold). A limiting factor for this compound is the poor solubility in water, which is reflected in not reproducible biological results. 6-BIO (**5**) has been tested in different neuronal systems, demonstrating neuroprotective effect against kainic acid- and MPTP-induced neuronal death and amelioration of many AD symptoms, including *tau* hyperphosphorylation and Aβ accumulation.[136,142] In addition, it has shown anti-convulsant activity in Zebrafish and mouse models and promotes differentiation of human embryonic stem cells (hESCs) or human induced pluripotent stem cells (hiPSCs) to hepatocyte-like cells and cardiomyocytes, respectively.[134]

Originally isolated from marine sponges *Axinella verrucosa* e *Acantella aurantiaca*, Hymenialdisine (**6**) has been identified as a potent, non-selective ATP-competitive inhibitor of different kinases, including GSK-3β (IC_{50}=10 nM) and CK-1 (IC_{50}=35 nM).[143] Hymenialdisine (**6**) was first isolated for its anti-inflammatory properties, possibly due to inhibition of GSK-3β in the NF-κB pathway. Moreover, it has demonstrated the ability to inhibit *in vivo tau* phosphorylation at sites which are hyperphosphorylated by GSK-3β in AD.[144] Another natural derivative reported in literature that inhibits GSK-3β (IC_{50}= 15 nM) is Staurosporine (**7**), an alkaloid isolated from the bacterium *Streptomyces Staurosporeus*, well known for its antimicrobial, hypotensive and cytotoxic properties. The lack of specificity has precluded its clinical use, but has made it a valuable research tool. In fact, Staurosporine has been the ancestor of a series of maleimide derivatives developed over the years.[145]

Recently, the citrus flavonoid luteolin (**8**) has been reported as a micromolar GSK-3β inhibitor; it was initially known to be a potent free radical scavenger, anti-inflammatory agent, immunomodulator and, in particular, it seems to have a potential role in colorectal cancer therapies, through interaction with the Wnt pathway, in which GSK-3β is surely involved. GSK-3β inhibition by luteolin (**8**) also resulted in a decrease of soluble Aβ levels and promotes the association between presenilin-1 and APP, both *in vitro* and *in vivo*.[146]

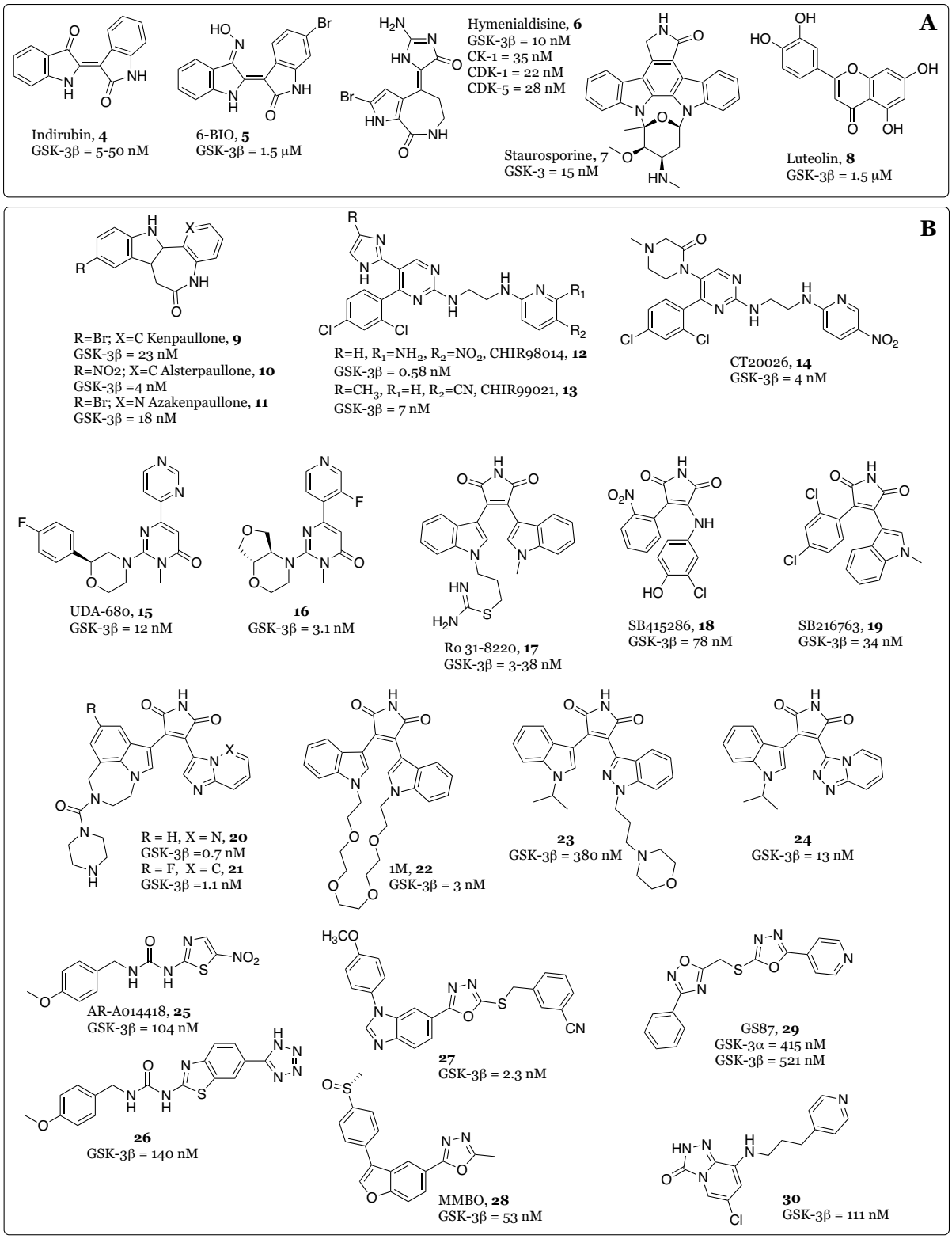

Figure 15 - Panel A) GSK-3 ATP-competitive inhibitors from natural sources (**4-8**). Panel B) Synthetic ATP-competitive GSK-3 inhibitors (**9-30**).

Among the first synthetic GSK-3 inhibitors reported (**Figure 15**, panel B) were the paullones, fused tetracyclic compounds that inhibit GSK-3 within the nanomolar concentration range but also some CDKs. Kenpaullone (**9**), alsterpaullone (**10**) and azakenpaullone (**11**) are widely used in various experimental settings as GSK-3 inhibitors.[147] It is reported that compound **9** reduces the production of Aβ in cells overexpressing APP and

promotes cell differentiation of dopaminergic neurons, useful in the case of PD. Recently, **9** was also reported to promote maturation of hepatocyte-like cells in combination with retinoic acid.[134] Treatment with the derivative **10** instead seems to prevent *tau* phosphorylation and block the LTD in cell cultures, while both present neuroprotective properties against various kinds of stress. Moreover, **10** slowed down the degradation of survival motor neuron (SMN) protein in spinal muscular atrophy (SMA) human fibroblasts, supporting the use of GSK-3 inhibitors in treatment of SMA.[136]

In early 2000s, Chiron developed a series of aminopyrimidines that inhibit GSK-3 within the nanomolar range.[136] The potent inhibitors CHIR98014 (**12**), CHIR99021 (**13**) and CT20026 (**14**) were initially investigated for the treatment of diabetes: the oral treatment for 30 days with CT20026 (**14**) reduced the disease progression in Zucker diabetic fatty (ZDF) rats; later the CHIRs have been tested in neuronal systems: the GSK-3β inhibition led to a reduction of *tau* phosphorylation, arrest of NMDA-mediated LTD and maintenance of pluripotency in mouse cells, through activation of the Wnt pathway.[136] Recently it has been reported that GSK-3 inhibitors may be used to enhance antigen-specific immunotherapy (antigen-SIT) by the induction of tolerance to an antigen (as "tolerogenic adjuvants"). In fact, it was demonstrated that combination of CHIR99021 (**13**) and a peptide (e.g. myelin basic protein to treat multiple sclerosis) can offer a potential for treatment and/or prevention of diseases associated with pro-inflammatory T cells such as allergies, autoimmune diseases and graft rejection. As well as 6-BIO (**5**), also **13** has shown promising results in the generation of cardiovascular cells from human pluripotent cells, through Wnt pathway modulation.[134]

Similarly, Fukunaga and collaborators reported the synthesis of different series of pyrimidinones (**15**, **16**) with a good pharmacokinetic profile and able to inhibit *in vivo tau* phosphorylation in mice after oral administration.[148,149]

As previously introduced, Staurosporine (**7**) inspired the research of a wide number of maleimide derivative as GSK-3β inhibitors. Among all, the bisindolylmaleimide Ro 31-8220 (**17**) resulted to be a potent GSK-3β inhibitor, through ATP-competition but also inhibition of voltage-dependent sodium channels.[96] GlaxoSmithKline also focused in the research of GSK-3 inhibitors, identifying different maleimides such as compounds SB415286 (**18**) and SB216763 (**19**). Both compounds (**18**, **19**) stimulate glycogen synthesis in human hepatocytes and induce the expression of β-catenin-LEF/TCF related genes. Moreover, they have shown neuroprotective effects via inhibition of PI3K-PKB both *in vitro* and *in vivo* in models of AD, schizophrenia and Huntington's disease (HD).[145] Recently, it was proposed the use of GSK-3 inhibitors **18** and **19** to promote immunity in subjects with chronic conditions, such as cancer and infections. GSK-3β in fact is involved in the control of transcription of immunosuppressive receptors, such as programmed death 1 (PD-1), and expression of the transcriptional regulator of Th1, named Tbet, in immune cells. SB216763 (**19**) has been claimed for the treatment of ovarian cancer, through modulation of FOXL2 transcription factor, since it has shown a reduction of tumor growth *in vivo*.[134]

Engler *et al.* reported the discovery of two series of potent and selective maleimides as GSK-3 inhibitors. In particular, compound **20** and **21** inhibit *tau* phosphorylation in a neuronal cell line and lower plasma glucose in the ZDF rat model of type 2 diabetes.[150,151] Finally, maleimide 1M (**22**), presenting polyoxygenated chain, resulted a potent GSK-3β inhibitor (IC_{50}= 3 nM) and robustly enhanced ESC self-renewal.[134,152]

New bisaryl maleimides (**23**, **24**), with high potency and selectivity towards GSK-3β, have been characterized by Ye *et al.*[153,154] In particular, compound **24** significantly reduced *tau* phosphorylation in primary neurons and prevented neuronal death in cerebral ischemic

stroke models. *In vivo*, **24** confirmed its neuroprotective activity reducing infarct size and improving the neurological deficit in cerebral ischemia animal models.[154]

The thiazole AR-A014418 (**25**) is another ATP-competitive inhibitor developed by AstraZeneca. It inhibits GSK-3 with an IC_{50}value of 104 nM and is selective for CDK2, CDK5 and many other kinases. AR-A014418 (**25**) showed to inhibit PI3K and other apoptotic pathways, thus exerting a neuroprotective action. It has shown beneficial effects in models of AD (prevention of Aβ-dependent neurodegeneration) and SLA (decreased motor neurons death and improved cognition). AR- A014418 (**25**) has also shown anti-depressive and anti-maniacal activities in mice. A structurally closed related compound (**26**) showed increased selectivity towards a wide panel of kinases.[136,155]

Takeda pharmaceuticals reported the synthesis and characterization of 1,3,4-oxadiazole derivatives as GSK-3β inhibitors (**27**, **28**). In particular MMBO (**28**) presents good water solubility, oral bioavailability and BBB permeability; it has been assayed in neuronal cell cultures and triple transgenic mice (3xTg-AD, mice overexpressing hyperphosphorylated *tau*, mutant forms of presenilin-1 and APP) and has proven to be effective in reducing *tau* phosphorylation both *in vitro* and *in vivo*.[156,157] GS87 (**29**) is a novel 1,3,4-oxadiazole GSK-3 inhibitor, with IC_{50} values in the nanomolar range for both α and β isoforms, identified in efforts to discover a small molecule optimized against acute myeloid leukemia (AML). GS87 (**29**) demonstrates high efficacy to induce differentiation with selective growth inhibition of leukemic cells in a mouse AML model system, probably due to the activation of GSK-3-dependent signaling components including MAPK signaling.[158]

The crystal structure of staurosporine (**7**) in the ATP binding pocket of GSK-3β has allowed the study of the interactions between the inhibitor and the enzyme and the design of several molecules that mimic this binding mode. Among them, the 8-amino-[1,2,4]triazolo[4,3-*a*]pyridin-3-onic derivative **30**, which showed good potency towards GSK-3β (IC_{50}= 111 nM), good water solubility (>10 mg/mL), good permeability of the BBB and oral pharmacokinetic profile.[159]

In these years many heteroaromatic bicyclic cores resulted suitable scaffolds for the synthesis of ATP-competitive GSK-3β inhibitors (**Figure 16**). The 4,6-disubstituted pyrrolopyrimidine derivative TWS119 (**31**), GSK-3β inhibitor with IC_{50} value of 30 nM, emerged after a phenotypic screen for compounds with the ability to induce neuronal differentiation of pluripotent mouse ESCs.[136] Other examples are furo[2,3-*d*]pyrimidines (**32**),[160] benzimidazoles (**33**),[161] pyrazolo-pyrimidines (**34**)[51] and purines (**35**).[162] A bicyclic moiety is also the core of the indazole derivative **36**, which showed efficacy *in vivo* in the low dose amphetamine test, a model used to mimic mania, a key symptom of mood disorders.[163] Also the carbohydrazide derivative **37** demonstrated *in vivo* antidepressant activity evaluated in the tail suspension test (TST) and forced swim test (FST), two behavioral models.[164] Notably, the 1*H*-pyrrolo[2,3-*b*]pyridine derivative **38**, developed with a fragment-based *de novo* design procedure, showed an IC_{50} values in the picomolar range and high selectivity.[165]

A different chemotype is represented by spiroquinolone **39** (IC_{50}= 12 nM) that showed a reducing effect on plasma glucose concentration in a dose dependent manner in mice.[166]

Recently, novel isonicotinamide GSK-3 inhibitors have been patented. Compound **40** is active towards both α and β isoform but resulted very selective towards a wide panel of kinases. In fact, it binds to the sugar pocket of the ATP binding site that is not highly conserved among different kinases. Moreover, it has shown good *in vivo* activity lowering p-*tau* levels in a triple transgenic AD mouse model after oral administration.[167] The pyridin-2-yl cyclopropanecarboxamide moiety is also present in compound **41**, a GSK-3β inhibitor with IC_{50} in the picomolar range, which showed significant p-*tau* reduction when dosed orally in a

triple transgenic AD mouse model.[168]

Finally, the pyrazolo-tetrahydroquinolinone scaffold, as present in compound BRD1652 (**42**), led to highly selective and potent GSK-3α/β inhibitors. **42** led to attenuation of *tau* and collapsin response mediator protein-2 (CRMP-2) phosphorylation and stabilization and nuclear translocation of β-catenin. Moreover, it demonstrated *in vivo* efficacy against amphetamine-induced hyperactivity (AIH), a model of dopaminergic-induced motor activation.[169]

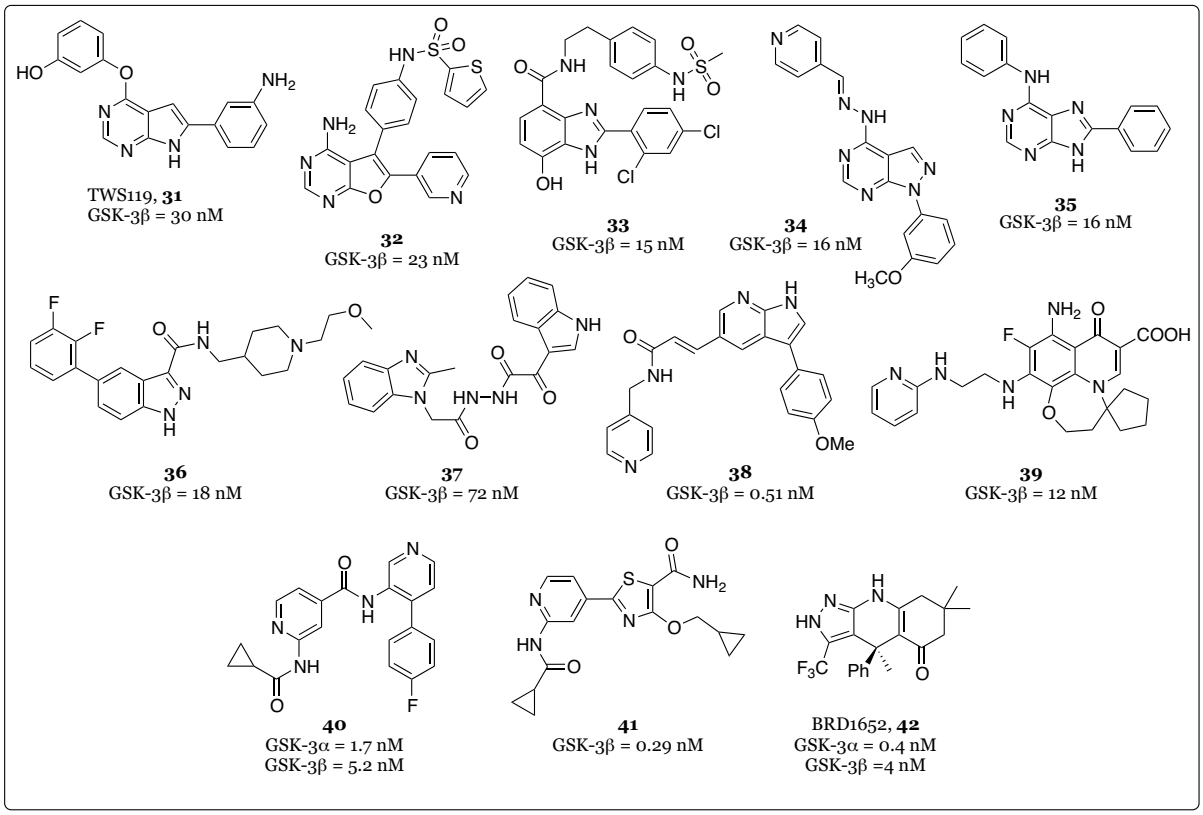

Figure 16 – Other ATP-competitive GSK-3 inhibitors (**31-42**).

1.5.1.2 Non-ATP-competitive inhibitors

Most of the GSK-3β inhibitors discovered so far, including those described above, bind to the enzyme in the ATP region, with a reversible and competitive mechanism of action. The ATP-binding site is highly conserved among different protein kinases, so these inhibitors often present lack of selectivity. In addition, the affinity for this pocket is usually very high, thus ATP-competitive inhibitors are generally able to inhibit the enzyme in a very potent form with lower concentrations. Since GSK-3β is a very ubiquitous enzyme whose activity is absolutely necessary for many different processes, a strong inhibition could cause undesired side effects. In recent years, research focused on the development of non-ATP competitive kinase inhibitors, which bind to the protein in more subtle way (**Figure 17**).[134,170]

In early 2000s, Martinez *et al.* reported the first class of non-ATP competitive GSK-3β inhibitors, the thiadiazolidindiones (**43**). TDZD-8 (**44**), considered one of the most interesting pharmacological tools together with the closely related Tideglusib (**2**), are reversible covalent inhibitors of GSK-3β that target Cys199 located at the entrance of the active site.[171] Once the disulfide bond between the enzyme and the TDZD derivative is formed, the thiadiazolidinone core decompose into carbon monoxide and the corresponding

N,N'-disubstituted urea, that could present a residual activity towards the kinase. In fact, the *N*-naphtyl-*N'*-benzylurea (**45**), that derives from Tideglusib (**2**), resulted to inhibit GSK-3β with an IC_{50} value of 17.1 μM, thus contributing to the long lasting activity of this compound.[134,172] TDZD-8 (**44**) has demonstrated neuroprotective activity *in vitro*, as it can reduce the phosphorylation of *tau* protein, and antidepressant activity in different animal models. In myeloma cells, TDZD-8 reduces cell growth and induces apoptosis, modulating the PI3K/PKB/GSK-3β pathway, while in colon cancer cells the inhibition of GSK-3β activates p53-dependent apoptotic processes slowing the progression of the tumor. Moreover, the administration of TDZD-8 (**44**) *in vivo* counteracts the systemic inflammation caused by the co-administration of LPS and peptidoglycan.[136]

The second family of non-ATP-competitive inhibitors is the halomethylketones family (**46**), including DIP3.18/HMK-32 (**47**). HMKs inhibit the enzyme in an irreversible manner by the formation of a carbon-sulfur covalent bond between the methyl ketone moiety and the thiol of Cys199.[173] The covalent and irreversible binding to the kinase was also confirmed through model reactions, docking studies and mass spectrometric analysis of the resultant product. Moreover, Perez *et al.* reported that the introduction of the halomethylketone warhead is able to convert a reversible inhibitor (**48**, **49**) into a more potent irreversible GSK-3 inhibitor (**50**, **51**).[174] Subsequent to the discovery of these compounds, other non-competitive GSK-3β inhibitors, such as the natural alkaloid Manzamine A (**52**) and the sesquiterpene Palinurin (**53**), both extracted from marine sponges, have been described.[136] The non-ATP competitive inhibitory mechanism of Manzamine A has been demonstrated experimentally, while a computational study proposed that **52** could bind to the substrate recognition region.[175] On the other hand, the mechanism of inhibition suggested for Palinurin (**53**) seems to be allosteric: in fact, it seems that the molecule binds the N-terminal portion of the enzyme, influencing the orientation of the third and fourth strand of the β sheet and the hydrogen bond usually formed between Ser66 and the γ phosphate of ATP, thus preventing the correct positioning of a substrate to this portion of the enzyme.[176]

Since GSK-3β requires preferentially pre-phosphorylated substrates, efforts have been directed in the synthesis of peptides showing a similar sequence to the one usually recognized by the kinase. The first example is L803-mts (**54**), which is a cell-permeable phosphorylated peptide composed by 11 residues, derived from the GSK-3 substrate heats shock factor-1 (HSF-1) with a myristic acid attached to the N-terminal end that enables cell permeability.[136] Protein-protein computational studies helped to clarify the interactions between the peptide and the kinase and revealed that **54** does not occupy exactly the same site occupied by the substrate. Both interact with the phosphate binding region but while the substrate binds mainly to the cavity delimitated by Gln89 and Asn95, L803-mts interacts with Phe93 and a hydrophobic portion of the enzyme, away from the ATP-binding site.[136] Administration of L803-mts in *in vivo* models of diabetes led to an improvement in glucose tolerance and a decrease of insulin levels; **54** also demonstrated neuroprotective properties both *in vitro* and *in vivo*.[136] Licht-Murava *et al.* have just reported a new type of GSK-3 inhibitor, L807-mts (**55**), that acts through a substrate-to-inhibitor conversion mechanism that occurs within the catalytic site of the enzyme. In specific, the peptide **55** binds GSK-3 (α or β) as a substrate and after phosphorylation is converted into an inhibitor.[177] Compared to L803-mts (**54**), L807-mts (**55**) is more potent, highly selective *in vitro*, and in mice it exhibits suitable pharmacological properties, including stability, brain permeability, pharmacokinetics, and safety. Moreover, L807-mts (**55**) enhanced the clearance of Aβ masses, reduced inflammation and improved cognitive and social skills in the 5XFAD AD mouse model.[177]

5-imino-1,2,4-thiadiazoles (ITDZs, **56**) were the first non-peptidic compounds able to

inhibit GSK-3 in a substrate competitive manner.[178] ITDZs were obtained modifying the skeleton of the TDZD compounds (**43**): the two carbonyl groups at the 3 and 5 positions of the thiadiazolic ring were in fact replaced with imino and alkyl/aryl moieties. Docking studies have shown that ITDZs interact with GSK-3 protein through a hydrogen bond between the proton of the imino-charged group and the backbone oxygen of Phe67 and an aromatic S-π interaction between the thiadiazole scaffold and the aromatic ring of the Phe67. The ITDZs resulted able to cross the BBB, to have a high affinity with albumin and, in general, a good pharmacokinetic profile. ITDZs, including **57**, have been shown to exert neuroprotective actions against different cell cultures of astrocytes and microglia treated with LPS. Moreover, ITDZs presented efficacy in promoting murine neural stem cells' differentiation and repairing damaged neuronal areas.[179]

Recently, different allosteric binding sites have been described on the GSK-3 surface, which could be targeted for a selective inhibition of the enzyme. In particular the quinolone derivative (VP0.7, **58,** IC_{50}= 3.01 μM) is considered the first allosteric inhibitor of GSK-3. **58** has been shown to have neuroprotective activities *in vitro*, while its *in vivo* activity has been presented in preclinical models of fragile X syndrome and multiple sclerosis.[134,180]

Starting from VP0.7 (**58**) scaffold, Zhang *et al.* reported two benzothiazinone (BTO) derivatives as GSK-3β inhibitors (**59**, **60**), presenting two different inhibitory mechanisms. BTO-5h (**59**) is in fact an allosteric modulator of GSK-3β, while BTO-5s (**60**) is a novel substrate competitive inhibitor. Compounds **59** and **60** showed good efficacy and selectivity towards a panel of related protein kinases. Moreover, both compounds have been able to reduce GS phosphorylation levels in an intact cell and greatly enhanced the glucose uptake in both HpG2 and 3T3-L1 cells.[181]

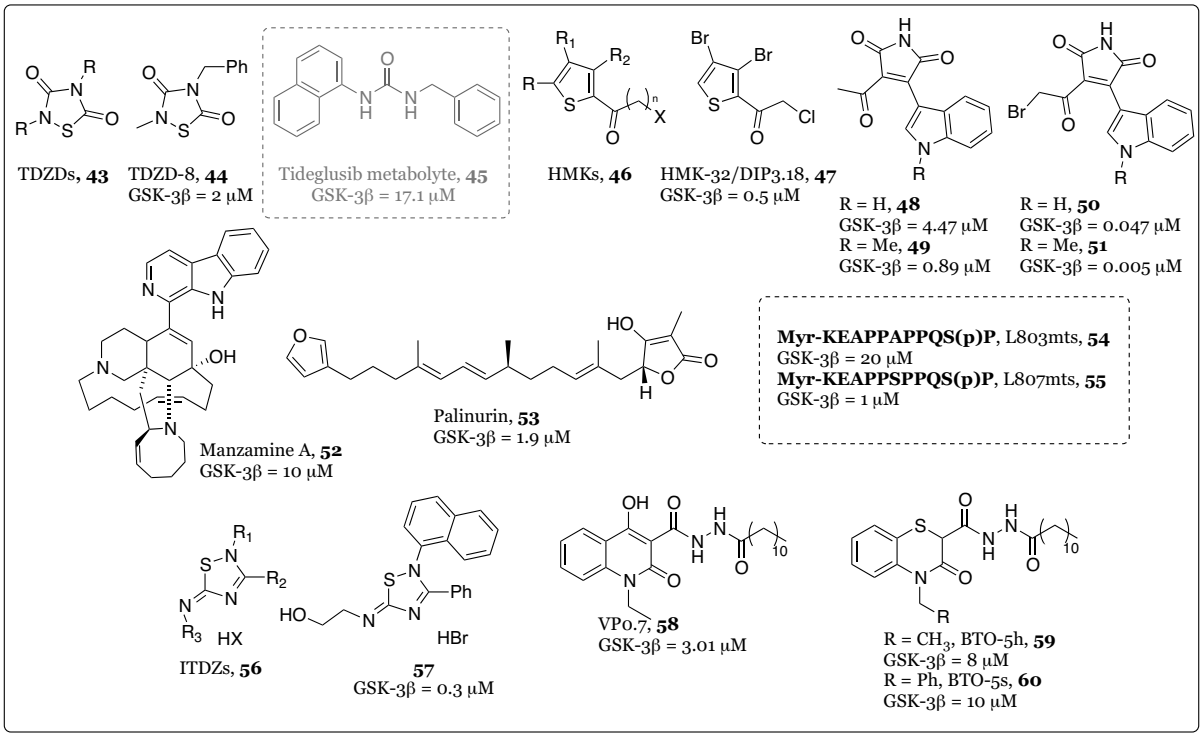

Figure 17 – Non-ATP competitive GSK-3 inhibitors (**43-60**).

1.5.1.3 Multi-target inhibitors

A current trend in drug-discovery is the idea that multi-target drugs could be more effective than single targeted therapy, in particular in the case of neurodegenerative diseases and cancer where the redundancy of signaling pathways may neutralize the treatment with a highly selective inhibitor. Recently, the multi-target strategy started to involve some new GSK-3 inhibitors (**Figure 18**). The first examples reported are compounds with dual activity on GSK-3 and BACE-1 (**61-63**). The synergic inhibition of these two targets is a promising strategy for the treatment of AD or other cognitive disorders where β-amyloid and GSK-3 are overexpressed.[182–184] Boulahjar and colleagues reported a Valmerin derivative (**64**) that could be considered a dual GSK-3/CDK-5 inhibitor (IC_{50} GSK-3/CDK5 32/84 nM). Both GSK-3 and CDK-5 are key mediators in embryonic development, protein synthesis, cell proliferation and differentiation and apoptosis, and deregulation of these PKs has been found in many human diseases.[185] The thiazolo[5,4-*f*]quinazolinone derivative (**65**) showed nanomolar IC_{50} values for CLK-1, DYRK-1A and GSK-3α/β, all kinases deregulated in AD.[186] Finally, the ITDZ derivative VP1.15 (**66**) is reported as substrate competitive GSK-3β inhibitor (IC_{50}=1.95 μM) and an allosteric inhibitor for the phosphodiesterase 7 (PDE-7, IC_{50}=1.11 μM). Both PDE-7 and GSK-3 are relevant therapeutic targets for neurological disorders, and PDE-7 inhibitors can also be considered potent indirect inhibitors of GSK-3 through the cAMP/PKA signaling pathway or phosphorylation of GSK-3 at Ser9. VP.1.15 (**66**) displayed antipsychotic activities and ameliorated cognitive processes in a schizophrenia mouse model. [178,187]

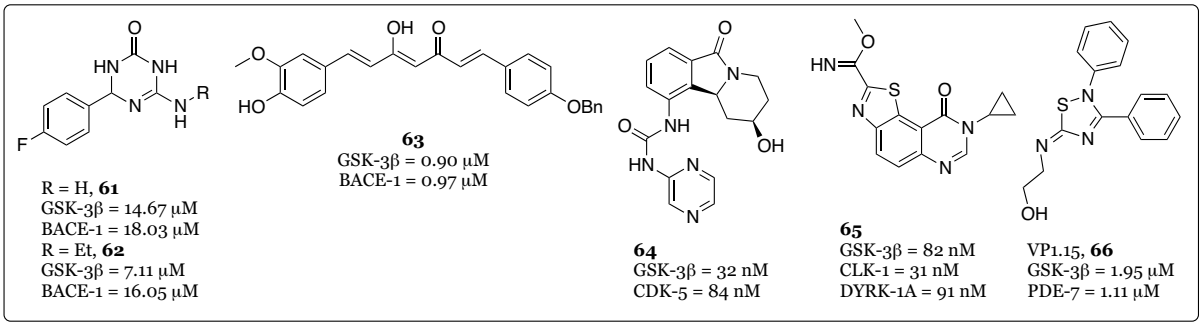

Figure 18 – Multi-target GSK-3 inhibitors (**61-66**).

1.5.2 CK-1 Inhibitors

Due to the involvement of CK-1 isoforms in the pathogenesis of several diseases, such as inflammatory, proliferative, neurodegenerative and sleeping disorders, the design and development of CK-1 inhibitors have earned more and more interest in the last years. However, only a relatively small number of CK-1 inhibitors, as compared to GSK-3β, have been described, all belonging to the ATP-competitive class.[15] Here is presented a brief overview of inhibitors of CK-δ isoform described in literature at the moment. When known, also inhibitory activities towards ε isoform were reported (**Figure 19**).

Even in this case, the natural environment has represented a promising source of new bioactive molecules (**Figure 19**, panel A). In addition to hymenialdesine [**6**, IC_{50}(CK-1)= 35 nM], already described in the GSK-3β inhibitor chapter (1.5.1.1), it is worth mentioning Meridianine E (**67**), a brominated 3-(2-aminopyrimidine)-indole isolated from the marine invertebrate *Aplidium meridianum*. It resulted an inhibitor with IC_{50} in the low micromolar range towards different protein kinases, including CK-1 and CDKs.[188] **67** has been reported to

prevent cell proliferation and promote apoptosis, but it also resulted cytotoxic in different cell lines.[58] (-)Matairenisol (**68**), a dibenzylbutyrolactone lignan, is a CK-1/PKC inhibitor with IC_{50} values of approximately 10 μM.[58] It was first reported to inhibit HIV replication in H9 lymphocyte and recently showed moderate inhibiting activity on NF-κB signaling pathway.[189] Lamellarin 3 (**69**), a synthetic analogue of the hexacyclic pyrrole alkaloids originally isolated from marine invertebrates, displays promising anti-tumor activity that can be related to the inhibition of different kinases relevant to cancer, such as CK-1 and DYRK-1A.[190] Harmine (**70**), isolated from medicinal herbs, is an extremely potent inhibitor of the DYRK family of protein kinases, but also inhibits CK-1 in the micromolar range. It exhibited a strong inhibitory effect on the growth and proliferation of carcinoma cells.[191] Recently, Esposito *et al.* reported the halogenated alkaloid chloromethylhalicyclamine B (**71**), isolated from the dichloromethane crude extract of the sponge *Acanthostrongylophora Ingens* that resulted to be a selective CK-1δ/ε inhibitor with an IC_{50} of 6 μM.[192]

The first inhibitor of CK-1δ was reported in 1989 and is the quinoline derivative CKI-7 (**72**)(**Figure 19**, panel B). It is unable to discriminate among the different CK-1 isoforms but showed quite kinase specificity; in N2A cells, it reduced Aβ plaques formation. In early 2000s, was identified the indolinone derivative IC261 (**73**), a specific inhibitor of δ/ε isoforms of CK-1. IC261 has been demonstrated to induce cell cycle arrest and apoptosis of human cancer cells (pancreatic and breast tumor cell lines).[193,194] The imidazole derivative D4476 (**74**, IC_{50}=0.3 μM) showed a good selectivity towards other kinases and thus is widely used for inhibiting CK-1 isoforms in cell-based assays. It has been shown able to reduce the β-amyloid formation acting during the γ-secretase cleavage, while in hepatoma cells it inhibited the phosphorylation of Forkhead Box O1 (FOXO1), a transcription factor involved in the regulation of metabolic homeostasis in response to oxidative stress.[58]

Amino-antraquinone derivatives were optimized as CK-1 inhibitors with the help of a structure-based virtual screening. In particular, the 1,4-diamino anthraquinone (DAA, **75**) resulted able to discriminate between the different isoforms, while in a cytotoxic profile on human ovarian carcinoma cell line showed DC_{50} value of 10 μM after a 48 h exposure.[193,195] The benzothiazole TG003 (**76**), originally identified as a CLK-2 inhibitor, has recently been shown to inhibit CK-1δ in the sub-micromolar range. Together with IC261 (**73**), it has been assayed in inflammatory pain models and both showed a decrease of the frequency of spontaneous excitatory postsynaptic currents (sEPSCs), suggesting a role for CK-1 in spinal inflammatory pain transmission.[196] Pfizer developed three potent and selective inhibitors for CK-1δ/ε: compounds **77** and **78** present an aminopyrimidine ring, while in compound **79** the same ring was fused with a pyrazole to give a pyrazolo[3,4-*d*]pyrimidin core. PF-4800567 (**79**) inhibits more effectively the isoform ε than δ. Compound **78** has been demonstrated to modulate dose-dependently circadian rhythm in both nocturnal and diurnal animal models and attenuate opioid drug-seeking behavior in a rodent model of abuse.[197] Further studies of circadian rhythm in mouse models revealed that the specific CK-1ε inhibitor **79** is not able to affect the circadian rhythm *in vivo*, thus suggesting that the δ-isoform could be predominant in circadian clock.[193] Following the [6+5] fused heterocycle series, Yang and colleagues reported the synthesis of pyrazolo[3,4-*d*]pyrimidine derivative **80**, which inhibits CK-1 with an IC_{50} value of 78 nM.[198] Roscovitine (or Seliciclib or CYC202, **81**) is a broad range inhibitor of CDKs, currently being investigated in clinical trials for advanced solid tumors, cystic fibrosis and Cushing's disease.[199] Different 2,6,9-trisubstituted purines were synthesized to inhibit protein kinases implicated in AD, specifically GSK-3, CDK-5, and CK-1. In this series, emerged compounds CR8 (**82**) and DRF053 (**83**); the latter inhibits CK-1δ/ε at a

concentration of 14 nM, while it is less effective towards CDK-5 (IC_{50}= 80 nM), CDK-1 (IC_{50}=0.22 μM) and GSK-3 (IC_{50}=4.1 μM).[200] It also has been shown able to reduce the production of Aβ in N2A cells.[193] Other adenine-like derivatives are SR-3029 (**84**) and SR-2890 (**85**), which show good *in vitro* and *in vivo* pharmacokinetics properties and were also highly potent in inhibiting A375 melanoma cell growth in a MTT viability assay.[84,201]

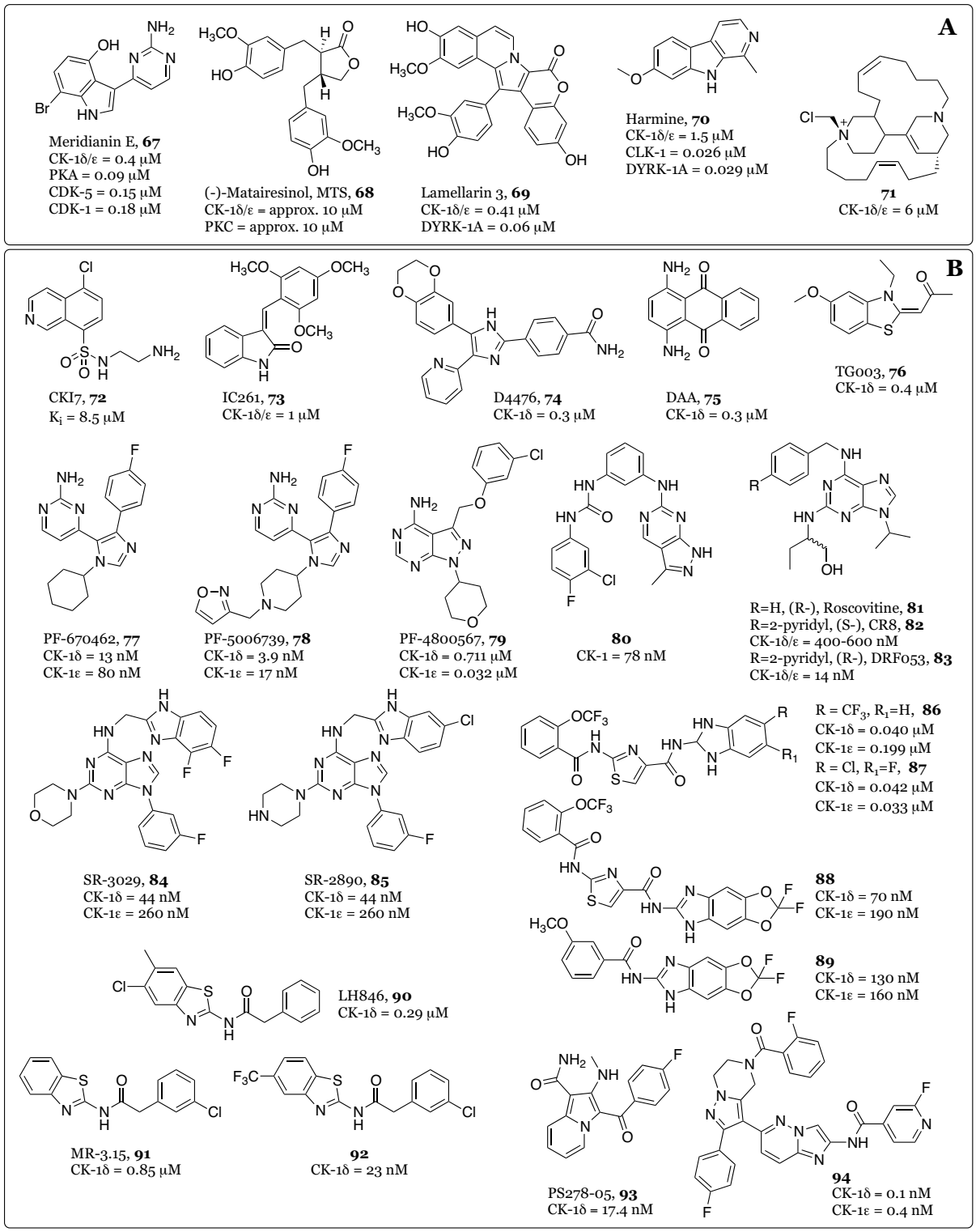

Figure 19 - Panel A) CK-1 ATP-competitive inhibitors from natural resources (**67-71**). Panel B) Synthetic ATP-competitive CK-1 inhibitors (**72-94**).

Furthermore, SR-3029 (**84**) promoted apoptosis of CK-1δ-expressing breast tumor cells *ex vivo* and tumor growth inhibition in human epidermal growth factor receptor 2–positive (HER2$^+$) breast cancer models, through Wnt pathway modulation.[202] Bischof *et al.* described the development of a series of potent and selective benzimidazoles as CK-1δ/ε inhibitors (**86,87**). Both compounds **86** (δ-selective) and **87** (δ/ε) resulted able to inhibit proliferation of tumor cell lines in a dose and cell line specific manner.[15] Optimization of the benzimidazole scaffold led to dioxolo-benzoimidazoles (**88,89**), which exhibited similar potency towards CK-1 with a remarkable selectivity for the δ isoform.[203] Moreover, newly designed compounds **88-89** showed increased growth inhibitory activity in different tumor cell lines.[203] A cell-permeable benzothiazole (**90**) resulted a potent and selective inhibitor of CK-1δ (IC_{50} = 290 nM). It was shown to block CK-1δ-dependent PER1 phosphorylation and to lengthen the circadian period (10 h) in cell culture.[204] Following a chemical genetic approach, Salado *et al.* identified novel benzothiazoles as selective CK-1δ inhibitors in the nanomolar range (**91-92**). They were predicted as BBB-permeable, presenting excellent pharmacokinetic properties and able to reduce TDP-43 phosphorylation, one of the hallmark of ALS.[117] Pike and collaborators claimed a new potent and selective CK-1δ inhibitor, derivative PS278-05 (**93**) for AD treatment; specifically, **93** showed reduction of CK-1δ specific phosphorylation of *tau* in human neuronal cell cultures and general improvement in cognitive behaviour in Thy-1 mutated human *tau* (TMHT) mouse model.[205,206] Finally, Bristol-Myers Squibb developed a series of imidazo-pyridazine derivatives, where the lead compound present sub-nanomolar IC_{50} values for both CK-1δ and ε isoforms (**94**).[207]

1.5.2.1 Multi-target inhibitors

In the last years, also CK-1 has been involved in development of multi-kinase inhibitors (**Figure 20**). Different isoxazole derivatives (**95-97**) have been recently reported as dual inhibitors of CK-1δ/ε and p38α kinases,[208–210] which are both involved in the Wnt pathway.[211] CKP138 (**98**) presents a peculiar acrylamide moiety, which could function as a Michael acceptor, able to target a chemically reactive residue (such as cysteine), thereby forming a covalent bond to the protein. According to the binding pose predicted for both CK-1δ and p38α, a residue capable of reacting through this mechanism cannot be found either in HRII of p38α or CK-1δ.[209] **98** resulted able to induce apoptotic processes in AC1-M88 cells,[193] while **97** is claimed to enhance the differentiation of pluripotent stem cells into cardiomyocytes.[208] On the other hand, the pyrazolo-pyridine derivative **99** is a CK-1/Chk-1 dual-specific inhibitor, which resulted able to stabilize and reactivate the p53 pathway, suppressed in many human cancer cells.[15,212] Finally, the new pyrido[3,4-*g*]quinazoline derivative **100** has been designed to inhibit different kinases involved in AD, in this case DYRK-1A, CLK-1 and marginally also CK-1.[213]

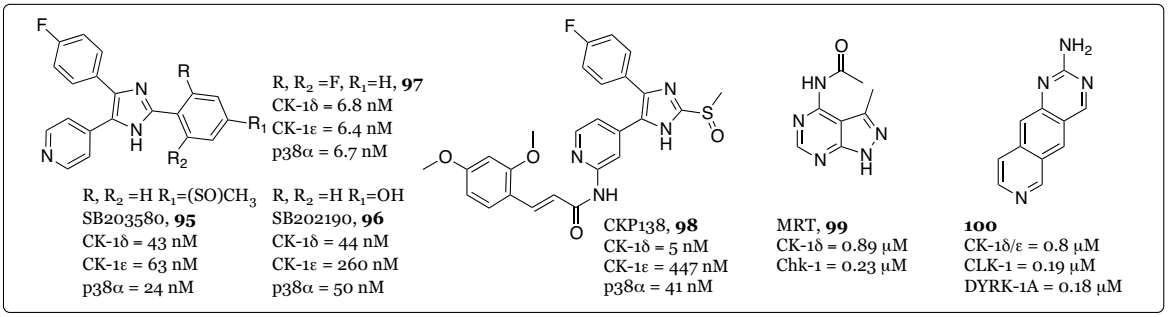

Figure 20 – Multi-target CK-1 inhibitors (**95-100**).

2 Aim of the Work

The implication of GSK-3β and CK-1δ proteins in various pathological conditions, such as neurodegenerative diseases and cancer, and the fact that only few inhibitors reached clinical trials highlighted the great interest in developing new inhibitors of these two enzymes for the treatment of different unmet diseases.

As previously mentioned, the ATP-binding domain is to some extent highly conserved among the kinase family members, and this is reflected in the difficulty of designing selective ATP-competitive kinase inhibitors; however it remains the most exploited kinase inhibition approach and, in fact, the majority of known GSK-3β and CK-1δ inhibitors are ATP-competitive.

The present Ph.D research project is aimed to the synthesis of novel small-molecule inhibitors of GSK-3β and CK-1δ to study their potential use as agents to counteract neuroinflammation and neurodegeneration. In particular, inhibitors were addressed to interact with the kinase ATP-binding domain due to their structural similarity to the adenine moiety of ATP itself. In fact, we focused on the design and decoration of fused 5 and 6 membered rings: [1,2,4]triazolo[1,5-*a*][1,3,5]triazines (**TT**)[214–217] and [1,2,4]triazolo[1,5-*c*]pyrimidines (**TP**),[218–220] two classes of adenine-like derivatives well known in literature (**Figure 21**).

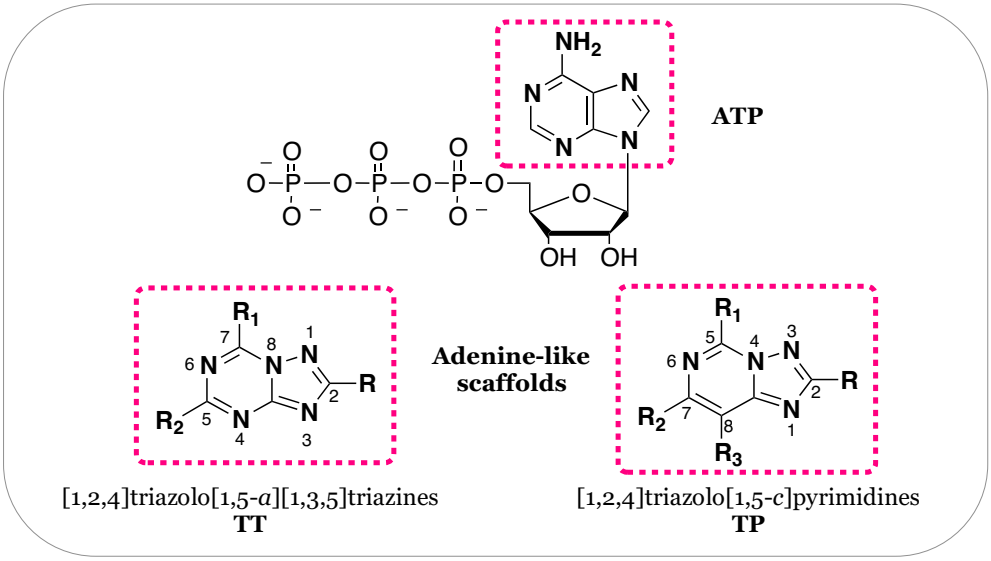

Figure 21. Rationale design of ATP-mimicking kinase inhibitors

Specifically, in the following chapters it will be described the design, synthesis and biological evaluation of:

-Chapter 3: 5,7-disubstituted [1,2,4]triazolo[1,5-*a*][1,3,5]triazines as ATP-competitive GSK-3β inhibitors.

-Chapter 4: 2,5,7- and 2,5,8-trisubstituted [1,2,4]triazolo[1,5-*c*]pyrimidines and 2,5,7-trisubstituted [1,2,4]triazolo[1,5-*a*][1,3,5]triazines as ATP-competitive CK-1δ inhibitors.

-Chapter 5: 2,5,7-trisubstituted [1,2,4]triazolo[1,5-*a*][1,3,5]triazines as dual GSK-3β/CK-1δ inhibitors.

3 Synthesis and Characterization of GSK-3β Inhibitors

3.1 INTRODUCTION

Over the past several decades, many purine and purine-bioisoster derivatives have been the subject of intensive structure-activity relationship (SAR) studies to identify potent protein kinase inhibitors. As mentioned before, the structure similarity between purine-like derivatives and the adenine moiety of ATP gives the possibility to easily obtain ATP-competitive inhibitors. In particular, the positive outcome of the purine derivative Roscovitine (**81**), a broad-range CDK inhibitor currently undergoing clinical trials as a candidate drug for some oncological and inflammatory indications, has prompted the development of a wide number of structurally related kinase inhibitors, mainly oriented towards the CDK and CK-1 families.[200,221] Furthermore among GSK-3β inhibitors reported in literature, we can find different examples of adenine-like derivatives showing good inhibitory potency (e.g. derivatives **31-35**, Chapter 1.5.1.1).[51,136,160–162,222]

The 1,2,4-triazolo[1,5-*a*][1,3,5]triazine scaffold (**TT**), widely exploited in our research group to obtain adenosine receptors ligands,[216,217,223] is an appealing purine bioisoster core not yet explored for the synthesis of protein kinase inhibitors. Therefore, this part of the thesis is directed to the design and synthesis of new 1,2,4-triazolo[1,5-*a*][1,3,5]triazine derivatives as GSK-3β inhibitors. Despite Roscovitine (**81**) and its analogues have been reported to exhibit low activities towards GSK-3β, they could however represent a valid starting point for the design of new inhibitors for this kinase, since GSK-3β and CDKs share high homology (86%, between GSK-3β and CDK2) within the two ATP-binding sites.[21,224] In fact, we decided to introduce on the TT scaffold some features present in Roscovitine (**81**) and its derivatives[200] and in particular we have substituted the 7-position with different arylmethylamino groups (e.g. benzylamino) or the cyclohexylamino moiety while the 2-position was maintained unsubstituted or substituted with a phenyl group. Most important, we focused our investigation on the 5-position by introducing the (R)-2-aminobutan-1-ol moiety, as present in Roscovitine (**81**),[200] and several other different groups in order to better understand the interactions required to gain affinity towards GSK-3β (**Figure 22**).

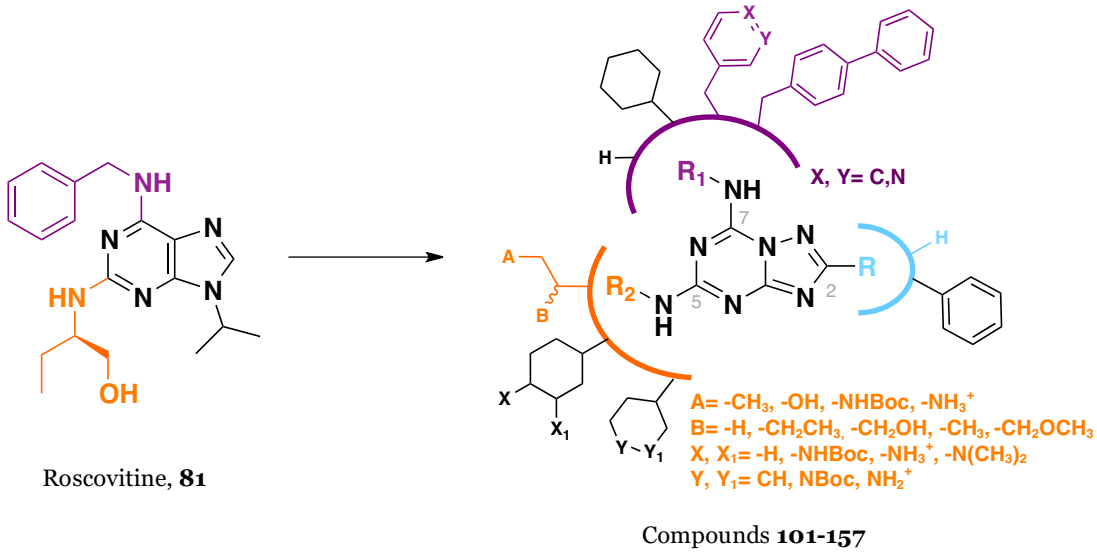

Figure 22. Rationale for the synthesis of novel GSK-3β inhibitors (**101-157**).

All the synthesized derivatives were evaluated towards GSK-3β (in collaboration with the group of Professor Sabrina Castellano at the University of Salerno) using the LANCE®*Ultra* kinase assay. In addition, since GSK-3β is considered a potential target for therapeutic

intervention in CNS diseases, the blood-brain barrier (BBB) permeability of some of the most promising triazolo-triazine derivatives was predicted.

3.1.1 Parallel Artificial Membrane Permeability Assay (PAMPA)

One of the main obstacles for the treatment of central nervous system (CNS) diseases is the drug's penetration into the BBB at therapeutic concentrations.[225] The BBB is a complex interface between blood and the CNS which strictly controls the exchanges between the blood and brain compartments.[226] This barrier is composed by endothelial cells with tight junctions which protect the brain from endogenous materials that could damage the brain tissues.[227] The majority of CNS drugs enter the brain by transcellular passive diffusion, due to the tight junction structure and limited transport pathways.[228] In early drug discovery stage, evaluation of ADME (Absorption, Distribution, Metabolism, Excretion) properties is of crucial importance to reduce the attrition rate in development process. PAMPA is a high throughput technique developed to predict passive permeability through biological membranes, described for the first time by Di et al.,[229] further developed in the research group of Professor Ana Martinez, at Centro de Investigaciones Biológicas (CIB, Madrid, ES), for poor water-soluble organic molecules[178] and here used to assay our newly synthetized derivatives.

This methodology is based on the ability of a compound to cross an artificial membrane impregnated with a porcine brain lipid from a donor plate containing the buffer and the assayed drug to an acceptor plate containing only the buffer. Thus, the effective permeability (*Pe*) of each compound is determined from the difference between the absorbance values obtained in the donor and the acceptor plates (**Figure 23**).

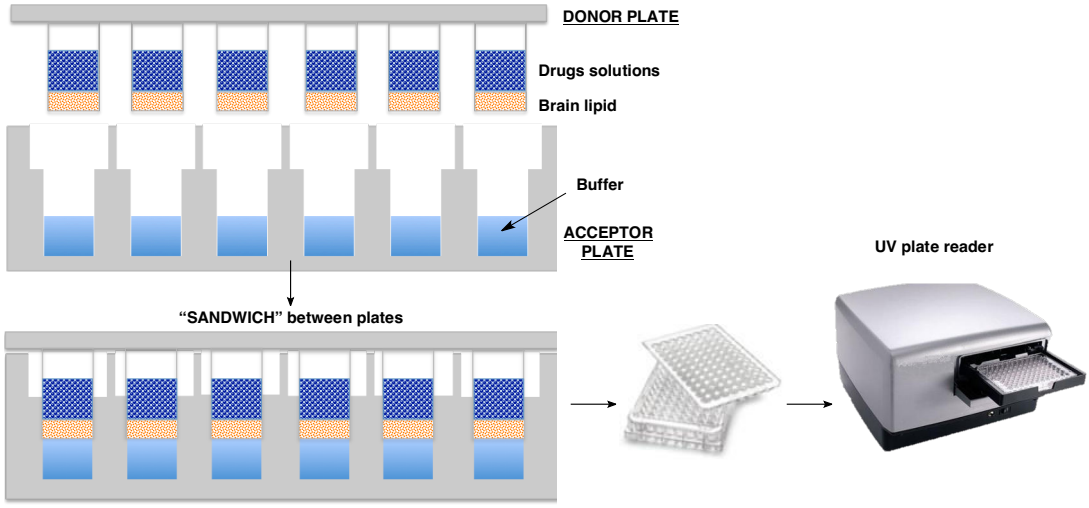

Figure 23. PAMPA assay representation.

3.2 RESULTS AND DISCUSSION

3.2.1 Chemistry

The synthesis of the 1,2,4-triazolo[1,5-*a*][1,3,5]triazine scaffold started by reacting the commercial available 2,4,6-trichloro[1,3,5]triazine (**158**) with phenol under reflux for 5 hours. The resulting 2,4,6-triphenoxy[1,3,5]triazine (**159**) was then treated with hydrazine monohydrate to afford the hydrazinyl derivative **160**, which was successively formylated with formic acid to give the intermediate **161**, useful for the synthesis of the 2-H TT scaffold. The latter synthesis derives from the optimization of the procedure described by Bakhite et al., where the hydrazinyl derivative **160** was reacted in formic acid under reflux for 6 hours (yield <10%).[230] In order to obtain higher yield, we decided to perform the reaction in milder conditions (room temperature), with a restrained excess of formic acid (10 equivalents) and in presence of an organic solvent as toluene,[231] and all these expedients allowed us to obtain the product **161** with an average yield of 69%. On the other hand, benzohydrazinyl derivative **164** was obtained by reacting **159** directly with the benzohydrazide **163** (obtained from the corresponding ethyl ester **162** after reaction with hydrazine) in the presence of 1,8-diazabicyclo[5.4.0]undec-7-ene (DBU) [**Scheme 1**].[214]

Scheme 1. Synthesis of *N*'-(4,6-diphenoxy-1,3,5-triazin-2-yl)hydrazides **161** and **164**[a]

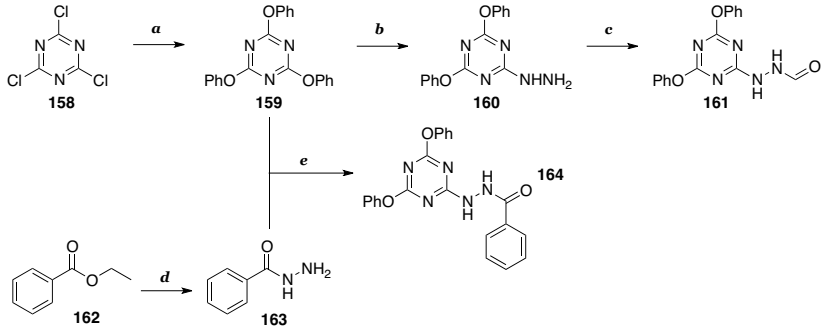

[a] ***a:*** phenol, reflux, 5 h; ***b:*** hydrazine monohydrate in THF, DCM, r.t., 12 h; ***c:*** formic acid, toluene, r.t., 4 h; ***d:*** hydrazine monohydrate, ethanol, reflux, 24-72 h; ***e:*** DBU, THF, r.t., 12 h.

Derivatives **161** and **164** underwent intramolecular cyclization to afford the 1,2,4-triazolo[1,5-*a*][1,3,5]triazine scaffold in dehydrative conditions. In literature, the formation of condensed heterocyclic systems is described to occur in xylene at reflux (bp=139°C) in presence of phosphorus pentoxide as dehydrating agent.[214] This reaction, however, requires long reaction times (> 14 hours) with consequent loss of material by thermal degradation. In fact, the 2-phenyl derivative **166** was initially synthesized following this procedure, however obtaining low yields (<30%). Later, it has been reported that the use of polyphosphoric acid trimethylsilyl esters (PPSE) as dehydrating agents affords better yields with lower reaction times. For this reason we decided to use the trimethylsilyl ester of polyphosphoric acid obtained by reacting phosphorus pentoxide with hexamethyldisiloxane (HMDSO) in xylene under argon [**Scheme 2**].[232] The condensation reaction involves initially a nucleophilic attack by the nitrogen of the triazine ring to the carbonyl of the hydrazide. This attack is severely disadvantaged due to both the low nucleophilicity of the tertiary nitrogen and the low electron-deficiency of carbonylic carbon. PPSEs can promote the condensation reaction in two ways: they can donate a trimethylsilyl group (TMS) to the carbonylic oxygen, thus rendering it electron-poor and susceptible to the nucleophilic attack, or polyphosphorylate it,

affording a mixed anhydride. In both cases, the silylated or the polyphosphorylated oxygen is now a good leaving group, whose exit promotes the final step of the condensation.[233,234] The desired 5,7-diphenoxy-[1,2,4]triazolo[1,5-*a*][1,3,5]triazine derivatives **165-166** were finally obtained after spontaneous Dimroth rearrangement, an amidine rearrangement whose driving force is represented by a major stability of the [1,5-*a*] isomer than the [4,3-*a*] one, which could not even be isolated. The mechanism of the Dimroth rearrangement involves opening and subsequent closure of the triazine ring annulated to the 1,2,4-triazole ring (**Figure 24**).[234]

Scheme 2. Synthesis of final compounds **101-143**[a]

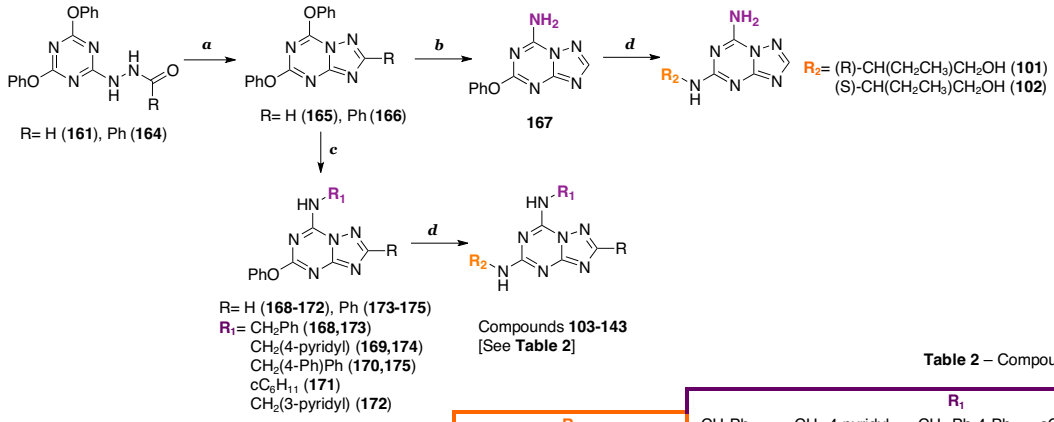

Table 2 – Compounds **103-143** (*R=Ph)

R_2	R_1: CH_2Ph	CH_2-4-pyridyl	CH_2-Ph-4-Ph	cC_6H_{11}	CH_2-3-pyridyl
(R)-$CH(CH_2CH_3)CH_2OH$	**103,106***	**104,107***	**105,108***	**112**	**114**
(S)-$CH(CH_2CH_3)CH_2OH$	**109**	**110**	**111**	**113**	**115**
$CH(CH_2CH_3)CH_2CH_3$		**116**	**117**		
$CH(CH_2OH)_2$		**118**	**119**		
(R)-$CH(CH_2CH_3)CH_3$		**120**	**122**		
(S)-$CH(CH_2CH_3)CH_3$		**121**	**123**		
CH_2CH_2OH		**124**	**125**		
CH_2CH_2NH-Boc		**126**	**127**		
cyclohexyl		**128**	**129**		
4-(NHBoc)cyclohexyl		**130**	**131**		
3-(NHBoc)cyclohexyl		**132,133**	**134,135**		**136,137**
4-(N-Boc-piperidine)		**138**	**139**		
3-(N-Boc-piperidine)		**140**	**141**		
4-($N(CH_3)_2$cyclohexyl)					**142**
(R,S)-$CH(CH_2CH_3)CH_2OCH_3$					**143**

[a] ***a:*** P_2O_5, HMDSO, xylene, from r.t. to 90°C, 2.5 h, reflux, 2-3 h; ***b:*** ammonia 7N in methanol, methanol, r.t., 2 h; ***c:*** R_1-NH_2, methanol, 50°C, 3 h; ***d:*** R_2-NH_2, ethanol, 95-100°C, sealed tube, 24-72 h

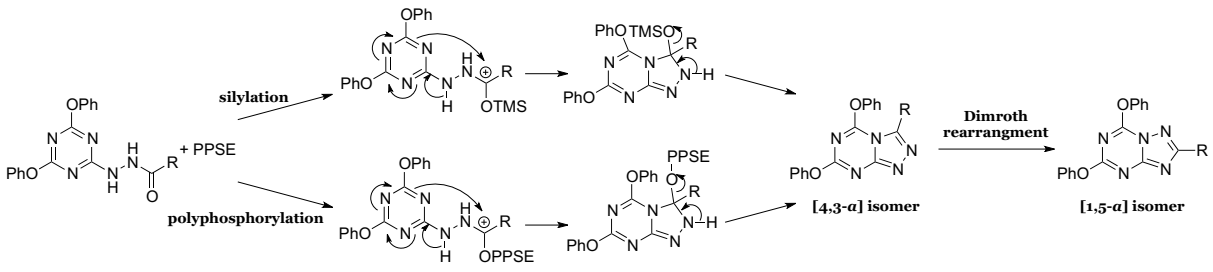

Figure 24. Mechanism of dehydrative cyclization and Dimroth rearrangement

Regarding derivative **165** (R=H) the very low yield (6%) led us to optimize the synthetic process: in fact, we tried to change temperature and reaction time (e.g. reflux 12 hours, 60°C for 36 hours) and also the solvent (mixture xylene/DCM or toluene). The results obtained in all the cases were even worse (yield <4%): probably derivative **165** easily decomposed during the work-up of the reaction. Therefore we decided to maintain the original reaction

conditions and purify the mixture with a fast filtration through a silica plug (3-4 cm length). Proceeding in this way the yield of the reaction increased to 25% of average. According to literature, the first nucleophilic substitution of the phenoxy group on the TT scaffold occurs at the 7-position,[214] proceeding with high yields both with methanolic ammonia 7N at room temperature to give derivative **167** and with different amines at 50°C (**168-175**). On the contrary, substitution at the 5-position of the TT ring requires harsher conditions: in fact, the 7-aminosubstituted 5-phenoxy-[1,2,4]triazolo[1,5-*a*][1,3,5]triazine derivatives **167-175** were reacted in ethanol, in a sealed tube at 95-100°C for 24-120 hours [**Scheme 2**]. In this case, yields of reaction were lower because of the low reactivity of this position that led to unconsumed starting material or, when the reaction is forced, to the formation of the corresponding 5,7-bis-substituted derivatives. The latter event occurred in particular with derivatives bearing a free amino group at the 7-position **101-102**, where the yields did not reach the 20%. Furthermore, the disubstituted, monosubstituted and the starting compounds showed very similar retention factors making more complicated the separation through chromatography.

The main feature of ^{1}H NMR spectra of triazolo-triazine derivatives is that the NH-proton of amino group at the 5-position typically resonates at δ 6.5-7.5 as a broad singlet, while those of the 7-amino group resonate at 8.0-10.0 ppm as a doubled broad singlet, which coalesces when registering the spectra at higher temperature (**Figure 25**). Moreover, in general, when the TT scaffold is substituted at both 5- and 7- positions, doubled peaks were observed due to the different conformational isomers, which complicate ^{1}H NMR spectra interpretation. At higher temperatures the spectrum is simplified since the equivalent peaks coalesced, as it can be observed in **Figure 25** for compound **121**.

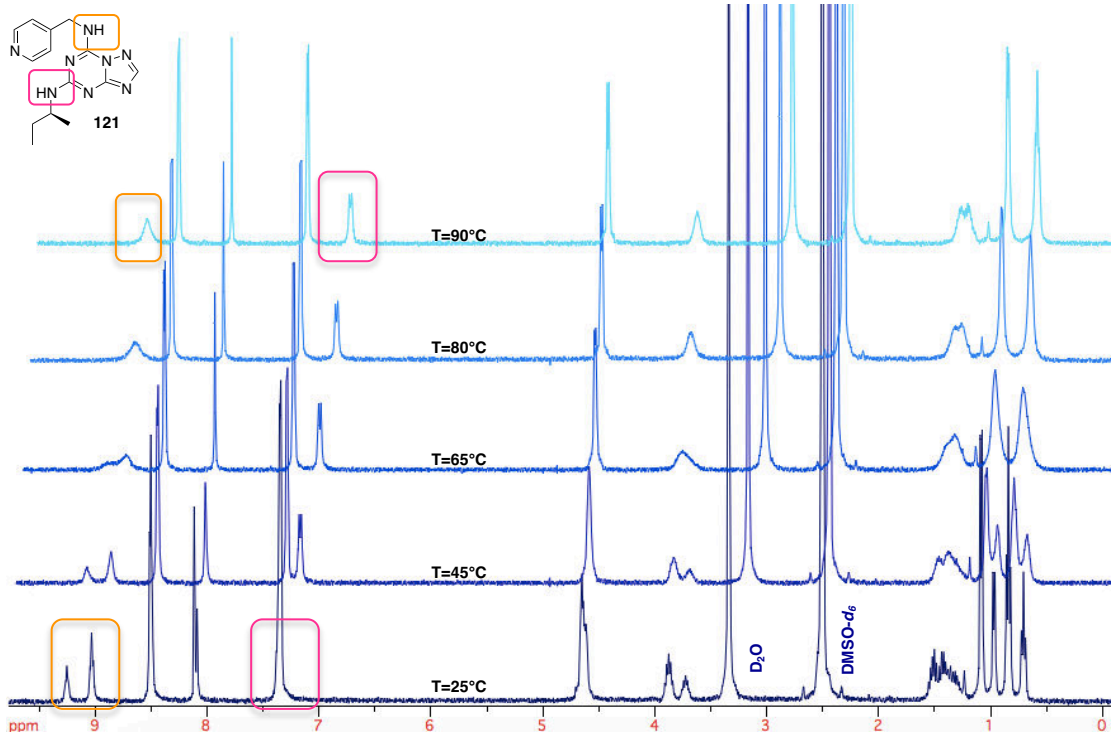

Figure 25. ^{1}H NMR spectrum of compound **121** at increasing temperature, from 25°C to 90°C.

Finally, N-Boc-amino derivatives **126-127**, **130-141** were deprotected with trifluoroacetic acid 10% in dichloromethane, giving the final amino derivatives **144-157** as trifluoroacetate salts in quantitative yields [**Scheme 3**].

Scheme 3. Synthesis of compounds **144-157**[a]

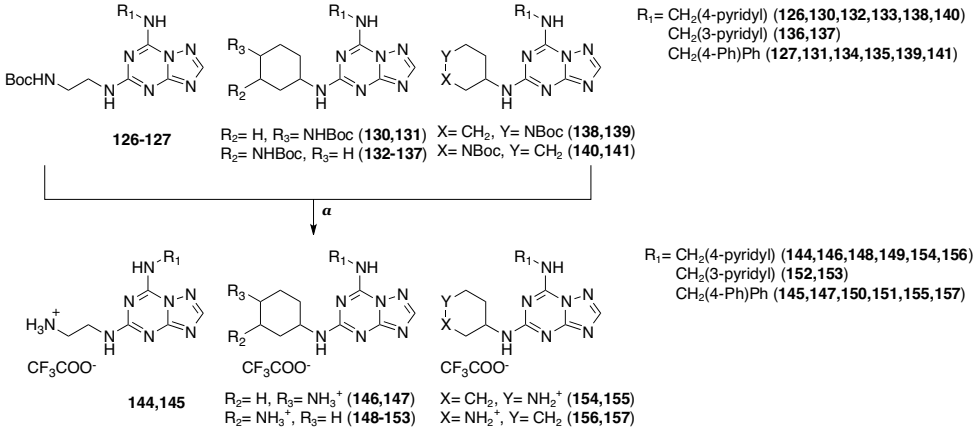

[a] ***a:*** CF_3COOH 10% in DCM, r.t., 2-3 h.

3.2.2 Enzymatic evaluation and structure activity relationship (SAR) analysis

All the synthesized derivatives were evaluated towards GSK-3β in collaboration with the group of Professor Sabrina Castellano at the University of Salerno, using the LANCE®*Ultra* kinase assay. In particular, their inhibitory potencies on human GSK-3β were measured in a cell-free environment on the phosphorylation of a peptide substrate, using a Time-resolved fluorescence energy transfer (TR-FRET) based method. The newly synthetized compounds were initially evaluated at 20, 10, 5 or 2.5 μM to obtain the percentage of GSK-3β residual activity. The concentrations of the compounds used in the single-dose screening were established after nephelometric solubility assay. For those compounds with a percentage of GSK-3β residual activity lower than 35% at the concentration of 5 μM, the dose-response curves were determined and the half-maximal inhibitory concentration (IC_{50}) calculated (**Table 3**). In each kinase assay, the commercial inhibitor of GSK-3β SB216763 (**18**) was used as a control.

In a preliminarily phase, we decided to introduce on the TT scaffold at the 7-position three different arylmethylamino groups (benzylamino, 4-pyridylmethyl, 4-phenylbenzylamino) and at the 5-position the (R)-2-aminobutan-1-ol chain as present in Roscovitine and its analogues (**81-83**).[200] The effect, upon biological activity, of introduction of a phenyl moiety at the TT 2-position was also investigated (**103-108**).

Table 3. TTs derivatives **103-108**

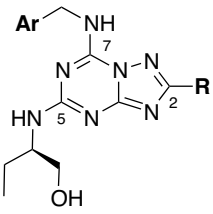

cmpd	R	Ar	IC_{50} (μM) or % residual activity (GSK-3β)[a]
103	H	phenyl	5.4
104	H	4-pyridyl	4.0
105	H	phenyl-4-phenyl	2.2
106	Ph	phenyl	13
107	Ph	4-pyridyl	83.7 ± 1.8 % @10μM
108	Ph	phenyl-4-phenyl	92.7 ± 0.8% @10μM

[a]GSK-3β inhibition data obtained with LANCE® *Ultra* kinase assay. Single-dose values are expressed ±SD (n=2).

As showed in **Table 3**, an activity in the micromolar range towards GSK-3β was found only with derivatives **103-105**, where the 2-position of TT is not substituted, thus rendering it the scaffold to work on to further improve the affinity towards GSK-3β (**Table 3**). On the contrary, the presence of a phenyl (**106-108**) resulted detrimental in terms of potency (**Table 2**). Later, we decided to investigate the role of stereochemistry in the interaction between GSK-3β and the active triazolo-triazines, thus preparing the (S)-analogues of derivatives **103-105**.

Table 4. TTs derivatives **109-111**

cmpd	Ar	R isomer	S isomer
		IC_{50} (μM) or %residual activity (GSK-3β)[a]	
103 (R) **109** (S)	phenyl	5.4	46.8% ±3.8 @5μM
104 (R) **110** (S)	4-pyridyl	4.0	7.0
105 (R) **111** (S)	phenyl-4-phenyl	2.2	2.5

[a]GSK-3β inhibition data obtained with LANCE® *Ultra* kinase assay. Single-dose values are expressed ±SD (n=2).

From results reported in **Table 4**, we can infer that optical properties of the 2-aminobutan-1-ol moiety slightly influence the affinity of TTs towards GSK-3β [**105**, IC_{50}(GSK-3β)= 2.2 μM *vs.* **111**, IC_{50}(GSK-3β)= 2.5 μM], with the only exception of 7-(4-pyridylmethylamino) derivatives **104** and **110**, where difference in kinase affinity between the two isomers resulted more pronounced [**104**, IC_{50}(GSK-3β)= 4.0 μM *vs.* **110**, IC_{50}(GSK-3β)= 7.0 μM].

Taking into account these preliminary results, structural modifications at the 7- and 5-positions of triazolo-triazine were considered in order to investigate the potency and outline a structure-activity relationship (SAR) of the novel GSK-3β inhibitors (**Figure 26**). In detail:

- **7-position**: we evaluated the role of substitution at the 7-position introducing other groups such as cyclohexylamino and 3-pyridylmethylamino or leaving the amino group free, while maintaining at the 5-position the (R-/S-) 2-aminobutan-1-ol chain.
- **5-position**: in order to investigate the role of the (R-/S-) 2-aminobutan-1-ol chain and its hydroxyl group, we introduced other alkyl chains of different length and nature, or substituted cyclohexylamino and piperidinamino systems. At the 7-position, 4-pyridylmethylamino and 4-biphenylmethylamino groups, as present in compounds **104** and **105**, were kept unchanged.

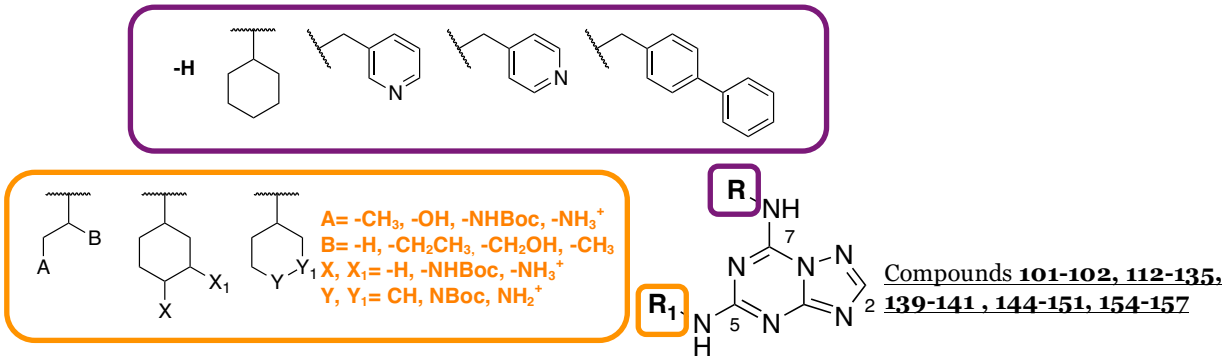

Figure 26. TTs as GSK-3β inhibitors.

Table 5. Inhibitory activities towards GSK-3β of compounds **101-102, 112-135**, **139-141**, **144-151**, **154-157**.

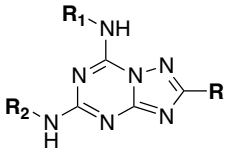

cmpd	**R**	**R_1**	**R_2**	IC_{50} (μM) or %residual activity (GSK-3β)[a]
104	H	4-pyridylmethyl	(*R*)-1-hydroxy-but-2-yl	4.0
105	H	4-phenylbenzyl	(*R*)-1-hydroxy-but-2-yl	2.2
101	H	H	(*R*)-1-hydroxy-but-2-yl	85.1 ± 7.9% @20μM
102	H	H	(*S*)-1-hydroxy-but-2-yl	85.4 ± 7.1% @20μM
112	H	cyclohexyl	(*R*)-1-hydroxy-but-2-yl	6.0
113	H	cyclohexyl	(*S*)-1-hydroxy-but-2-yl	5.8
114	H	3-pyridylmethyl	(*R*)-1-hydroxy-but-2-yl	1.4
115	H	3-pyridylmethyl	(*S*)-1-hydroxy-but-2-yl	0.63
116	H	4-pyridylmethyl	pentan-3-yl	46.4 ± 13.7% @20μM
117	H	4-phenylbenzyl	pentan-3-yl	88.3 ± 24.3% @10μM
118	H	4-pyridylmethyl	1,3-dihydroxy-prop-2-yl	64.8 ± 0.4 % @5μM
119	H	4-phenylbenzyl	1,3-dihydroxy-prop-2-yl	4.0
120	H	4-pyridylmethyl	(*R*)-*sec*-but-2-yl	2.4
121	H	4-pyridylmethyl	(*S*)-*sec*-but-2-yl	4.4
122	H	4-phenylbenzyl	(*R*)-*sec*-but-2-yl	38.8 ± 3.7% @5μM
123	H	4-phenylbenzyl	(*S*)-*sec*-but-2-yl	36.7 ± 7.6% @5μM
124	H	4-pyridylmethyl	hydroxyethyl	62.7 ± 7.3% @5μM
125	H	4-phenylbenzyl	hydroxyethyl	2.4
126	H	4-pyridylmethyl	N^1-Boc-aminoeth-2-yl	60.0 ± 9.6%@10μM
127	H	4-phenylbenzyl	N^1-Boc-aminoeth-2-yl	82.3 ± 8.4% @2.5μM
144	H	4-pyridylmethyl	1-aminoeth-2-yl (TFA salt)	55.1 ± 6.9% @5μM
145	H	4-phenylbenzyl	1-aminoeth-2-yl (TFA salt)	31.6 ± 0.2% @5μM[b]
128	H	4-pyridylmethyl	cyclohexyl	2.8
129	H	4-phenylbenzyl	cyclohexyl	43.7 ± 16.3% @5μM
130	H	4-pyridylmethyl	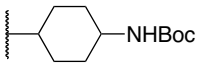	46.9 ± 3.1% @5μM
131	H	4-phenylbenzyl	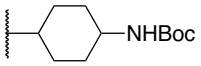	34.6 ± 13.6% @5μM[c]
146	H	4-pyridylmethyl	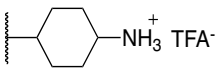	3.4
147	H	4-phenylbenzyl	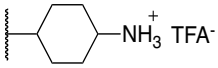	2.3
132	H	4-pyridylmethyl	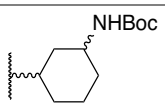 1,3-trans mixture	55.0 ± 2.0% @5μM
133	H	4-pyridylmethyl	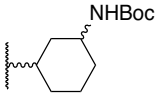 1,3-cis mixture	1.7

134	H	4-phenylbenzyl	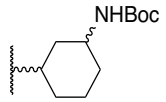 1,3-trans mixture	57.3 ± 15.3% @5μM
135	H	4-phenylbenzyl	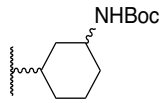 1,3-cis mixture	0.80
148	H	4-pyridylmethyl	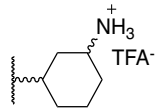 1,3-trans mixture	44.8 ± 9.3% @5μM
149	H	4-pyridylmethyl	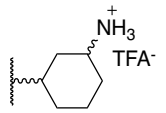 1,3-cis mixture	66.6 ± 3.8% @5μM
150	H	4-phenylbenzyl	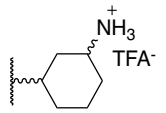 1,3-trans mixture	3.5
151	H	4-phenylbenzyl	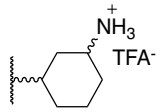 1,3-cis mixture	2.3
139	H	4-phenylbenzyl	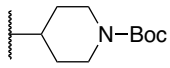	65.2 ± 21.9% @5μM
154	H	4-pyridylmethyl	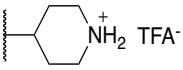	68.9 ± 11.7% @5μM
155	H	4-phenylbenzyl	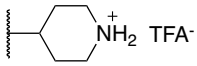	3.8
140	H	4-pyridylmethyl	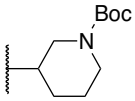	61.3 ± 10.8% @5μM
141	H	4-phenylbenzyl	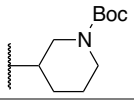	19.5 ± 1.5% @5μM[c]
156	H	4-pyridylmethyl	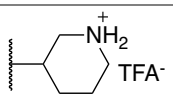	51.9 ± 14.2% @5μM
157	H	4-phenylbenzyl	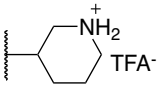	5.2

[a]GSK-3β inhibition data obtained with LANCE® *Ultra* kinase assay; single-dose values are reported as the mean of two independent experiments ± SD; [b]IC_{50} not determinable, false positive at the single-dose screening; [c]IC_{50} not calculated due to solubility issue.

As shown in **Table 5**, the presence of the free amino group at the 7-position of TT scaffold, as in compounds **101** and **102**, led to inactive compounds towards GSK-3β, while the presence of a cycloalkylamino group, such as the cyclohexylamino one, allowed a recovery of inhibitory activity [**113**, IC_{50}(GSK-3β)= 5.8 μM], although less effective than aromatic systems [**112**, IC_{50}(GSK-3β)= 6.0 μM *vs.* **105**, IC_{50}(GSK-3β)= 2.2 μM]. In fact, the most

interesting results were obtained with the introduction of the 3-pyridylmethylamino group at the 7-position, that led to the most potent GSK-3β inhibitor of the series, with an IC_{50} value in the sub-micromolar range [**115**, IC_{50}(GSK-3β)= 0.63 μM]. It is worth noting how the position of the nitrogen in the pyridyl moiety influenced the affinity towards the kinase: in fact, the 3-pyridylmethyl derivative **114** resulted almost three times more potent than then 4-pyridylmethyl compound **104** [**114**, IC_{50}(GSK-3β)= 1.4 μM *vs.* **104**, IC_{50}(GSK-3β)= 4 μM], and in the case of (S-)2-aminobutan-1-ol derivatives the difference was even more than one order of magnitude [**115**, IC_{50}(GSK-3β)= 0.63 μM *vs.* **110**, IC_{50}(GSK-3β)= 7 μM].

Concerning 5-position, the effect of the substituent on the affinity of TT derivatives towards the enzyme was evaluated maintaining at the 7-position the two most effective groups, which emerged from the preliminary series of compounds (**103-108**), the 4-pyridylmethylamino and the 4-phenylbenzylamino groups.

Definitely, the presence of the hydroxyl group of 2-aminobutanol is important for the interaction with GSK-3β pocket, since its replacement with a methyl led to poorly active compounds (**116** and **117**); this suggests the formation of a hydrogen bond between the hydroxyl group and one of the amino acid residues within the kinase ATP binding pocket. However, the introduction of a second hydroxyl group on the chain led to derivatives **118** and **119** with comparable IC_{50} values in respect to reference compounds [**119**, IC_{50}(GSK-3β)= 4 μM *vs.* **105**, IC_{50}(GSK-3β)= 2.2 μM]. Nevertheless, the complete removal of the hydroxyl group, with the consequent shortening of the chain, led again to inhibitors with IC_{50} values in the micromolar range (**120-123**). In all these cases, when both enantiomers of optically active compounds were synthetized, no differences in the inhibitory activity towards GSK-3β were detected, thus revealing no enantioselective interactions with the ATP-binding pocket.

The removal of the ramification of the chain at the 5-position (**124**, **125**) and the substitution of the hydroxyl group with an amino one (**144**, **145**) did not lead to any remarkable result compared to inhibitory activities of **104** and **105**.

The further synthetized derivatives (**128-135, 139-141, 146-151, 154-157**) were designed to elucidate the effect of introducing at the 5-position cyclic substituents bearing or not H-bond donor groups. In particular, the cyclohexyl derivative **128**, even not presenting any polar groups attached to the alkylic ring, showed a slightly improved activity than that of compound **104**, while it resulted certainly more active in comparison to the pentan-3-yl derivative **116** [**104**, IC_{50}(GSK-3β)= 4 μM *vs.* **128**, IC_{50}(GSK-3β)= 2.8 μM *vs.* **116**, IC_{50}(GSK-3β)~20 μM]. Then, an amino group at the 4- or 3-position of the cyclohexyl ring was introduced, and also the *N*-Boc intermediates were assayed on GSK-3β. Concerning the 4-substituted cyclohexyl derivatives (**130-131, 146-147**), free amino derivatives (**146**, **147**) showed IC_{50} values in the micromolar range, comparable to those of cyclohexyl derivative **128** and reference compound **104** [**104**, IC_{50}(GSK-3β)= 4 μM *vs.* **128**, IC_{50}(GSK-3β)= 2.8 μM *vs* **146**, IC_{50}(GSK-3β)= 3.4 μM]. In the case of the 3-substituted cyclohexyl derivatives, we managed to resolve the 1,3-trans and the 1,3-cis racemic mixtures and assayed them separately. Concerning the *N*-Boc derivatives, we can notice a substantial difference in affinity with the kinase between 1,3-trans (**132,134**) and the 1,3-cis (**133-135**), with the latters presenting better IC_{50} value [**132**, IC_{50}(GSK-3β)> 5 μM *vs.* **133**, IC_{50}(GSK-3β)= 1.7 μM; **134**, IC_{50}(GSK-3β)> 5 μM *vs.* **135**, IC_{50}(GSK-3β)= 0.80 μM]. This may reflect a steric control of the kinase-binding pocket towards the entrance of different ligands or a different pose of the two isomers within the cavity. With the removal of the *N*-Boc protecting group, the differences in inhibitory activity between the isomers were bridged [**150**, IC_{50}(GSK-3β)= 3.5 μM *vs.* **151**, IC_{50}(GSK-3β)= 2.3 μM], while the effect of the substituent at the 7-position of the TT scaffold emerged: in fact, in this case, the 4-phenylbenzylamino moiety resulted better

than the 4-pyridylmethylamino group [**149**, IC_{50}(GSK-3β)> 5 μM *vs.* **151**, IC_{50}(GSK-3β)= 2.3 μM]. However, it is worth noting that *N*-Boc derivative **135** resulted more potent than the corresponding free amino derivative **151** [**135**, IC_{50}(GSK-3β)= 0.80 μM *vs.* **151**, IC_{50}(GSK-3β)= 2.3 μM], and in general one of the best results achieved in this part of the work.

Finally, we decided to move the amino group in endocyclic position, thus introducing at the 5-position *N*-Boc protected 3-amino or 4-aminopiperidines. All the 7-(4-pyridylmethylamino) derivatives assayed (**154**, **140**, **156**) presented IC_{50} values in the range of 5-10 μM, while, even in this case, the 4-phenylbenzylamino derivatives (**155**, **141**, **157**) resulted more active. However, retaining the amino group within the alkylic ring did not improve the affinity of these compounds towards GSK-3β.

From this series of novel triazolo-triazines emerged in particular two derivatives as promising GSK-3β inhibitors: compound **115**, characterized by the presence of the 3-pyridylmethylamino group at the 7-position of the TT scaffold, and **135**, the 1,3-cis racemic mixture of isomers bearing the *N*-Boc-3-aminocyclohexylamino moiety at the 5-position. So, we decided to converge these two substitutions on the TT scaffold, to verify if they could exert a synergistic effect on the affinity towards GSK-3β (**136-137, 152-153**). Then, with the aim of investigating the role of the *N*-Boc protecting group in the interaction with the kinase and with the purpose of having a more metabolically stable compound, we replaced the *tert*-butyloxycarbamate with a dimethyl amino group (**142**). Finally, to complete our SAR analysis we masked the hydroxyl group of the 2-aminobutan-1-ol chain of compounds **114** and **115** with a methyl ether, to elucidate if the oxygen atom could act only as H-bond donor or also as an acceptor (**143**) (**Figure 27**).

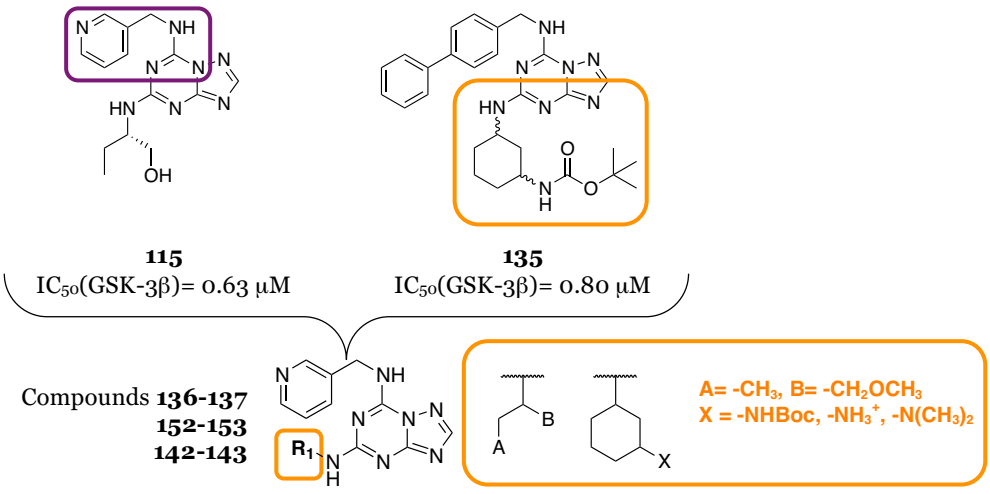

Figure 27. Second generation of TTs as GSK-3 inhibitors (**136-137, 152-153, 142-143**).

Table 6. Inhibitory activities towards GSK-3β of compounds **136-137, 152-153, 142-143**[a]

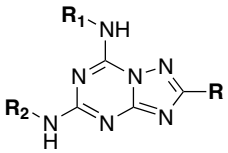

cmpd	**R**	**R₁**	**R₂**	%residual activity (GSK-3β) @10 μM[a]
136	H	3-pyridylmethyl	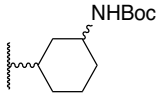 1,3-trans mixture	82.9 ±9.2%
137	H	3-pyridylmethyl	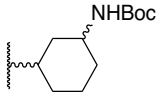 1,3-cis mixture	22.0 ±0.6%
152	H	3-pyridylmethyl	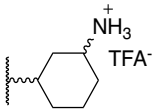 1,3-trans mixture	100%
153	H	3-pyridylmethyl	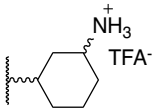 1,3-cis mixture	88.9 ±5.5%
142	H	3-pyridylmethyl	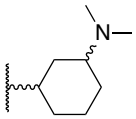 1,3-trans/1,3-cis mixture 1:3 ratio	100%
143	H	3-pyridylmethyl	(*R*),(*S*)-1-methoxy-but-2-yl	50.7 ±0.2%

[a]GSK-3β inhibition data obtained with LANCE® *Ultra* kinase assay, expressed ±SD (n=2).

Results reported in **Table 6** confirmed a positive effect of *N*-Boc-3-aminocyclohexylamino moiety at the 5-position of TT scaffold on the affinity towards GSK-3β, but limited to the 1,3-cis racemic mixture of isomers. In fact, as it happens with compounds **132-135**, a substantial difference in inhibitory potency was detected between the 1,3-cis (**137**) and the 1,3-trans (**136**) mixture of isomers [**136**, GSK-3β residual activity at 10 μM: 82.9% *vs.* **137**, GSK-3β residual activity at 10 μM: 22.0%]. However, the synergistic effect we were aiming to, with the introduction of the *N*-Boc-3-aminocyclohexylamino moiety at the 5-position and the 3-pyridylmethylamino group at the 7-position, could be evaluated once obtained the IC_{50} value; it will also allow a comparison between derivative **137** and the 4-phenylbenzylamino (**135**) and the 4-pyridylmethylamino (**133**) derivatives.

Again, the deprotected derivative **153** resulted less active than the *N*-Boc protected derivative **137** [**153**, GSK-3β residual activity at 10 μM: 88.9% *vs.* **137**, GSK-3β residual activity at 10 μM: 22.0%]. Similarly, the replacement of the *tert*-butyloxycarbamate moiety with a dimethyl amino group (**142**) resulted detrimental in terms of potency [**142**, GSK-3β residual activity at 10 μM: 100% *vs.* **137**, GSK-3β residual activity at 10 μM: 22.0%]. In this case, it is correct to point out that a mixture of 1,3-cis and 1,3-trans isomers was tested on the

kinase, but, to really assess a detrimental effect of *N,N*-dimethylamino group on inhibition of GSK-3β, the 1,3-cis isomers should be isolated and tested alone. Finally, the methoxy derivative **143** showed a certain activity towards GSK-3β (residual activity at 10 μM: 50.7%); however the corresponding 2-aminobutan-1-ol chain, as present in compound **115** [IC_{50}(GSK-3β)= 0.63 μM], remains one of the most likely substituents for pursuing GSK-3β inhibition.

3.2.3 Kinetic Assays on GSK-3β

To experimentally confirm the inhibitory mechanism of triazolo-triazine derivatives towards GSK-3β, enzymatic kinetic studies were performed in collaboration with the research group of Professor Ana Martinez (CIB, Madrid, ES), using the luminescence ADP-Glo™ kinase kit. In order to analyse the competition of our inhibitors with ATP, the two reference compounds **104** and **105** were chosen and kinetic experiments were performed by varying concentrations of both ATP [from 1 to 50 μM, ATP(K_m)= 13 μM[169]] and inhibitors (**104**, from 5 to 10 μM; **105**, from 2.5 to 5 μM), while the kinase substrate was kept constant (GS-2, 12.5 μM). Concentrations were chosen taking in consideration the affinity of ligands towards the enzyme. The Lineweaver-Burk plots are shown in **Figure 28**, and in both **104** and **105** the intercept of the plot in the vertical axis (1/V) does not change when the concentration of compounds increases, which means that these compounds act as ATP competitive inhibitors of GSK-3β, in agreement with our starting hypothesis.

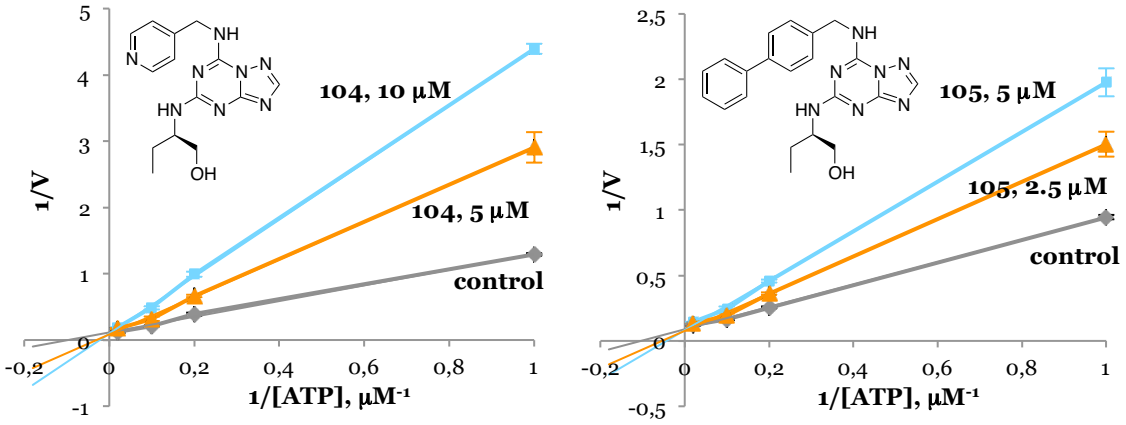

Figure 28. Double-reciprocal plots for compounds **104** and **105**.

3.2.4 Prediction of CNS permeation

As mentioned before, since GSK-3β is considered a potential target for therapeutic intervention in CNS diseases and one of the main obstacles for the treatment of the diseases of the CNS is the drug's penetration into the BBB at therapeutic concentrations,[225] we decided to apply the Parallel Artificial Membrane Permeability Assay (PAMPA) to predict the BBB-permeability of the triazolo-triazine derivatives for which IC_{50} values were determined.[229] Following the PAMPA methodology, as described in detail in the Experimental Section 3.4.2.2, a good correlation between experimental and reported values was obtained *Pe* (exp)= 0.9422 (bibl) + 0.9285 (R^2= 0.9822) (**Figure 29**).

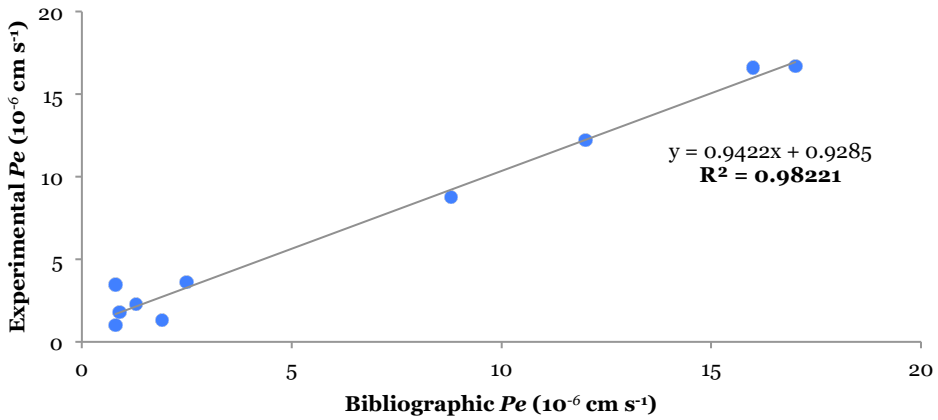

Figure 29. Linear correlation between experimental and reported permeability of commercial drugs using the PAMPA-BBB assay.

The *in vitro* permeabilities (*Pe*) of commercial drugs through lipid membrane extract (porcine brain lipid) together with our selected compounds were determined and described in **Table 7**. For each experiment, according to the values described in the literature for BBB permeation prediction in humans[235], where the value of $4 \cdot 10^{-6}$ cm/s is considered the lower limit to establish the compounds permeable to BBB and $2 \cdot 10^{-6}$ cm/s the limit to establish derivatives not able to cross the blood-brain barrier, it is possible to calculate from the equation of calibration curve the corresponding experimental *Pe* limits. Thus, in this experiment, we were able to classify compounds as CNS permeable (CNS+) when they present a permeability > 4.7 x 10^{-6} cm s^{-1} and CNS not-permeable (CNS-) when they present a permeability < 2.8 x 10^{-6} cm s^{-1}. Values between these two limits are in the zone of uncertainty and therefore for these compounds an univocal prediction cannot be given (CNS-/+). Based on these results we can consider that seven of the assayed compounds resulted able to cross the BBB by passive permeation (**Table 7**), including **135** [IC_{50}(GSK-3β)= 0.80 μM], one of the most promising derivatives. We can notice that all the CNS+ derivatives present at the 7-position of the TT scaffold the 4-phenylbenzylamino moiety that confers them the right apolar character, with the exception of derivative **106**, which instead brings an additional phenyl ring at the 2-position.

Table 7. Permeability (*Pe* 10^{-6} cm s^{-1}) in the PAMPA-BBB assay of 10 commercial drugs (used in the experiment validation) and different compounds with their predictive penetration in the CNS.

compd	Bibl.[229]	*Pe* (10^{-6} cm s^{-1})[a]	Prediction	compd	Bibl.[229]	*Pe* (10^{-6} cm s^{-1})[a]	Prediction
Atenolol	0.8	1.0 ± 1.3		**113**		1.0 ± 0.08	**CNS-**
Caffeine	1.3	2.3 ± 1.0		**114**		1.9 ± 0.2	**CNS-**
Desipramine	12	12.2 ± 2.9		**115**		2.7 ± 0.2	**CNS-**
Enoxacin	1.6	1.8 ± 0.7		**119**		4.0 ±0.11	**CNS-/+**
Hydrocortisone	2.4	1.3 ± 0.5		**121**		3.5 ±0.04	**CNS-/+**
Ofloxacine	0.8	3.4 ± 0.07		**120**		3.7 ±0.07	**CNS-/+**
Piroxicam	2.5	3.6 ± 0.2		**125**		8.9 ±0.71	**CNS+**
Promazine	8.8	8.8 ± 1.0		**128**		3.2 ±0.07	**CNS-/+**
Testosterone	17	16.7 ± 0.5		**146**		4.2 ±0.11	**CNS-/+**
Verapamil	16	16.6 ± 3.7		**147**		3.7 ±1.75	**CNS-/+**
103[b]		1.5 ± 0.5	**CNS-**	**133**		3.1 ±0.54	**CNS-/+**
104[b]		0.8 ± 0.02	**CNS-**	**135**		15.3 ±0.44	**CNS+**
105[b]		13.5 ± 1.3	**CNS+**	**150**		4.7 ± 0.7	**CNS+**
106		6.1 ±0.83	**CNS+**	**151**		4.5 ±0.57	**CNS-/+**
110		3.0 ±0.45	**CNS-/+**	**155**		4.7 ± 0.4	**CNS+**
111		5.1 ±0.36	**CNS+**	**157**		4.1 ±1.63	**CNS-/+**
112		1.4 ±1.66	**CNS-**				

[a]Data are the mean ± SD of 2 independent experiments. [b]Data obtained in a different experiment: *Pe*(exp)= 1.2156 (bibl) - 0.8366 (R^2= 0.9679), CNS + ≥ 4.0, CNS - ≤ 1.6

3.3 CONCLUSIONS

In conclusion, we have validated the 1,2,4-triazolo[1,5-*a*][1,3,5]triazine byciclic system as suitable scaffold for the development of novel ATP-competitive GSK-3β inhibitors. In fact, the initial introduction on the TT ring of functional groups characterizing the Roscovitine-like kinase inhibitors and then the further decoration of the scaffold led to a new series of GSK-3β inhibitors with IC_{50} values in the micromolar range and a first SAR for this nucleus (**Figure 30**). In particular, we focused on nucleophilic substitutions with different primary amines at 7- and 5-positions, while 2-position needed to remain unsubstituted. Concerning 7-position, substitutions are required to obtain stabilizing interactions with the kinase binding pocket. In general, arylmethylamino groups are well tolerated, with the most interesting results achieved with the 3-pyridylmethylamino group (as in compound **115** [IC_{50}(GSK-3β)= 0.63 μM]) or with the 4-phenylbenzylamino one (as in **135** [IC_{50}(GSK-3β)= 0.80 μM]). A deeper investigation at the 5-position was carried out, introducing various alkyl chains of different lengths and nature or cycloalkyl groups. The 2-aminobutan-1-ol chain, borrowed from Roscovitine (**81**), was confirmed suitable to reach good affinities towards GSK-3β. Shorter or not-branching chains led in some cases (compounds **121** and **125**) to comparable results. The introduction of cyclohexyl substituents led to controversial results but, in general, we can see that a substitution at the 3-position of the ring with an amino (**151**) or even better with a *N*-Boc-amino group (**133, 135**, **137**) led to good GSK-3β inhibitors. Notably, interactions between the *N*-Boc-3-aminocyclohexyl moiety at the 5-position and the enzyme resulted to be stereoselective, with 1,3-cis racemic mixture of isomers significantly preferred to 1,3-trans ones.

Interestingly, some of the most active derivatives (IC_{50} <10 μM) resulted to be able to pass the blood-brain barrier (BBB) according to the PAMPA assay, an essential feature for all those drugs that target CNS diseases. In particular, the positive result achieved by compound **135** emerged, which showed a good affinity towards GSK-3β (IC_{50}= 0.80 μM) and also a high permeability value (*Pe*= $15.3 \cdot 10^{-6}$ cm·s^{-1}), thus representing a good candidate on the chance of *in vitro* studies with neurodegenerative disease models.

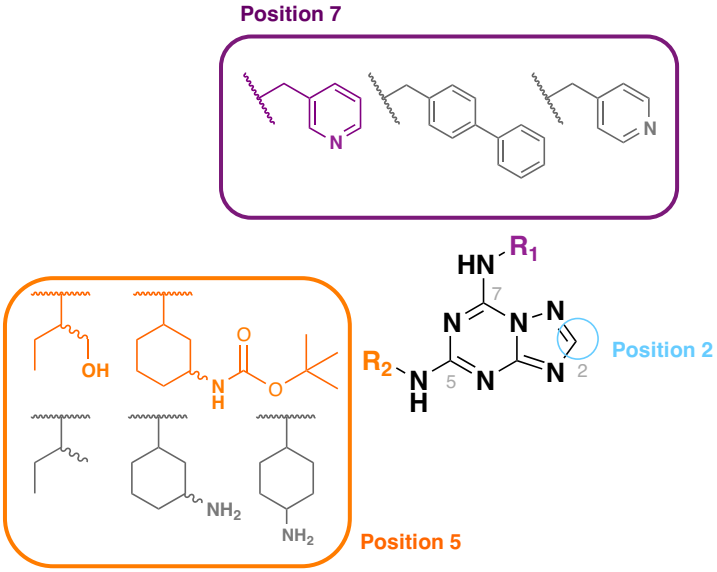

Figure 30. Schematic SAR of triazolo-triazines as GSK-3β inhibitors.

3.4 EXPERIMENTAL SECTION

3.4.1 Chemistry

3.4.1.1 General material and methods used in the synthetic process

Reagents were obtained from commercial suppliers and used without further purification. Reactions were monitored by TLC, on precoated silica gel plates (Macherey-Nagel, $60F_{UV254}$) or aluminium oxide plates (Macherey-Nagel, $60N_{UV254}$). Final compounds and intermediates were purified by flash chromatography using as stationary phases silica gel (Macherey-Nagel, silica 60, 240-400 mesh) or aluminium oxide (Macherey-Nagel, aluminium oxide 90 neutral, 50–200 μm). When used, light petroleum ether refers to the fractions boiling at 40-60°C. Melting points were determined with a Stuart SMP10 melting point apparatus and were not corrected. The ^{1}H NMR and ^{13}C NMR spectra were determined in $CDCl_3$, DMSO-d_6, D_2O, acetone-d_6 or DMF-d_7 solutions and recorded on Jeol GX 270 MHz, Jeol 400 MHz, Varian 400 MHz or Varian 500 MHz spectrometers; chemical shifts (δ scale) are reported in parts per million (ppm) and referenced to residual solvent peak, with splitting patterns abbreviated to: s (singlet), d (doublet), dd (doublet of doublets), dt (doublet of triplets), t (triplet), m (multiplet) and bs (broad signal). Coupling constants (*J*) are given in Hz. MS-ESI analysis were performed using ESI Bruker 4000 Esquire spectrometer.

Compound purities were determined by HPLC-DAD (*Waters* 515 HPLC pump; *Waters* PDA 2998 Detector) using Luna C8(2) HPLC column (150 x 4.6 mm, particle size 3 μm). Isocratic elution was performed for 40 min at a flow rate of 300 μL/min in water-methanol 30:70 either containing 2 mM ammonium acetate. UV absorption was detected from 200 to 400 nm using a diode array detector; purity was determined at maximum absorption wavelength of compound and at 254 nm. All compounds showed a purity >95% at the detected wavelengths.

3.4.1.2 Synthesis of compounds 101-157

Synthesis of 2,4,6-triphenoxy-[1,3,5]triazine (**159**)

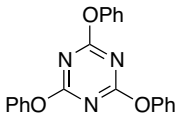

A mixture of 2,4,6-trichloro-[1,3,5]triazine (**158**, 184.4 g, 1.0 mol) was dissolved in phenol (3.0-4.0 mol) and refluxed for 5h. The hot reaction was extracted with methanol and a white solid (253.7 g) was obtained. Yield 71%; mp 235°C (EtOAc-light petroleum); ^{1}H NMR (270 MHz, $CDCl_3$): δ 7.39 (m, 6H), 7.32–7.22 (m, 3H), 7.17 (m, 6H).

Synthesis of (4,6-diphenoxy-[1,3,5]triazin-2-yl)-hydrazine (**160**)

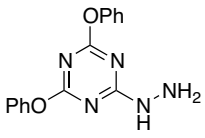

To a solution of 2,4,6-triphenoxy-[1,3,5]triazine (**159**, 20 g, 0.056 mol) in DCM (200 mL), hydrazine monohydrate (3.3 mL, 0.067 mol) in 20 mL of THF was added dropwise and the reaction was stirred overnight. The solvent was removed, the residue suspended in methanol and EtOAc and precipitated with light petroleum and used in the next step without further purification (yield 72%, 23.0 g).

Synthesis of *N*'-(4,6-diphenoxy-[1,3,5]triazin-2-yl)-formohydrazide (**161**)

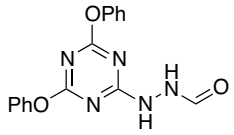

Formic acid (15.5 mL, 0.41 mol) was added dropwise to a solution of compound **160** (12.0 g, 0.041 mol) in toluene (50 mL). The biphasic mixture was stirred for 4h at room temperature, then volatiles were removed under vacuum and the residue was purified by gradient elution flash chromatography (DCM to DCM-MeOH 98:2). Yield 69% (9.2 g); white solid; mp 192-193°C (EtOEt-light petroleum); ^{1}H NMR (400 MHz, DMSO-d_6): δ 10.05 (s, 1H), 9.92 (s, 1H), 8.00 (s, 1H), 7.47–7.36 (m, 4H), 7.35–7.09 (m, 6H). ES-MS (methanol) m/z: 324.1 $[M+H]^+$, 346.1 $[M+Na]^+$.

3.4.1.2.1 General procedure (I) for the synthesis of hydrazide derivatives

To a solution of the desired ester (0.1 mol) in ethanol (500 mL), hydrazine hydrate (0.3-0.5 mol) was added and the solution heated under reflux for 24-72 h. When the reaction terminated, the solvent was removed under reduced pressure and the residue purified by flash chromatography or filtrated and washed with EtOEt and methanol.

Synthesis of benzoic hydrazide (**163**)

Flash chromatography eluent: EtOAc-light petroleum 9:1 to EtOAc-MeOH 9:1. Yield 62%

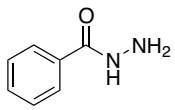

(8.4 g); white solid; mp 112-114°C (EtOEt-light petroleum); ^{1}H NMR (270 MHz, DMSO-d_6): δ 9.77 (s, 1H), 7.82 (d, J = 7.0 Hz, 2H), 7.60 – 7.29 (m, 3H), 4.58 (s, 2H). ES-MS (methanol) m/z: 137.4 $[M+H]^+$, 159.3 $[M+Na]^+$.

3.4.1.2.2 General procedure (II) for the preparation of substituted *N*'-(4,6-diphenoxy-1,3,5-triazin-2-yl)hydrazides

2,4,6-triphenoxy-[1,3,5]triazine (**159**, 10.0 g, 0.028 mol) and the required hydrazide (0.0476 mmol) were dissolved in anhydrous THF (200 mL) while DBU (7.1 mL, 0.0476 mmol) was added dropwise at 0°C. The mixture was stirred at room temperature for 12 h. The solvent was then removed, the residue was dissolved in DCM (300 mL), and the resulting solution washed with water (3x100 mL). The organic layer was dried over anhydrous sodium sulphate, concentrated and purified by flash chromatography.

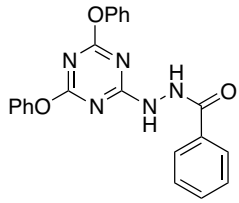

N'-(4,6-diphenoxy-1,3,5-triazin-2-yl)benzohydrazide (**164**)
Flash chromatography eluent: DCM-EtOAc 95:5. Yield 62% (4.95 g); white solid; mp 204-207°C (EtOEt-light petroleum); ^{1}H NMR (270 MHz, $CDCl_3$): δ 8.54 (s, 1H), 7.66 (d, J = 7.6 Hz, 2H), 7.52 (q, J = 7.0 Hz, 1H), 7.46 – 7.31 (m, 4H), 7.31 – 7.19 (m, 4H), 7.11 (dd, J = 12.8, 7.8 Hz, 5H). ES-MS (methanol) m/z: 400.3 $[M+H]^+$, 422.2 $[M+Na]^+$, 438.2 $[M+K]^+$.

3.4.1.2.3 General procedure (III) for the preparation of the 5,7-diphenoxy-[1,2,4]triazolo[1,5-*a*][1,3,5]triazines

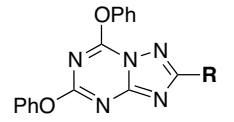

R = H (**165**), Ph (**166**)

The mixture of phosphorous pentoxyde [0.045 mol (procedure **III$_a$**) or 0.075 mol (procedure **III$_b$**)] and hexamethyldisiloxane [0.045 mol (procedure **III$_a$**) or 0.075 mol (procedure **III$_b$**)] in anhydrous xylene (150 mL) was heated to 90°C over 1.5 hours and then stirred for 1 hour at 90°C, under argon atmosphere. The well-dried *N*'-(4,6-diphenoxy-1,3,5-triazin-2-yl)hydrazides (0.015 mol) were then added to the clear solution and the

temperature increased to reflux and stirred for 2-3 hours. The solvent was then removed, the residue dissolved in DCM (300 mL) and the resulting solution was washed with water (3x100 mL). The organic layer was dried over anhydrous sodium sulphate, concentrated and purified to afford the desired compounds.

5,7-diphenoxy-[1,2,4]triazolo[1,5-*a*][1,3,5]triazine (**165**)
Procedure **III$_a$**. Purification on silica plug (3-4 cm length) in light petroleum-EtOAc 6.5:3.5. Yield 25% (1.1 g); white solid; mp 120-121°C (EtOEt-light petroleum); ^{1}H NMR (400 MHz, acetone-d_6): δ 8.41 (s, 1H), 7.60–7.49 (m, 4H), 7.48-7.40 (m, 3H), 7.31-7.21 (m, 3H). ^{13}C NMR (101 MHz, acetone-d_6): δ 165.6, 161.1, 157.6, 156.5, 153.3, 151.9, 130.8, 130.4, 128.1, 126.8, 122.36, 122.30. ES-MS (acetonitrile) m/z: 306.1 $[M+H]^+$, 328.1 $[M+Na]^+$.

2-phenyl-5,7-diphenoxy-[1,2,4]triazolo[1,5-*a*][1,3,5]triazine (**166**)
Procedure **III$_a$**. Flash chromatography eluent: DCM. Yield 75% (4.3 g); white solid; mp 246-250°C (EtOEt-light petroleum); ^{1}H NMR (270 MHz, $CDCl_3$) δ: 8.38-8.28 (m, 2H), 7.65-7.34 (m, 9H), 7.34–7.10 (m, 4H). ^{13}C NMR (68 MHz, $CDCl_3$): δ 167.36, 164.72, 160.49, 154.80, 151.83, 150.55, 131.24, 130.08, 129.62, 129.41, 128.73, 127.81, 127.52, 126.20, 121.47, 121.17. ES-MS (methanol) m/z: 382.2 $[M+H]^+$, 404.2 $[M+Na]^+$, 420.1 $[M+K]^+$.

3.4.1.2.4 General procedure (IV) for the preparation of 5-phenoxy-[1,2,4]triazolo[1,5-*a*][1,3,5]triazin-7-amines

A solution of the 5,7-diphenoxy-[1,2,4]triazolo[1,5-*a*][1,3,5]triazine derivative (2 mmol) in methanol (20 mL) with methanolic ammonia 7 N (12 mmol) was stirred for 3 hours at room temperature. The solvent was removed under reduced pressure and the residue purified by flash chromatography, when required, or directly crystallized from EtOEt-light petroleum to afford the desired compounds as solids.

5-phenoxy-[1,2,4]triazolo[1,5-*a*][1,3,5]triazin-7-amine (**167**)

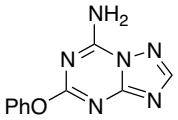

Yield 86% (0.39 g); white solid; mp 130-131°C (EtOEt-light petroleum); ^{1}H NMR (400 MHz, DMSO-d_6) δ: 9.15-8.77 (bd, 2H), 8.34 (s, 1H), 7.50-7.41 (m, 2H), 7.31-7.20 (m, 3H). ^{13}C NMR (68 MHz, DMSO-d_6): δ 165.2, 158.7, 155.5, 152.7, 152.5, 129.9, 125.7, 122.1. ES-MS (methanol) m/z: 229.4 $[M+H]^+$, 251.4 $[M+Na]^+$, 267.4 $[M+K]^+$.

3.4.1.2.5 General procedure (V) for the preparation of *N*^{7}-substituted 5-phenoxy-[1,2,4]triazolo[1,5-*a*][1,3,5]triazin-7-amines

A solution of 5,7-diphenoxy-[1,2,4]triazolo[1,5-*a*][1,3,5]triazine derivatives (2 mmol) with 6 mmol of the required amine in methanol (20 mL) was stirred at 50°C for 3 hours. The solvent was removed under reduced pressure and the residue was purified, when necessary, by flash chromatography or directly precipitated from EtOEt-light petroleum and washed with a small amount of methanol to afford the desired compounds as solids.

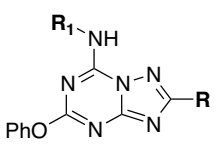

R= H (**168-172**), Ph (**173-175**)
R_1= CH_2Ph (**168, 173**)
CH_2(4-pyridyl) (**169,174**)
CH_2(4-Ph)Ph (**170,175**)
cC_6H_{11} (**171**)
CH_2(3-pyridyl) (**172**)

N-benzyl-5-phenoxy-[1,2,4]triazolo[1,5-*a*][1,3,5]triazin-7-amine (**168**)
Yield 78% (0.501 g); white solid; mp 149-151°C (EtOEt-light petroleum). ^{1}H NMR (400 MHz; DMSO-d_6): δ 8.39 (s, 1H), 7.49-7.43 (m, 2H), 7.35-7.20 (m, 9H), 4.60-4.57 (m, 2H). ^{13}C NMR (101 MHz, DMSO-d_6): δ 165.1, 158.7, 155.6, 152.7, 150.9, 138.0, 129.9, 128.8, 128.1, 127.7, 125.9, 122.3, 44.3. ES-MS (methanol) m/z: 319.5 $[M+H]^+$, 341.5 $[M+Na]^+$, 357.4 $[M+K]^+$.

N-benzyl-5-phenoxy-2-phenyl-[[1,2,4]triazolo[1,5-*a*][1,3,5]triazin-7-amine (**173**)
Yield 98% (0.773 g); white solid; mp 196°C (EtOEt-light petroleum). ^{1}H NMR (270 MHz; DMSO-d_6): δ 9.85 (m, 1H), 8.20-8.12 (m, 2H), 7.62-7.42 (m, 5H), 7.41-7.19 (m, 8H), 4.66-4.63 (m, 2H). ^{13}C NMR (101 MHz, DMSO-d_6): δ 165.1, 164.2, 159.3, 152.8, 150.8, 138.1, 131.0, 130.6, 129.9, 129.3, 128.8, 128.2, 127.7, 127.2, 125.9, 122.3, 44.3. ES-MS (methanol) m/z: 395.4 $[M+H]^+$, 417.4 $[M+Na]^+$, 433.3 $[M+K]^+$.

N-(pyridin-4-yl-methyl)-5-phenoxy-[1,2,4]triazolo[1,5-*a*][1,3,5]triazin-7-amine (**169**)
Yield 79% (0.505 g); white solid; mp 117-118°C (EtOEt-light petroleum). ^{1}H NMR (400 MHz; DMSO-d_6): δ 9.91-9.87 (m, 1H), 8.50 (dd, J = 4.4, 1.6 Hz, 2H), 8.41 (s, 1H), 7.46-7.41 (m, 2H), 7.30-7.26 (m, 3H), 7.22-7.17 (m, 2H), 4.64-4.61 (m, 2H). ^{13}C NMR (101 MHz, DMSO-d_6): δ 165.0, 158.7, 155.7, 152.7, 151.2, 150.0, 146.9, 129.9, 125.9, 122.7, 122.2, 43.3. ES-MS (methanol) m/z: 320.2 $[M+H]^+$, 342.1 $[M+Na]^+$.

N-(pyridin-4-yl-methyl)-5-phenoxy-2-phenyl-[1,2,4]triazolo[1,5-*a*][1,3,5]triazin-7-amine (**174**)
Yield 89% (0.704 g); white solid; mp 241-241°C (EtOEt-light petroleum). ^{1}H NMR (400 MHz; DMSO-d_6): δ 9.91-9.84 (m, 1H), 8.55-8.50 (m, 2H), 8.20-8.12 (m, 2H), 7.56-7.52 (m, 3H), 7.49-7.81 (m, 2H), 7.35-7.28 (m, 3H), 7.22 (d, J = 8.1 Hz, 2H), 4.68-4.62 (m, 2H). ^{13}C NMR (101 MHz, DMSO-d_6): δ 165.0, 164.3, 159.3, 152.7, 151.0, 149.9, 147.2, 131.1, 130.6, 129.9, 129.4, 127.2, 125.9, 122.9, 122.2, 43.4. ES-MS (methanol) m/z: 396.2 $[M+H]^+$, 418.1 $[M+Na]^+$, 434.2 $[M+K]^+$.

N-((1,1'-biphenyl)-4-ylmethyl)-5-phenoxy-[1,2,4]triazolo[1,5-*a*][1,3,5]triazin-7-amine (**170**)
Yield 78% (0.615 g); white solid; mp 113°C (EtOEt-light petroleum). ^{1}H NMR (400 MHz; DMSO-d_6): δ 9.94-9.90 (m, 1H), 8.40 (s, 1H), 7.66-7.59 (m, 4H), 7.52-7.21 (m, 10H), 4.63-4.60 (m, 2H). ^{13}C NMR (101 MHz, DMSO-d_6): δ 165.1, 158.7, 155.6, 152.8, 150.9, 140.3, 139.6, 137.2, 129.9, 129.4, 128.8, 127.8, 127.11, 127.06, 126.0, 122.3, 44.0. ES-MS (methanol) m/z: 395.2 $[M+H]^+$, 417.2 $[M+Na]^+$, 433.1 $[M+K]^+$.

N-((1,1'-biphenyl)-4-ylmethyl)-5-phenoxy-2-phenyl-[1,2,4]triazolo[1,5-*a*][1,3,5]triazin-7-amine (**175**)
Yield 77% (0.725 g); white solid; mp 238-240°C (EtOEt-light petroleum). ^{1}H NMR (270 MHz; DMSO-d_6): δ 9.91-9.85 (m, 1H), 8.19-8.13 (m, 2H), 7.68-7.24 (m, 17H), 4.70-4.63 (m, 2H). ^{13}C NMR (101 MHz, DMSO-d_6): δ 165.1, 164.3, 159.3, 152.8, 150.8, 143.0, 140.3, 139.7, 137.3, 130.6, 129.9, 129.4, 129.3, 128.9, 127.9, 127.2, 127.1, 127.06, 126.0, 122.3, 44.0. ES-MS (methanol) m/z: 471.2 $[M+H]^+$, 493.2 $[M+Na]^+$.

N-cyclohexyl-5-phenoxy-[1,2,4]triazolo[1,5-*a*][1,3,5]triazine-7-amine (**171**)
Flash chromatography eluent: EtOAc-light petroleum 7:3. Yield 94% (0.583 g); sticky foam; ^{1}H NMR (270 MHz; DMSO-d_6): δ 9.26-9.21 (m, 1H), 8.36 (s, 1H), 7.48-7.42 (m, 2H), 7.31-7.23 (m, 3H), 3.92-3.77 (m, 1H), 1.88-1.71 (m, 4H), 1.64-1.42 (m, 3H), 1.33-1.00 (m, 3H). ^{13}C NMR (101 MHz, DMSO-d_6): δ 165.2, 158.7, 155.3, 152.7, 149.9, 129.8, 125.9, 122.3, 51.1, 31.9, 25.3. ES-MS (methanol) m/z: 311.0 $[M+H]^+$, 333.0 $[M+Na]^+$, 348.9 $[M+K]^+$.

N-(pyridin-3-yl-methyl)-5-phenoxy-[1,2,4]triazolo[1,5-*a*][1,3,5]triazin-7-amine (**172**)
Flash chromatography eluent: DCM-EtOAC 5%. Yield 66% (0.421 g); white solid; mp 219-

221°C (EtOEt-light petroleum). ^{1}H NMR (400 MHz, DMSO-d_6): δ 9.95-9.81 (m, 1H), 8.59-8.43 (m, 2H), 8.39 (s, 1H), 7.75-7.63 (m, 1H), 7.54-7.41 (m, 2H), 7.40–7.26 (m, 2H), 7.27.7.16 (m, 2H), 4.64-4.60 (m, 2H). ^{13}C NMR (101 MHz, DMSO-d_6): δ 165.1, 158.7, 155.6, 152.7, 151.0, 149.5, 149.0, 136.0, 133.6, 129.9, 126.0, 123.9, 122.3, 42.0. ES-MS (methanol) m/z: 320.1 $[M+H]^+$, 342.0 $[M+Na]^+$.

3.4.1.2.6 General procedure (VI) for the preparation of *N*^{5}-substituted [1,2,4]triazolo[1,5-*a*][1,3,5]triazin-5,7-diamines and *N*^{5},*N*^{7}-disubstituted [1,2,4]triazolo[1,5-*a*][1,3,5]triazin-5,7-diamines

A mixture of 7-amino substituted 5-diphenoxy-[1,2,4]triazolo[1,5-*a*][1,3,5]triazine derivatives (0.3 mmol) and the required amine (0.9 mmol) in absolute ethanol (3-4 mL) was poured into a sealed tube and heated at 90-100 °C for 48-120 h. When the reaction completed, the solvent was removed under reduced pressure, the residue was purified by flash chromatography and then precipitated to afford the desired compounds as solids.

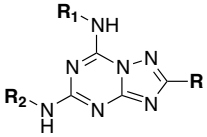

Compounds **101-143**

*R= Ph

	R₁					
R₂	H	CH_2Ph	CH_2-4-pyridyl	CH_2-Ph-4-Ph	cC_6H_{11}	CH_2-3-pyridyl
(R)-$CH(CH_2CH_3)CH_2OH$	**101**	**103,106***	**104,107***	**105,108***	**112**	**114**
(S)-$CH(CH_2CH_3)CH_2OH$	**102**	**109**	**110**	**111**	**113**	**115**
$CH(CH_2CH_3)CH_2CH_3$			**116**	**117**		
$CH(CH_2OH)_2$			**118**	**119**		
(R)-$CH(CH_2CH_3)CH_3$			**120**	**122**		
(S)-$CH(CH_2CH_3)CH_3$			**121**	**123**		
CH_2CH_2OH			**124**	**125**		
CH_2CH_2NH-Boc			**126**	**127**		
cyclohexyl			**128**	**129**		
4-(NHBoc)cyclohexyl			**130**	**131**		
3-(NHBoc)cyclohexyl			**132,133**	**134,135**		**136,137**
4-(N-Boc-piperidine)			**138**	**139**		
3-(N-Boc-piperidine)			**140**	**141**		
4-($N(CH_3)_2$cyclohexyl)						**142**
(R,S)-$CH(CH_2CH_3)CH_2OCH_3$						**143**

(R)-2-((7-amino-[1,2,4]triazolo[1,5-*a*][1,3,5]triazin-5-yl)amino)butan-1-ol (**101**)
Flash chromatography eluent: EtOAc-MeOH 98:2. Yield 20% (13 mg); white solid; mp 180-187°C (EtOEt-light petroleum). ^{1}H NMR (400 MHz, DMSO-d_6): δ 8.63-7.70 (m, 3H), 7.17-6.83 (m, 1H), 4.64 (bs, 1H), 3.84 (bs, 1H), 3.44 (bs, 2H), 1.73-1.55 (m, 1H), 1.51-1.31 (m, 1H), 0.98-0.75 (m, 3H). ES-MS (methanol) m/z: 224.4 $[M+H]^+$, 246.3 $[M+Na]^+$.

(*R*)-2-((7-(benzylamino)-[1,2,4]triazolo[1,5-*a*][1,3,5]triazin-5-yl)amino)butan-1-ol (**103**)
Flash chromatography eluent: DCM-MeOH 97.5:2.5. Yield 21% (20 mg); white solid; mp 146-149°C (EtOEt-light petroleum). ^{1}H NMR (270 MHz; DMSO-d_6): δ 9.20 + 9.00 (bs, 1H), 8.10 + 8.06 (s, 1H), 7.44-7.13 (m, 6H), 4.72-4.55 (m, 3H), 3.91-3.80 (m, 1H), 3.50-3.27 (m, 2H), 1.70-1.34 (m, 2H), 0.90-0.75 (m, 3H). ES-MS (methanol) m/z: 314.2 $[M+H]^+$, 336.2 $[M+Na]^+$.

(*R*)-2-((7-((pyridin-4-ylmethyl)amino)-[1,2,4]triazolo[1,5-*a*][1,3,5]triazin-5-yl)amino)butan-1-ol (**104**)
Flash chromatography eluent: EtOAc-MeOH 99:1. Yield 41% (39 mg); white solid; mp 200-

202°C (EtOEt-light petroleum). ^{1}H NMR (400 MHz; DMSO-d_6, 90°C): δ 8.82 (bs, 1H), 8.53-8.58 (m, 2H), 8.04 (s, 1H), 7.38-7.34 (m, 2H), 6.77 (d, J = 8.2 Hz, 1H), 4.73-4.60 (m, 2H), 4.34-4.27 (m, 1H), 3.90–3.79 (m, 1H), 3.52–3.37 (m, 2H), 1.69-1.54 (m, 1H), 1.52-1.38 (m, 1H), 0.84 (t, J = 6.6 Hz, 3H). ES-MS (methanol) m/z: 315.1 $[M+H]^+$, 337.1 $[M+Na]^+$.

(R)-2-((7-(([1-1'-biphenyl]4-ylmethyl)amino)-[1,2,4]triazolo[1,5-*a*][1,3,5]triazin-5-yl)amino)butan-1-ol (**105**)
Flash chromatography eluent: DCM-MeOH 98:2. Yield 34% (40 mg); white solid; mp 192°C (EtOEt-light petroleum). ^{1}H NMR (400 MHz; DMSO-d_6): δ 9.24 + 9.06 (bs, 1H), 8.11 + 8.07 (s, 1H), 7.68-7.13 (m, 10H), 4.76-4.56 (m, 3H), 3.94-3.78 (m, 1H), 3.52-3.33 (m, 2H), 1.72-1.31 (m, 2H), 0.90-0.74 (m, 3H). ES-MS (methanol) m/z: 388.1 $(M-H)^-$.

(*R*)-2-((7-(benzylamino)-2-phenyl-[1,2,4]triazolo[1,5-*a*][1,3,5]triazin-5-yl)amino)butan-1-ol (**106**)
Flash chromatography eluent: DCM-MeOH 97:3. Yield 46% (54 mg); white solid; mp 204-206°C (EtOEt-light petroleum). ^{1}H NMR (400 MHz; DMSO-d_6): δ 9.19 + 8.89 (bs, 1H), 8.14 + 8.11 (s, 1H), 7.53-7.25 (m, 10H), 4.66-4.65 (m, 3H), 3.97-3.79 (m, 1H), 3.56-3.25 (m, 2H), 1.71-1.53 (m, 1H), 1.52-1.32 (m, 1H), 0.91-0.78 (m, 3H). ES-MS (methanol) m/z: 390.2 $[M+H]^+$, 412.2 $[M+Na]^+$, 428.1 $[M+K]^+$.

(*R*)-2-((7-((pyridin-4-ylmethyl)amino)-2-phenyl-[1,2,4]triazolo[1,5-*a*][1,3,5]triazin-5-yl)amino)butan-1-ol (**107**)
Flash chromatography eluent: DCM-MeOH 97:3. Yield 44% (51 mg); white solid; mp 271°C (EtOEt-light petroleum). ^{1}H NMR (400 MHz, DMSO-d_6, 90°C): δ 8.78 (bs, 1H), 8.52 (d, J = 5.6 Hz, 2H), 8.15-8.12 (m, 2H), 7.54-7.47 (m, 3H), 7.40 (d, J = 5.5 Hz, 2H), 6.85-6.80 (m, 1H), 4.74-4.68 (m, 2H), 4.35-4.31 (m, 1H), 3.90-3.84 (m, 1H), 3.53-3.41 (m, 2H), 1.67-1.46 (m, 2H), 0.92-0.83 (m, 3H). MS (methanol) m/z: 391.2 $[M+H]^+$, 413.2 $[M+Na]^+$, 429.2 $[M+K]^+$.

(*R*)-2-((7-(([1-1'-biphenyl]4-ylmethyl)amino)-2-phenyl-[1,2,4]triazolo[1,5-*a*][1,3,5]triazin-5-yl)amino)butan-1-ol (**108**)
Flash chromatography eluent: DCM-EtOAc gradient from 95:5 to 85:15. Yield 16% (22 mg); white solid; mp 244°C (EtOEt-light petroleum). ^{1}H NMR (270 MHz; DMSO-d_6): 9.21 + 9.02 (bs, 1H), 8.12 + 8.09 (s, 2H), 7.77-7-41 (m, 12H), 7.40-7.20 (m, 1H), 4.77-4.62 (m, 3H), 3.94-3.84 (m, 1H), 3.58-3.30 (m, 2H), 1.69-1.60 (m, 1H), 1.49-1.40 (m, 1H), 0.94-0.78 (m, 3H). MS (methanol) m/z: 466.3 $[M+H]^+$, 488.2 $[M+Na]^+$, 504.2 $[M+K]^+$.

(R)-2-((7-(cyclohexylamino)-[1,2,4]triazolo[1,5-*a*][1,3,5]triazin-5-yl)amino)butan-1-ol (**112**)
Flash chromatography eluent: DCM-MeOH 97:3. Yield 50% (46 mg); white solid; mp 147-151°C (EtOEt-light petroleum). ^{1}H NMR (400 MHz, DMSO-d_6, 90°C): δ 7.99 (s, 1H), 7.77 (bs, 1H), 6.74-6.70 (m, 1H), 4.32 (bs, 1H), 3.98-3.86 (m, 2H), 3.56-3.49 (m, 2H), 1.93-1.90 (m, 2H), 1.80-1.72 (m, 2H), 1.72-1.62 (m, 2H), 1.60-1.47 (m, 3H), 1.39-1.27 (m, 2H), 1.24-1.13 (m, 1H), 0.93-0.83 (m, 3H). ES-MS (methanol) m/z: 306.4 $[M+H]^+$.

(R)-2-((7-((pyridin-3-ylmethyl)amino)-[1,2,4]triazolo[1,5-*a*][1,3,5]triazin-5-yl)amino)butan-1-ol (**114**)
Flash chromatography eluent: EtOAc-MeOH 95:5. Yield 47% (44 mg); white solid; mp 166-168°C (EtOEt-light petroleum). ^{1}H NMR (400 MHz, DMSO-d_6): δ 9.25 + 9.05 (bs, 1H), 8.74-8.54 (m, 1H), 8.47 (s, 1H), 8.18-7.99 (m, 1H), 7.80 (s, 1H), 7.46-7.30 (m, 1H), 7.30-7.11 (m, 1H), 4.79-4.47 (m, 3H), 3.83 (bs, 1H), 3.60-3.39 (m, 2H), 1.74-1.51 (m, 1H), 1.51-1.30 (m, 1H), 0.99-0.65 (m, 3H). ES-MS (methanol) m/z: 315.0 $[M+H]^+$, 337.0 $[M+Na]^+$.

(S)-2-((7-amino-[1,2,4]triazolo[1,5-*a*][1,3,5]triazin-5-yl)amino)butan-1-ol (**102**)
Flash chromatography eluent: EtOAc-MeOH 98:2. Yield 23% (15 mg); white solid; mp 177-181°C (EtOEt-light petroleum). ^{1}H NMR (400 MHz, DMSO-d_6, 90°C): δ 8.00 (s, 1H), 7.78 (bs, 2H), 6.70-6.53 (m, 1H), 3.95-3.85 (m, 1H), 3.54-3.40 (m, 2H), 1.74-1.60 (m, 1H), 1.59-1.44 (m, 1H), 0.86 (t, J = 7.3 Hz, 3H). ES-MS (methanol) m/z: 224.4 $[M+H]^+$, 246.3 $[M+Na]^+$.

(*S*)-2-((7-(benzylamino)-[1,2,4]triazolo[1,5-*a*][1,3,5]triazin-5-yl)amino)butan-1-ol (**109)**
Flash chromatography eluent: DCM-MeOH 97:3. Yield 39% (37 mg); white solid; mp 159-163°C (EtOEt-light petroleum). ^{1}H NMR (400 MHz, DMSO-d_6): 9.21 + 9.00 (bs, 1H), 8.09 + 8.07 (s, 1H), 7.41-7.12 (m, 6H), 4.69-4.53 (m, 3H), 3.87-3.79 (m, 1H), 3.48-3.40 (m, 1H), 3.38-3.27 (m, 1H), 1.67-1.56 (m, 1H), 1.47-1.33 (m, 1H), 0.90-0.75 (m, 3H). ES-MS (methanol) m/z: 314.0 $[M+Na]^+$.

(S)-2-((7-((pyridin-4-ylmethyl)amino)-[1,2,4]triazolo[1,5-*a*][1,3,5]triazin-5-yl)amino)butan-1-ol (**110**)
Flash chromatography eluent: DCM-MeOH 98:2. Yield 15% (14 mg); white solid; mp 188-190°C (EtOEt-light petroleum). ^{1}H NMR (400 MHz, DMSO- d_6, 90°C): δ 8.77 (bs, 1H), 8.51-8.42 (m, 2H), 8.04 (s, 1H), 7.37-7.33 (m, 2H), 6.75 (d, J = 8.4 Hz, 1H), 4.72-4.61 (m, 2H), 4.38-4.29 (m, 1H), 3.92-3.78 (m, 1H), 3.59-3.32 (m, 2H), 1.71-1.53 (m, 1H), 1.53-1.39 (m, 1H), 0.92-0.77 (m, 3H). ES-MS (methanol) m/z: 315.4 $[M+H]^+$.

(S)-2-((7-(([1,1'-biphenyl]-4-ylmethyl)amino)-[1,2,4]triazolo[1,5-*a*][1,3,5]triazin-5-yl)amino)butan-1-ol (**111**)
Flash chromatography eluent: DCM-MeOH 97:3. Yield 32% (37 mg); white solid; mp 192-195°C (EtOEt-light petroleum). ^{1}H NMR (400 MHz, DMSO-d_6): δ 9.25 + 9.06 (s, 1H), 8.11 + 8.07 (s, 1H), 7.78-7.55 (m, 4H), 7.55-7.39 (m, 4H), 7.39- 7.32 (m, 1H), 7.31-7.08 (m, 1H), 4.87-4.48 (m, 3H), 3.86 (bs, 1H), 3.55-3.24 (m, 2H), 1.74-1.53 (m, 1H), 1.53-1.30 (m, 1H), 0.96-0.68 (m, 3H). ES-MS (methanol) m/z: 390.4 $[M+H]^+$, 412.4 $[M+Na]^+$.

(S)-2-((7-(cyclohexylamino)-[1,2,4]triazolo[1,5-*a*][1,3,5]triazin-5-yl)amino)butan-1-ol (**113**)
Flash chromatography eluent: DCM-MeOH 98:2. Yield 53% (49 mg); white solid; mp 104-109°C (EtOEt-light petroleum). ^{1}H NMR (400 MHz, DMSO- d_6): δ 7.99 (s, 1H), 7.77 (s, 1H), 6.75-6.71 (m, 2H), 4.32 (s, 1H), 4.05-3.75 (m, 2H), 3.63-3.32 (m, 2H), 1.93-1.71 (m, 4H), 1.70-1.57 (m, 2H), 1.56-1.36 (m, 3H), 1.35-1.18 (m, 2H), 1.17-1.03 (m, 1H), 0.95-0.78 (m, 3H). ES-MS (methanol) m/z: 306.5 $[M+H]^+$, 328.5 $[M+Na]^+$.

(S)-2-((7-((pyridin-3-ylmethyl)amino)-[1,2,4]triazolo[1,5-*a*][1,3,5]triazin-5-yl)amino)butan-1-ol (**115**)
Flash chromatography eluent: EtOAc + 5% MeOH. Yield 46% (43 mg); white solid; mp 177-179°C (EtOEt-light petroleum). ^{1}H NMR (400 MHz, DMSO- d_6): δ 9.25 + 9.05 (bs, 1H), 8.64 + 8.61 (s, 1H), 8.47 (s, 1H), 8.09 + 8.07 (s, 1H), 7.88-7.74 (m, 1H), 7.42-7.31 (m, 1H), 7.41-7.32 + 7.28-7.14 (m, 1H), 4.77-4.49 (m, 3H), 3.92-3.75 (m, 1H), 3.54-3.19 (m, 2H), 1.76-1.52 (m, 1H), 1.51-1.29 (m, 1H), 0.86 + 0.78 (t, J = 7.3 Hz, 3H). ES-MS (methanol) m/z: 315.0 $[M+H]^+$, 336.9 $[M+Na]^+$.

N^5-(pentan-3-yl)-N^7-(pyridin-4-ylmethyl)-[1,2,4]triazolo[1,5-*a*][1,3,5]triazine-5,7-diamine (**116**)
Flash chromatography eluent: from EtOAc-light petroleum 8:2 to EtOAc-MeOH 9.5:0.5. Yield 43% (40 mg); white solid; mp 163-166°C (EtOEt-light petroleum). ^{1}H NMR (400 MHz; DMSO-d_6, 90°C): δ 8.78 (bs, 1H), 8.51-8.46 (m, 2H), 8.03 (s, 1H), 7.35 (d, J = 5.6 Hz, 2H), 6.96.6.86 (m, 1H), 4.70-4.61 (m, 2H), 3.79-3.70 (m, 1H), 1.55-1.38 (m, 4H), 0.89-0.72 (m,

6H). ES-MS (methanol) m/z: 313.2 $[M+H]^+$, 335.1 $[M+Na]^+$.

*N*5-(pentan-3-yl)-*N*7-([1,1'-biphenyl]-4-ylmethyl)-[1,2,4]triazolo[1,5-*a*][1,3,5]triazine-5,7-diamine (**117**)
Flash chromatography eluent: light petroleum-EtOAc 1:1. Yield 20% (23 mg); white solid; mp 146-150°C (EtOEt-light petroleum). ^{1}H NMR (400 MHz; DMSO-d_6): δ 9.24 + 9.01 (bs, 1H), 8.09 + 8.06 (s, 1H), 7.70-7.54 (m, 4H), 7.54-7.26 (m, 6H), 4.73-4.59 (m, 2H), 3.83-3.74 (m, 1H), 1.62-1.33 (m, 4H), 0.94-0.73 (m, 6H). ES-MS (methanol) m/z: 388.2 $[M+H]^+$, 410.2 $[M+Na]^+$, 426.1 $[M+K]^+$.

2-((7-((pyridin-4-ylmethyl)amino)-[1,2,4]triazolo[1,5-*a*][1,3,5]triazin-5-yl)amino)propane-1,3-diol (**118**)
Flash chromatography eluent: DCM-MeOH 95:5. Yield 39% (37 mg); white solid; mp 192-195°C (EtOEt-light petroleum). ^{1}H NMR (400 MHz, DMSO-d_6): δ 9.30 + 9.11 (bs, 1H), 8.48 (d, J = 5.69 Hz, 2H), 8.13 + 8.10 (s, 1H), 7.39-7.33 (m, 2H), 6.99 (d, J = 8.07 Hz, 1H), 4.69-4.55 (m, 4H), 3.94-3.83 (m, 1H), 3.52-3.37 (m, 4H). ES-MS (methanol) m/z: 317.1 $[M+Na]^+$, 339.1 $[M+Na]^+$.

2-((7-(([1,1'-biphenyl]-4-ylmethyl)amino)-[1,2,4]triazolo[1,5-*a*][1,3,5]triazin-5-yl)amino)propane-1,3-diol (**119**)
Flash chromatography eluent: DCM-MeOH 95:5. Yield 55% (65 mg); white solid; mp 184-186°C (EtOEt-light petroleum). ^{1}H NMR (400 MHz, DMSO-d_6): δ 9.28 + 9.11 (bs, 1H), 8.11 + 8.09 (s, 1H), 7.67-7.58 (m, 4H), 7.55-7.41 (m, 4H), 7.38-7.32 (m, 1H), 7.03-6.97 (m, 1H), 4.70-4.60 (m, 4H), 4.05-3.90 (m, 1H), 3.56-3.44 (m, 4H). ES-MS (methanol) m/z: 392.1 $[M+Na]^+$, 414.1 $[M+K]^+$.

(R)-*N*7-(pyridin-4-ylmethyl)-*N*5-(*sec*-butyl)-[1,2,4]triazolo[1,5-*a*][1,3,5]triazine-5,7-diamine (**120**)
Flash chromatography eluent: DCM-MeOH 97.5:2.5. Yield 43% (38 mg); white solid; mp 190-191°C (EtOEt-light petroleum). ^{1}H NMR (400 MHz, DMSO-d_6): δ 9.25 + 9.02 (bs, 1H), 8.59-8.35 (m, 2H), 8.11 + 8.08 (s, 1H), 7.41-7.28 (m, 3H), 4.77-4.53 (m, 2H), 3.96-3.80 + 3.79-3.65 (m, 1H), 1.59-1.21 (m, 2H), 1.08 + 0.97 (d, J = 6.4 Hz, 3H), 0.84 + 0.70 (t, J = 7.2 Hz, 3H). ES-MS (methanol) m/z: 299.2 $[M+H]^+$, 321.1 $[M+Na]^+$.

(S)-*N*7-(pyridin-4-ylmethyl)-*N*5-(*sec*-butyl)-[1,2,4]triazolo[1,5-*a*][1,3,5]triazine-5,7-diamine (**121**)
Flash chromatography eluent: DCM-MeOH 99:1. Yield 40% (36 mg); white solid; mp 181-182°C (EtOEt-light petroleum). ^{1}H NMR (400 MHz, DMSO-d_6, 90°C): δ 8.79 (bs, 1H), 8.54-8.48 (m, 2H), 8.03 (s, 1H), 7.38-7.32 (m, 2H), 6.99-6.95 (m, 1H), 4.67 (d, J = 6.0 Hz, 2H), 3.87 (bs, 1H), 1.67 – 1.36 (m, 2H), 1.10 (d, J = 6.1 Hz, 3H), 0.84 (t, J = 6.8 Hz, 3H). ES-MS (methanol) m/z: 299.1 $[M+H]^+$, 321.1 $[M+Na]^+$.

(R)-*N*7-([1,1'-biphenyl]-4-ylmethyl)-*N*5-(*sec*-butyl)-[1,2,4]triazolo[1,5-*a*][1,3,5]triazine-5,7-diamine (**122**)
Flash chromatography eluent: DCM-MeOH 99.5:0.5. Yield 71% (79 mg); white solid; mp 184-186°C (EtOEt-light petroleum). ^{1}H NMR (400 MHz, DMSO-d_6): δ 9.26 + 9.04 (bs, 1H), 8.11 + 8.08 (s, 1H), 7.64 (s, 4H), 7.55-7.28 (m, 6H), 4.68 (s, 2H), 3.89 (s, 1H), 1.64-1.32 (m, 2H), 1.20-0.98 (m, 3H), 0.96-0.70 (m, 3H). ES-MS (methanol) m/z: 374.2 $[M+H]^+$, 396.2 $[M+Na]^+$, 412.1 $[M+K]^+$.

(S)-*N*7-([1,1'-biphenyl]-4-ylmethyl)-*N*5-(*sec*-butyl)-[1,2,4]triazolo[1,5-*a*][1,3,5]triazine-5,7-diamine (**123**)
Flash chromatography eluent: DCM-MeOH 99:1. Yield 77% (86 mg); white solid; mp 177-

178°C (EtOEt-light petroleum). ^{1}H NMR (400 MHz, DMSO-d_6, 90°C): δ 8.74 (bs, 1H), 8.02 (s, 1H), 7.73-7.54 (m, 4H), 7.53-7.39 (m, 4H), 7.38-7.27 (m, 1H), 7.00 (bs, 1H), 4.70 (s, 2H), 4.02-3.85 (m, 1H), 1.67-1.38 (m, 2H), 1.13 (d, *J* = 5.8 Hz, 3H), 0.87 (s, 3H). ES-MS (methanol) m/z: 374.2 $[M+H]^+$, 396.2 $[M+Na]^+$.

2-((7-((pyridin-4-ylmethyl)amino)-[1,2,4]triazolo[1,5-*a*][1,3,5]triazin-5-yl)amino)ethanol (**124**)
Flash chromatography eluent: EtOAc-MeOH 9:1. Yield 47% (40 mg); white solid; mp 189-191°C (EtOEt-light petroleum). ^{1}H NMR (400 MHz, DMSO-d_6): δ 9.31 + 9.11 (s, 1H), 8.59-8.42 (m, 2H), 8.14 + 8.11 (s, 1H), 7.43 (bs, 1H), 7.36 (bs, 2H), 4.70 (bs, 1H), 4.75-4.54 (m, 2H), 3.63 – 3.43 (m, 2H), 3.41 – 3.15 (m, 2H). ES-MS (methanol) m/z: 287.4 $[M+H]^+$.

2-((7-(([1,1'-biphenyl]-4-ylmetil)amino)-[1,2,4]triazolo[1,5-*a*][1,3,5]triazin-5-yl)amino)ethanol (**125**)
Flash chromatography eluent: DCM-MeOH 97.5:2.5. Yield 62% (67 mg); white solid; mp 219-221°C (EtOEt-light petroleum). ^{1}H NMR (400 MHz, DMSO- d_6): δ 9.29 + 9.10 (t, *J* = 5.8 Hz, 1H), 8.12 + 8.08 (s, 1H), 7.74-7.56 (m, 4H), 7.55-7.39 (m, 5H), 7.40-7.31 (m, 1H), 4.74-4.59 (m, 3H), 3.59-3.43 (m, 2H), 3.41-3.20 (m, 2H). ES-MS (methanol) m/z: 362.0 $[M+H]^+$, 383.7 $[M+Na]^+$.

tert-butyl-(2-((7-((pyridin-4-ylmethyl)amino)-[1,2,4]triazolo[1,5-*a*][1,3,5]triazin-5-yl)amino)ethyl)carbamate (**126**)
Flash chromatography eluent: DCM-MeOH 95:5. Yield 31.5% (36 mg); white solid; mp 195-197°C (EtOEt-light petroleum). ^{1}H NMR (400 MHz, DMSO-d_6): δ 9.31 + 9.11 (bs, 1H), 8.54-8.46 (m, 2H), 8.14 + 8.10 (s, 1H), 7.53-7.29 (m, 3H), 6.88-6.79 (m, 1H), 4.70-4.58 (m, 2H), 3.34-2.94 (m, 4H), 1.51-1.19 (m, 9H). ES-MS (methanol) m/z: 286.1 $[M+H\text{-}Boc]^+$, 330.1 $[M+H\text{-}(tert\text{-}Bu)]^+$, 386.1 $[M+H]^+$, 408.2 $[M+Na]^+$, 424.1 $[M+K]^+$.

tert-butyl-(2-((7-(([1,1'-biphenyl]-4-ylmethyl)amino)-[1,2,4]triazolo[1,5-*a*][1,3,5]triazin-5-yl)amino)ethyl)carbamate (**127**)
Yield 77% (106 mg); white solid; mp 240-244°C (EtOEt-light petroleum). ^{1}H NMR (400 MHz, DMSO-d_6): δ 9.31 + 9.11 (bs, 1H), 8.13 + 8.09 (s, 1H), 7.68-7.32 (m, 10H), 6.90-6.83 (m, 1H), 4.71-4.61 (m, 2H), 3.34-3.24 (m, 2H), 3.15-3.04 (m, 2H), 1.44-1.25 (m, 9H). ES-MS (methanol) m/z: 361.1 $[M+H\text{-}Boc]^+$, 405.1 $[M+H\text{-}(tert\text{-}Bu)]^+$, 461.2 $[M+H]^+$, 483.2 $[M+Na]^+$, 499.1 $[M+K]^+$.

N^5-cyclohexyl-N^7-(pyridin-4-ylmethyl)-[1,2,4]triazolo[1,5-*a*][1,3,5]triazine-5,7-diamine (**128**)
Flash chromatography eluent: DCM-MeOH 98:2. Yield 74% (72 mg); white solid; mp 242-245°C (EtOEt-light petroleum). ^{1}H NMR (400 MHz, DMSO-d_6, 90°C): δ 8.80 (bs, 1H), 8.61-8.39 (m, 2H), 8.04 (s, 1H), 7.44-7.24 (m, 2H), 7.00 (d, *J* = 7.4 Hz, 1H), 4.66 (d, *J* = 6.1 Hz, 2H), 3.70 (bs, 1H), 1.99-1.48 (m, 5H), 1.43-1.01 (m, 5H). ES-MS (methanol) m/z: 325.5 $[M+H]^+$, 347.4 $[M+Na]^+$.

N^5-cyclohexyl-N^7-([1,1'-biphenyl]-4-ylmethyl)-[1,2,4]triazolo[1,5-*a*][1,3,5]triazine-5,7-diamine (**129**)
Flash chromatography eluent: DCM-MeOH 98:2. Yield 73% (87 mg); white solid; mp 233-234°C (EtOEt-light petroleum). ^{1}H NMR (400 MHz, DMSO-d_6): δ 9.29 + 9.03 (bs, 1H), 8.11 + 8.07 (s, 1H), 7.68-7.56 (m, 4H), 7.53-7.39 (m, 5H), 7.38-7.32 (m, 1H), 4.74-4.54 (m, 2H), 3.72 (bs, 1H), 1.97-1.52 (m, 5H), 1.40-0.99 (m, 5H). ES-MS (methanol) m/z: 400.4 $[M+H]^+$.

tert-butyl-(4-((7-((pyridin-4-ylmethyl)amino)-[1,2,4]triazolo[1,5-*a*][1,3,5]triazin-5-yl)amino) cyclohexyl)carbamate (**130**)
Flash chromatography eluent: EtOAc-MeOH 95:5. Yield 77% (101 mg); white solid; mp 256-258°C (EtOEt-light petroleum). ^{1}H NMR (400 MHz, DMSO-d_6): δ 9.30 + 9.05 (bs, 1H), 8.50 (s, 2H), 8.24 – 7.99 (m, 1H), 7.56 – 7.15 (m, 3H), 6.75 + 6.65 (bs, 1H), 4.81 – 4.46 (m, 2H), 3.89 – 2.99 (m, 2H), 1.93 – 0.98 (m, 17H). ES-MS (methanol) m/z: 340.2 [M+H-Boc]$^+$, 384.2 [M+H-(*tert*-Bu)]$^+$, 440.2 [M+H]$^+$, 462.2 [M+Na]$^+$, 478.1 [M+K]$^+$.

tert-butyl-(4-((7-(([1,1'-biphenyl]-4-ylmethyl)amino)-[1,2,4]triazolo[1,5-*a*][1,3,5]triazin-5-yl) amino)cyclohexyl)carbamate (**131**)
Flash chromatography eluent: DCM + 0.5% MeOH. Yield 27% (42 mg); white solid; mp 208-209°C (EtOEt-light petroleum). ^{1}H NMR (400 MHz, DMSO-d_6): δ 9.31 + 9.07 (bs, 1H), 8.12 + 8.09 (s, 1H), 7.63 (s, 4H), 7.56-7.15 (m, 6H), 6.80 + 6.68 (bs, 1H), 4.79-4.52 (m, 2H), 3.78 + 3.65 (bs, 1H), 3.42 + 3.17 (s, 1H), 1.99-1.07 (m, 17H). ES-MS (methanol) m/z: 415.3 [M+H-Boc]$^+$, 459.2 [M+H-(*tert*-Bu)]$^+$, 515.3 [M+H]$^+$, 537.3 [M+Na]$^+$, 553.3 [M+K]$^+$.

tert-butyl-(3-((7-((pyridin-4-ylmethyl)amino)-[1,2,4]triazolo[1,5-*a*][1,3,5]triazin-5-yl)amino)cyclohexyl)carbamate (1,3-trans racemic mixture) (**132**)
Flash chromatography eluent: DCM + 5% MeOH. Yield 18% (24 mg); white solid; mp 153-155°C (EtOEt-light petroleum). ^{1}H NMR (400 MHz, DMSO-d_6): δ 9.31 + 9.04 (bs, 1H), 8.72 + 8.51 + 8.49 (m, 2H), 8.15-8.07 (m, 1H), 7.75 + 7.50-7.28 (m, 3H), 6.91-6.76 (m, 1H), 4.72-4.56 (m, 2H), 4.14-3.95 (m, 1H), 3.73-3.60 (m, 1H), 1.77-1.15 (m, 17H). ES-MS (methanol) m/z: 384.2 [M+H-(*tert*-Bu)]$^+$, 440.2 [M+H]$^+$, 462.3 [M+Na]$^+$.

tert-butyl-(3-((7-((pyridin-4-ylmethyl)amino)-[1,2,4]triazolo[1,5-*a*][1,3,5]triazin-5-yl)amino)cyclohexyl)carbamate (1,3-cis racemic mixture) (**133**)
Flash chromatography eluent: DCM:MeOH 95:5. Yield 18% (24 mg); white solid; mp 166-169°C (EtOEt-light petroleum). ^{1}H NMR (400 MHz, DMSO- d_6): δ 9.32 + 9.04 (bs, 1H), 8.53-8.45 (m, 2H), 8.14-8.07 (m, 1H), 7.52-7.29 (m, 3H), 6.84-6.78 (m, 1H), 4.68-4.56 (m, 2H), 3.79-3.57 (m, 1H), 3.36-3.20 (m, 1H) 2.02-1.50 (m, 4H), 1.50-0.91 (m, 13H). ES-MS (methanol) m/z: 340.2 [M+H-Boc]$^+$, 384.1 [M+H-(*tert*-Bu)]$^+$, 440.2 [M+H]$^+$, 462.2 [M+Na]$^+$, 478.2 [M+K]$^+$.

tert-butyl-(3-((7-(([1,1'-biphenyl]-4-ylmethyl)amino)-[1,2,4]triazolo[1,5-*a*][1,3,5]triazin-5-yl)amino)cyclohexyl)carbamate (1,3-trans racemic mixture) (**134**)
Flash chromatography eluent: EtOAc-light petroleum 7:3. Yield 22% (34 mg); white solid; mp 140-143°C (EtOEt-light petroleum). ^{1}H NMR (400 MHz, DMSO- d_6, 90°C): δ 8.79-8.67 (m, 1H), 8.03 (s, 1H), 7.67-7.31 (m, 9H), 7.06-6.98 (m, 1H), 6.37-6.28 (m, 1H), 4.72 (d, J = 5.6 Hz, 2H), 4.21-4.13 (m, 1H), 3.75-3.68 (m, 1H), 1.81-1.52 (m, 6H), 1.52-1.22 (m, 11H). ES-MS (methanol) m/z: 415.2 [M+H-Boc]$^+$, 459.1 [M+H-(*tert*-Bu)]$^+$, 515.0 [M+H]$^+$, 537.1 [M+Na]$^+$, 553.0 [M+K]$^+$.

tert-butyl-(3-((7-(([1,1'-biphenyl]-4-ylmethyl)amino)-[1,2,4]triazolo[1,5-*a*][1,3,5]triazin-5-yl)amino)cyclohexyl)carbamate (1,3-cis racemic mixture) (**135**)
Flash chromatography eluent: EtOAc-light petroleum 7:3. Yield 19% (29 mg); white solid; mp 154-156°C (EtOEt-light petroleum). ^{1}H NMR (400 MHz, DMSO-d_6, 90°C): δ 8.85-8.71 (m, 1H), 8.03 (s, 1H), 7.72-7.32 (m, 9H), 7.17-7.11 (m, 1H), 6.42-6.32 (m, 1H), 4.69 (d, J = 6.0 Hz, 2H), 3.87-3.77 (m, 1H), 3.41-3.30 (m, 1H), 2.12-2.05 (m, 1H), 1.89-1.66 (m, 3H), 1.42-1.06 (m, 13H). ES-MS (methanol) m/z: 415.2 [M+H-Boc]$^+$, 459.0 [M+H-(*tert*-Bu)]$^+$, 514.7 [M+H]$^+$, 537.2 [M+Na]$^+$, 553.1 [M+K]$^+$.

tert-butyl-(3-((7-((pyridin-3-ylmethyl)amino)-[1,2,4]triazolo[1,5-*a*][1,3,5]triazin-5-yl)amino)cyclohexyl)carbamate (1,3-trans racemic mixture) (**136**)
Flash chromatography eluent: DCM-MeOH 98:2 (stationary phase: neutral aluminium oxide). Yield 21% (28 mg); white solid; mp 154-156°C (EtOAc-EtOEt). ^{1}H NMR (400 MHz, DMSO-d_6, 80°C): δ 9.24 + 9.00 (bs, 1H), 8.61 (s, 1H), 8.47-8.42 (m, 1H), 8.07-8.03 (m, 1H), 7.83-7.77 (m, 1H), 7.46-7.30 (m, 2H), 6.87-6.75 (m, 1H), 4.69-4.55 (m, 2H), 4.15-4.03 (m, 1H), 3.73-3.63 (m, 1H), 1.73-1.17 (m, 17H). ES-MS (methanol) m/z: 340.2 $[M+H-Boc]^+$, 384.2 $[M+H-(tert\text{-}Bu)]^+$, 440.3 $[M+H]^+$, 462.2 $[M+Na]^+$, 478.2 $[M+K]^+$.

tert-butyl-(3-((7-((pyridin-3-ylmethyl)amino)-[1,2,4]triazolo[1,5-*a*][1,3,5]triazin-5-yl)amino)cyclohexyl)carbamate (1,3-cis racemic mixture) (**137**)
Flash chromatography eluent: DCM-MeOH 98:2 (stationary phase: neutral aluminium oxide). Yield 27% (35 mg); pale brown solid; mp 178-180°C (EtOAc-EtOEt). ^{1}H NMR (400 MHz, DMSO-d_6, 80°C): δ 9.26 + 9.03 (bs, 1H), 8.65-8.58 (s, 1H), 8.47-8.40 (m, 1H), 8.09-8.04 (m, 1H), 7.81-7.75 (m, 1H), 7.54-7.44 (m, 1H), 7.40-7.30 (m, 1H), 6.85-6.75 (m, 1H), 4.68-4.54 (m, 2H), 3.81-3.64 (m, 1H), 3.42-3.19 (m, 1H), 2.05-1.59 (m, 4H), 1.59-0.95 (m, 13H). ES-MS (methanol) m/z: 384.2 $[M+H-(tert\text{-}Bu)]^+$, 440.2 $[M+H]^+$, 462.2 $[M+Na]^+$, 478.2 $[M+K]^+$.

tert-butyl-4-((7-((pyridin-4-ylmethyl)amino)-[1,2,4]triazolo[1,5-*a*][1,3,5]triazin-5yl)amino) piperidine-1-carboxylate (**138**)
Flash chromatography eluent: DCM-MeOH 95:5. Yield 39% (55 mg); white solid; mp 158-161°C (EtOEt-light petroleum). ^{1}H NMR (400 MHz, DMSO-d_6, 90°C): δ 8.85 (bs, 1H), 8.51-8.48 (m, 2H), 8.05 (s, 1H), 7.36-7.33 (m, 2H), 7.17-7.15 (m, 1H), 4.67 (d, J = 6.1 Hz, 2H), 3.89-3.86 (m, 3H), 2.89-2.76 (m, 2H), 1.85-1.69 (m, 2H), 1.48-1.26 (m, 11H). ES-MS (acetonitrile) m/z: 326.1 $[M+H-Boc]^+$, 370.0 $[M+H-(tert\text{-}Bu)]^+$, 426.1 $[M+H]^+$. The ^{1}H NMR spectrum revealed the presence of impurities.

tert-butyl-4-((7-(([1,1'-biphenyl]-4-ylmethyl)amino)-[1,2,4]triazolo[1,5-*a*][1,3,5]triazin-5-yl)amino)piperidine-1-carboxylate (**139**)
Flash chromatography eluent: DCM-MeOH 97:3. Yield 38% (57 mg); white solid; mp 147-149°C (EtOEt-light petroleum). ^{1}H NMR (400 MHz, DMSO-d_6): δ 9.34 + 9.08 (bs, 1H), 8.10 + 8.12 (s, 1H), 7.67-7.32 (m, 10H), 4.70-4.60 (m, 2H), 3.98-3.78 (m, 3H), 2.93-2.71 (m, 2H), 1.86-1.60 (m, 2H), 1.50-1.17 (m, 11H). ES-MS (acetonitrile) m/z: 401.2 $[M+H-Boc]^+$, 445.2 $[M+H-(tert\text{-}Bu)]^+$, 501.3 $[M+H]^+$.

tert-butyl-3-((7-((pyridin-4-ylmethyl)amino)-[1,2,4]triazolo[1,5-*a*][1,3,5]triazin-5-yl)amino)piperidine-1-carboxylate (**140**)
Flash chromatography eluent: DCM-MeOH 95:5. Yield 37% (47 mg); white solid; mp 164-167°C (EtOEt-light petroleum). ^{1}H NMR (400 MHz, DMSO-d_6, 90°C): δ 8.87 (bs, 1H), 8.50 (d, J = 4.45 Hz, 2H), 8.07 (s, 1H), 7.36 (d, J = 4.52 Hz, 2H), 7.12-7.04 (m, 1H), 4.75-4.63 (m, 2H), 3.93-3.61 (m, 3H), 3.00-2.82 (m, 2H), 1.93-1.64 (m, 2H), 1.57-1.15 (m, 11H). ES-MS (methanol) m/z: 326.1 $[M+H-Boc]^+$, 426.2 $[M+H]^+$, 448.2 $[M+Na]^+$.

tert-butyl-3-((7-(([1,1'-biphenyl]-4-ylmethyl)amino)-[1,2,4]triazolo[1,5-*a*][1,3,5]triazin-5-yl)amino)piperidine-1-carboxylate (**141**)
Flash chromatography eluent: DCM-MeOH 97:3. Yield 43% (64 mg); white solid; mp 125-128°C (EtOEt-light petroleum). ^{1}H NMR (400 MHz, DMSO-d_6): δ 9.35 + 9.11 (bs, 1H), 8.13 + 8.11 (s, 1H), 7.69-7.31 (m, 10H), 4.78-4.56 (m, 2H), 4.29-3.46 (m, 3H), 3.23-2.66 (m, 2H), 2.00-1.04 (m, 13H). ES-MS (acetonitrile) m/z: 401.2 $[M+H-Boc]^+$, 445.2 $[M+H-(tert\text{-}Bu)]^+$, 501.2 $[M+H]^+$, 523.2 $[M+Na]^+$, 539.2 $[M+K]^+$.

*N*5-(3-(dimethylamino)cyclohexyl)-*N*7-(pyridin-3-ylmethyl)-[1,2,4]triazolo[1,5-*a*][1,3,5] triazine-5,7-diamine (1,3-*trans*-1,3-*cis* approximately 1:3.4 mixture) (**142**)
Flash chromatography eluent: DCM-MeOH-NH_4OH 9:0.75:0.25. Yield 42.5% (47 mg); white solid; mp 155-157°C (EtOAc-EtOEt). ^{1}H NMR (400 MHz, DMSO-d_6, 80°C): δ 9.01-8.71 (m, 1H), 8.71-8.60 (m, 1H), 8.54-8.44 (m, 1H), 8.06 + 8.02 (s, 1H), 7.88-7.77 (m, 1H), 7.41-7.30 (m, 1H), 7.28-7.17 + 7.09-7.03 (m, 1H), 4.72-4.62 (m, 2H), 4.25-4.17 + 3.86-3.71 (m, 1H), 2.38-2.11 (m, 7H), 2.09-1.96 (m, 1H), 1.95-1.38 (m, 4H), 1.38-1.00 (m, 3H). ES-MS (methanol) m/z: 368.2 $[M+H]^+$.

*N*5-(1-methoxybutan-2-yl)-*N*7-(pyridin-3-ylmethyl)-[1,2,4]triazolo[1,5-*a*][1,3,5]triazine-5,7-diamine (racemic mixture) (**143**)
Flash chromatography eluent: EtOAc-MeOH 99:1. Yield 14.5% (14 mg); white solid; mp 141-144°C (EtOEt-light petroleum). ^{1}H NMR (400 MHz, DMSO-d_6): δ 9.25 + 9.05 (bs, 1H), 8.69-8.54 + 8.46 (m, 2H), 8.13-8.03 (m, 1H), 7.86-7.73 (m, 1H), 7.49-7.13 (m, 2H), 4.71-4.52 (m, 2H), 4.07-3.94 (m, 1H), 3.44-3.11 (m, 5H), 1.65-1.30 (m, 2H), 0.94-0.69 (m, 3H). ES-MS (methanol) m/z: 329.2 $[M+H]^+$, 351.2 $[M+Na]^+$.

3.4.1.2.7 General procedure (VII) for the *N*-Boc deprotection

0.10 mmol of the appropriate *N*-Boc derivative were suspended in a 10% solution of trifluoroacetic acid in DCM (4 mL) and stirred at room temperature for 3 h. Once completed, the solvent was removed under reduced pressure and the residue precipitated from EtOAc-light petroleum to give the desired trifluoroacetate salts.

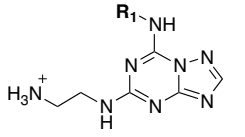

R_1= CH_2(4-pyridyl) (**144**)
CH_2(4-Ph)Ph (**145**)

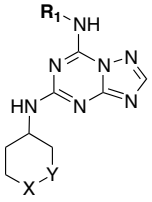

R_1= CH_2(4-pyridyl) (**146,148,149,154,156**)
CH_2(3-pyridyl) (**152,153**)
CH_2(4-Ph)Ph (**147,150,151,155,157**)
X = $CHNH3^+$, Y = CH_2 (**146,147**)
X = CH_2, Y = $CHNH3^+$ (**148-153**)
X = NH_2^+, Y = H (**154,155**)
X = H, Y = NH_2^+ (**156,157**)

*N*7-(pyridin-4-ylmethyl)-*N*5-(2-aminoethyl)-[1,2,4]triazolo[1,5-*a*][1,3,5]triazine-5,7-diamine, trifluoroacetate salt (**144**)
Yield 78% (31 mg from 0.06 mmol of **126**); white solid; mp 155-158°C; ^{1}H NMR (400 MHz, DMSO-d_6,): δ 9.54 + 9.32 (m, 1H), 8.73-8.70 (m, 2H), 8.26 + 8.24 (s, 1H), 7.86-7.60 (m, 6H), 4.86-4.75 (m, 2H), 3.50-3.39 (m, 2H), 3.01-2.81 (m, 2H). ES-MS (methanol) m/z: 286.1 $[M+H]^+$, 308.1 $[M+Na]^+$.

*N*7-([1,1'-biphenyl]-4-ylmethyl)-*N*5-(2-aminoethyl)-[1,2,4]triazolo[1,5-*a*][1,3,5]triazine-5,7-diamine, trifluoroacetate salt (**145**)
Yield 75% (36 mg); white solid; mp 125-128°C; ^{1}H NMR (400 MHz, DMSO-d_6,): δ 9.43 + 9.26 (bs, 1H), 8.19 (s, 1H), 7.86-7.33 (m, 13H), 4.74-4.64 (m, 2H), 3.58-3.48 (m, 2H), 3.04-2.93 (m, 2H). ES-MS (methanol) m/z: 361.1 $[M+H]^+$.

*N*7-(pyridin-4-ylmethyl)-*N*5-(4-aminocyclohexyl)-[1,2,4]triazolo[1,5-*a*][1,3,5]triazine-5,7-diamine, trifluoroacetate salt (**146**)
Yield 94% (41 mg); white solid; mp 137-140°C; ^{1}H NMR (400 MHz, DMSO-d_6, 90°C): δ 8.96 (bs, 1H), 8.57 (d, J = 4.8 Hz, 2H), 8.11 (s, 1H), 7.72 (bs, 3H), 7.46 (s, 2H), 7.19 + 7.01 (bs, 1H), 4.90-4.54 (m, 2H), 3.86 + 3.66 (bs, 1H), 3.15 + 2.98 (bs, 1H), 2.16-1.54 (m, 6H), 1.52-1.23 (m, 2H). ES-MS (methanol) m/z: 340.2 $[M+H]^+$.

N^7-([1,1'-biphenyl]-4-ylmethyl)-*N*^{5}-(4-aminocyclohexyl)-[1,2,4]triazolo[1,5-*a*][1,3,5]triazine-5,7-diamine, trifluoroacetate salt (**147**)
Quantitative yield (32 mg from 0.06 mmol of **131**); white solid; mp 190-193°C; ^{1}H NMR (400 MHz, DMSO-d_6): δ 9.55-9.41 + 9.09 (m, 1H), 8.20 + 8.26 (s, 1H), 7.91 – 7.54 (m, 8H), 7.53-7.30 (m, 5H), 4.83-4.52 (m, 2H), 3.86 + 3.69 (bs, 1H), 3.13 + 2.97 (bs, 1H), 2.06-1.52 (m, 6H), 1.52-1.19 (m, 2H). ES-MS (methanol) m/z: 415.2 $[M+H]^+$.

N^7-(pyridin-4-ylmethyl)-*N*^{5}-(3-aminocyclohexyl)-[1,2,4]triazolo[1,5-*a*][1,3,5]triazine-5,7-diamine, trifluoroacetate salt (1,3-trans racemic mixture) (**148**)
Yield 91% (16 mg from 0.04 mmol of **132**); sticky foam; ^{1}H NMR (400 MHz, DMSO-d_6): δ 9.49 + 9.20 (bs, 1H), 8.71-8.62 (m, 2H), 8.23 + 8.19 (s, 1H), 7.88-7.53 (m, 6H), 4.84-4.69 (m, 2H), 4.27-4.09 (m, 1H), 3.45-3.34 (m, 1H), 1.95-1.27 (m, 8H). ES-MS (methanol) m/z: 340.1 $[M+H]^+$.

N^7-(pyridin-4-ylmethyl)-*N*^{5}-(3-aminocyclohexyl)-[1,2,4]triazolo[1,5-*a*][1,3,5]triazine-5,7-diamine, trifluoroacetate salt (1,3-cis racemic mixture) (**149**)
Yield 84% (15 from 0.04 mmol of **133**); sticky foam; ^{1}H NMR (400 MHz, DMSO-d_6, 90°C): δ 8.91 (bs, 1H), 8.56 (d, J = 4.7 Hz, 2H), 8.09 (s, 1H), 7.80-7.68 (m, 3H), 7.44 (d, J = 4.6 Hz, 2H), 7.35-7.27 (m, 1H), 4.80-4.64 (m, 2H), 3.82-3.77 (m, 1H), 3.14-3.08 (m, 1H), 2.25-2.20 (m, 1H), 1.95-1.76 (m, 3H), 1.40-1.16 (m, 4H). ES-MS (methanol) m/z: 340.2$[M+H]^+$.

N^7-([1,1'-biphenyl]-4-ylmethyl)-*N*^{5}-(3-aminocyclohexyl)-[1,2,4]triazolo[1,5-*a*][1,3,5]triazine-5,7-diamine, trifluoroacetate salt (1,3-trans racemic mixture) (**150**)
Yield 89.5% (24 mg from 0.05 mmol of **134**); white solid; mp 183-185°C; ^{1}H NMR (400 MHz, DMSO-d_6, 90°C): δ 8.85 (bs, 1H), 8.08 (s, 1H), 7.90-7.23 (m, 14H), 4.88-4.67 (m, 2H), 4.34-4.27 (m, 1H), 3.51-3.39 (m, 1H), 2.15-2.00 (m, 1H), 1.90-1.39 (m, 6H). ES-MS (methanol) m/z: 415.2 $[M+H]^+$.

N^7-([1,1'-biphenyl]-4-ylmethyl)-*N*^{5}-(3-aminocyclohexyl)-[1,2,4]triazolo[1,5-*a*][1,3,5]triazine-5,7-diamine, trifluoroacetate salt (1,3-cis racemic mixture) (**151**)
Yield 93% (20 mg from 0.04 mmol of **135**); white solid; mp 211-213°C; ^{1}H NMR (400 MHz, DMSO-d_6, 90°C): δ 8.81 (m, 1H), 8.06 (s, 1H), 7.83-7.27 (m, 13H), 4.77-4.65 (m, 2H), 3.91-3.81 (m, 1H), 3.28-3.10 (m, 1H), 2.33-2.24 (m, 1H), 1.98-1.66 (m, 3H), 1.50-1.15 (m, 4H). ES-MS (methanol) m/z: 415.2 $[M+H]^+$.

N^7-(pyridin-4-ylmethyl)-*N*^{5}-(3-aminocyclohexyl)-[1,2,4]triazolo[1,5-*a*][1,3,5]triazine-5,7-diamine, trifluoroacetate salt (1,3-trans racemic mixture) (**152**)
Yield 67.3% (13 mg from 0.045 mmol of **136**); white solid; mp 207-209°C; ^{1}H NMR (400 MHz, DMSO-d_6): δ 9.42 + 9.14 (bs, 1H), 8.76 (m, 1H), 8.56 (m, 1H), 8.21 + 8.16 (s, 1H), 8.01-7.95 (m, 1H), 7.87-7.71 (m, 3H), 7.61-7.46 (m, 2H), 4.79-4.62 (m, 2H), 4.30-4.20 (m, 1H), 3.49-3.35 (m, 1H), 1.99-1.83 (m, 2H), 1.85.-1.40 (m, 6H). ES-MS (methanol) m/z: 340.2 $[M+H]^+$.

N^7-(pyridin-4-ylmethyl)-*N*^{5}-(3-aminocyclohexyl)-[1,2,4]triazolo[1,5-*a*][1,3,5]triazine-5,7-diamine, trifluoroacetate salt (1,3-cis racemic mixture) (**153**)
Yield 45% (9 mg from 0.045 mmol of **137**); white solid; mp 223-225°C; ^{1}H NMR (400 MHz, DMSO-d_6): δ 9.42 + 9.12 (bs, 1H), 8.73-8.66 (m, 1H), 8.57-8.51 (m, 1H), 8.18 + 8.14 (s, 1H), 8.06-7.84 (m, 4H), 7.84-7.64 (m, 1H), 7.54-7.49 (m, 1H), 4.82-4.64 (m, 2H), 3.89-3.70 (m, 1H), 3.18-3.08 (m, 1H), 2.25-2.08 (m, 1H), 1.92-1.60 (m, 3H), 1.45-1.14 (m, 4H). ES-MS (methanol) m/z: 340.2$[M+H]^+$.

*N*7-(pyridin-4-ylmethyl)-*N*5-(piperidin-4-yl)-[1,2,4]triazolo[1,5-*a*][1,3,5]triazine-5,7-diamine, trifluoroacetate salt (**154**)
Yield 93% (41 mg); white solid; mp 176-180°C; ^{1}H NMR (400 MHz, DMSO-d_6,): δ 9.54 + 9.24 (bs, 1H), 8.80-8.57 (m, 3H), 8.45-8.30 (m, 1H), 8.25 + 8.21 (m, 1H), 7.89-7.63 (m, 3H), 4.85-4.71 (m, 2H), 4.07-3.76 (m, 1H), 3.47-2.82 (m, 4H), 2.06-1.92 (m, 2H), 1.79-1.45 (m, 2H). ES-MS (methanol) m/z: 326.1 $[M+H]^+$.

*N*7-([1,1'-biphenyl]-4-ylmethyl)-*N*5-(piperidin-4-yl)-[1,2,4]triazolo[1,5-*a*][1,3,5]triazine-5,7-diamine, trifluoroacetate salt (**155**)
Yield 83% (43 mg); white solid; mp 149-151°C (d); ^{1}H NMR (400 MHz, DMSO-d_6,): δ 9.43 + 9.18 (bs, 1H), 8.60-8.46 (m, 1H), 8.38-8.21 (m, 1H), 8.15 (s, 1H), 7.84-7.56 (m, 5H), 7.55-7.31 (m, 5H), 4.80-4.62 (m, 2H), 4.09-3.93 (m, 1H), 3.37-3.18 (m, 2H), 3.14-2.93 (m, 2H), 2.08-1.80 (m, 2H), 1.73-1.50 (m, 2H). ES-MS (methanol) m/z: 401.2 $[M+H]^+$.

*N*7-(pyridin-4-ylmethyl)-*N*5-(piperidin-3-yl)-[1,2,4]triazolo[1,5-*a*][1,3,5]triazine-5,7-diamine, trifluoroacetate salt (**156**)
Yield 71.5% (25 mg from 0.08 mmol of **140**); sticky foam; ^{1}H NMR (400 MHz, DMSO-d_6,): δ 9.53 + 9.29 (bs, 1H), 8.68-8.59 (m, 4H), 8.22 (s, 1H), 7.67-7.58 (m, 3H), 4.77-4.74 (m, 2H), 4.12 (m, 1H), 3.39-3.17 (m, 2H), 2.81-2.66 (m, 2H), 1.92-1.49 (m, 4H). ES-MS (methanol) m/z: 326.2 $[M+H]^+$.

*N*7-([1,1'-biphenyl]-4-ylmethyl)-*N*5-(piperidin-3-yl)-[1,2,4]triazolo[1,5-*a*][1,3,5]triazine-5,7-diamine, trifluoroacetate salt (**157**)
Yield 90% (46 mg); white solid; mp 141-144°C; ^{1}H NMR (400 MHz, DMSO-d_6,): δ 9.46 + 9.24 (bs, 1H), 8.74-8.58 (m, 2H), 8.18 + 8.16 (s, 1H), 7.73-7.32 (m, 10H), 4.73-4.64 (m, 2H), 4.18-4.09 (m, 1H), 3.47-3.16 (m, 2H), 2.87-2.66 (m, 2H), 1.98-1.81 (m, 2H), 1.74-1.46 (m, 2H). ES-MS (methanol) m/z: 401.2 $[M+H]^+$.

3.4.2 Biological Procedures

3.4.2.1 GSK-3β Kinase Assay – LANCE® *Ultra* TR-FRET kit

These studies were performed by Dr. Alessandra Feoli, in the research group of Professor Sabrina Castellano, University of Salerno, Fisciano (Italy).

The assays were performed in white Optiplate-384 at room temperature (22°C) in a final volume of 25 μL, using the following buffer: 50 mM HEPES pH 7.5, 1 mM EGTA, 10 mM $MgCl_2$, 2 mM DTT and 0.01% Tween-20.

The candidate compounds were dissolved in DMSO and then diluted in the assay buffer, keeping constant the concentration of DMSO (1 or 2%) in each well. In each assay, the compound SB216763 (**18**) was used as positive control, while DMSO was used as reference.

GSK-3β (0.25 nM, final concentration) was first incubated with compounds for 30 minutes, then a mixture of ATP (10 μM, final concentration) and U*Light*-GS (Ser641/pSer657) peptide (50 nM, final concentration) was added. The reaction was incubated for 1 h, afterwards it was stopped by adding 24 mM EDTA and 2 nM (final concentration) Eu-anti-phospho-GS (Ser641) antibody, both diluted in Lance Detection Buffer. After an incubation of 1 h, the TR-FRET signal was read with the EnVision Multilabel Reader (excitation at 320 nm and emissions at 615 and 665 nm).

First, enzyme activity percentage was determined at 20, 10, 5 or 2.5 μM (depending on compounds solubility) for each inhibitor with respect to DMSO; subsequently, the most

active compounds were tested in 10 to 16-dose IC_{50} mode (twofold serial dilutions). Data were analysed using Excel and GraphPad Prism software (version 6.0, GraphPad) for IC_{50} curve fits using sigmoidal dose–response (variable slope) equations.

3.4.2.2 GSK-3β Kinetic Assays – ADP-Glo™ Kinase Assay

These studies were performed by Dr. Concepcioń Perez in the research group of Professor Ana Martinez, Instituto de Quimica Medica-CSIC, Madrid (Spain).

Kinetic experiments varying both the ATP (from 1 to 50 μM) and the concentrations of candidate compounds (**104**, from 5 to 10 μM; **105**, from 2.5 to 5 μM), were performed using the ADP-Glo Kinase Assay in black 96-well plates and using the following buffer: 50 mM HEPES (pH 7.5), 1 mM EDTA, 1 mM EGTA, and 15 mM magnesium acetate. In a typical assay, 10 μL of test compound (dissolved in DMSO at 1 mM concentration and diluted in advance in assay buffer to the desired concentration) and 10 μL (20 ng) of GSK-3β were added to each well followed by 20 μL of assay buffer containing 25 μM substrate and the desired concentrations of ATP. The final DMSO concentration in the reaction mixture did not exceed 1%. After 30 min of incubation at 30°C, the enzymatic reaction was stopped with 40 μL of ADP-Glo™Reagent, followed by Kinase Detection Reagent addition. Glow-type luminescence was recorded after 10 min using a FLUOstar Optima (BMG Labtechnologies GmbH, Offenburg, Germany) multimode reader. The enzyme activity is proportional to the difference of the total and consumed ATP.

3.4.2.3 Prediction of CNS permeation: PAMPA-BBB assay

Prediction of the brain penetration was evaluated using a parallel artificial membrane permeability assay (PAMPA).[229] Test compounds (2-6 mg of Caffeine, Enoxacine, Hydrocortisone, Desipramine, Ofloxacine, Piroxicam, Testosterone, 12-15 mg of Promazine and Verapamil and 23 mg of Atenolol) were dissolved in EtOH (1000 μL). 100 microlitres of this compound stock solution was taken and 1400 μL of EtOH and 3500 μL of PBS pH=7.4 buffer were added to reach 30% of EtOH concentration in the experiment. Likewise, 1-2 mg of every compound to be determined their ability to pass the brain barrier were dissolved in 1500 μL of EtOH and 3500 μL of PBS pH=7.4 buffer. All the solutions were then filtered with PDVF membrane filters (diameter 30 mm, pore size 0.45 μm). The acceptor indented 96-well microplate was filled with 180 μL of PBS/EtOH (70/30). The donor 96-well filtrate plate (Multiscreen® IP Sterile Plate PDVF membrane, pore size is 0.45 μM) was coated with 4 μL of porcine brain lipid in dodecane (20 mg mL^{-1}) and after 5 minutes, 180 μL of each compound solution was added. Then the donor plate was carefully put on the acceptor plate to form a "sandwich", which was left undisturbed for 2h and 30 min at 25 °C. During this time the compounds diffused from the donor plate through the brain lipid membrane into the acceptor plate. After incubation, the donor plate was removed. The concentrations of compounds and commercial drugs were determined measuring the absorbance in the acceptor (before the incubation) and the donor wells (after the incubation) with UV plate reader Tecan Infinite M1000. Every sample was analyzed at two to five wavelengths, in 3 wells and in two independent runs. Results are given as the mean ± standard deviation (SD) and the average of the two runs is reported. 10 quality control compounds (previously mentioned) of known BBB permeability were included in each experiment to validate the analysis set.

4 Synthesis and Characterization of CK-1 Inhibitors

4.1 INTRODUCTION

Although deregulation of CK-1 isoforms is involved in the pathogenesis of several diseases, including neurodegenerative and sleeping disorders and cancer, no CK-1 inhibitors have reached preclinical trials so far. In particular, CK-1δ is nowadays considered an appealing target and the design and development of ligands able to modulate its activity have become topical in the last years.[15,193]

Since the 2-aminopyrimidine, as present in Meridianine E (**67**) or derivative PF-5006739 (**78**), and purine/purine-like (**79-85**) moieties are recurring features of several CK-1 inhibitors described in literature, we initially focused our attention on the [1,2,4]triazolo[1,5-*c*]pyrimidine (TP) scaffold with the aim of obtaining new potent inhibitors for this kinase.

Over the years, several research groups have developed [1,2,4]triazolo[1,5-*c*]pyrimidine derivatives, which have been reported to bind different protein targets depending on the pattern of substitutions present on their structure,[220] such as adenosine receptors,[219] splenic tyrosine kinase (Syk)[236] and AXL receptor tyrosine kinase.[237] So, we decided to synthesize a triazolo-pyrimidine series (**177-200**), introducing various substituents at 2-, 5- and 8-positions to address the affinity towards CK-1δ (**Figure 31**).

Furthermore, in a preliminary biological screening, aimed to identify potential kinase inhibitors among our in-house set of adenine-like derivatives, we identified the [1,2,4]triazolo[1,3,5][1,5-*a*]triazine derivative **SF46** (**176**), that presents an IC_{50} towards CK-1δ in the micromolar range. Thus, we implemented our set of compounds with novel 2,5,7-trisubstituted triazolo-triazine derivatives and 2,5,7-trisubstituted triazolo-pyrimidines (**201-212**), bearing at 5(TT)/7(TP) positions a benzylamino group, as present in compound **SF46** (**176**). In particular, concerning 2-position (TT/TP), we inserted different alkyl (e.g. methyl) and aromatic groups (e.g. 2-indolyl and variously substituted phenyl) to evaluate their effects on affinity towards the kinase, while at 7(TT)/5(TP) positions we introduced the free amino group, as present in Meridianine E (**67**), the methylamino group or benzyl groups (e.g. 4-phenylbenzyl), resembling to those present in Roscovitine-like derivatives CR-8 (**82**) and DRF053 (**83**). Finally, at the 8-position of TP the influence of carboxylic acid, ethyl esters or amides was evaluated (**Figure 31**).

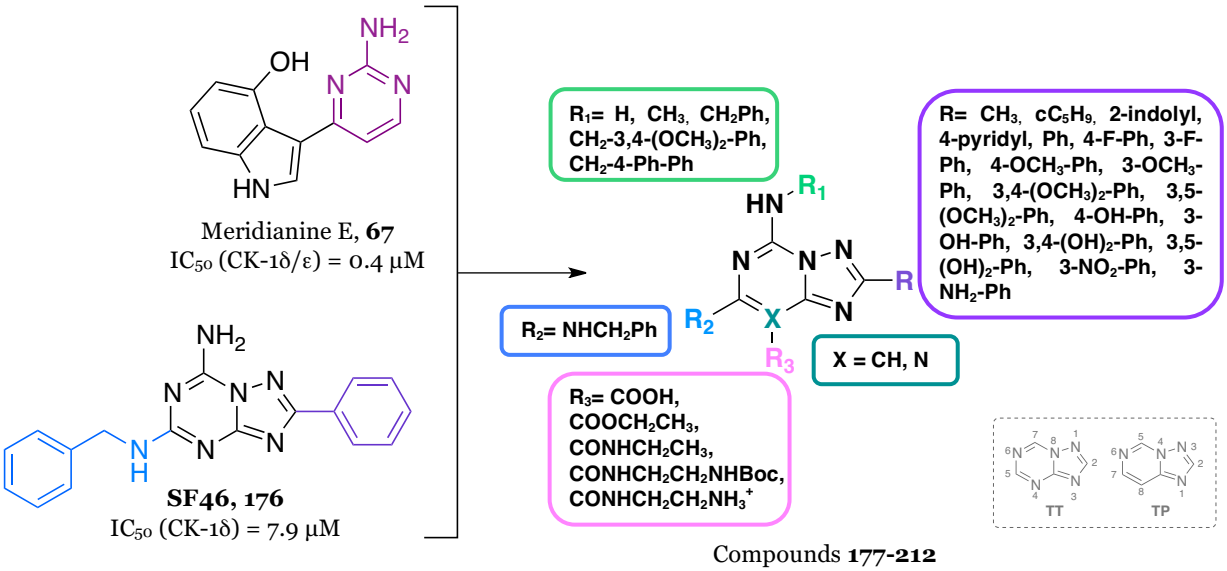

Figure 31. TTs and TPs derivatives **177-212** as CK-1δ inhibitors

All the synthesized derivatives were evaluated towards CK-1δ. In particular, we set up in our laboratory a high-throughput bioluminescent screening assay,[238] using the commercial KinaseGlo® kit and following a procedure implemented in the research group of Prof. Ana Martinez (CIB, Madrid, ES).[117] This assay is a luciferase-based assay for the determination of residual ATP. In order to validate the obtained results, the first series of compounds was assayed also with the well-recognized radiolabeled kinase assay (performed by Dr. Giorgio Cozza, at the University of Padua).[195] The bioluminescent method avoids the use of radioactive species, thus reducing safety and equipment issues for the researchers.

After biological characterization upon kinase assay, the most interesting derivatives were evaluated in the PAMPA assay, to obtain a prediction of their BBB permeability, and molecular modelling studies on CK-1δ model were performed in order to understand interactions that occurred between kinase and synthesized inhibitors.

4.2 RESULTS AND DISCUSSION

4.2.1 Chemistry

4.2.1.1 Synthesis of 2,5,8-trisubstituted [1,2,4]triazolo[1,5-*c*]pyrimidines

All the 2,5,8-trisubstituted triazolo-pyrimidines derivatives **177-200** have been synthesized following the strategy of Kyowa Hakko Kogyo Co.,[218] adjusting it to our synthetic purposes as summarized below [**Scheme 4**].

Scheme 4. Synthesis of 2,5-disubstituted (**185-186,262-264**) or 2-substituted ethyl 5-amino-[1,2,4]triazolo[1,5-*c*]pyrimidine-8-carboxylates (**177-184, 258-261**)[a]

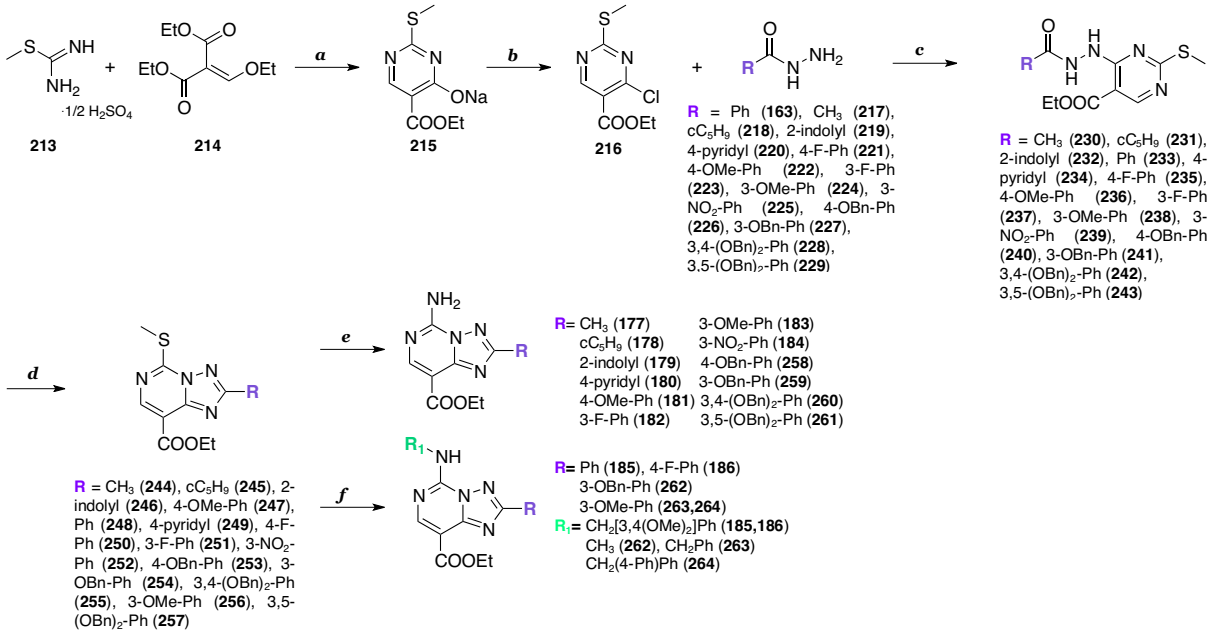

[a] ***a:*** NaOH, H_2O, ethanol, r.t., 24 h; ***b:*** $POCl_3$, reflux, 5 h; ***c:*** DBU, THF, r.t., 12 h; ***d:*** P_2O_5, HMDSO, xylene, from r.t. to 90°C, 2.5 h, reflux, 12 h; ***e:*** ammonia 7N in methanol, ethanol, 70°C, sealed tube, 3-12 h; ***f:*** R_1-NH_2, ethanol, 90°C, sealed tube, 3-12 h;.

Condensation between S-methylisothiourea **213** and diethyl ethoxymethylene malonate **214** in basic condition led to the pyrimidine sodium salt **215**, which after treatment with phosphorous oxychloride under reflux afforded the chloro derivative **216** that was immediately coupled with the required hydrazides (**163, 217-229**) in the presence of DBU,

to obtain derivatives **230-243**. The intramolecular cyclization that led to the [1,2,4]triazolo[1,5-*c*]pyrimidine system was conducted in the same conditions of the triazolo-triazine scaffold, previously discussed in Chapter 3.2.1; but in this case, the closure of the ring and the Dimroth rearrangement required longer reaction time (at least 20 hours), probably due to the lower difference in stability of the two isomers. In confirmation, in the case of the 2-phenyl derivative (**248**), we succeeded in isolating also the [4,3-*c*] derivative **265**, that was in turn converted into the desired [1,5-*c*] isomer **248** after reaction in acid conditions at reflux [**Scheme 5**].

Scheme 5. Reagents and conditions of conversion of compound **265** into **248**[a]

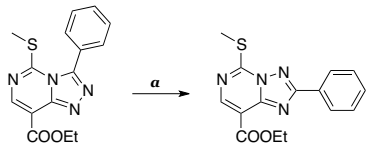

265 **248**

[a] ***a:*** acetic acid, reflux, 48 h.

Comparing the ^{1}H NMR spectra of compounds **265** and **248**, we can observe that hydrogen atoms of [4,3-*c*]-isomer **265** are moderately shifted up-field, but the main difference is represented by the pattern of signals of the phenyl ring: in the [1,5-*c*]-isomer spectra *ortho*-protons resulted more deshielded than the others, while in the [4,3-*c*] one all the phenyl protons resonate at the same ppm values (**Figure 32**).

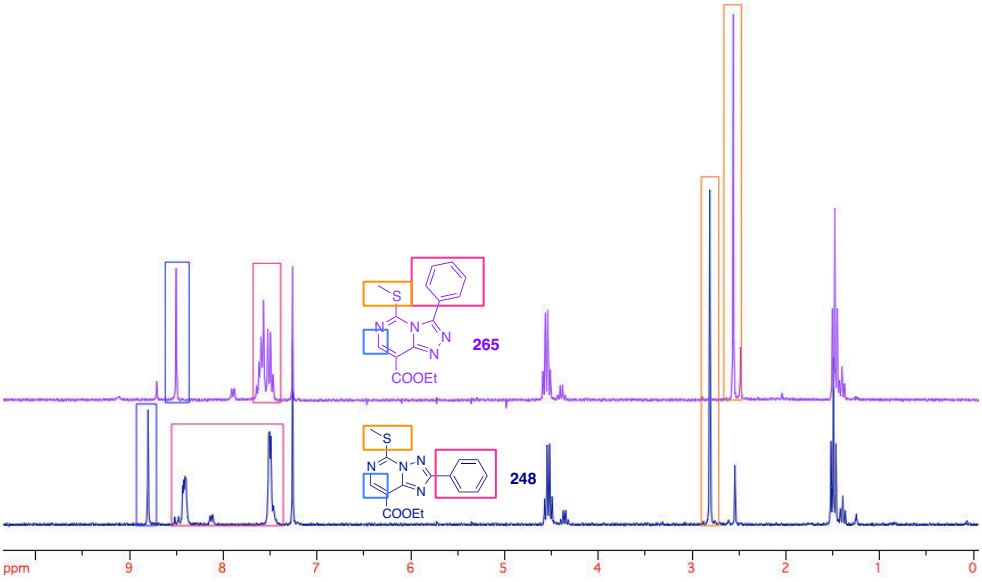

Figure 32. ^{1}H NMR of compounds **265** and **248**

In general, the cyclization products **244-255** were obtained in low yields. In attempts to optimize reaction conditions, we decided to increase the equivalents of phosphorus pentoxide and HMDSO from three to five and this led to a noticeable improvement in the yield. In particular, the yield of the synthesis of 3-methoxy derivative **256** increased from 10% to 59%. Therefore, we applied this strategy in all the following synthesis.

For those compounds presenting at the 2-position of the triazolo-pyrimidine scaffold polar groups susceptible of secondary reactions (-OH, -NH_2), a protective group was required in the initial steps of the synthetic pathway. So we decided to protect the hydroxyl groups with a benzyl group, easily introduced in high yields trough Williamson reaction (**270-273**) and removed in mild conditions by catalytic hydrogenolysis (**188-192**). The same conditions were applied also in the palladium-catalyzed reduction of the nitro group of compound **184**

used to protect the amino group of compound **187** [**Scheme 6**].

Scheme 6. Reagents and conditions of benzyl protection (**270-273**) and hydrogenolysis (**187-192**)[a]

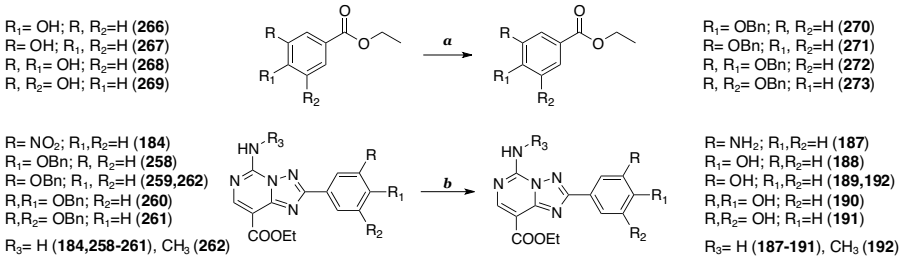

[a] ***a:*** benzyl bromide, K_2CO_3, acetone, reflux, 12 h; ***b:*** Pd/C, ammonium formate, methanol, reflux, 3-12 h.

Nucleophilic substitutions of methylthio group with ammonia or a primary amine were conducted heating the mixture in a sealed tube [**Scheme 4**]. The 2-phenyl (**193**) and 2-(4-fluoro)phenyl (**194**) derivatives were obtained following the two-step strategy reported in literature[218,219] which consists in the synthesis of the 3,4-dimethoxybenzylamino derivatives (**185, 186**) and the subsequent deprotection with trifluoromethanesulfonic acid, anisole and trifluoroacetic acid, leading to the desired derivative with the 5-amino group free [**Scheme 7**]. This strategy allowed to avoid the possible ammonolysis of the ethyl ester,[239] that could occur proceeding with a direct replacement of methylthio group with ammonia. Since the overall yields were not high, we tried to directly substitute the 5-methylthio derivatives **244-247** and **250-257** with ammonia using milder conditions (heating temperature not above 70°C), obtaining the desired 5-amino derivatives **177-184**, **258-261** in a single step with acceptable yields most of the time (16%-93%)[**Scheme 4**].

Scheme 7. Synthesis of compounds **193** and **194**[a]

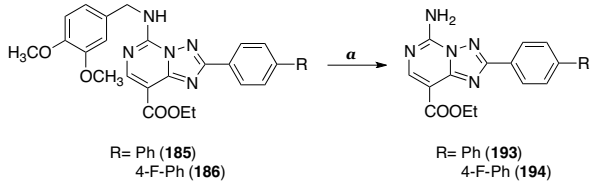

[a] ***a:*** TFA, trifluoromethanesulfonic acid, anisole, r.t., overnight.

The 5-benzylamino derivatives **196-197**, the 8-amido derivatives **198-199** and the carboxylic acid **195** were all obtained from the 3-methoxyphenyl derivatives **183** and **263-264**. Beyond being potential inhibitors of CK-1δ, these compounds in fact have proven to be key intermediates of the synthetic pathway since the methoxy group is considered to be one of the most effective protection methodologies for phenolic hydroxyl moieties. In fact, in the case of the 5-benzylamino derivatives **196-197**, it was necessary to find another suitable protection since the removal of the benzyl group from the 3-hydroxyphenyl moiety at the 2-position of the TP scaffold could have led also to the undesired loss of the benzyl and 4-phenylbenzyl groups present at the 5-position. Different conditions for the removal of the methoxy protecting group were investigated, including refluxing with HBr/CH_3COOH[240] or with pyridine hydrochloride[241], but all resulted ineffective. By contrast, demethylation was achieved in 3-12 hours using boron tribromide (BBr_3), the classical but harsh reagent used for this purpose. Unfortunately, the reactivity of BBr_3 led also to the hydrolysis of the ethyl ester at the 8-position, even using the minimum excess of reagent (1.1 equivalents) and maintaining the temperature below the 0°C. So we decided to force the reaction using an

excess of BBr_3 that ensured the complete consumption of starting material. Therefore, compounds **196-197** were obtained after re-esterification of **274-275**, *via* acyl chloride formation [**Scheme 8**].

In the case of 8-amido derivatives **198-199**, methoxy protecting group was preferred to the benzyl one for two reasons: the first is that this methodology allowed to avoid one synthetic step, leading directly to the carboxylic acid derivative **195**; the second is the higher yielding synthetic route that conducted to compound **183** (overall yield 20.5%) rather than the 3-benzyloxy derivative **259** (overall yield 1.1%).

Compound **198** was obtained in low yield using the acyl chloride formation strategy, since all the previous attempts of amide or ester formation using coupling reagents have been ineffective. The reaction was repeated several times using different chlorinating agents and solvents, leading most of the times the carboxylic acid **195** unaltered. The maximum yield, 9.1% [**Scheme 8**], was obtained by reacting the carboxylic acid **195** with a large excess of thionyl chloride (15 eq), as chlorinating agent, and a large excess of ethylamine (15 eq) using pyridine as solvent.

Synthesis of 5-amino-*N*-(2-aminoethyl)-2-(3-hydroxyphenyl)-[1,2,4]triazolo[1,5-*c*]pyrimidin-8-carboxamide **199** [**Scheme 8**] proceeded through amide formation by reaction of **195** with mono protected *N*-Boc-ethylendiamine, that after simple deprotection with TFA led to the desired compound **200**. Likewise synthesis of the derivative **198**, substrate **195** was reacted with excess of thionyl chloride and amine (15 eq) in anhydrous pyridine, but unfortunately **199** was obtained with only 5% yield. The procedure was then optimized [**Scheme 8**] and derivative **195** was reacted with 4 equivalents of thionyl chloride and a catalytic amount of DMF in anhydrous chloroform, at reflux for 3 hours, yielding the corresponding acyl chloride, which after treatment triethylamine and of Boc-ethylenediamine (2 eq) in THF gave the amide product **199** (yield 19%).

Scheme 8. Synthesis of compounds **195-200** [a]

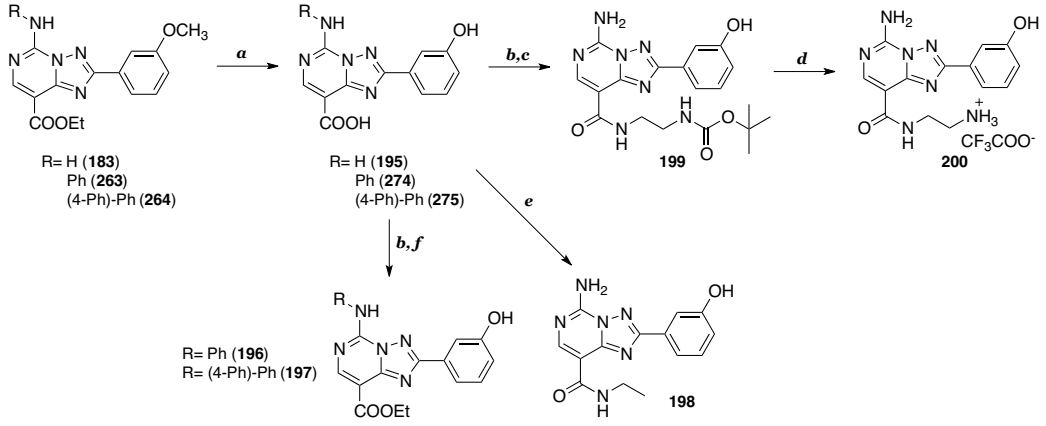

[a] ***a:*** BBr_3 1M in DCM, DCM, from -78°C to r.t., 12 h; ***b:*** $SOCl_2$, DMF, chloroform, reflux, 5 h; ***c:*** $NH_2(CH_2)_2NHBoc$, TEA, THF, r.t., 12 h; ***d:*** CF_3COOH 10% in DCM, r.t., 2 h; ***e:*** $SOCl_2$, ethylamine, pyridine, from 0°C to r.t., 12 h; ***f:*** ethanol, r.t., 12 h.

4.2.1.2 Synthesis of 2,5,7-trisubstituted [1,2,4]triazolo[1,5-*c*]pyrimidines

Compounds **201** and **202** were obtained following the approach used by Schering Co. for the synthesis of 2,5,7-trisubstituted triazolo-pyrimidines [**Scheme 9**].[242]

Scheme 9. Synthesis of compounds **201** and **202**[a]

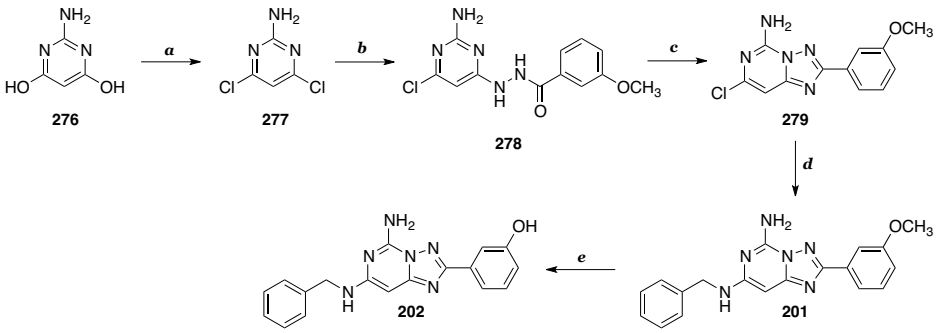

[a] ***a:*** $POCl_3$, TEA, acetonitrile, reflux, 1 h; ***b:*** 3-methoxybenzohydrazide (**224**), DBU, THF, r.t., 12 h; ***c:*** BSA, reflux, 12 h; ***d:*** benzylamine, K_2CO_3, ethanol, 95°C, sealed tube, 4 days; ***e:*** BBr_3 1M in DCM, DCM, from -78°C to r.t., 12h.

The commercial available 2-amino-4,6-dihydroxypyrimidine **276** was converted to the dichloride derivative **277** with phosphorus oxychloride and triethylamine in refluxing acetonitrile, that was in turn reacted with 3-methoxyphenylhydrazide (**224**) and DBU in THF, to obtain *N*'-(2-amino-6-chloropyrimidin-4-yl)-3-methoxybenzohydrazide **278**. Compound **278** was then cyclized in dehydrating conditions leading to the 5-amino-7-chloro-[1,2,4]triazolo[1,5-*c*]-pyrimidine **279**. In this case cyclization conditions were different from those used to prepare TT and TP derivatives described hitherto, and in particular the reaction was carried out in *N,O*-bis(trimethylsilyl)acetamide (BSA), a silylating agent that works similarly to PPSE (**Figure 33**).[243]

Figure 33. BSA-mediated cyclization

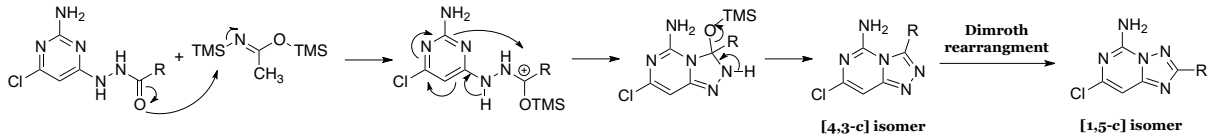

Nucleophilic substitution of chlorine at the 7-position of the TP scaffold with benzylamine yielded derivative **201**, which was then demethylated with boron tribromide to afford the 3-hydroxyphenyl derivative **202**.

4.2.1.3 Synthesis of 2,5,7-trisubstituted [1,2,4]triazolo[1,5-*a*][1,3,5]triazines

Compounds **203-212** were obtained following the same synthetic pathway discussed in Chapter 3.2.1 [**Scheme 10**]. The 2,4,6-triphenoxy[1,3,5]triazine **159** was reacted with the required arylhydrazides (**222, 224, 280-281**) and DBU to give 4,6-diphenoxy-[1,3,5]triazin-2-yl-hydrazides **282-285**, that successively underwent dehydrative cyclization with phosphorus pentoxide and HMDSO in xylene at reflux, yielding the 2-substituted 5,7-diphenoxy[1,2,4]triazolo[1,5-*a*][1,3,5]triazines **286-289**. Addition of methanolic ammonia to derivatives **286-289** led to the corresponding 7-amino derivatives **290-293**, while nucleophilic substitution at the 5-position with benzylamine occurred after heating the mixture in ethanol in sealed tube at 95-100°C for days. During the synthesis of the 3-methoxy derivative **204**, also the N^5,N^7-bisbenzylamino derivative **205** was isolated and characterized. Finally, removal of the methoxy group with an excess of boron tribromide afforded the hydroxyphenyl derivatives **208-212**. Both N^5,N^7-bisbenzylamino derivatives

205 and **210** were also assayed towards CK-1δ because they are interesting to complete the SAR of this series of derivatives.

Scheme 10. Synthesis of compounds **203-212** [a]

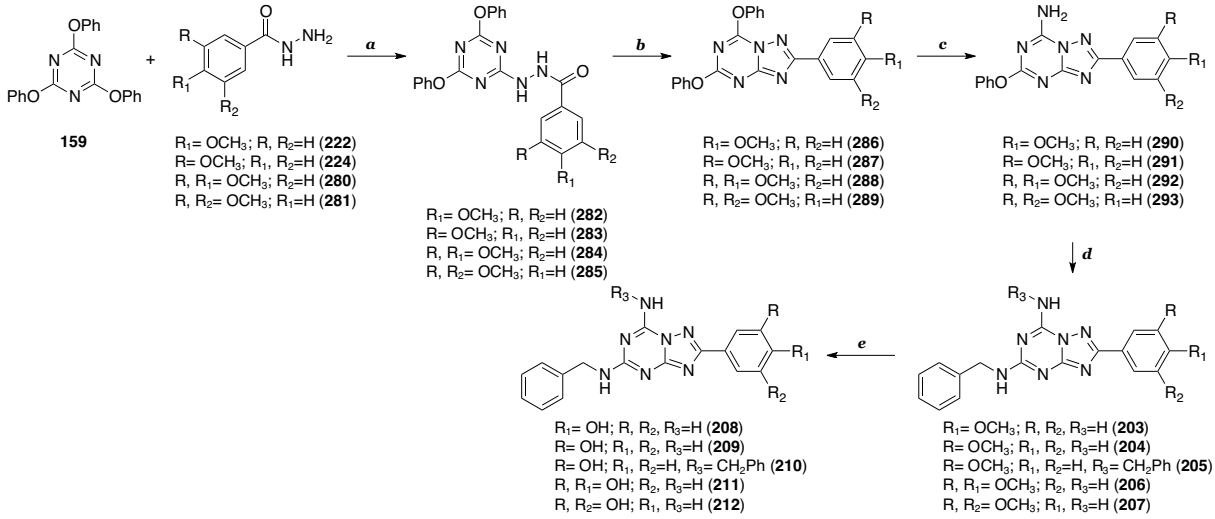

[a] ***a:*** DBU, THF, r.t., 12 h; ***b:*** P_2O_5, HMDSO, xylene, from r.t. to 90°C, 2.5 h, reflux, 2-4 h; ***c:*** ammonia 7N in methanol, methanol, r.t., 2 h; ***d:*** benzylamine, ethanol, 95-100°C, sealed tube, 24-72 h; ***e:*** BBr_3 1M in DCM, DCM, from -78°C to r.t., 12 h.

4.2.1.4 Synthesis of hydrazide derivatives

Hydrazide derivatives **218-219**, **221-223**, **225-229**, **280-281** were obtained by reacting the corresponding esters with a moderate excess of monohydrate hydrazine at reflux for several hours. Acetic hydrazide (**217**), pyridyn-4-carbohydrazide (**220**) and 3-methoxybenzohydrazide (**224**) were commercial available, while synthesis of benzhydrazide **163** was already reported in Chapter 3.4.1.2.

Scheme 11. Synthesis of hydrazides **218-219**, **221-223**, **225-229**, **280-281** [a]

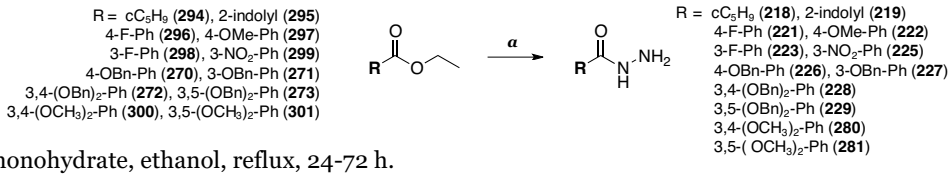

[a] ***a:*** hydrazine monohydrate, ethanol, reflux, 24-72 h.

4.2.2 Enzymatic evaluation and structure activity relationship (SAR) analysis

All the synthesized derivatives were evaluated towards CK-1δ, through radiometric kinase assay and/or KinaseGlo® luminescence assay. Initially they were evaluated at 40 μM to obtain the percentage of CK-1δ residual activity. For those compounds with a percentage of CK-1δ residual activity lower than 45%, the dose-response curves were determined and the half-maximal inhibitory concentration (IC_{50}) calculated (**Table 8**).

In a preliminarily phase, we decided to introduce modifications on the TP scaffold only at the 2-position: in particular, we inserted alkyl groups (methyl, cyclohexyl), different aromatic groups (phenyl, 4-pyridyl and 2-indolyl) which comprise different substituted phenyl rings (4-F, 4-OCH_3, 4-OH, 3-OH). At the 5-position, we left the amino group free, such as in Meridianine E (**67**) [IC_{50}(CK-1δ/ε)= 0.4 μM], but we evaluated also the N^5-3,4-dimethoxybenzyl derivatives **185** and **186**.

Table 8. TPs derivatives **177-181, 185-186, 188-189, 193-194**

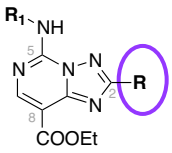

cmpd	R	R_1	CK-1δ IC_{50} (μM) or % residual activity @40 μM	
			[γ-^{32}P]ATP kinase assay	KinaseGlo® luminescence assay[a]
177	CH_3	H	>40	33.4% ±1.1[b]
178	cC_5H_9	H	15.9	12.32 ±5.17
179	2-indolyl	H	31.7	77.6% ±3.5
193	Ph	H	29.8	8.67 ±4.73
185	Ph	3,4-$(OCH_3)_2$-benzyl	>40	20.3% ±6.0[b]
180	4-pyridyl	H	33.5	20.19 ±5.57
194	Ph-4-F	H	>40	55.3% ±12.3
186	Ph-4-F	3,4-$(OCH_3)_2$-benzyl	>40	88.7% ±8.1
181	Ph-4-OCH_3	H	33.2	49.7% ±9.35
188	Ph-4-OH	H	29.0	23.2% ±3.0[b]
189	Ph-3-OH	H	5.9	2.06 ±0.28

[a]IC_{50} data are expressed ± SD (n=3); single-dose data are expressed ± SD (n=2); [b]False positive in the single-dose screening. IC_{50} not calculable.

In order to validate data deriving from luminescent kinase assay, this first series of derivatives was assayed both with the radiometric [γ-^{32}P]ATP assay and KinaseGlo® luminescence assay (**Table 8**). Even if the IC_{50} values determined applying the two different assays are not identical, the rank-ordering of inhibitor potency was maintained. As depicted in **Table 8**, most of the assayed compounds showed activities towards CK-1δ in the high micromolar range (>20 μM). The most interesting results were obtained with cyclopentyl derivative **178** [IC_{50}(CK-1δ)= 15.9/12.3 μM] and 3-hydroxyphenyl derivative **189** [IC_{50}(CK-1δ)= 5.9/2.1 μM]. The latter, in particular, in both assays resulted more effective in CK-1δ inhibition than the phenyl (**193**) and the 4-hydroxyphenyl (**188**) derivatives, thus providing first information about the requirement of a polar H-bond donor group with a specific orientation to gain affinity towards the kinase.

Taking into account these preliminary observations, we decided to further investigate the role of the substituent at the 2-position, introducing at the *meta* position of the phenyl ring other different substituents (3-F, 3-OCH_3, 3-NO_2, 3-NH_2) or inserting two hydroxyl groups [3,4-$(OH)_2$-, 3,5-$(OH)_2$-] (**Table 9**).

Table 9. TPs derivatives **182-184, 187, 190-191**

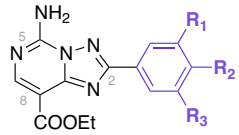

cmpd	R_1	R_2	R_3	CK-1δ IC_{50} (μM) or % residual activity @40 μM[a]
189	OH	H	H	2.06 ±0.28
182	F	H	H	46.3% ±4.4
183	OCH_3	H	H	48.0% ±9.2
184	NO_2	H	H	78.4% ±10.3
187	NH_2	H	H	16.59 ±5.03
190	OH	OH	H	4.75 ±0.35
191	OH	H	OH	0.48 ±0.20

[a]CK-1δ inhibition data obtained with KinaseGlo® luminescence kinase assay; IC_{50} data are expressed ± SD (n=3); single-dose data are expressed ± SD (n=2).

From **Table 9**, it is worth noting that any group different from the hydroxyl one had a detrimental effect in terms of inhibition potency towards CK-1δ, while interesting results were obtained with the dihydroxyphenyl derivatives **190** and especially **191**. The *meta*,*para*-disubstituted derivative **190** resulted less active than the *meta*-derivative **189** [**190**, IC_{50}(CK-1δ)= 4.75 μM *vs.* **189**, IC_{50}(CK-1δ)= 2.06 μM], while more effective than the *para*- [**188**, %residual activity at 40 μM (CK-1δ)= 23.2%] and the not substituted phenyl derivatives [**193**, IC_{50}(CK-1δ)= 8.67 μM]. Notably, with the di-*meta*-substituted derivative **191** we reached the submicromolar range of inhibiting concentrations [IC_{50}(CK-1δ)= 0.48 μM], with a 4-fold increase in inhibition potency if compared with the mono-*meta*-substituted derivative **189** [IC_{50}(CK-1δ)= 2.06 μM].

At the same time, modifications at the 5- and 8-positions were introduced in the scaffold of compound **189** (**Table 10**). In particular, in order to assess if a substitution at the 5-position of the TP scaffold could be tolerated, the free amino group was substituted with methyl, benzyl and a 4-phenyl-benzyl groups (**192**, **196-197**), with the latter two groups resembling the substituents present in Roscovitine (**81**) and other analogues (**82**,**83**). Concerning 8-position, the ethyl ester was hydrolysed to the carboxylic acid (**195**) and then three different amides were synthesized (ethyl **198**, N-Boc-aminoethyl **199**, aminoethyl **200**), to explore if stabilizing interactions could be reached in the part of the kinase pocket occupied by this moiety.

Table 10. TPs derivatives **192, 195-200**

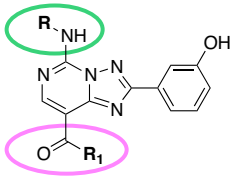

cmpd	R	R_1	CK-1δ IC_{50} (μM) or % residual activity @40 μM[a]
189	H	OCH_2CH_3	2.06 ±0.28
195	H	H	26.75 ±6.03
192	CH_3	OCH_2CH_3	92.9% ±7.1
196	CH_2Ph	OCH_2CH_3	98.8% ±3.5
197	CH_2Ph-4-Ph	OCH_2CH_3	100%
198	H	$NHCH_2CH_3$	0.32 ±0.10
199	H	$NHCH_2CH_2NHBoc$	83.2% ±25.9
200	H	$NHCH_2CH_2NH_3^+$ (TFA salt)	1.26 ±0.19

[a]CK-1δ inhibition data obtained with KinaseGlo® luminescence kinase assay; IC_{50} data are expressed ± SD (n=3); single-dose data are expressed ± SD (n=2).

From what can be seen from **Table 10**, the substitution at the 5-position led to inactive compounds at 40 μM (**192**, **196-197**), thus confirming the necessity of a free amino group at that position of TP scaffold. On the contrary, the results obtained with the modifications produced at the 8-position are more interesting. In fact, while the carboxylic acid **195** resulted less active than the corresponding ethyl ester [**195**, IC_{50}(CK-1δ)= 26.75 μM *vs.* **189**, IC_{50}(CK-1δ)= 2.06 μM], introducing an amido moiety led to improved inhibition potencies of derivatives **198** [IC_{50}(CK-1δ)= 0.32 μM] and **200** [IC_{50}(CK-1δ)= 1.26 μM] in comparison to compound **189** [IC_{50}(CK-1δ)= 2.06 μM]. Notably, derivative **198** [IC_{50}(CK-1δ)= 0.32 μM] represents the best result achieved in these TP series.

In the light of these results, in the second part of this project, we decided to combine the peculiar substitutions of TP derivatives just described and those of **SF46** (**176**) [IC_{50}(CK-1δ)= 7.9 μM], a TT derivative previously identified in our research group, thus implementing our set of compounds addressed to CK-1δ with novel 2,5,7-trisubstituted triazolo-triazine derivatives and 2,5,7-trisubstituted triazolo-pyrimidines (**201-212**). In particular, we maintained the free amino group at the 7(TT)/5(TP) positions and a benzylamino group at the 5(TT)/7(TP) positions, as present in compound **SF46** (**176**), but also the N^7,N^5-dibenzyl derivatives **205** and **210** were evaluated. While, concerning 2-position, we inserted at the *meta* and/or *para* positions hydroxyl groups which demonstrated to be favorable in the TP derivatives reported in **Table 8** and **9** (**Figure 34**).

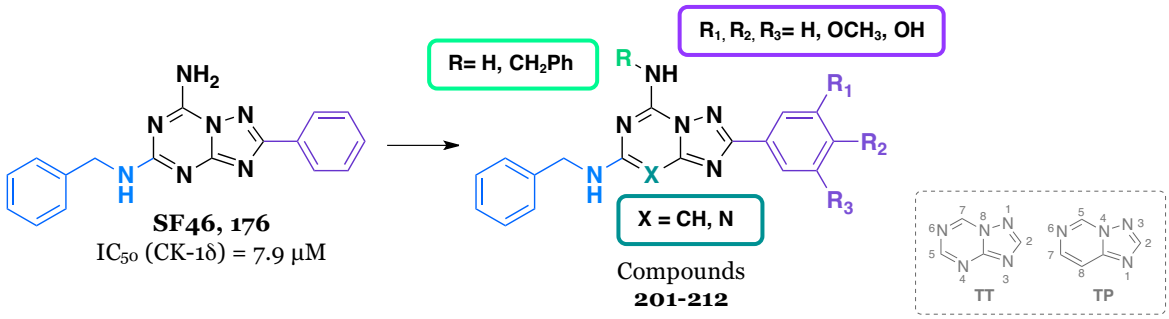

Figure 34. 2,5,7 trisubstituted TTs and TPs derivatives **201-212** as CK-1δ inhibitors

Table 11. TTs and TPs derivatives **201-212**

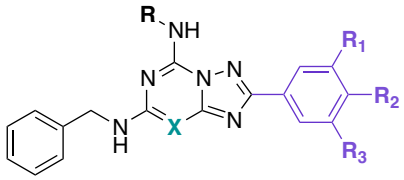

cmpd	X	R	R_1	R_2	R_3	CK-1δ IC_{50} (μM) or % residual activity @40 μM[a]
203	N	H	H	OCH_3	H	84.4% ±21.9
208	N	H	H	OH	H	1.32 ±0.51
204	N	H	OCH_3	H	H	81.9% ±7.7
205	N	CH_2Ph	OCH_3	H	H	100%
201	C	H	OCH_3	H	H	100%
209	N	H	OH	H	H	0.46 ±0.15
210	N	CH_2Ph	OH	H	H	100%
202	C	H	OH	H	H	0.30 ±0.07
206	N	H	OCH_3	OCH_3	H	5.65 ±1.34
211	N	H	OH	OH	H	0.91 ±0.30
207	N	H	OCH_3	H	OCH_3	95.5% ±2.3
212	N	H	OH	H	OH	0.18 ±0.04

[a]CK-1δ inhibition data obtained with KinaseGlo® luminescence kinase assay; IC_{50} data are expressed ± SD (n=3); single-dose data are expressed ± SD (n=2).

As we can observe in **Table 11**, the presence of a hydroxyl group on the phenyl ring at the 2-position has been confirmed to confer affinity to CK-1δ. In fact, all these derivatives resulted more potent than the reference compounds **189** [IC_{50}(CK-1δ)= 2.06 μM] and **SF46** (**176**) [IC_{50}(CK-1δ)= 7.9 μM], confirming the validity of our rationale. In particular, again we

can see that the best results were obtained with the *meta* [**209**, IC_{50}(CK-1δ)= 0.46 μM**, 202** IC_{50}(CK-1δ)= 0.30 μM] and di-*meta*-substituted derivatives [**212**, IC_{50}(CK-1δ)= 0.18 μM], probably due to the formation of important interactions between the hydroxyl group and an amino-acid residue of the ATP-binding pocket.

It is worth noting that all the methoxy derivatives resulted mostly inactive at the concentration used in the screening assay (40 μM), with the only exception of the 3,4-dimethoxy derivative **206** [IC_{50}(CK-1δ)= 5.65 μM]. Notably, from the comparison between the 3-hydroxyphenyl TT **209** and the 3-hydroxyphenyl TP **202** we can see that the two scaffold are mostly superimposable, with the TP derivative **202** slightly more potent than the corresponding TT **209** [**209**, IC_{50}(CK-1δ)= 0.46 μM *vs.* **202** IC_{50}(CK-1δ)= 0.30 μM]. We can also notice that, even in this case, the introduction of substituents on the amino group at the 7(TT) or 5(TP) position had a detrimental effect in terms of potency: in fact, both derivative **205**, isolated as side-product of the nucleophilic substitution at the 5-position, and the corresponding hydroxyl-derivative **210**, presenting a benzylamino group also at the 7-position, have no effects on CK-1δ activity at 40 μM.

4.2.3 Binding-mode studies on CK-1δ

Aimed to study the interactions of triazolo-pyrimidine and triazolo-triazine compounds with the catalytic pocket of CK-1δ and to rationalize the results obtained from the pharmacological evaluation, molecular docking simulations were performed by the research group of Prof. Stefano Moro, at the University of Padua. To this purpose, some of the most promising inhibitors were docked into the crystallographic structure of CK-1δ [PDB code: 4HNF] (**Figure 35**).

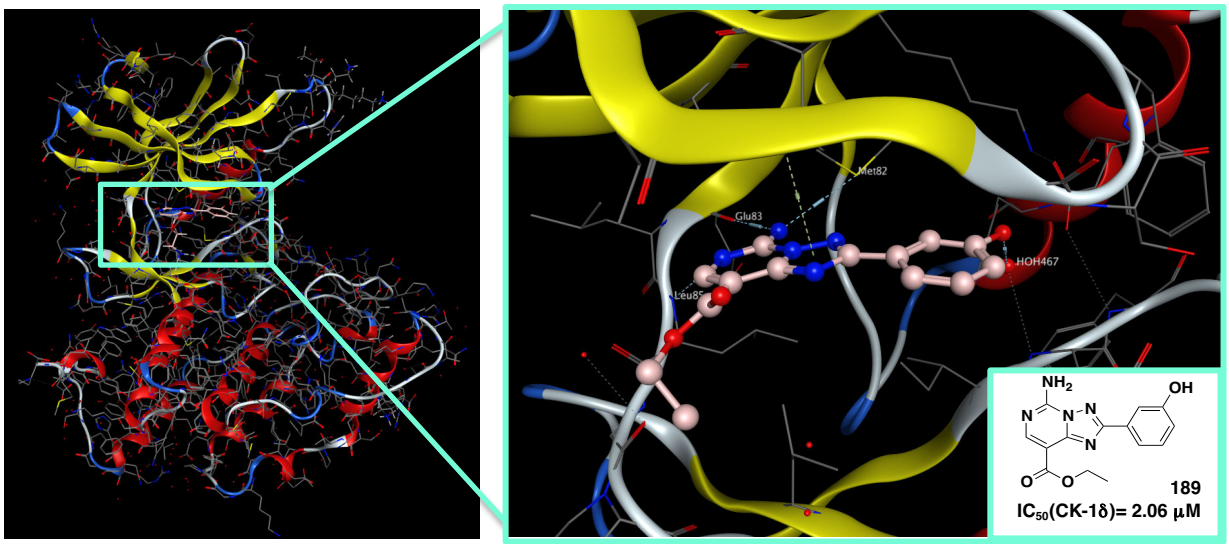

Figure 35. Docking studies with CK-1δ (PDB code: 4HNF) of compound **189**. The ligand is reported in pale pink x-sticks. Hydrogen bond interactions are highlighted by dotted lines.

Docking analysis on **189** revealed the usually observed adenine-type interactions with residues of the hinge-region: in detail, the amino group at the 5-position establishes two H-bonds with the gatekeeper Met82[15] and Glu83 while the lone pair of N^6 acts as H-bond acceptor for Leu85. Furthermore, hydrophobic interactions between the triazole ring and the kinase backbone have been detected. Most important, a hydrogen bond is formed between the key 3-hydroxyl group on the phenyl at the 2-position and a water molecule, which in turn interacts with the NH of Asp149, a residue belonging to the phosphate-binding region of the

ATP-binding site. This interaction probably is responsible of the better IC_{50} value of this compound **189** respect to the para-hydroxyl (**188**) and unsubstituted (**193**) derivatives [**189**, IC_{50}(CK-1δ)= 2.06 μM *vs* **188**, % residual activity at 40 μM (CK-1δ)= 23.2% and **193**, IC_{50}(CK-1δ)= 8.67 μM]. The same docking study applied to the TT derivative **209** (**Figure 36**), also bearing the 3-hydroxyphenyl moiety at 2-position, confirms the same orientation found for compound **189**.

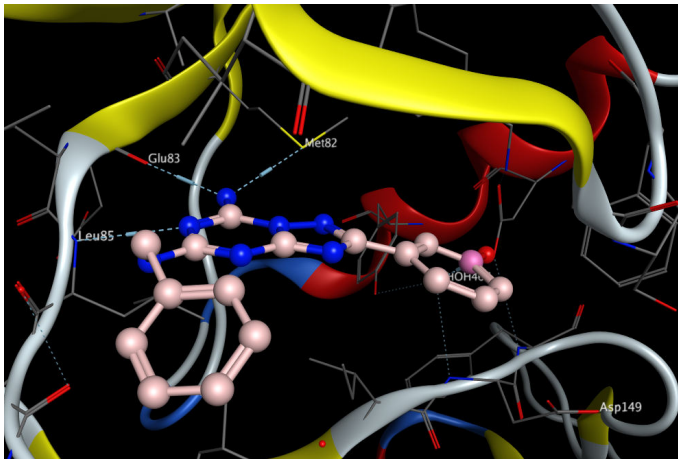

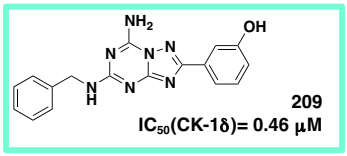

Figure 36. Docking studies with CK-1δ (PDB code: 4HNF) of compound **209**. The ligand is reported in pale pink x-sticks. Hydrogen bond interactions are highlighted by dotted lines.

Searching for a plausible structural explanation of the superiority of *m,m*-dihydroxyphenyl (**191, 212**) and the amide derivatives (**198, 200**) as CK-1δ inhibitors, a simulation was performed also for compound **191** (**Figure 37**) and **200** (**Figure 38**). Interestingly, the docking pose of compound **191** revealed, beyond the interactions with the hinge region, three stabilizing H-bonds for the hydroxyl groups of the TP scaffold: one hydroxyl group made interactions with Lys38 and a water molecule while the other one with Asp149. The presence of more interactions between the ligand and the kinase could provide an explanation of the improved affinity of the *m,m*-dihydroxyl analogue **191** towards CK-1δ (**Figure 37**). On the other hand, the pose observed for the aminoethylamide derivative **200** highlighted new interactions with residues in the hydrophobic region II, in particular between the N-terminal amino group at the 8-position and Asp91 and between the amido group and Gly86, once again providing a justification for its interesting inhibitory profile (**Figure 38**).

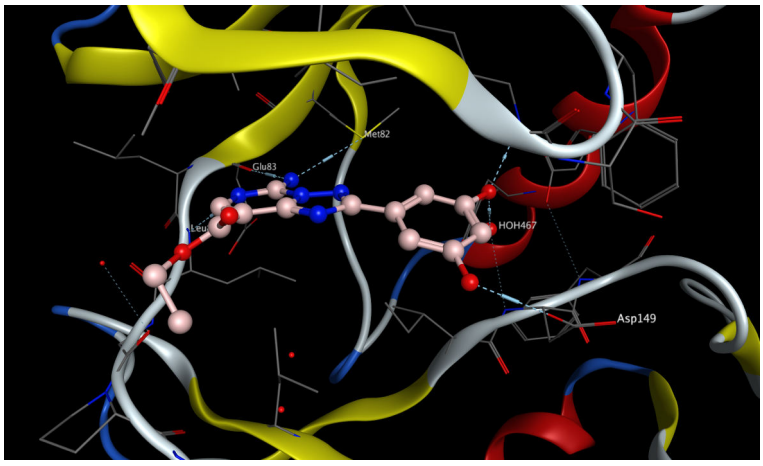

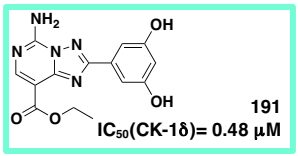

Figure 37. Docking studies with CK-1δ (PDB code: 4HNF) of compound **191**. The ligand is reported in pale pink x-sticks. Hydrogen bond interactions are highlighted by dotted lines.

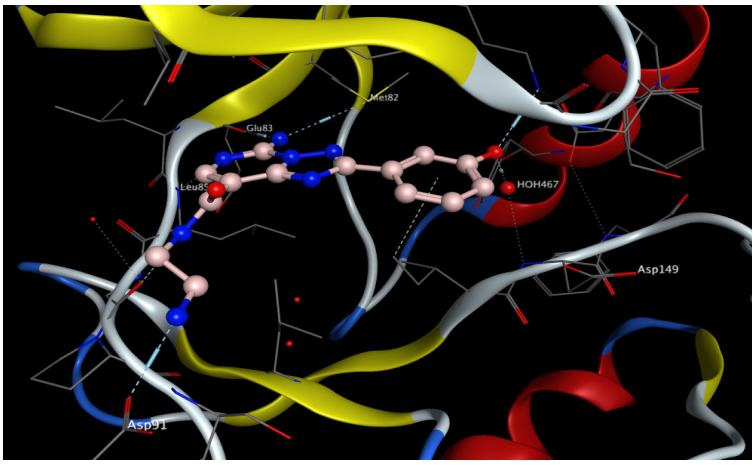

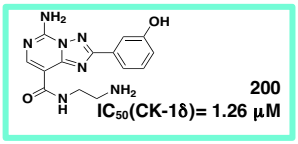

Figure 38. Docking studies with CK-1δ (PDB code: 4HNF) of compound **200**. The ligand is reported in pale pink x-sticks. Hydrogen bond interactions are highlighted by dotted lines.

3.2.4 Prediction of CNS permeation

Similarly to GSK-3β, CK-1δ inhibitors could have a clinical relevance in the field of CNS diseases and therefore it is important to assess if they are able to penetrate the BBB. Also in this case, we decided to predict the BBB-permeability of the most active compounds (IC_{50}<10 μM) using the PAMPA assay (**Table 12**).

Table 12. Permeability (*Pe* 10^{-6} cm s^{-1}) in the PAMPA-BBB assay of selected CK-1δ inhibitors with their predictive penetration in the CNS.

compd	IC_{50}(CK-1δ) μM	*Pe* (10^{-6} cm s^{-1})[a]	Prediction	compd	IC_{50}(CK-1δ) μM	*Pe* (10^{-6} cm s^{-1})[a]	Prediction
189[b]	2.06	1.3 ± 0.1	**CNS-**	**SF46**	7.9	9.7 ±2.29	**CNS+**
190[b]	4.75	0.84 ± 0.9	**CNS-**	**202**	0.30	13.1 ± 0.01	**CNS+**
191	0.48	3.0 ±0.04	**CNS-/+**	**206**	5.65	10.9 ±0.19	**CNS+**
193[b]	8.67	4.9. ± 1.6	**CNS+**	**208**	1.32	1.7 ±0.12	**CNS-**
198	0.32	3.5 ±0.15	**CNS-/+**	**209**	0.46	3.9 ±0.03	**CNS-/+**
200	1.26	4.1 ±0.18	**CNS+**	**211**	0.91	5.2 ± 0.16	**CNS+**
				212	0.18	3.7 ±10.17	**CNS-/+**

[a]Data are the mean ± SD of 2 independent experiments. *Pe*(exp)= 0.9324 (bibl) + 0.1988 (R^2= 0.8978), CNS+ >3.9, CNS - < 2.1.

As we can see from **Table 12**, many of the tested 2,5,8-trisubstituted TPs, presenting one or more hydroxyl groups on the scaffold, found difficult to pass the BBB in the *in vitro* assay (e.g. **190**, P_e= 0.84·10^{-6} cm/s). However, the same substitutions on the TT scaffold or on the 2,5,7-trisubstituted TPs are better tolerated, leading to more BBB-permeable derivatives (e.g. **189**, P_e= 1.3·10^{-6} cm/s *vs.* **209**, P_e= 3.9·10^{-6} cm/s *vs.* **202**, P_e= 13.1·10^{-6} cm/s). In particular, it is worth noting that the 2,5,7-trisubstituted TP derivative **202** presents a good inhibition potency towards CK-1δ (IC_{50} = 0.30 μM) and a high BBB-permeability according PAMPA, and therefore it could represent a valuable starting point for further structural optimizations and biological evaluations.

4.3 CONCLUSIONS

In the present Chapter the design and development of novel triazolo-pyrimidines and triazolo-triazines as CK-1δ inhibitors have been described. Both adenine-like scaffolds, opportunely decorated, resulted nearly superimposable and suitable to achieve CK-1δ inhibition, reaching IC_{50} values in the submicromolar range. The different modifications allowed outlining a SAR (summarized in **Figure 39**) for these novel CK-1δ inhibitors, and in particular:

- Position 2(TT/TP): the introduction of hydroxyphenyl or dihydroxyphenyl groups led to improved affinities for CK-1δ. In particular, *meta* and di-*meta* [**212**, IC_{50}(CK-1δ)= 0.18 μM] substitutions are preferred.
- Position 7(TT)/5(TP): primary amino group is required; any other substitution led to poorly active compounds.
- Position 5(TT)/7(TP): at this position a benzylamino group was maintained, as present in TT derivative **SF46** (**176**), and no other modifications were produced.
- Position 8(TP): ethyl ester is preferred to carboxylic acid, while different alkyl amides (e.g. ethylamide) contributed to gain affinity towards the kinase.

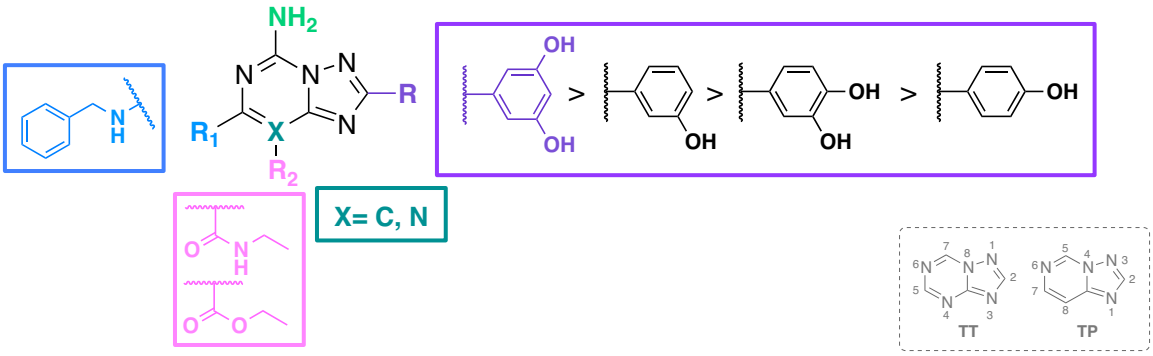

Figure 39. SAR for TTs and TPs derivatives **177-212** as CK-1δ inhibitors.

Molecular docking simulations, performed on few representative derivatives, helped us to rationalize the results obtained from the pharmacological evaluation, highlighting stabilizing interactions between the hydroxyl group at the 2-position of the ligand and CK-1δ ATP-binding pocket; on the other hand, PAMPA assay provided us a preliminary BBB-permeability prediction of the most promising derivatives and, in general, 5-benzylamino TTs and 7-benzylamino TPs presented the structural features required to have a good CNS-permeability. Among them, derivative **202** [IC_{50}(CK-1δ)= 0.30 μM] resulted BBB-permeable and so could be considered the reference compound for further studies on CK-1δ and its pharmacological implications.

4.4 EXPERIMENTAL SECTION

4.4.1 Chemistry

General material and methods used in the synthetic process are reported in Chapter 3.4.1.1

4.4.1.1 Synthesis of 2,5,8-trisubstituted [1,2,4]triazolo[1,5-c]pyrimidines

4.4.1.1.1 Synthesis of 4-hydroxy-2-methylthio-5-carbethoxypyrimidine sodium salt (215)

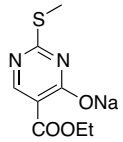

To a solution of 34.4 g (0.860 mol) of sodium hydroxide in 215 mL of water were added 59.8 g of 2-methyl-2-thio-pseudourea hemisulfate (**213**, 0.430 mol). The mixture was stirred for 5 min, by which time most of the pseudothiourea had dissolved. Diethyl ethoxymethylenemalonate (**214**, 0.430 mol, 92.9 g), dissolved in 500 mL of ethanol, was added under stirring over a period of 1 h. After the addition was completed, stirring was continued for 3 h and then the solid mixture was allowed to stand for 24 h. Finally, the mixture was filtered and washed using the minimum amount of water to give a pink solid (81.2 g). Yield 40%; mp >300°C. ^{1}H NMR (400 MHz, D_2O): δ 8.35 (s, 1H), 4.16 (q, *J* = 7.1 Hz, 2H), 2.33 (s, 3H), 1.20 (t, *J* = 7.1 Hz, 3H).

4.4.1.1.2 General procedure (VIII) for the synthesis of ethyl 4-(2-hydrazinyl)-2-(methylthio)pyrimidine-5-carbocarboxylate derivatives

To 10.0 g (42 mmol) of dried **215** were added 30 mL of phosphoryl oxychloride dropwise at 0°C (ice-bath). After the addition was completed, the mixture was refluxed for 5 h. The excess of phosphoryl oxychloride was then removed under reduced pressure and ice and cold water were added to the solid residue (150 mL). The mixture was extracted with EtOEt (3 x 50 mL), dried over sodium sulfate and the solvent was removed by evaporation under reduced pressure to give the 4-chloro-2-methylthio-5-carbethoxypyrimidine (**216**), which was weighted and readily used in the next step without purification. The chloropyrimidine obtained (**216**) and 1.76 equivalents of the required hydrazide were dissolved in THF (40 mL/0.015 mol of **216**), while 1.76 equivalents of DBU were added dropwise at 0°C. The mixture was stirred at room temperature overnight. The solvent was then removed, the residue was dissolved in dichloromethane (300 mL) and the resulting solution was washed with water (3 x 100 mL). The organic layer was dried over anhydrous sodium sulfate, concentrated under reduced pressure and purified by flash chromatography.

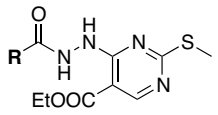

R= CH_3 (**230**)
cC_5H_9 (**231**)
2-indolyl (**232**)
Ph (**233**)
4-pyridyl (**234**)
4-F-Ph (**235**)
4-OCH_3-Ph (**236**)
3-F-Ph (**237**)
3-OCH_3-Ph (**238**)
3-NO_2-Ph (**239**)
4-OBn-Ph (**240**)
3-OBn-Ph (**241**)
3,4-$(OBn)_2$-Ph (**242**)
3,5-$(OBn)_2$-Ph (**243**)

ethyl 4-(2-acetylhydrazinyl)-2-(methylthio)pyrimidine-5-carboxylate (**230**)
Flash chromatography eluent: light petroleum-EtOAc 6:4. Yield 42% (4.76 g); pale yellow solid; mp 155°C (EtOEt-light petroleum). ^{1}H NMR (400 MHz; $CDCl_3$): 10.17 (s, 1H), 9.60 (s, 1H), 8.62 (s, 1H), 4.30 (q, *J* = 7.0 Hz, 2H), 2.46 (s, 3H), 1.92 (s, 3H), 1.29 (t, *J* = 7.1 Hz, 3H). ES-MS (methanol) m/z: 293.0 $[M+Na]^+$.

ethyl 4-[2-(cyclopentancarbonyl)hydrazinyl]-2-(methylthio)pyrimidine-5-carboxylate (**231**)
Flash chromatography eluent: light petroleum-EtOAc 8:2. Yield 24% (3.27 g); pale yellow solid; mp 127°C (EtOEt-light petroleum). ^{1}H NMR (270 MHz, $CDCl_3$): δ 10.05 (bs, 1H), 8.67 (s, 1H), 8.20 (bs, 1H), 4.35 (q, *J* = 7.0 Hz, 2H), 2.80-2.57 (m, 1H), 2.52 (s, 3H), 2.06-1.49 (m, 8H), 1.37 (t, *J* = 7.0 Hz, 3H). ES-MS (methanol) m/z: 323.0 $[M-H]^-$.

ethyl 4-[2-(1*H*-indol-2-carbonyl)hydrazinyl]-2-(methylthio)pyrimidine-5-carboxylate (**232**)
Flash chromatography eluent: light petroleum-EtOAc 8:2. Yield 46% (7.18 g); pale yellow solid; mp 253-255°C (EtOEt-light petroleum). ^{1}H NMR (400 MHz, DMSO-d_6): δ 11.71 (s, 1H), 10.69 (s, 1H), 9.76 (s, 1H), 8.68 (s, 1H), 7.65 (d, *J* = 8.0 Hz, 1H), 7.43 (d, *J* = 8.3 Hz, 1H), 7.27 (d, *J* = 1.3 Hz, 1H), 7.20 (t, *J* = 7.6 Hz, 1H), 7.05 (t, *J* = 7.3 Hz, 1H), 4.34 (q, *J* = 7.1 Hz, 2H), 2.29 (s, 3H), 1.33 (t, *J* = 7.1 Hz, 3H). ES-MS (methanol) m/z: 370.0 $[M-H]^-$.

ethyl 4-(2-benzoylhydrazinyl)-2-(methylthio)pyrimidine-5-carboxylate (**233**)
Flash chromatography eluent: DCM-EtOAc 95:5. Yield 34% (4.75 g); white solid; mp 168°C (EtOEt-light petroleum). ^{1}H NMR (270 MHz, $CDCl_3$): δ 10.43 (bs, 1H), 8.96 (bs, 1H), 8.75 (s, 1H), 7.91 (d, *J* = 7.5 Hz, 2H), 7.67 – 7.41 (m, 3H), 4.43 (q, *J* = 7.2 Hz, 2H), 2.52 (s, 3H), 1.44 (t, *J* = 7.2 Hz, 3H). ES-MS (methanol) m/z: 331.0 $[M-H]^-$.

ethyl 4-(2-isonicotinoylhydrazinyl)-2-(methylthio)pyrimidine-5-carboxylate (**234**)
Flash chromatography eluent: EtOAc-light petroleum 8:2. Yield 24% (4.12 g); white solid; mp 203-206°C (EtOEt-light petroleum). ^{1}H NMR (270 MHz, DMSO-d_6): δ 11.04 (bs, 1H), 9.85 (bs, 1H), 8.80 (d, *J* = 4.7 Hz, 2H), 8.70 (s, 1H), 7.81 (d, *J* = 4.7 Hz, 2H), 4.35 (q, *J* = 7.1 Hz, 2H), 2.34 (s, 3H), 1.34 (t, *J* = 7.1 Hz, 3H). ES-MS (methanol) m/z: 333.9 $[M+H]^+$, 355.9 $[M+Na]^+$.

ethyl 4-(2-(4-fluorobenzoyl)hydrazinyl)-2-(methylthio)pyrimidine-5-carboxylate (**235**)
Flash chromatography eluent: DCM-EtOAc 9:1. Yield 28%; white solid; mp 200°C (EtOEt-light petroleum). ^{1}H NMR (270 MHz, DMSO-d_6): δ 10.77 (bs, 1H), 9.78 (bs, 1H), 8.68 (s, 1H), 7.98 (dd, J_H= 8.8, J_{HF} = 5.6 Hz, 2H), 7.37 (t, $J_{H,HF}$ = 8.8 Hz, 2H), 4.34 (q, *J* = 7.0 Hz, 2H), 2.33 (s, 3H), 1.33 (t, *J* = 7.0 Hz, 3H). ES-MS (methanol) m/z: 348.9 $[M-H]^-$.

ethyl 4-(2-(4-methoxybenzoyl)hydrazinyl)-2-(methylthio)pyrimidine-5-carboxylate (**236**)
Flash chromatography eluent: light petroleum-EtOAc 6:4. Yield 57% (8.68 g); white solid; mp 186°C (EtOEt-light petroleum). ^{1}H NMR (400 MHz, $CDCl_3$): δ 10.57 (s, 1H), 9.71 (s, 1H), 8.66 (s, 1H), 7.88 (d, *J* = 8.8 Hz, 2H), 7.04 (d, *J* = 8.8 Hz, 2H), 4.33 (q, *J* = 7.1 Hz, 2H), 3.81 (s, 3H), 2.31 (s, 3H), 1.32 (t, *J* = 7.1 Hz, 3H). ES-MS (methanol) m/z: 361.0 $[M-H]^-$.

ethyl 4-(2-(3-fluorobenzoyl)hydrazinyl)-2-(methylthio)pyrimidine-5-carboxylate (**237**)
Flash chromatography eluent: DCM-EtOAc 9:1. Yield 66% (9.7 g); white solid; mp 175°C (EtOEt-light petroleum). ^{1}H NMR (400 MHz, $CDCl_3$): δ 10.82 (s, 1H), 9.78 (s, 1H), 8.67 (s, 1H), 7.75 (d, *J* = 7.8 Hz, 1H), 7.67 (dt, *J* = 8.0 Hz, *J* = 2.4 Hz, 1H), 7.61-7.55 (m, 1H), 7.45 (td, *J* = 8.0, *J* = 2.4 Hz, 1H), 4.33 (q, *J*= 7.1 Hz, 2H), 2.33 (s, 3H), 1.32 (t, *J*= 7.1 Hz, 3H). ES-MS (methanol) m/z: 351.0 $[M+H]^+$, 373.0 $[M+Na]^+$.

ethyl 4-(2-(3-methoxybenzoyl)hydrazinyl)-2-(methylthio)pyrimidine-5-carboxylate (**238**)
Flash chromatography eluent: from DCM-EtOAc 95:5 to DCM-MeOH 9:1.Yield 43% (6.54 g); white solid; mp 145-150°C (EtOEt-light petroleum). ^{1}H NMR (400 MHz, $CDCl_3$): δ 10.34 (bs,

1H), 8.88 (bs, 1H), 8.71 (s, 1H), 7.44 – 7.33 (m, 3H), 7.10 (bs, 1H), 4.39 (q, *J* = 7.1 Hz, 2H), 3.87 (s, 3H), 2.49 (s, 3H), 1.41 (t, *J* = 7.1 Hz, 3H). ES-MS (methanol) m/z: 363.1 $[M+H]^+$, 385.1 $[M+Na]^+$.

ethyl 4-(2-(3-nitro)hydrazinyl)-2-(methylthio)pyrimidine-5-carboxylate (**239**)
Flash chromatography eluent: from light petroleum-EtOAc 9:1 to 4:6. Yield 63% (10.0 g); white solid; mp 204-208°C (EtOEt-light petroleum). ^{1}H NMR (400 MHz, DMSO-d_6): δ 11.14 (s, 1H), 9.90 (s, 1H), 8.74 (s, 1H), 8.70 (s, 1H), 8.49 – 8.44 (m, 1H), 8.36 – 8.31 (m, 1H), 7.86 (t, *J* = 8.0 Hz, 1H), 4.36 (q, *J* = 7.1 Hz, 2H), 2.35 (s, 3H), 1.34 (t, *J* = 7.1 Hz, 3H).). ES-MS (methanol) m/z: 378.3 $[M+H]^+$, 400.3 $[M+Na]^+$.

ethyl 4-(2-(4-(benzyloxy)benzoyl)hydrazinyl)-2-(methylthio)pyrimidine-5-carboxylate (**240**)
Flash chromatography eluent: DCM-EtOAc 9:1. Yield 40.5% (7.46 g); yellow solid; mp 202-205°C (EtOEt-light petroleum). ^{1}H NMR (400 MHz, DMSO-d_6): δ 10.58 (bs, 1H), 9.75 (bs, 1H), 8.67 (s, 1H), 7.89 (d, *J* = 7.9 Hz, 2H), 7.47-7.35 (m, 5H), 7.14 (d, *J* = 7.9 Hz, 2H), 5.19 (s, 2H), 4.34 (q, *J* = 6.6 Hz, 2H), 2.33 (s, 3H), 1.33 (t, *J* = 6.6 Hz, 3H). ES-MS (methanol) m/z: 439.2 $[M+H]^+$, 461.1 $[M+Na]^+$, 477.1 $[M+K]^+$.

ethyl 4-(2-(3-(benzyloxy)benzoyl)hydrazinyl)-2-(methylthio)pyrimidine-5-carboxylate (**241**)
Flash chromatography eluent: DCM-EtOAc 9:1. Yield 33.5% (6.17 g); white solid; mp 117°C (EtOEt-light petroleum). ^{1}H NMR (270 MHz, DMSO-d_6): δ 10.72 (bs, 1H), 9.77 (bs, 1H), 8.68 (s, 1H), 7.71 – 7.11 (m, 9H), 5.17 (s, 2H), 4.34 (q, *J* = 7.1 Hz, 2H), 2.33 (s, 3H), 1.33 (t, *J* = 7.1 Hz, 3H). ES-MS (methanol) m/z: 438.9 $[M+H]^+$, 460.8 $[M+H]^+$.

ethyl 4-(2-(3,4-bis(benzyloxy)benzoyl)hydrazinyl)-2-(methylthio)pyrimidine-5-carboxylate (**242**)
Flash chromatography eluent: from DCM-light petroleum 9.5:0.5 to DCM-EtOAc 8:2. Yield 30% (6.86 g); white solid; mp 186°C (EtOEt-light petroleum). ^{1}H NMR (270 MHz, DMSO-d_6): δ 10.59 (bs, 1H), 9.74 (bs, 1H), 8.68 (s, 1H), 7.62 (s, 1H), 7.60-7.26 (m, 11H), 7.20 (d, *J* = 8.4 Hz, 1H), 5.21 (d, *J* = 9.9 Hz, 4H), 4.35 (q, *J* = 6.7 Hz, 2H), 2.31 (s, 3H), 1.33 (t, *J* = 6.7 Hz, 3H). ES-MS (methanol) m/z: 544.9 $[M+H]^+$, 566.9 $[M+Na]^+$.

ethyl 4-(2-(3,5-bis(benzyloxy)benzoyl)hydrazinyl)-2-(methylthio)pyrimidine-5-carboxylate (**243**)
Flash chromatography eluent: from DCM-EtOAc 9:1 to DCM-EtOAc 8.5:1.5. Yield 54% (12.35 g); white solid; mp 184-188°C (EtOEt-light petroleum). ^{1}H NMR (400 MHz, DMSO-d_6): δ 10.69 (s, 1H), 9.77 (s, 1H), 8.68 (s, 1H), 7.49 – 7.33 (m, 10H), 7.16 (s, 2H), 6.91 (s, 1H), 5.16 (s, 4H), 4.35 (q, *J* = 7.0 Hz, 2H), 2.33 (s, 3H), 1.34 (t, *J* = 7.0 Hz, 3H). ES-MS (methanol) m/z: 545.2 $[M+H]^+$, 567.3 $[M+Na]^+$.

4.4.1.1.3 Synthesis of 2-substituted 5-(methylthio)-[1,2,4]triazolo[1,5-c]pyrimidine-8-carboxylate derivatives (244-257)

- **General procedure (IX) for the preparation of compounds 244-247**
  To 150 mL of dry xylene were added 0.030 mol of phosphorus pentoxide and hexamethyldisiloxane, and the mixture was heated at 90°C for 2 h. Compounds **230-232, 236** (0.010 mol) were then added, and the reaction was refluxed for 2 days. After that, the solvent was removed under reduced pressure, and the residue was dissolved in EtOAc (200 mL) and washed with water (3 x 70 mL). The organic layer was then dried over anhydrous sodium sulfate, concentrated under reduced pressure and purified by flash chromatography.

- Compounds **248-257** were obtained according to **General Procedure (IIIa/IIIb)** (Chapter 3.4.1.2.3), from 0.010 mol of compounds **233-235, 237-243** and refluxed for 20 hours.

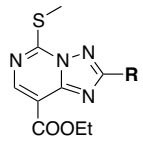

R= CH_3 (**244**), cC_5H_9 (**245**), 2-indolyl (**246**), 4-OCH_3-Ph (**247**), Ph (**248**), 4-pyridyl (**249**), 4-F-Ph (**250**), 3-F-Ph (**251**), 3-NO_2-Ph (**252**), 4-OBn-Ph (**253**), 3-OBn-Ph (**254**), 3,4-$(OBn)_2$-Ph (**255**), 3-OCH_3-Ph (**256**), 3,5-$(OBn)_2$-Ph (**257**)

ethyl 2-methyl-5-(methylthio)-[1,2,4]triazolo[1,5-*c*]pyrimidine-8-carboxylate (**244**)
Procedure **IX**. Flash chromatography eluent: light petroleum-EtOAc 6:4. Yield 32% (0.807 g); pale yellow solid; mp 120°C (EtOEt-light petroleum). ^{1}H NMR (400 MHz, $CDCl_3$): δ 8.76 (s, 1H), 4.50 (q, *J* = 7.1 Hz, 2H), 2.78 (s, 3H), 2.70 (s, 3H), 1.44 (t, *J* = 7.1 Hz, 3H). ES-MS (methanol) m/z: 225.0 $[M+H-(CH_2CH_3)]^+$, 253.0 $[M+H]^+$, 275.0 $[M+Na]^+$.

ethyl 2-cyclopentyl-5-(methylthio)-[1,2,4]triazolo[1,5-*c*]pyrimidine-8-carboxylate (**245**)
Procedure **IX**. Flash chromatography eluent: light petroleum-EtOAc 8:2. Yield 28% (0.858 g); white solid; mp 95°C (EtOEt-light petroleum). ^{1}H NMR (400 MHz, $CDCl_3$): δ 8.74 (s, 1H), 4.49 (q, *J* = 7.1 Hz, 2H), 3.48 (p, *J* = 8.3 Hz, 1H), 2.77 (s, 3H), 2.21-2.13 (m, 2H), 2.09-1.99 (m, 2H), 1.90-1.82 (m, 2H), 1.76-1.67 (m, 2H), 1.44 (d, *J* = 7.1 Hz, 3H). ES-MS (methanol) m/z: 307.1 $[M+H]^+$, 329.1 $[M+Na]^+$.

ethyl 2-(1-*H*-indol-2-yl)-5-(methylthio)-[1,2,4]triazolo[1,5-*c*]pyrimidine-8-carboxylate (**246**)
Procedure **IX**. Flash chromatography eluent: light petroleum-EtOAc 7:3. Yield 28% (0.989 g); yellow solid; mp 187-190°C (EtOEt-light petroleum). ^{1}H NMR (400 MHz, $CDCl_3$): δ 9.39 (s, 1H), 8.80 (s, 1H), 7.71 (d, *J* = 8.0 Hz, 1H), 7.50-7.45 (m, 2H), 7.31-7.27 (m, 1H), 7.17-7.13 (m, 1H), 4.54 (q, *J* = 7.1 Hz, 2H), 2.82 (s, 3H), 1.49 (t, *J* = 7.1 Hz, 3H). ES-MS (methanol) m/z: 354.1 $[M+H]^+$, 376.0 $[M+Na]^+$.

ethyl 2-(4-methoxyphenyl)-5-(methylthio)-[1,2,4]triazolo[1,5-*c*]pyrimidine-8-carboxylate (**247**)
Procedure **IX**. Flash chromatography eluent: DCM (stationary phase: neutral aluminium oxide). Yield 57% (1.96 g); white solid; mp 182-184°C (EtOEt-light petroleum). ^{1}H NMR (400 MHz, $CDCl_3$): δ 8.78 (s, 1H), 8.35 (d, *J* = 8.9 Hz, 2H), 7.01 (d, *J* = 8.9 Hz, 2H), 4.52 (q, *J* = 7.1 Hz, 2H), 3.88 (s, 3H), 2.80 (s, 3H), 1.49 (t, *J* = 7.1 Hz, 3H). ES-MS (methanol) m/z: 345.2 $[M+H]^+$, 367.1 $[M+Na]^+$.

ethyl 2-phenyl-5-(methylthio)-[1,2,4]triazolo[1,5-*c*]pyrimidine-8-carboxylate (**248**)
Procedure **III$_a$**. Flash chromatography eluent: light petroleum-EtOAc from 9:1 to 4:6 (stationary phase: neutral aluminium oxide). Yield 16% (0.503 g); white solid; mp 169-171°C (EtOEt-light petroleum). ^{1}H NMR (270 MHz, $CDCl_3$): δ 8.80 (s, 1H), 8.41 (m, 2H), 7.51 (m, 3H), 4.53 (q, J = 6.5 Hz, 2H), 2.81 (s, 3H), 1.49 (t, J = 6.5 Hz, 3H). ES-MS (methanol) m/z: 315.2 $[M+H]^+$, 337.2 $[M+Na]^+$, 353.1 $[M+K]^+$.

ethyl 2-(pyridin-4-yl)-5-(methylthio)-[1,2,4]triazolo[1,5-*c*]pyrimidine-8-carboxylate (**249**)
Procedure **III$_a$**. Flash chromatography eluent: DCM-MeOH 97:3. Yield 8% (0.252 g); white solid; mp 183-185°C (EtOEt-light petroleum). ^{1}H NMR (400 MHz, DMSO-d_6): δ 8.83-8.81 (m, 3H), 8.14 (dd, J = 4.4, 1.6 Hz, 2H), 4.43 (q, *J* = 7.1 Hz, 2H), 2.80 (s, 3H), 1.40 (t, *J* = 7.1 Hz, 3H). ES-MS (methanol) m/z: 316.4 $[M+H]^+$, 338.3 $[M+Na]^+$.

ethyl 2-(4-fluorophenyl)-5-(methylthio)-[1,2,4]triazolo[1,5-*c*]pyrimidine-8-carboxylate (**250**)
Procedure **III$_a$**. Flash chromatography eluent: DCM-EtOAc from 95:5. Yield 6% (0.199 g);

white solid; mp 188-190°C (EtOEt-light petroleum). ^{1}H NMR (270 MHz, $CDCl_3$): δ 8.80 (s, 1H), 8.41 (dd, J_H= 8.2 Hz, J_{HF}= 5.7 Hz, 2H), 7.18 (t, $J_{H,HF}$=8.2Hz, 2H), 4.53 (q, J=7.1 Hz, 2H), 2.80 (s, 3H) 1.48 (t, J=7.1 Hz, 3H). ES-MS (methanol) m/z: 332.9 $[M+H]^+$, 354.9 $[M+Na]^+$, 370.8 $[M+K]^+$.

ethyl 2-(3-fluorophenyl)-5-(methylthio)-[1,2,4]triazolo[1,5-*c*]pyrimidine-8-carboxylate (**251**)
Procedure **III$_a$**. Flash chromatography eluent: light petroleum-EtOAc 95:5 (stationary phase: neutral aluminium oxide). Yield 14% (0.465 g); white solid; mp 153-156°C (EtOEt-light petroleum). ^{1}H NMR (400 MHz, $CDCl_3$): 8.81 (s, 1H), 8.20 (m, 1H), 8.12-8.09 (m, 1H), 7.47 (td, J = 8.0, J_{HF} = 5.7 Hz, 1H), 7.23-7.17 (m, 1H), 4.53 (q, J = 7.1 Hz, 2H), 2.81 (s, 3H), 1.49 (t, J = 7.1 Hz, 3H). ES-MS (methanol) m/z: 333.0 $[M+H]^+$.

ethyl 2-(3-nitrophenyl)-5-(methylthio)-[1,2,4]triazolo[1,5-*c*]pyrimidine-8-carboxylate (**252**)
Procedure **III$_a$**. Flash chromatography eluent: DCM-light petroleum 8:2 (stationary phase: neutral aluminium oxide). Yield 7% (0.252 g); white solid; mp 210-215°C (EtOEt-light petroleum). ^{1}H NMR (400 MHz, $CDCl_3$): δ 9.23 (s, 1H), 8.84 (s, 1H), 8.77 – 8.72 (m, 1H), 8.39 – 8.33 (m, 1H), 7.70 (t, J = 8.0 Hz, 1H), 4.54 (q, J = 7.1 Hz, 2H), 2.83 (s, 3H), 1.49 (t, J = 7.1 Hz, 3H). ES-MS (methanol) m/z: 332.3 $[M+H-(CH_2CH_3)]^+$, 360.3 $[M+H]^+$, 382.3 $[M+Na]^+$.

ethyl 2-(4-(benzyloxy)phenyl)-5-(methylthio)-[1,2,4]triazolo[1,5-*c*]pyrimidine-8-carboxylate (**253**)
Procedure **III$_a$**. Flash chromatography eluent: DCM. Yield 7% (0.294 g); white solid; mp 190-192°C (EtOEt-light petroleum). ^{1}H NMR (400 MHz, $CDCl_3$): δ 8.79 (s, 1H), 8.37 (d, J = 8.7 Hz, 2H), 7.56–7.30 (m, 5H), 7.09 (d, J = 8.7 Hz, 2H), 5.14 (s, 2H), 4.53 (q, J = 7.1 Hz, 2H), 2.80 (s, 3H), 1.49 (t, J = 7.1 Hz, 3H). ES-MS (methanol) m/z: 421.0 $[M+H]^+$, 443.0 $[M+Na]^+$, 458.9 $[M+K]^+$.

ethyl 2-(3-(benzyloxy)phenyl)-5-(methylthio)-[1,2,4]triazolo[1,5-*c*]pyrimidine-8-carboxylate (**254**)
Procedure **III$_a$**. Flash chromatography eluent: light petroleum-EtOAc 8:2. Yield 7% (0.294 g); white solid; mp 167-169°C (EtOEt-light petroleum). ^{1}H NMR (270 MHz, $CDCl_3$): δ 8.81 (s, 1H), 8.03 (d, J = 8.0 Hz, 2H), 7.57-7.30 (m, 6H), 7.12 (d, J = 6.6 Hz, 1H), 5.18 (s, 2H), 4.53 (q, J = 7.1 Hz, 2H), 2.81 (s, 3H), 1.49 (t, J = 7.1 Hz, 3H). ES-MS (methanol) m/z: 421.4 $[M+H]^+$, 443.3 $[M+Na]^+$.

ethyl 2-(3,4-bis(benzyloxy)phenyl)5-(methylthio)-[1,2,4]triazolo[1,5-*c*]pyrimidine-8-carboxylate (**255**)
Procedure **III$_a$**. Flash chromatography eluent: DCM-EtOAc 99:1. Yield 6.5% (0.342 g); white solid; mp 170-172°C (EtOEt-light petroleum). ^{1}H NMR (270 MHz; $CDCl_3$): δ 8.80 (s, 1H), 8.08-7.97 (m, 2H), 7.57-7.28 (m, 10H), 7.08-6.99 (m, 1H), 5.34-5.17 (m, 4H), 4.59-4.48 (q, J = 6.5 Hz, 2H), 2.81 (s, 3H), 1.55-1.43 (t, J = 6.5 Hz, 3H). ES-MS (methanol) m/z: 527.2 $[M+H]^+$, 549.2 $[M+Na]^+$, 565.1 $[M+K]^+$.

ethyl 2-(3-methoxyphenyl)-5-(methylthio)-[1,2,4]triazolo[1,5-*c*]pyrimidine-8-carboxylate (**256**)
Procedure **III$_b$**. Flash chromatography eluent: light petroleum-EtOAc 8:2. Yield 59% (2.03 g)); white solid; mp 154°C (EtOEt-light petroleum). ^{1}H NMR (270 MHz, $CDCl_3$): δ 8.80 (s, 1H), 8.06-7.87 (m, 2H), 7.41 (t, J = 7.8 Hz, 1H), 7.06 (dd, J = 7.8, 2.7 Hz, 1H), 4.53 (q, J = 7.1 Hz, 2H), 3.93 (s, 3H), 2.81 (s, 3H), 1.49 (t, J = 7.1 Hz, 3H). ES-MS (methanol) m/z: 345.4 $[M+H]^+$, 367.3 $[M+Na]^+$.

ethyl 2-(3,5-bis(benzyloxy)phenyl)5-(methylthio)-[1,2,4]triazolo[1,5-*c*]pyrimidine-8-carboxylate (**257**)
Procedure **III$_b$**. Flash chromatography eluent: light petroleum-EtOAc 8:2. Yield 5% (0.263 g); white solid; mp 170-175°C (EtOEt-light petroleum). ^{1}H NMR (400 MHz, $CDCl_3$): δ 8.80 (s, 1H), 7.69 (s, 2H), 7.53 7.30 (m, 10H), 6.76 (s, 1H), 5.14 (s, 4H), 4.53 (q, *J* = 7.0 Hz, 2H), 2.80 (s, 3H), 1.48 (t, *J* = 7.0 Hz, 3H). ES-MS (methanol) m/z: 527.3 $[M+H]^+$, 549.2 $[M+Na]^+$.

4.4.1.1.4 General procedure (X) for the preparation of 2-substituted 5-amino-[1,2,4]triazolo[1,5-*c*]pyrimidine-8-carboxylate derivatives

1 mL of methanolic ammonia 7N and 4 mL of methanol were added to 0.5 mmol of 5-(methylthio)-[1,2,4]triazolo[1,5-*c*]pyrimidine-8-carboxylate derivatives and the mixture was heated at 70°C in a sealed tube for 3-12 hours. The solvent was then removed under vacuum and the solid purified by flash chromatography.

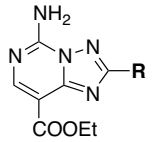

R= CH_3 (**177**)
cC_5H_9 (**178**)
2-indolyl (**179**)
4-pyridyl (**180**)
4-OCH_3-Ph (**181**)
3-F-Ph (**182**)
3-OCH_3-Ph (**183**)
3-NO_2-Ph (**194**)
4-OBn-Ph (**258**)
3-OBn-Ph (**259**)
3,4-$(OBn)_2$-Ph (**260**)
3,5-$(OBn)_2$-Ph (**261**)

ethyl 5-amino-2-methyl-[1,2,4]triazolo[1,5-*c*]pyrimidine-8-carboxylate (**177**)
Flash chromatography eluent: light petroleum-EtOAc 8:2. Yield 52% (57 mg); white solid; mp 238-241°C (EtOEt-light petroleum). ^{1}H NMR (270 MHz, DMSO-d_6): δ 8.90-8.35 (m, 3H), 4.30 (q, *J* = 7.1 Hz, 2H), 2.51 (s, 3H), 1.31 (t, *J* = 7.1 Hz, 3H). ^{1}H NMR (270 MHz, DMSO-d_6/D_2O) δ: 8.44 (s, 1H), 4.27 (bs, 2H), 2.46 (s, 3H), 1.27 (bs, 3H). ^{13}C NMR (101 MHz, DMSO-d_6): δ 164.5, 163.5, 152.2, 151.6, 150.2, 103.0, 60.5, 14.80, 14.70. ES-MS (methanol) m/z: 222.4 $[M+H]^+$, 244.4 $[M+Na]^+$.

ethyl 5-amino-2-cyclopentyl-[1,2,4]triazolo[1,5-*c*]pyrimidine-8-carboxylate (**178**)
Flash chromatography eluent: light petroleum-EtOAc 1:1. Yield 27% (37 mg); white solid; mp 179-181°C (EtOEt-light petroleum). ^{1}H NMR (400 MHz, $CDCl_3$): δ 8.80-8.29 (m, 3H), 4.29 (q, *J* = 7.1 Hz, 2H), 3.36-3.28 (m, 1H), 2.09-2.00 (m, 2H), 1.98-1.85 (m, 2H), 1.83-1.73 (m, 2H), 1.73-1.61 (m, 2H), 1.31 (t, *J* = 7.1 Hz, 3H). ^{13}C NMR (101 MHz, DMSO-d_6): δ 171.6, 163.4, 152.0, 151.7, 150.2, 103.1, 60.5, 39.0, 32.4, 25.8, 14.7. ES-MS (methanol) m/z: 276.1 $[M+H]^+$, 298.1 $[M+Na]^+$.

ethyl 5-amino-2-(1*H*-indol-2-yl)-[1,2,4]triazolo[1,5-*c*]pyrimidine-8-carboxylate (**179**)
Flash chromatography eluent: light petroleum-EtOAc 6:4. Yield 16% (26 mg); white solid; mp 296-299°C (EtOEt-light petroleum). ^{1}H NMR (400 MHz, DMSO-d_6): δ 11.76 (s, 1H), 8.95-8.30 (m, 3H), 7.64 (d, *J* = 7.9 Hz, 1H), 7.53 (d, *J* = 8.1 Hz, 1H), 7.19-7.15 (m, 2H), 7.04 (t, *J* = 7.3 Hz, 1H), 4.34 (q, *J* = 7.1 Hz, 2H), 1.35 (t, *J* = 7.1 Hz, 3H). ^{13}C NMR (101 MHz, DMSO-d_6): δ 163.2, 159.4, 152.4, 152.2, 150.4, 137.8, 128.7, 128.2, 123.3, 121.4, 120.2, 112.8, 110.0, 103.4, 60.6, 14.8. ES-MS (methanol) m/z: 323.2 $[M+H]^+$, 345.1 $[M+Na]^+$.

ethyl 5-amino-2-(piridin-4-yl)-[1,2,4]triazolo[1,5-*c*]pyrimidine-8-carboxylate (**180**)
Flash chromatography eluent: EtOAc-MeOH 99:1. Yield 58.5% (83 mg); white solid; mp 268-270°C (EtOEt-light petroleum). ^{1}H NMR (400 MHz, DMSO-d_6): δ 9.08 (bs, 1H), 8.82 (d, *J* =

5.9 Hz, 2H), 8.71–8.47 (m, 2H), 8.12 (d, *J* = 5.9 Hz, 2H), 4.34 (q, *J* = 7.1 Hz, 2H), 1.36 (t, *J* = 7.1 Hz, 3H). ^{13}C NMR (270 MHz, $CDCl_3$-CF_3COOD): δ 161.7, 152.6, 149.0, 145.9, 142.9, 142.3, 125.6, 123.6, 106.7, 63.1, 14.2. ES-MS (methanol) m/z: 284.9 $[M+H]^+$, 306.9 $[M+Na]^+$.

ethyl 5-amino-2-(4-methoxyphenyl)-[1,2,4]triazolo[1,5-*c*]pyrimidine-8-carboxylate (**181**)
Flash chromatography eluent: DCM-MeOH 98:2. Yield 40% (63 mg); white solid; mp 232°C (EtOEt-light petroleum). ^{1}H NMR (270 MHz, DMSO-d_6): δ 8.90 (s, 1H), 8.65-8.28 (m, 2H), 8.18 (d, *J* = 8.8 Hz, 2H), 7.13 (d, *J* = 8.8 Hz, 2H), 4.33 (q, *J* = 7.1 Hz, 2H), 3.85 (s, 3H), 1.35 (t, *J* = 7.1 Hz, 3H). ^{13}C NMR (68 MHz, DMSO-d_6): δ 163.86, 163.23, 161.43, 152.07, 151.97, 150.19, 128.99, 122.53, 114.46, 102.98, 60.18, 55.36, 14.25. ES-MS (methanol) m/z: 314.1 $[M+H]^+$, 336.1 $[M+Na]^+$.

ethyl 5-amino-2-(3-fluorophenyl)-[1,2,4]triazolo[1,5-*c*]pyrimidine-8-carboxylate (**182**)
Flash chromatography eluent: DCM-MeOH 96:4. Yield 40% (60 mg); white solid; mp 223-225°C (EtOEt-light petroleum). ^{1}H NMR (270 MHz, DMSO-d_6): δ 9.17-8.34 (m, 3H), 8.09 (d, *J* = 7.0 Hz, 1H), 7.95 (m, 1H), 7.70-7.59 (m, 1H), 7.42 (m, 1H), 4.34 (q, *J* = 7.0 Hz, 2H), 1.35 (t, *J* = 7.0 Hz, 3H). ^{13}C NMR (68 MHz, DMSO-d_6): δ 163.1, 162.8, 162.6 (d, J_{CF} = 244.1 Hz), 152.4, 152.2, 150.3, 132.5 (d, J_{CF} = 8.8 Hz), 131.4 (d, J_{CF} = 8.4 Hz), 123.5 (d, J_{CF} = 2.8 Hz), 117.7 (d, J_{CF} = 21.0 Hz), 113.75 (d, J_{CF} = 23.1 Hz), 103.2, 60.3, 14.25. ES-MS (methanol) m/z: 274.4 $[M+2H-(CH_2CH_3)]^+$, 302.5 $[M+H]^+$, 324.4 $[M+Na]^+$, 340.3 $[M+K]^+$.

ethyl 5-amino-2-(3-methoxyphenyl)-[1,2,4]triazolo[1,5-*c*]pyrimidine-8-carboxylate (**183**)
Flash chromatography eluent: light petroleum-EtOAc 8:2. Yield 81% (127 mg); white solid; mp 200-204°C (EtOEt-light petroleum). ^{1}H NMR (400 MHz, DMSO-d_6): δ 8.99 (s, 1H), 8.52 (bs, 2H), 7.89-7.74 (m, 2H), 7.50 (t, *J* = 7.9 Hz, 1H), 7.13 (d, *J* = 7.9 Hz, 1H), 4.34 (q, *J* = 7.0 Hz, 2H), 3.87 (s, 3H), 1.36 (t, *J* = 7.0 Hz, 3H). ^{13}C NMR (68 MHz, DMSO-d_6): δ 163.8, 163.2, 159.8, 152.2, 152.1, 150.3, 131.5, 130.3, 119.8, 116.6, 112.4, 103.15, 60.3, 55.3, 14.3. ES-MS (methanol) m/z: 286.3 $[M+2H-(CH_2CH_3)]^+$, 314.4 $[M+H]^+$, 336.3 $[M+Na]^+$.

ethyl 5-amino-2-(3-nitrophenyl)-[1,2,4]triazolo[1,5-*c*]pyrimidine-8-carboxylate (**184**)
Flash chromatography eluent: light petroleum-EtOAc 6:4. Yield 91% (149 mg); white solid; mp 275-280°C (EtOEt-light petroleum). ^{1}H NMR (400 MHz, DMSO-d_6): δ 9.07 (bs, 1H), 9.01 (s, 1H), 8.73-8.48 (m, 3H), 8.42 (d, *J* = 7.6 Hz, 1H), 7.91 (t, *J* = 7.6 Hz, 1H), 4.35 (q, *J* = 7.1 Hz, 2H), 1.37 (t, *J* = 7.1 Hz, 3H). ^{13}C NMR (68 MHz, DMSO-d_6): 163.05, 162.0, 152.6, 152.4, 150.4, 148.5, 133.4, 131.8, 131.1, 125.4, 121.7, 103.2, 60.3, 14.27. ES-MS (methanol) m/z: 329.4 $[M+H]^+$, 351.4 $[M+Na]^+$.

ethyl 5-amino-2-(4-(benzyloxy)phenyl)-[1,2,4]triazolo[1,5-*c*]pyrimidine-8-carboxylate (**258**)
Flash chromatography eluent: DCM-methanol 95:5. Yield 93% (185 mg); white solid; mp 277-280°C (EtOEt-light petroleum). ^{1}H NMR (400 MHz, DMSO-d_6): δ 8.86 (bs, 1H), 8.65 - 8.32 (m, 2H), 8.18 (d, *J* = 8.4 Hz, 2H), 7.44 (m, 5H), 7.22 (d, *J* = 8.4 Hz, 2H), 5.20 (s, 2H), 4.33 (q, *J* = 6.9 Hz, 2H), 1.35 (t, *J* = 6.9 Hz, 3H). ^{13}C NMR (68 MHz, $CDCl_3$): δ 163.26, 161.81, 160.57, 152.11, 151.99, 150.21, 136.92, 129.00, 128.66, 128.16, 128.04, 115.28, 102.98, 69.48, 60.18, 14.26. ES-MS (methanol) m/z: 390.2 $[M+H]^+$, 412.1 $[M+Na]^+$, 428.1 $[M+K]^+$.

ethyl 5-amino-2-(3-(benzyloxy)phenyl)-[1,2,4]triazolo[1,5-*c*]pyrimidine-8-carboxylate (**259**)
Flash chromatography eluent: EtOAc-light petroleum 6:4. Yield 45% (88 mg); white solid; mp 196-198°C (EtOEt-light petroleum). ^{1}H NMR (400 MHz, DMSO-d_6): δ 9.26-8.35 (m, 3H), 7.88 (m, 2H), 7.71-7.28 (m, 6H), 7.21 (s, 1H), 5.21 (s, 2H), 4.33 (bs, 2H), 1.35 (bs, 3H). ^{13}C NMR (68 MHz, DMSO-d_6): δ 163.4, 162.9, 158.6, 151.95, 151.78, 150.0, 136.9, 131.3, 130.1, 128.5, 127.9, 127.7, 119.8, 117.1, 113.4, 103.0, 69.3, 60.2, 14.3. ES-MS (methanol) m/z: 390.0 $[M+H]^+$, 412.0 $[M+Na]^+$.

ethyl 5-amino-2-(3,4-bis(benzyloxy)phenyl)-[1,2,4]triazolo[1,5-*c*]pyrimidine-8-carboxylate (**260**)

Flash chromatography eluent: DCM-MeOH 99:1. Yield 65% (161 mg); white solid; mp 200-202°C (EtOEt-light petroleum). ^{1}H NMR (270 MHz; DMSO-d_6): δ 9.01-8.84 (m, 1H), 8.56-8.36 (m, 2H), 7.94-7.80 (m, 2H), 7.56-7.24 (m, 11H), 5.29-5.16 (m, 4H), 4.33 (q, *J* = 7.0 Hz, 2H), 1.36 (t, *J* = 7.0 Hz, 3H). ^{13}C NMR (68 MHz, DMSO-d_6): δ 163.5, 163.0, 151.9, 151.7, 150.5, 150.0, 148.2, 137.0, 136.9, 128.4, 127.9, 127.6, 122.9, 121.0, 114.1, 113.0, 102.9, 70.3, 70.0, 60.2, 14.3. ES-MS (methanol) m/z: 496.2 $[M+H]^+$, 518.2 $[M+Na]^+$, 534.1 $[M+K]^+$.

ethyl 5-amino-2-(3,5-bis(benzyloxy)phenyl)-[1,2,4]triazolo[1,5-*c*]pyrimidine-8-carboxylate (**261**)

Flash chromatography eluent: DCM-MeOH 99:1. Yield 70% (173 mg); white solid; mp 245-248°C (EtOEt-light petroleum). ^{1}H NMR (400 MHz; DMSO-d_6): δ 9.00-8.52 (m, 3H), 7.68-7.24 (m, 12H), 6.89 (s, 1H), 5.20 (s, 4H), 4.34 (q, *J* = 7.0 Hz, 2H), 1.35 (t, *J* = 7.0 Hz, 3H). ^{13}C NMR (68 MHz, DMSO-d_6): δ 163.6, 163.2, 160.05, 152.2, 152.0, 150.3, 137.0, 132.1, 128.7, 128.1, 127.9, 106.4, 104.2, 103.2, 69.55, 60.2, 14.3. ES-MS (methanol) m/z: 496.2 $[M+H]^+$, 518.2 $[M+Na]^+$, 534.2 $[M+K]^+$.

4.4.1.1.5 General procedure (XI) for the synthesis of the N^5-substituted 2-aryl-5-amino-8-ethoxycarbonyl-[1,2,4]triazolo[1,5-*c*]pyrimidine derivatives

Compounds **248-249, 252, 256** (0.5 mmol) were dissolved in 4 mL of ethanol and reacted with 1.5 mmol of the required amine, heating at 90°C for 3 hours in a sealed tube. Once the reaction was completed, the solvent was evaporated and the crude products purified through flash chromatography.

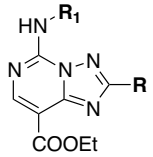

R= Ph (**185**)
4-F-Ph (**186**)
3-OBn-Ph (**262**)
3-OCH_3-Ph (**263-264**)

R_1= CH_2[3,4$(OCH_3)_2$]Ph (**185, 186**)
CH_3 (**262**)
CH_2Ph (**263**)
CH_2(4-Ph)Ph (**264**)

ethyl 5-((3,4-dimethoxybenzyl)amino)-2-phenyl-[1,2,4]triazolo[1,5-*c*]pyrimidine-8-carboxylate (**185**)

Flash chromatography eluent: light petroleum-EtOAc 8:2. Yield 38% (82 mg); white solid; mp 163-166°C (EtOEt-light petroleum). ^{1}H NMR (270 MHz, DMSO-d_6): δ 9.41 (t, *J* = 6.1 Hz, 1H), 8.58 (s, 1H), 8.39-8.13 (m, 2H), 7.70-7.42 (m, 3H), 7.08 (s, 1H), 6.95 (d, *J* = 7.9Hz, 1H), 6.88 (d, *J* = 7.9 Hz, 1H), 4.75 (d, *J* = 6.1 Hz, 2H), 4.34 (q, *J* = 6.8 Hz, 2H), 3.73 (s, 3H), 3.71 (s, 3H), 1.35 (t, *J* = 6.8 Hz, 3H). ^{13}C NMR (68 MHz, DMSO-d_6): δ 163.9, 163.2, 151.87, 151.7, 148.8, 148.5, 148.3, 130.9, 130.1, 129.1, 127.4, 120.0, 111.9, 103.4, 60.3, 55.6, 55.51, 43.9, 14.25. ES-MS (methanol) m/z: 434.1 $[M+H]^+$, 456.1 $[M+Na]^+$, 472.0 $[M+K]^+$.

ethyl 5-((3,4-dimethoxybenzyl)amino)-2-(4-fluorophenyl)-[1,2,4]triazolo[1,5-*c*]-8-carboxylate (**186**)

Flash chromatography eluent: light petroleum-EtOAc 8:2. Yield 73% (165 mg); white solid; mp 156°C (EtOEt-light petroleum). ^{1}H NMR (400 MHz, DMSO-d_6): δ 9.42 (bs, 1H), 8.58 (s, 1H), 8.29 (m, 2H), 7.43 (t, $J_{H,HF}$ = 8.4 Hz, 2H), 7.07 (s, 1H), 6.94 (d, *J* = 8.0 Hz, 1H), 6.88 (d,

J = 8.0 Hz, 1H), 4.74 (d, *J* = 5.5 Hz, 2H), 4.34 (q, *J* = 6.8 Hz, 2H), 3.73 (s, 3H), 3.71 (s, 3H), 1.35 (t, *J* = 6.8 Hz, 3H). ^{13}C NMR (68 MHz, DMSO-d_6): δ 163.85 (d, J_{CF}= 247.3 Hz), 163.16, 163.05, 151.95, 151.81, 148.85, 148.45, 148.29, 130.82, 129.72 (d, J_{CF} = 8.7 Hz), 126.70 (d, J_{CF} = 2.7 Hz), 119.96, 116.21 (d, J_{CF} = 22.1 Hz), 111.92, 111.82, 103.40, 60.29, 55.56, 55.51, 43.91, 14.24. ES-MS (methanol) m/z: 452.1 $[M+H]^+$, 474.1 $[M+Na]^+$, 490.0 $[M+K]^+$.

ethyl 5-(methylamino)-2-(3-(benzyloxy)phenyl)-[1,2,4]triazolo[1,5-*c*]-8-carboxylate (**262**)
Flash chromatography eluent: light petroleum-EtOAc 8:2. Yield 29% (58 mg); white solid; mp 174-175°C (EtOEt-light petroleum). ^{1}H NMR (400 MHz, DMSO-d_6): 8.85 (s, 1H), 8.57 (s, 1H), 7.96-7.76 (m, 2H), 7.61-7.26 (m, 6H), 7.26-7.12 (m, 1H), 5.20 (s, 2H), 4.33 (q, J = 7.1 Hz, 2H), 3.10 (s, 3H), 1.34 (t, J = 7.1 Hz, 3H). ^{13}C NMR (68 MHz, DMSO-d_6): δ 163.4, 163.1, 158.7, 151.7, 151.5, 148.6, 136.9, 131.4, 130.2, 128.5, 128.0, 127.7, 119.8, 117.2, 113.4, 102.9, 69.4, 60.3, 27.9, 14.4. ES-MS (methanol) m/z: 404.2 $[M+H]^+$, 426.1 $[M+Na]^+$.

ethyl 5-(benzylamino)-2-(3-methoxyphenyl)-[1,2,4]triazolo[1,5-*c*]-8-carboxylate (**263**)
Flash chromatography eluent: DCM-methanol 98.5:1.5. Yield 74% (149 mg); white solid; mp 159-160°C (EtOEt-light petroleum). ^{1}H NMR (400 MHz, DMSO-d_6): δ 9.48 (s, 1H), 8.54 (s, 1H), 7.97-7.73 (m, 2H), 7.58-7.23 (m, 6H), 7.19-7.05 (m, 1H), 4.83 (s, 2H), 4.34 (q, *J* = 7.1 Hz, 2H), 3.86 (s, 3H), 1.35 (t, *J* = 7.1 Hz, 3H). ^{13}C NMR (101 MHz, DMSO-d_6): δ 164.0, 163.3, 160.0, 152.05, 151.91, 148.8, 138.8, 131.7, 130.6, 128.8, 127.9, 127.6, 120.1, 117.0, 112.6, 103.8, 60.7, 55.7, 44.5, 14.7. ES-MS (methanol) m/z: 404.2 $[M+H]^+$, 426.1 $[M+Na]^+$.

ethyl 5-(([1,1'-biphenyl]-4-ylmethyl)amino)-2-(3-methoxyphenyl)-[1,2,4]triazolo[1,5-*c*]-8-carboxylate (**264**)
Flash chromatography eluent: DCM-methanol 99:1. Yield 68% (163 mg); white solid; mp 160°C (EtOEt-light petroleum). ^{1}H NMR (270 MHz, DMSO-d_6): 9.56 (s, 1H), 8.58 (s, 1H), 7.98-7.73 (m, 2H), 7.71-7.29 (m, 10H), 7.21-7.05 (m, 1H), 4.87 (s, 2H), 4.34 (q, *J* = 7.1 Hz, 2H), 3.87 (s, 3H), 1.35 (t, *J* = 7.1 Hz, 3H). ^{13}C NMR (101 MHz, DMSO-d_6): δ 164.0, 163.3, 162.8, 160.0, 157.7, 151.9, 148.8, 138.0, 131.7, 131.4, 129.3, 128.5, 127.13, 127.03, 121.8, 117.0, 114.3, 112.6, 110.0, 103.9, 60.7, 55.7, 49.0, 14.7. ES-MS (methanol) m/z: 480.2 $[M+H]^+$, 502.2 $[M+Na]^+$.

4.4.1.1.6 General procedure (XII) for the removal of the 3,4-dimethoxybenzyl group

To 0.2 mol of compounds **185** and **186**, TFA (1 mL), anisole (0.8 mmol) and trifluoromethanesulfonic acid (HOTf) (0.8 mmol) were added at 0°C and the reaction proceeded for 12 hours at room temperature. The solvent was evaporated, DCM added (15 mL) and washed with three aliquots of water (5 mL). After drying the organic phase over anhydrous sodium sulfate, the solvent is evaporated and the residue purified by flash chromatography.

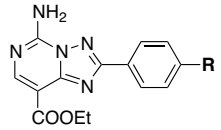

R= H (**193**)
F (**194**)

ethyl 5-amino-2-phenyl-[1,2,4]triazolo[1,5-*c*]pyrimidine-8-carboxylate (**193**)
Flash chromatography eluent: DCM-EtOAc from 9:1 to 8:2. Yield 22% (12 mg); white solid; mp 195-198°C (EtOEt-light petroleum). ^{1}H NMR (400 MHz, DMSO-d_6): δ 8.98 (bs, 1H), 8.52-8.33 (m, 2H), 8.25 (m, 2H), 7.58 (m, 3H), 4.34 (q, *J* = 7.1 Hz, 2H), 1.35 (t, *J* = 7.1 Hz, 3H). ^{13}C NMR (68 MHz, $CDCl_3$): δ 163.90, 163.20, 152.20, 152.07, 150.29, 130.84, 130.17, 129.08, 127.39, 103.14, 60.22, 14.26. ES-MS (methanol) m/z: 284.0 $[M+H]^+$, 305.9 $[M+Na]^+$, 321.9 $[M+K]^+$.

ethyl 5-amino-2-(4-fluorophenyl)-[1,2,4]triazolo[1,5-*c*]pyrimidine-8-carboxylate (**194**)
Flash chromatography eluent: DCM-EtOAc from 9:1 to 8:2. Yield 73% (44.0 mg); pale pink solid; mp 263°C (EtOEt-light petroleum). ^{1}H NMR (400 MHz, DMSO-d_6): δ 8.99 (bs, 1H), 8.61-8.37 (m, 2H), 8.28 (dd, J = 8.8 Hz, J_{HF} = 5.6 Hz, 2H), 7.43 (t, $J_{H,HF}$ = 8.8 Hz, 2H), 4.33 (q, J = 7.1 Hz, 2H), 1.35 (t, J = 7.1 Hz, 3H). ^{13}C NMR (68 MHz, DMSO-d_6): δ 163.84 (d, J_{CF} = 247.5 Hz), 163.19, 163.06, 152.29, 152.14, 150.29, 129.70 (d, J_{CF} = 8.8 Hz), 126.76 (d, J_{CF}= 1.2 Hz), 116.19 (d, J_{CF} = 22.0 Hz), 103.12, 60.22, 14.26. ES-MS (methanol) m/z: 323.9 $[M+Na]^+$.

4.4.1.1.7 General procedure (XIII) for the removal of benzyl group or the reduction of nitro group to amine

To a stirred suspension of compounds **184** and **258-262** (0.2 mmol) and an equal weight of 10% Pd-C in dry methanol (10 mL), ammonium formate (2 mmol) was added in a single portion. The resulting reaction mixture was stirred under argon atmosphere at 60°C for 3-24 hours. Once completed, the catalyst was removed by filtration through a celite pad, which was then washed with methanol. The solvent was evaporated under reduced pressure and the crude product dissolved in EtOAc (50 mL) and washed with water (3 x 15 mL). Finally, the organic phase was dried over anhydrous sodium sulfate, the solvent evaporated under vacuum and, if necessary, the residue purified by flash chromatography or precipitated with EtOEt and light petroleum to afford the desired derivatives.

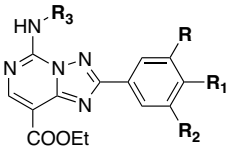

R= NH_2; R_1,R_2=H (**187**) R_3= H (**187-191**)
R_1= OH; R,R_2=H (**188**) CH_3 (**192**)
R= OH; R_1,R_2=H (**189,192**)
R,R_1= OH; R_2=H (**190**)
R,R_2= OH; R_1=H (**191**)

ethyl 5-amino-2-(3-aminophenyl)-[1,2,4]triazolo[1,5-*c*]pyrimidine-8-carboxylate (**187**)
Flash chromatography eluent: DCM-methanol 95:5. Yield 65% (39 mg); white solid; mp 245-250°C (EtOEt-light petroleum). ^{1}H NMR (270 MHz, DMSO-d_6): δ 8.97 - 8.50 (m, 3H), 7.49 (s, 1H), 7.41 (d, J = 7.3 Hz, 1H), 7.18 (t, J = 7.9 Hz, 1H), 6.76-6.72 (m, 1H), 5.37 (s, 2H), 4.33 (q, J = 7.0 Hz, 2H), 1.35 (t, J = 7.0 Hz, 3H). ^{13}C NMR (68 MHz, DMSO-d_6): δ 164.7, 163.2, 152.0, 151.8, 150.24, 149.3, 130.7, 129.4, 116.20, 115.0, 112.8, 103.1, 60.2, 14.3. ES-MS (methanol) m/z: 299.1 $[M+H]^+$, 321.1 $[M+Na]^+$.

ethyl 5-amino-2-(4-hydroxyphenyl)-[1,2,4]triazolo[1,5-*c*]pyrimidine-8-carboxylate (**188**)
Flash chromatography eluent: DCM-methanol from 98:2 to 95:5. Yield 72% (43 mg); white solid; mp >300°C (EtOEt-light petroleum). ^{1}H NMR (400 MHz, DMSO-d_6): δ 10.01 (bs, 1H), 8.89 (bs, 1H), 8.50–8.19 (m, 2H), 8.07 (d, J = 7.7 Hz, 2H), 6.93 (d, J = 7.7 Hz, 2H), 4.33 (q, J = 6.3 Hz, 2H), 1.35 (t, J = 6.3 Hz, 3H). ^{13}C NMR (68 MHz, DMSO-d_6): δ 164.2, 163.3, 160.0, 152.00, 151.9, 150.2, 129.15, 120.9, 115.8, 102.9, 60.2, 14.3. ES-MS (methanol) m/z: 322.1 $[M+Na]^+$, 338.0 $[M+K]^+$.

ethyl 5-amino-2-(3-hydroxyphenyl)-[1,2,4]triazolo[1,5-*c*]pyrimidine-8-carboxylate (**189**)
Flash chromatography eluent: DCM-methanol 98:2. Yield 51% (30 mg); white solid; mp 282-284°C (EtOEt-light petroleum). ^{1}H NMR (400 MHz, DMSO-d_6): δ 9.76 (s, 1H), 8.97 (bs, 1H), 8.64-8.25 (m, 2H), 7.76 – 7.63 (m, 2H), 7.36 (t, J = 8.1 Hz, 1H), 7.02 -6.85 (m, 1H), 4.34 (q, J = 7.1 Hz, 2H), 1.36 (t, J = 7.1 Hz, 3H). ^{13}C NMR (68 MHz, DMSO-d_6): δ 164.0, 163.2, 157.9,

152.1, 152.0, 150.3, 131.4, 130.1, 118.2, 117.8, 114.25, 103.1, 60.2, 14.3. ES-MS (methanol) m/z: 299.8 $[M+H]^+$, 321.8 $[M+Na]^+$, 337.8 $[M+K]^+$.

ethyl 5-amino-2-(3,4-bis(hydroxy)phenyl)-[1,2,4]triazolo[1,5-*c*]pyrimidine-8-carboxylate (**190**)
Yield 64% (40 mg); white solid; mp 270-272°C (EtOEt-light petroleum). ^{1}H NMR (400 MHz, DMSO-d_6): δ 9.50-8.80 (m, 3H), 8.50-8.25 (m, 2H), 7.68 (s, 1H), 7.60-7.53 (m, 1H), 6.88 (d, J = 8.2 Hz, 1H), 4.33 (q, J = 7.1 Hz, 2H), 1.35 (t, J = 7.1 Hz, 3H). ^{13}C NMR (68 MHz, DMSO-d_6): δ 164.1, 163.0, 151.68, 151.57, 149.9, 148.0, 145.4, 121.1, 119.2, 115.8, 114.8, 102.8, 60.1, 14.3. ES-MS (methanol) m/z: 316.1 $[M+H]^+$, 338.1 $[M+Na]^+$.

ethyl 5-amino-2-(3,5-bis(hydroxy)phenyl)-[1,2,4]triazolo[1,5-*c*]pyrimidine-8-carboxylate (**191**)
Yield 54% (34 mg); white solid; mp 255-260°C (EtOEt-light petroleum). ^{1}H NMR (270 MHz, DMSO-d_6): 9.55 (bs, 2H), 8.50 (m, 3H), 7.20-7.11 (m, 2H), 6.36 (m, 1H), 4.33 (q, J = 7.1 Hz, 2H), 1.35 (t, J = 7.1 Hz, 3H). ^{13}C NMR (68 MHz, DMSO-d_6): δ 164.3, 163.2, 158.95, 152.1, 151.8, 150.2, 131.7, 105.7, 104.95, 103.1, 60.2, 14.3. ES-MS (methanol) m/z: 316.1 $[M+H]^+$, 338.0 $[M+Na]^+$.

ethyl 5-methylamino-2-(3-hydroxyphenyl)-[1,2,4]triazolo[1,5-*c*]pyrimidine-8-carboxylate (**192**)
Yield 66%; white solid (41 mg); mp 234°C (EtOEt-light petroleum). ^{1}H NMR (400 MHz, DMSO-d_6): δ 9.73 (s, 1H), 8.81 (bs, 1H), 8.56 (s, 1H), 7.75-7.61 (m, 2H), 7.34 (t, J = 8.1 Hz, 1H), 6.98-6.84 (m, 1H), 4.33 (q, J = 7.1 Hz, 2H), 3.10 (s, 3H), 1.34 (t, J = 7.1 Hz, 3H). ^{13}C NMR (68 MHz, DMSO-d_6) δ 163.0, 157.7, 153.9, 153.1, 151.5, 148.6, 131.1, 129.9, 117.9, 117.6, 114.0, 102.9, 60.2, 27.9, 14.3. ES-MS (methanol) m/z: 314.1 $[M+H]^+$, 336.1 $[M+Na]^+$.

4.4.1.1.8 General procedure (XIV) for the synthesis of 2-(3-hydroxyphenyl)-[1,2,4]triazolo[1,5-c]pyrimidine-8-carboxylic acids

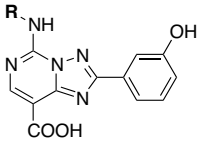

R= H (**195**)
CH_2Ph (**274**)
CH_2(4-Ph)Ph (**275**)

A solution of boron tribromide (1M in DCM, 3 mmol) was slowly added to a cooled (-78°C) solution of methoxy-derivatives (0.25 mmol) in DCM (2.5 mL) under argon atmosphere. The cooling bath was removed and the suspension was slowly warmed up to room temperature and stirred for 12 h. Once completed, an equal volume of cool methanol was added dropwise and the solution stirred for 15 minutes. Then the volatile species were removed under vacuum, thus giving the corresponding carboxylic acids derivatives. Compounds **274-275** were immediately used in the next step without any characterization.

ethyl 5-amino-2-(3-hydroxyphenyl)-[1,2,4]triazolo[1,5-*c*]pyrimidine-8-carboxylic acid (**195**)
Recrystallized from methanol and EtOAc. Yield 91.5% (62 mg); white solid; mp 290-295°C. ^{1}H NMR (270 MHz, DMSO-d_6): δ 8.93-8.49 (m, 3H), 7.74-7.65 (m, 2H), 7.35 (t, J = 7.9 Hz, 1H), 6.93 (d, J = 8.1 Hz, 1H). ^{13}C NMR (68 MHz, DMSO-d_6): δ 164.6, 163.85, 158.0, 157.7, 152.2, 150.15, 131.25, 130.2, 118.2, 117.9, 114.3, 103.65. ES-MS (methanol) m/z: 272.0 $[M+H]^+$, 294.0 $[M+Na]^+$.

4.4.1.1.9 Synthesis of N^5-substituted ethyl 2-(3-hydroxyphenyl)-5-amino-[1,2,4]triazolo[1,5-*c*]pyrimidine-8-carboxylates (196-197)

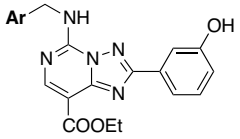

Ar= Ph (**196**)
(4-Ph)-Ph (**197**)

Carboxylic acids **274-275** (0.25 mmol) were reacted with thionyl chloride (1 mmol) and DMF (catalytic) in chloroform at reflux for 5 hours. Then, the volatile species were removed under reduced pressure, the crude product was suspended in ethanol and triethylamine was added (0.375 mmol), then the reaction was stirred at room temperature overnight. When completed, the solvent was removed under reduced pressure and the product purified by flash chromatography.

ethyl 5-(benzylamino)-2-(3-hydroxyphenyl)-[1,2,4]triazolo[1,5-*c*]pyrimidine-8-carboxylate (**196**)
Flash chromatography eluent: DCM-methanol 98.5:1.5. Yield 13% (12 mg); white solid; mp 219-220°C (EtOEt-light petroleum). ^{1}H NMR (400 MHz, DMSO-d_6): δ 9.72 (s, 1H), 9.44 (s, 1H), 8.54 (s, 1H), 7.77-7.63 (m, 2H), 7.44-7.18 (m, 6H), 6.99-6.84 (m, 1H), 4.81 (s, 2H), 4.32 (q, J = 7.1 Hz, 2H), 1.33 (t, J = 7.1 Hz, 3H). ^{13}C NMR (101 MHz, DMSO-d_6): δ 164.3, 163.3, 158.1, 151.97, 151.82, 148.8, 138.8, 131.6, 130.4, 128.8, 127.8, 127.5, 118.4, 118.1, 114.6, 103.9, 60.7, 14.7. ES-MS (methanol) m/z: 390.1 $[M+H]^+$, 412.1 $[M+Na]^+$.

ethyl 5-(([1,1'-biphenyl]-4-ylmethyl)amino)-2-(3-hydroxyphenyl)-[1,2,4]triazolo[1,5-*c*]pyrimidine-8-carboxylate (**197**)
Flash chromatography eluent: DCM-methanol 99.5:0.5. Yield 19.5% (23 mg); white solid; mp 227-229°C (EtOEt-light petroleum). ^{1}H NMR (400 MHz, DMSO-d_6): δ 9.72 (s, 1H), 9.48 (s, 1H), 8.55 (s, 1H), 7.69 (s, 2H), 7.66-7.57 (m, 4H), 7.54-7.30 (m, 6H), 6.97-6.88 (m, 1H), 4.85 (s, 2H), 4.32 (q, J = 7.1 Hz, 2H), 1.33 (t, J = 7.1 Hz, 3H). ^{13}C NMR (68 MHz, DMSO-d_6): δ 163.8, 162.9, 157.7, 151.5, 151.35, 139.9, 139.8, 139.0, 137.6, 131.1, 129.9, 128.9, 128.0, 126.7, 126.6, 118.0, 117.7, 115.9, 114.1, 103.4, 60.2, 14.3. ES-MS (methanol) m/z: 465.9 $[M+H]^+$, 487.9 $[M+Na]^+$.

4.4.1.1.10 Synthesis of 5-amino-*N*-ethyl-2-(3-hydroxyphenyl)-[1,2,4]triazolo[1,5-*c*]pyrimidine-8-carboxamide (198)

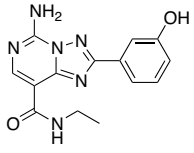

The mixture of 100 mg of **195** (0.37 mmol) dissolved in 1 mL of dry pyridine was cooled to 0 °C and 0.405 mL (5.55 mmol) of thionyl chloride were added dropwise. The reaction was then allowed to warm up to 10 °C, and 15 eq of ethylamine were added (0.368 mL, 5.55 mmol). The mixture was left to reach room temperature and stirred overnight. When the reaction was terminated, the pyridine was removed under reduced pressure, water was added (20 mL) to the mixture and the product was extracted with EtOAc (5x10 mL). The crude was then purified by column chromatography, eluting in EtOAc. Yield 9% (10 mg); white solid; mp 170-175°C (EtOEt-light petroleum). ^{1}H NMR (400 MHz, DMSO-d_6): δ 9.80 (s, 1H), 8.99-8.13 (m, 4H), 7.79-7.74 (m, 2H), 7.38 (t, J = 7.6 Hz, 1H), 6.96 (d, J = 7.6 Hz, 1H), 3.48-3.41 (m, 2H), 1.23 (t, J = 6.5 Hz, 3H). ^{13}C NMR (68 MHz, DMSO-d_6): δ 174.4, 163.9, 162.9, 161.9, 157.9, 151.9, 149.41, 130.7, 118.3, 114.2, 108.3, 105.1, 33.7, 15.0. ES-MS (methanol) m/z: 299.1 $[M+H]^+$, 321.1 $[M+Na]^+$.

4.4.1.1.11 Synthesis of *tert*-butyl (2-(5-amino-2-(3-hydroxyphenyl)-[1,2,4]triazolo[1,5-c]pyrimidine-8-carboxamido)ethyl)carbamate (199)

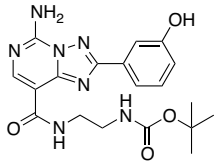

To carboxylic acid derivative **195** (100 mg, 0.37 mmol) in chloroform (3 mL), thionyl chloride (0.107 mL,1.48 mmol) and DMF (catalytic, 20 μL) were added and the mixture was heated under reflux for 5 h. The solvent was removed under reduced pressure to yield the corresponding chloride derivative (yellowish oil), which was immediately dissolved in THF (3 mL). The mixture was then cooled to 0°C and an equimolar amount of triethylamine (0.051 mL, 0.37 mmol) was added to the solution; afterward, *tert*-butyl 2-aminoethylcarbamate (118 mg, 0.74 mmol) was added slowly. The solution was allowed to warm to room temperature and stirred overnight. Once completed, the solvent was then removed under reduced pressure and the residue suspended in EtOAc (30 mL) and washed with water (3x10 mL). The organic phase was then dried over sodium sulfate and chromatographed with EtOAc and methanol 98:2, to obtain derivative **199** as white solid. Yield 19% (29 mg); white solid; mp 220-223°C (EtOEt-light petroleum). ^{1}H NMR (400 MHz, DMSO-d_6): δ 9.78 (s, 1H), 8.79 (s, 1H), 8.46 (s, 1H), 7.77 (d, J = 7.8 Hz, 1H), 7.70 (s, 1H), 7.36 (t, J = 7.9 Hz, 1H), 7.03-6.94 (m, 2H), 3.47 (d, J = 5.4 Hz, 2H), 3.16 (d, J = 5.6 Hz, 2H), 1.31 (m, 11H). ES-MS (methanol) m/z: 436.1 $[M+Na]^+$.

4.4.1.1.12 Synthesis of 5-amino-*N*-(2-aminoethyl)-2-(3-hydroxyphenyl)-[1,2,4]triazolo[1,5-c]pyrimidine-8-carboxamide, trifluoroacetate salt (200)

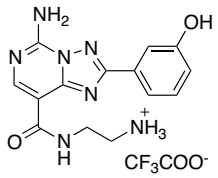

Compound **200** was obtained according to **General Procedure (VII)** (Chapter 3.4.1.2.7).

Yield 95% (20 mg from 0.05 mol of **199**); white solid; mp 210-212°C (EtOEt-light petroleum). ^{1}H NMR (270 MHz, DMSO-d_6): δ 9.84 (bs, 1H), 8.93-8.40 (m, 4H), 7.80 (m, 5H), 7.38 (m, 1H), 6.98 (s, 1H), 3.78-3.55 (m, 2H), 3.17-2.92 (m, 2H). ^{13}C NMR (68 MHz, DMSO-d_6): δ 163.0, 162.8, 157.7, 151.6, 150.0, 149.3, 130.5, 129.9, 118.4, 118.0, 114.3, 104.7, 56.4, 37.0. ES-MS (methanol) m/z: 314.1 $[M+H]^+$, 336.0 $[M+Na]^+$.

4.4.1.1.13 General procedure (XV) for O-protection with a benzyl group[244]

To a solution of ethyl hydroxybenzoate (**266-267**, 0.1 mol) or ethyl dihydroxybenzoate (**268-269**, 0.1 mol) in dry acetone (400 mL) were added K_2CO_3 (0.11 mol for **266-267** or 0.22 mol for **268-269**) and benzyl bromide (0.11 mol for **266-267** or 0.22 mol for **268-269**), and the reaction mixture was heated to reflux overnight. The solvent was evaporated and the residue was suspended in 150 mL of water and extracted with dichloromethane (3 x 50 mL). The combined organic layers were dried over sodium sulphate and concentrated. The crude product was purified by flash chromatography, if necessary.

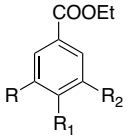

R_1= OBn; R, R_2=H (**270**)
R= OBn; R_1, R_2=H (**271**)
R, R_1= OBn; R_2=H (**272**)
R, R_2= OBn; R_1=H (**273**)

ethyl 4-benzyloxybenzoate (**270**)
Flash chromatography eluent: light petroleum-DCM 6:4. Yield 89% (22.8 g); yellow oil. ^{1}H NMR (270 MHz, DMSO-d_6): δ 8.00 (d, J = 8.9 Hz, 2H), 7.52–7.30 (m, 5H), 6.99 (d, J = 8.9

Hz, 2H), 5.12 (s, 2H), 4.34 (q, *J* = 7.1 Hz, 2H), 1.37 (t, *J* = 7.1 Hz, 3H). ES-MS (methanol) m/z: 257.1 $[M+H]^+$, 279.0 $[M+Na]^+$.

ethyl 3-benzyloxybenzoate (**271**)
Flash chromatography eluent: light petroleum-DCM 6:4. Yield 81% (20.8 g); yellow oil. ^{1}H NMR (270 MHz, DMSO-d_6): δ 7.80–7.55 (m, 2H), 7.55–7.27 (m, 6H), 7.20-7.15 (m, 1H), 5.11 (s, 2H), 4.38 (q, *J* = 7.1 Hz, 2H), 1.39 (t, *J* = 7.1 Hz, 3H). ES-MS (methanol) m/z: 257.0 $[M+H]^+$, 279.0 $[M+Na]^+$.

ethyl 3,4-dibenzyloxybenzoate (**272**)
Yield 89.5% (32.4 g); white solid; mp 113-114°C (acetone-light petroleum). ^{1}H NMR (270 MHz; $CDCl_3$): δ 7.67-7.61 (m, 2H), 7.50-7.28 (m, 10H), 6.95-6.91 (m, 1H), 5.25 (s, 2H), 5.18 (s, 2H), 4.37-4.28 (q, *J* = 7.1 Hz, 2H), 1.40-1.33 (t, *J* = 7.1 Hz, 3H). ES-MS (methanol) m/z: 363.2 $[M+H]^+$, 385.2 $[M+Na]^+$.

ethyl 3,5-dibenzyloxybenzoate (**273**)
Yield 79% (28.6 mg); white solid; mp 74-78°C (acetone-light petroleum). ^{1}H NMR (400 MHz; $CDCl_3$): δ 7.45–7.29 (m, 12H), 6.79 (s, 1H), 5.06 (s, 4H), 4.35 (q, *J* = 7.1 Hz, 2H), 1.38 (t, *J* = 7.1 Hz, 3H). ES-MS (methanol) m/z: 363.1 $[M+H]^+$, 385.1 $[M+Na]^+$.

4.4.1.2 Synthesis of 2,5,7-trisubstituted [1,2,4]triazolo[1,5-c]pyrimidines

4.4.1.2.1 Synthesis of *N'*-(2-amino-6-chloropyrimidin-4-yl)-3-methoxybenzohydrazide (278)[245,246]

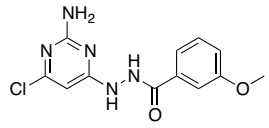

To 2-amino-4,6-dihydroxy-pyrimidine **276** (3.2 g, 25 mmol) in 15 ml of acetonitrile was added TEA (6.97 mL, 50 mmol) followed by the dropwise addition of phosphorous oxychloride (2.34 mL, 25 mmol). The solution was refluxed for 1 h, cooled to room temperature and ice was added. The resulting brown solid was filtered, washed with cold water and directely reacted with 3-methoxybenzohydrazide (**224**, 4.82 g, 29 mmol) and DBU (5.05 mL, 34 mmol) in 40 ml of THF. The solution was stirred at room temperature overnight. After evaporation of the solvent under vacuum, the mixture was suspended with 300 mL of EtOAc and washed with three aliquots of water (100 mL). Then, the organic phase was dried over sodium sulphate, concentrated and purified by flash chromatography (DCM-methanol from 98:2 to 95:5) and the product obtained as a white solid (1.32 g). Yield 18%; mp 253°C (EtOEt-light petroleum). ^{1}H NMR (270 MHz, DMSO-d_6): δ 10.45 (s, 1H), 9.09 (s, 1H), 7.45 (m, 3H), 7.15 (d, *J* = 8.0 Hz, 1H), 6.64 (s, 2H), 5.80 (bs, 1H), 3.82 (s, 3H). ES-MS (methanol) m/z: 294.1 $[M+H]^+$.

4.4.1.2.2 Synthesis of 7-chloro-2-(3-methoxyphenyl)-[1,2,4]triazolo[1,5-c]pyrimidine-5-amine (279)

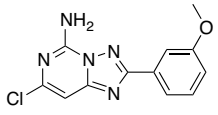

1.24 grams of **278** (4 mmol) in bis(trimethylsilyl)acetamide (BSA, 35 mL) are refluxed under argon atmosphere overnight. When the starting material was consumed, 40 mL of ice methanol were added slowly keeping the temperature near 0°C and then the volatile species removed under vacuum. The crude material, dissolved in dichloromethane (200 mL), was washed with water (3 x 65 mL) and the mixture purified by flash chromatography (DCM-methanol 99:1), using neutral aluminium oxide as stationary phase. Yield 50% (0.551 g); white solid; mp 249-250°C (EtOEt-light petroleum). ^{1}H NMR (400 MHz, DMSO-d_6): δ 8.43 (bs, 2H), 7.90-7.58 (m, 2H),

7.48 (s, 1H), 7.11 (s, 2H), 3.85 (s, 3H). ^{13}C NMR (68 MHz, DMSO-d_6): δ 163.99, 159.78, 154.71, 148.28, 147.27, 131.47, 130.31, 119.58, 116.76, 112.12, 96.92, 55.30. ES-MS (methanol) m/z: 276.0 $[M+H]^+$.

4.4.1.2.3 Synthesis of *N*^{7}-benzyl-2-(3-methoxyphenyl)-[1,2,4]triazolo[1,5-*c*]pyrimidine-5,7-diamine (201)

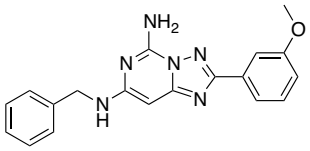

325 mg (1.18 mmol) of derivative **279** were reacted with 244 μL of benzylamine (2.35 mmol) and 476 mg (3.53 mmol) of potassium carbonate in 5 mL of ethanol in sealed tube at 90°C for 4 days. When reaction was completed, the solvent was evaporated and the crude material purified by chromatography in gradient from DCM-MeOH 99.5:0.5 to 99:1. Yield 28% (114 mg); white solid; mp 207°C (EtOEt-light petroleum). ^{1}H NMR (270 MHz, DMSO-d_6): δ 7.75-7.56 (m, 2H), 7.56-7.15 (m, 9H), 7.07-6.99 (m, 1H), 5.66 (s, 1H), 4.42 (d, *J* = 6.0 Hz, 2H), 3.82 (s, 3H). ^{13}C NMR (101 MHz, DMSO-d_6): δ 163.2, 159.8, 158.0, 156.5, 147.0, 140.3, 132.8, 130.2, 128.7, 127.5, 127.1, 119.6, 116.2, 112.2, 55.6, 45.2. ES-MS (methanol) m/z: 347.1 $[M+H]^+$.

4.4.1.2.4 Synthesis of *N*^{7}-benzyl-2-(3-hydroxyphenyl)-[1,2,4]triazolo[1,5-*c*]pyrimidine-5,7-diamine (202)

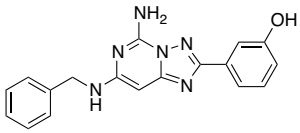

Compound **202** was obtained according to **General Procedure (XIV)** (Chapter 4.4.1.1.8), but using 3 equivalents of boron tribromide.

Flash chromatography eluent: DCM-MeOH 98.5:1.5. Yield 39% (38 mg from 0.29 mmol of **205**); white solid; mp 267°C (EtOEt-light petroleum). ^{1}H NMR (270 MHz, DMSO-d_6): δ 9.60 (s, 1H), 7.56-7.42 (m, 4H), 7.39-7.19 (m, 7H), 6.85 (d, *J* = 7.9 Hz, 1H), 5.65 (s, 1H), 4.42 (d, *J* = 6.1 Hz, 2H). ^{13}C NMR (101 MHz, DMSO-d_6): δ 163.4, 157.91, 157.88, 156.4, 146.9, 140.3, 132.6, 130.0, 128.7, 127.5, 127.1, 118.1, 117.3, 114.1, 45.2. ES-MS (methanol) m/z: 333.2 $[M+H]^+$.

4.4.1.3 Synthesis of 2,5,7-trisubstituted [1,2,4]triazolo[1,5-*a*][1,3,5]triazines

4.4.1.3.1 Synthesis of substituted *N*'-(4,6-diphenoxy-1,3,5-triazin-2-yl)hydrazides (282-285)

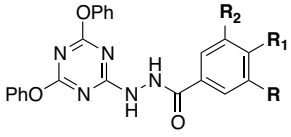

R_1= OCH_3; R, R_2=H (**282**)
R= OCH_3; R_1, R_2=H (**283**)
R, R_1= OCH_3; R_2=H (**284**)
R, R_2= OCH_3; R_1=H (**285**)

Compounds **282-285** were obtained according to **General Procedure (II)** (Chapter 3.4.1.2.2).

N'-(4,6-diphenoxy-1,3,5-triazin-2-yl)-4-methoxybenzohydrazide (**282**)
Flash chromatography eluent: DCM-EtOAc 98:2. Yield 48% (5.77 g); white solid; mp 220-221°C (EtOEt-light petroleum). ^{1}H NMR (270 MHz, $CDCl_3$): δ 8.59 (bs, 1H), 7.68 (d, *J* = 8.7

Hz, 2H), 7.42-7.32 (m, 2H), 7.30-7.19 (m, 4H), 7.21-7.06 (m, 5H), 6.87 (d, *J* = 8.7 Hz, 2H), 3.84 (s, 3H). ES-MS (methanol) m/z: 430.2 $[M+H]^+$, 452.2 $[M+Na]^+$.

N'-(4,6-diphenoxy-1,3,5-triazin-2-yl)-3-methoxybenzohydrazide (**283**)
Flash chromatography eluent: DCM-EtOAc 95:5. Yield 39% (4.69 g); white solid; mp 182-184°C (EtOEt-light petroleum). ^{1}H NMR (400 MHz, DMSO-d_6): δ 10.45 (s, 1H), 10.05 (s, 1H), 7.49-7.21 (m, 10H), 7.18-7.09 (m, 4H), 3.80 (s, 3H). ES-MS (methanol) m/z: 430.1 $[M+H]^+$, 452.1 $[M+Na]^+$.

N'-(4,6-diphenoxy-1,3,5-triazin-2-yl)-3,4-dimethoxybenzohydrazide (**284**)
Flash chromatography eluent: DCM-EtOAc 90:10. Yield 25% (3.22 g); white solid; mp 146-149°C (EtOEt-light petroleum). ^{1}H NMR (270 MHz, DMSO-d_6): δ 10.34 (s, 1H), 9.99 (s, 1H), 7.55-6.97 (m, 13H), 3.83 (s, 3H), 3.79 (s, 3H). ES-MS (methanol) m/z: 460.2 $[M+H]^+$, 482.2 $[M+Na]^+$.

N'-(4,6-diphenoxy-1,3,5-triazin-2-yl)-3,5-dimethoxybenzohydrazide (**285**)
Flash chromatography eluent: DCM-EtOAc 90:10. Yield 38% (4.89 g); white solid; mp 212-213°C (EtOEt-light petroleum). ^{1}H NMR (270 MHz, DMSO-d_6): δ 10.45 (s, 1H), 10.05 (s, 1H), 7.53-7.35 (m, 2H), 7.35-7.04 (m, 8H), 7.04-6.89 (m, 2H), 6.73-6.68 (m, 1H), 3.79 (s, 6H). ES-MS (methanol) m/z: 460.2 $[M+H]^+$, 482.1 $[M+Na]^+$.

4.4.1.3.2 Synthesis of 5,7-diphenoxy-[1,2,4]triazolo[1,5-*a*][1,3,5]triazines (286-289)

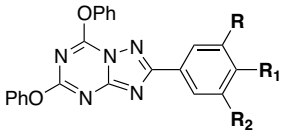

R_1= OCH_3; R, R_2=H (**286**)
R= OCH_3; R_1, R_2=H (**287**)
R, R_1= OCH_3; R_2=H (**288**)
R, R_2= OCH_3; R_1=H (**289**)

Compounds **286-289** were obtained according to **General Procedure ($III_{a/b}$)** (Chapter 3.4.1.2.3).

2-(4-methoxyphenyl)-5,7-diphenoxy-[1,2,4]triazolo[1,5-*a*][1,3,5]triazine (**286**).
Procedure **III_a**. Flash chromatography eluent: DCM. Yield 39% (2.41 g); white solid; mp 216°C (EtOEt-light petroleum). ^{1}H NMR (270 MHz, $CDCl_3$): δ 8.28 (d, *J* = 8.8 Hz, 2H), 7.56-7.47 (m, 2H), 7.44-7.34 (m, 5H), 7.24-7.15 (m, 3H), 7.00 (d, *J* = 8.8 Hz, 2H), 3.88 (s, 3H). ES-MS (acetonitrile) m/z: 412.2 $[M+H]^+$.

2-(3-methoxyphenyl)-5,7-diphenoxy-[1,2,4]triazolo[1,5-*a*][1,3,5]triazine (**287**)
Procedure **III_b**. Flash chromatography eluent: DCM. Yield 71% (4.38 g); white solid; mp 235°C (EtOEt-light petroleum). ^{1}H NMR (400 MHz, DMSO-d_6): δ 7.80 (d, *J* = 7.6 Hz, 1H), 7.70 (s, 1H), 7.65-7.39 (m, 8H), 7.32 (t, *J* = 7.3 Hz, 1H), 7.28-7.19 (m, 2H), 7.18-7.11 (m, 1H), 3.85 (s, 3H). ^{13}C NMR (68 MHz, $CDCl_3$): δ 167.51, 164.98, 160.68, 160.18, 155.03, 152.06, 150.78, 130.91, 130.35, 130.05, 129.90, 127.79, 126.47, 121.73, 121.42, 120.44, 118.42, 112.20, 55.59. ES-MS (acetonitrile) m/z: 412.1 $[M+H]^+$, 434.1 $[M+Na]^+$.

2-(3,4-dimethoxyphenyl)-5,7-diphenoxy-[1,2,4]triazolo[1,5-*a*][1,3,5]triazine (**288**)
Procedure **III_b**. Flash chromatography eluent: DCM-MeOH 99:1. Yield 51.5% (3.41 g); white solid; mp 248-249°C (EtOEt-light petroleum). ^{1}H NMR (270 MHz, $CDCl_3$): δ 8.06-7.88 (m, 1H), 7.84 (m, 1H), 7.58-7.47 (m, 2H), 7.47-7.32 (m, 5H), 7.32-7.13 (m, 3H), 6.98 (m, 1H), 3.98 (s, 3H), 3.95 (s, 3H). ^{13}C NMR (68 MHz, DMSO-d_6): δ 165.5, 164.4, 160.4, 155.1, 152.0, 151.5, 150.7, 149.1, 130.2, 129.8 127.4, 126.2, 121.9, 121.6, 121.4, 120.5, 112.0, 109.7, 55.6, 55.5. ES-MS (acetonitrile) m/z: 442.2 $[M+H]^+$, 464.2 $[M+Na]^+$.

2-(3,5-dimethoxyphenyl)-5,7-diphenoxy-[1,2,4]triazolo[1,5-*a*][1,3,5]triazine (**289**)
Procedure **III$_b$**. Flash chromatography eluent: DCM. Yield 25% (1.65 g); white solid; mp 211°C (EtOEt-light petroleum). ^{1}H NMR (270 MHz, $CDCl_3$): δ 7.59-7.47 (m, 4H), 7.47-7.34 (m, 5H), 7.34-7.12 (m, 3H), 6.68-6.55 (m, 1H), 3.86 (s, 6H). ^{13}C NMR (101 MHz, $CDCl_3$): δ 167.18, 164.67, 161.00, 160.32, 154.72, 151.77, 150.51, 131.19, 130.09, 129.64 , 127.53, 126.22, 121.49 121.18, 105.27, 104.65, 55.64. ES-MS (acetonitrile) m/z: 442.2 $[M+H]^+$, 464.1 $[M+Na]^+$.

4.4.1.3.3 Synthesis of 5-phenoxy-[1,2,4]triazolo[1,5-*a*][1,3,5]triazin-7-amines (290-293)

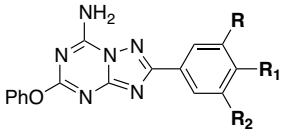

R_1= OCH_3; R, R_2=H (**290**)
R= OCH_3; R_1, R_2=H (**291**)
R, R_1= OCH_3; R_2=H (**292**)
R, R_2= OCH_3; R_1=H (**293**)

Compounds **290-293** were obtained according to **General Procedure (IV)** (Chapter 3.4.1.2.4).

2-(4-methoxyphenyl)-5-phenoxy-[1,2,4]triazolo[1,5-*a*][1,3,5]triazin-7-amine (**290**)
Flash chromatography eluent: DCM-MeOH 99:1. Yield 86% (0.575 g); white solid; mp >300°C (EtOEt-light petroleum).^{1}H NMR (400 MHz, DMSO-d_6)*:* δ 9.07 (s, 1H), 8.72 (s, 1H), 8.06 (d, *J* = 8.8 Hz, 2H), 7.46 (t, *J* = 7.9 Hz, 2H), 7.39-7.20 (m, 3H), 7.09 (d, *J* = 8.8 Hz, 2H), 3.83 (s, 3H). ^{13}C NMR (101 MHz, DMSO-d_6): δ 165.2, 164.2, 161.6, 159.4, 152.9, 152.3, 130.0, 128.8, 125.8, 123.1, 122.3, 114.7, 55.8. ES-MS (methanol) m/z: 335.1 $[M+H]^+$, 357.1 $[M+Na]^+$.

2-(3-methoxyphenyl)-5-phenoxy-[1,2,4]triazolo[1,5-*a*][1,3,5]triazin-7-amine (**291**)
Flash chromatography eluent: DCM-MeOH 99:1. Yield 91% (0.608 g); white solid; mp 226-229°C (EtOEt-light petroleum). ^{1}H NMR (400 MHz, DMSO-d_6)*:* δ 9.13 (s, 1H), 8.80 (s, 1H), 7.73 (d, *J* = 7.7 Hz, 1H), 7.67 (s, 1H), 7.57-7.40 (m, 3H), 7.37-7.19 (m, 3H), 7.10 (d, *J* = 7.7, 1H), 3.83 (s, 3H). ^{13}C NMR (101 MHz, DMSO-d_6): δ 165.3, 164.1, 159.9, 159.4, 152.9, 152.4, 132.0, 130.5, 130.0, 125.9, 122.3, 119.6, 116.9, 112.2, 55.7. ES-MS (methanol) m/z: 335.1 $[M+H]^+$, 357.1 $[M+Na]^+$, 373.0 $[M+K]^+$.

2-(3,4-dimethoxyphenyl)-5-phenoxy-[1,2,4]triazolo[1,5-*a*][1,3,5]triazin-7-amine (**292**)
Flash chromatography eluent: DCM-MeOH 99:1. Yield 89.5% (0.652 g); white solid; mp 276-278°C (EtOEt-light petroleum). ^{1}H NMR (270 MHz, DMSO-d_6): δ 9.02 (bs, 1H), 8.83 (bs, 1H), 7.76-7.73 (m, 2H), 7.53-7.41 (m, 2H), 7.34-7.21 (m, 3H), 7.17-7.08 (m, 1H), 3.83 (s, 6H). ^{13}C NMR (101 MHz, DMSO-d_6): δ 165.2, 164.3, 159.4, 152.9, 152.3, 151.3, 149.2, 130.0, 125.8, 123.1, 122.3, 120.4, 112.2, 110.2, 56.0, 55.9. ES-MS (methanol) m/z: 365.2 $[M+H]^+$, 387.1 $[M+Na]^+$.

2-(3,5-dimethoxyphenyl)-5-phenoxy-[1,2,4]triazolo[1,5-*a*][1,3,5]triazin-7-amine (**293**)
Yield 95% (0.692 mg); white solid; mp 274°C (EtOEt-light petroleum). ^{1}H NMR (400 MHz, DMSO-d_6): δ 9.12 (s, 1H), 8.78 (s, 1H), 7.46 (t, *J* = 7.8 Hz, 2H), 7.36-7.20 (m, 5H), 6.65 (s, 1H), 3.81 (s, 6H). ^{13}C NMR (101 MHz, DMSO-d_6): δ 165.3, 164.0, 161.1, 159.4, 152.8, 152.4, 132.5, 130.0, 125.9, 122.3, 110.0, 105.0, 103.1, 55.8. ES-MS (methanol) m/z: 365.1 $[M+H]^+$, 387.1 $[M+Na]^+$.

4.4.1.3.4 Synthesis of N^5-benzyl-[1,2,4]triazolo[1,5-*a*][1,3,5]triazin-5,7-diamine (203-204, 206-207) and N^7,N^5-dibenzyl-[1,2,4]triazolo[1,5-*a*][1,3,5]triazin-5,7-diamine (205)

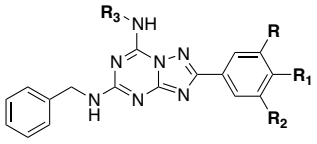

R_1= OCH_3; R, R_2, R_3=H (**203**)
R= OCH_3; R_1, R_2, R_3=H (**204**)
R_1= OCH_3; R, R_2=H, R_3=CH_2Ph (**205**)
R, R_1= OCH_3; R_2,R_3=H (**206**)
R, R_2= OCH_3; R_1,R_3=H (**207**)

Compounds **203-207** were obtained according to **General Procedure (V)** (Chapter 3.4.1.2), starting from 0.5 mmol of compounds (**290-293**).

N^5-benzyl-2-(4-methoxyphenyl)-[1,2,4]triazolo[1,5-*a*][1,3,5]triazine-5,7-diamine (**203**)
Flash chromatography eluent: DCM-MeOH 99:1. Yield 12% (21 mg); white solid; mp 266-269°C (EtOEt-light petroleum). ^{1}H NMR (400 MHz, DMSO-d_6): δ 8.51-7.75 (m, 5H), 7.49-7.14 (m, 5H), 7.14-6.92 (m, 2H), 4.50 (d, *J* = 6.9 Hz, 2H), 3.81 (s, 3H). ^{13}C NMR (101 MHz, DMSO-d_6): δ 161.2, 160.1, 154.5, 140.4, 136.2, 132.9, 128.6, 127.5, 125.2, 123.7, 122.6, 114.5, 55.7, 44.2. ES-MS (methanol) m/z: 348.1 $[M+H]^+$, 370.1 $[M+Na]^+$.

N^5-benzyl-2-(3-methoxyphenyl)-[1,2,4]triazolo[1,5-*a*][1,3,5]triazine-5,7-diamine (**204**)
Flash chromatography eluent: DCM-MeOH 97:3. Yield 46% (80 mg); white solid; mp 271°C (EtOEt-light petroleum). ^{1}H NMR (400 MHz, DMSO-d_6): δ 8.54-8.01 (m, 2H), 7.98 (t, *J* = 6.3 Hz, 1H) 7.73-7.61 (m, 2H), 7.42 (t, *J* = 7.9 Hz, 1H), 7.37-7.28 (m, 4H), 7.28-7.19 (m, 1H), 7.09-7.01 (m, 1H), 4.57-4.45 (m, 2H), 3.82 (s, 3H). ^{13}C NMR (101 MHz, DMSO-d_6): δ 162.94, 161.6, 159.8, 151.1, 150.6, 140.4, 132.6, 130.3, 128.6, 127.5, 127.0, 119.4, 116.5, 112.0, 55.6, 44.2. ES-MS (methanol) m/z: 348,1 $[M+H]^+$, 370,1 $[M+Na]^+$.

In this case was also isolated the N^5,N^7-dibenzyl-2-(3-methoxyphenyl)-[1,2,4]triazolo[1,5-*a*][1,3,5]triazine-5,7-diamine (**205**). Yield 15% (33 mg); white solid; mp 169-170°C (EtOEt-light petroleum). ^{1}H NMR (400 MHz, DMSO-d_6): δ 9.22 + 9.07 (m, 1H), 8.20-8-09 (m, 1H), 7.70 (d, *J* = 7.6 Hz, 1H), 7.64 (s, 1H), 7.51-7.16 (m, 11H), 7.10-7.03 (m, 1H), 4.72-4.56 (m, 2H), 4.50 (d, *J* = 6.2 Hz, 2H), 3.82 (s, 3H). ^{13}C NMR (101 MHz, DMSO-d_6): δ 163.0, 161.4, 159.9, 149.2, 140.2, 138.9, 132.6, 130.3, 128.8, 128.6, 128.2, 127.9, 127.6, 127.5, 127.1, 119.4, 116.6, 111.9, 55.6, 44.3, 43.7. ES-MS (methanol) m/z: 438.2 $[M+H]^+$, 460.2 $[M+Na]^+$.

N^5-benzyl-2-(3,4-dimethoxyphenyl)-[1,2,4]triazolo[1,5-*a*][1,3,5]triazine-5,7-diamine (**206**)
Flash chromatography eluent: DCM-MeOH 97:3. Yield 33% (62 mg); white solid; mp 234-235°C (EtOEt-light petroleum). ^{1}H NMR (270 MHz, DMSO-d_6): δ 8.42-7.81 (m, 3H), 7.72-7.55 (m, 2H), 7.44-7.18 (m, 6H), 7.08 (d, *J* = 8.4 Hz, 1H), 4.50 (m, 1H), 3.82 (s, 6H). ^{13}C NMR (101 MHz, DMSO-d_6): δ 160.0, 159.6, 150.9, 150.5, 149.1, 140.5, 136.1, 130.7, 128.6, 127.5, 127.0, 120.1, 112.1, 110.2, 55.99, 55.81, 44.24. ES-MS (methanol) m/z: 378.2 $[M+H]^+$, 400.1 $[M+Na]^+$, 416.1 $[M+K]^+$.

N^5-benzyl-2-(3,5-dimethoxyphenyl)-[1,2,4]triazolo[1,5-*a*][1,3,5]triazine-5,7-diamine (**207**)
Flash chromatography eluent: EtOAc-light petroleum 7:3. Yield 10% (19 mg); white solid; mp 279-281°C (EtOEt-light petroleum). ^{1}H NMR (400 MHz, DMSO-d_6): δ 8.46-7.84 (m, 3H), 7.43-7.13 (m, 7H), 6.59 (bs, 1H), 4.51 (bs, 2H), 3.79 (s, 6H). ES-MS (methanol) m/z: 378.1 $[M+H]^+$, 400.1 $[M+Na]^+$, 416.1 $[M+K]^+$.

4.4.1.3.5 Deprotection of the hydroxyl groups (208-212)

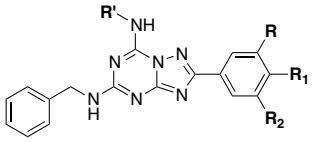

R_1= OH; R, R_2, R'=H (**208**)
R= OH; R_1, R_2, R'=H (**209**)
R_1= OH; R, R_2=H, R'=CH_2Ph (**210**)
R, R_1= OH; R_2,R'=H (**211**)
R, R_2= OH; R_1,R'=H (**212**)

Compounds **208-212** were obtained according to **General Procedure (XIV)** (Chapter 4.4.1.1.8), from 0.25 mmol of methoxy-derivatives and 0.75 mmol of boron tribromide (1M solution in DCM).

4-(7-amino-5-(benzylamino)-[1,2,4]triazolo[1,5-*a*][1,3,5]triazin-2-yl)phenol (**208**)
Flash chromatography eluent: DCM-MeOH 95:5. Yield 30% (25 mg); white solid; mp 295°C (EtOEt-light petroleum). ^{1}H NMR (400 MHz, DMSO-d_6): δ 9.87 (s, 1H), 8.51-7.80 (m, 5H), 7.41-7.15 (m, 5H), 6.86 (d, *J* = 8.2 Hz, 2H), 4.50 (d, *J* = 6.7 Hz, 2H). ^{13}C NMR (101 MHz, DMSO-d_6): δ 163.0, 161.6, 159.7, 150.5, 140.4, 138.5, 133.8, 128.7, 128.6, 127.5, 127.0, 115.8, 44.2. ES-MS (methanol) m/z: 334.1 $[M+H]^+$, 356.1 $[M+Na]^+$, 372.0 $[M+K]^+$.

3-(7-amino-5-(benzylamino)-[1,2,4]triazolo[1,5-*a*][1,3,5]triazin-2-yl)phenol (**209**)
Flash chromatography eluent: DCM-MeOH 96:4. Yield 30% (25 mg); white solid; mp 237-238°C (EtOEt-light petroleum). ^{1}H NMR (400 MHz, DMSO-d_6): δ 9.65 (s, 1H), 8.50-7.82 (m, 3H), 7.61-7.45 (m, 2H), 7.45-7.17 (m, 6H), 6.86 (d, *J* = 7.1 Hz, 1H), 4.51 (d, *J* = 6.5 Hz, 2H). ^{13}C NMR (101 MHz, DMSO-d_6): δ 163.6, 163.2, 161.6, 157.9, 150.6, 140.4, 132.5, 130.1, 128.6, 127.5, 127.0, 117.9, 117.5, 114.0, 44.2. ES-MS (methanol) m/z: 334.1 $[M+H]^+$, 356.1 $[M+Na]^+$.

3-(5,7-bis(benzylamino)-[1,2,4]triazolo[1,5-*a*][1,3,5]triazin-2-yl)phenol (**210**)
Flash chromatography eluent: DCM-MeOH 98:2 (stationary phase: neutral aluminium oxide). Yield 15% (16 mg); white solid; mp 275-276°C (EtOEt-light petroleum). ^{1}H NMR (400 MHz, DMSO-d_6): δ 9.65 (s, 1H), 9.09 (m, 1H), 8.12 (s, 1H), 7.69-7.08 (m, 13H), 6.87 (d, *J* = 8.2 Hz, 1H), 4.77-4.40 (m, 4H). ^{13}C NMR (101 MHz, DMSO-d_6): δ 161.4, 157.9, 151.7, 140.2, 138.9, 132.4, 130.1, 128.76, 128.72, 128.64, 128.1, 127.9, 127.64, 127.50, 127.1, 117.9, 117.6, 114.0, 44.3, 44.1. ES-MS (methanol) m/z: 424.2 $[M+H]^+$, 346.2 $[M+Na]^+$.

4-(7-amino-5-(benzylamino)-[1,2,4]triazolo[1,5-*a*][1,3,5]triazin-2-yl)benzen-1,2-diol (**211**)
Flash chromatography eluent: EtOAc-MeOH 8:2. Yield 33% (29 mg); white solid; mp 233°C (EtOEt-light petroleum). ^{1}H NMR (270 MHz, DMSO-d_6): δ 9.32 (s, 1H), 9.19 (s, 1H), 8.36 – 7.77 (m, 4H), 7.65 – 7.16 (m, 6H), 6.81 (d, *J* = 8.2 Hz, 1H), 4.56-4.41 (m, 2H). ^{13}C NMR (101 MHz, DMSO-d_6): δ 163.4, 161.6, 159.6, 158.9, 150.5, 143.2, 140.4, 132.9, 128.6, 127.5, 127.0, 105.5, 104.7, 44.2. ES-MS (methanol) m/z: 350.1 $[M+H]^+$.

5-(7-amino-5-(benzylamino)-[1,2,4]triazolo[1,5-*a*][1,3,5]triazin-2-yl)benzen-1,3-diol (**212**)
Flash chromatography eluent: DCM-MeOH 96:4. Yield 40% (35 mg); white solid; mp >300°C (EtOEt-light petroleum). ^{1}H NMR (400 MHz, DMSO-d_6): δ 9.39 (s, 2H), 7.93-7.82 (m, 2H), 7.39-7.14 (m, 6H), 7.00-6.92 (m, 2H), 6.28 (bs, 1H), 4.57-4.43 (m, 2H). ^{13}C NMR (101 MHz, DMSO-d_6): δ 163.5, 161.5, 159.6, 158.9, 150.5, 140.5, 132.9, 128.6, 127.5, 127.0, 105.5, 104.7, 44.2. ES-MS (methanol) m/z: 350.1 $[M+H]^+$.

4.4.1.4 Synthesis of hydrazide derivatives

Hydrazides **218-219**, **221-223**, **225-229** and **280-281** were obtained according to **General Procedure (I)** (Chapter 3.4.1.2.1).

cyclopentancarbohydrazide (**218**)
Flash chromatography eluent: light petroleum-EtOAc 1:1. Yield 50% (6.41 g); white solid; mp 106-109°C (d)(EtOEt-light petroleum). ^{1}H NMR (270 MHz, DMSO-d_6): δ 8.94 (bs, 1H), 3.89 (bs, 2H), 2.47-2.35 (m, 1H), 1.80-1.38 (m, 8H). ES-MS (methanol) m/z: 129.0 $[M+H]^+$, 151.0 $[M+Na]^+$.

1-*H*-indol-2-carbohydrazide (**219**)
Flash chromatography eluent: EtOAc. Yield 55% (9.63 g); white solid; mp 235-237°C (EtOEt-light petroleum). ^{1}H NMR (400 MHz, DMSO-d_6): δ 11.63 (bs, 1H), 9.81 (bs, 1H), 7.67-7.28 (m, 2H), 7.26-6.85 (m, 3H), 4.49 (bs, 2H). ES-MS (methanol) m/z: 176.0 $[M+H]^+$, 198.0 $[M+Na]^+$.

4-fluorobenzohydrazide (**221**)
Flash chromatography eluent: from EtOAc-light petroleum 8:2 to EtOAc-MeOH 9:1. Yield 47% (7.24 g); white solid; mp 163°C (EtOEt-light petroleum). ^{1}H NMR (270 MHz, DMSO-d_6): δ 9.77 (bs, 1H), 7.87 (dd, J= 8.9 Hz, J_{HF}= 5.5 Hz, 2H), 7.27 (t, $J_{H,HF}$= 8.9 Hz, 2H), 4.47 (s, 2H). ES-MS (methanol) m/z: 155.0 $[M+H]^+$, 177.0 $[M+Na]^+$.

4-methoxybenzohydrazide (**222**)
Flash chromatography eluent: from EtOAc-light petroleum 9:1 to EtOAc. Yield 41% (6.81 g); white solid; mp 89-92°C (EtOEt); ^{1}H NMR (270 MHz; DMSO-d_6): δ 9.62 (bs, 1H), 7.80 (d, J = 8.9 Hz, 2H), 6.98 (d, J = 8.9 Hz, 2H), 4.40 (bs, 2H), 3.80 (s, 3H). ES-MS (methanol) m/z: 167.1 $[M+H]^+$, 189.0 $[M+Na]^+$.

3-fluorobenzohydrazide (**223**)
Flash chromatography eluent: EtOAc. Yield 83.5% (12.9 g); white solid; mp 137-139°C (EtOEt); ^{1}H NMR (400 MHz, DMSO-d_6): δ 9.87 (s, 1H), 7.69-7.67 (m, 1H), 7.64-7.58 (m, 1H), 7.55-7.48 (m, 1H), 7.39-7.34 (m, 1H), 4.54 (s, 2H). ES-MS (methanol) m/z: 155.0 $[M+H]^+$.

3-nitrobenzohydrazide (**225**)
Yield 90% (16.3 g); white solid; mp 132°C (EtOEt); ^{1}H NMR (270 MHz; DMSO-d_6): δ 10.17 (bs, 1H), 8.63 (s, 1H), 8.40–8.31 (m, 1H), 8.30-8.21 (m, 1H), 7.76 (t, J = 8.0 Hz, 1H), 4.65 (bs, 2H). ES-MS (acetonitrile) m/z: 182.0 $[M+H]^+$.

4-benzyloxybenzohydrazide (**226**)
Flash chromatography eluent: from EtOAc to EtOAc-MeOH 9:1. Yield 38% (9.21 g); white solid; mp 125°C (EtOEt-light petroleum). ^{1}H NMR (270 MHz, DMSO-d_6): δ 9.61 (s, 1H), 7.79 (d, J = 8.7 Hz, 2H), 7.60 – 7.21 (m, 5H), 7.05 (d, J = 8.7 Hz, 2H), 5.16 (s, 2H), 4.41 (s, 2H). ES-MS (methanol) m/z: 242.9 $[M+H]^+$, 264.9 $[M+Na]^+$.

3-benzyloxybenzohydrazide (**227**)
Flash chromatography eluent: EtOAc. Yield 68% (16.5 g); white solid; mp 113°C (EtOEt-light petroleum). ^{1}H NMR (270 MHz, DMSO-d_6): δ 9.76 (s, 1H), 7.62 – 7.24 (m, 8H), 7.15 (d, J = 7.8 Hz, 1H), 5.15 (s, 2H), 4.49 (s, 2H). ES-MS (methanol) m/z: 242.8 $[M+H]^+$, 264.8 $[M+Na]^+$.

3,4-dibenzyloxybenzohydrazide (**228**)
Yield 85% (29.6 g); white solid; mp 146-149°C (EtOEt-light petroleum). ^{1}H NMR (270 MHz, DMSO-d_6): δ 9.61 (s, 1H), 7.56 (s, 1H), 7.52-7.24 (m, 11H), 7.11 (d, J = 8.4 Hz, 1H), 5.19 + 5.17

(s, 4H), 4.43 (s, 2H). ES-MS (methanol) m/z: 348.9 $[M+H]^+$, 370.9 $[M+Na]^+$.

3,5-dibenzyloxybenzohydrazide (**229**)
Quantitative yield (34.8 g); white solid; mp 128-135°C (EtOEt-light petroleum). ^{1}H NMR (400 MHz, DMSO-d_6): δ 9.73 (s, 1H), 7.48–7.32 (m, 10H), 7.09 (s, 2H), 6.81 (s, 1H), 5.12 (s, 4H), 4.49 (s, 2H). ES-MS (methanol) m/z: 349.1 $[M+H]^+$, 371.1 $[M+Na]^+$.

3,4-dimethoxybenzohydrazide (**280**)

Yield 70% (13.7 g); white solid; mp 152-154°C (EtOEt-light petroleum). ^{1}H NMR (270 MHz, DMSO-d_6): δ 9.62 (s, 1H), 7.55-7.38 (m, 2H), 7.03-6.95 (m, 1H), 4.44 (s, 2H), 3.79 (s, 6H). ES-MS (methanol) m/z: 197.0 $[M+H]^+$.

3,5-dimethoxybenzohydrazide (**281**)
Flash chromatography eluent: DCM-MeOH 97:3. Yield 78% (17.0 g); white solid; mp 176°C (EtOEt-light petroleum). ^{1}H NMR (270 MHz, DMSO-d_6): δ 9.74 (s, 1H), 7.01-6.95 (m, 2H), 6.65-6.60 (m, 1H), 4.47 (s, 2H), 3.77 (s, 6H). ES-MS (methanol) m/z: 197.0 $[M+H]^+$, 219.0 $[M+Na]^+$.

4.4.2 Biological Procedures

4.4.2.1 CK-1δ Kinase Assay - KinaseGlo® kit

The Kinase-Glo Kit was used to screen compounds for activity towards CK-1δ. In detail, CK-1δ luminescent assays were performed in black 96-well plates and using the following buffer: 50 mM HEPES (pH 7.5), 1 mM EDTA, 1 mM EGTA, and 15 mM magnesium acetate. In each assay, the compound CR8 (**82**) was used as positive control, while DMSO/buffer solution was used as reference.

In a typical assay, 10 μL of test compound (dissolved in DMSO at 1 mM concentration and diluted in advance in assay buffer to the desired concentration) and 10 μL (16 ng) of enzyme were added to each well followed by 20 μL of assay buffer containing 0.1% casein as substrate and 4 μM ATP. The final DMSO concentration in the reaction mixture did not exceed 1-2%. After 60' incubation at 30°C, the enzymatic reaction was stopped with 40 μL of Kinase-Glo reagent. Luminescence signal (relative light unit, RLU) was recorded after 10 min at 25°C using a Tecan Infinite M100 multimode reader.

The activity is proportional to the difference of the total and consumed ATP. The inhibitory activities were calculated on the basis of maximal activities measured in the absence of inhibitor, following this equation:

$$\textbf{Inhibition (\%)} = (RLU_X - RLU_{CTRL-}) / (RLU_{CTRL+} - RLU_{CTRL-}) \cdot 100$$

where RLU_X is the luminescence signal measured in the well of the test compound, RLU_{CTRL-} the luminescence measured in absence of inhibitor, RLU_{CTRL+} the luminescence of the well containing the reference compound CR8 (**82**), at a concentration that ensure total enzyme inhibition (100 μM). Initially, enzyme activity percentage was determined at 40 μM for each inhibitor, in two independent experiments; subsequently, the most active compounds were tested in 10-dose IC_{50} mode (2.5-fold serial dilutions), in three independent experiments. Data were analyzed using Excel and GraphPad Prism software (version 6.0) for IC_{50} curve fits using sigmoidal dose–response (variable slope) equations.

4.4.2.2 CK-1δ Kinase Assay – Radiometric Assay

These studies were performed by Dr. Giorgio Cozza, University of Padua, Padua (Italy).

CK-1δ phosphorylation assays were carried out at 37°C in the presence of increasing amounts of each inhibitor in a final volume of 25 µL containing 50 mM Tris-HCl pH 7.5, 100 mM NaCl, 12 mM MgCl2, 0.02 mM [γ^{33}P-ATP] (500-1000 cpm/pmol). The phosphorylatable substrate was the synthetic peptide RRKHAAIGDDDDAYSITA (200 µM). Reaction started with the addition of the kinase and was stopped after 10 minutes by addition of 5 µL of 0.5 M orthophosphoric acid before spotting aliquots onto phosphocellulose filters. Filters were washed in 75 mM phosphoric acid (5-10 mL/each) four times and then once in methanol and dried before counting. IC_{50} values were calculated using 5 concentrations of each inhibitor.

4.4.2.3 Prediction of CNS permeation: PAMPA-BBB assay

Prediction of the brain penetration was assessed using a parallel artificial membrane permeability assay (PAMPA), following the procedure described in Chapter 3.4.2.3.[229] Data obtained for the 10 commercial drugs used as assay validation were reported in **Table 13** and in **Figure 40**:

Table 13. Permeability (*Pe* 10^{-6} cm s^{-1}) in the PAMPA-BBB assay for 10 commercial drugs used in the experiment validation

Compound	Bibl.[229]	*Pe* (10^{-6} cm s^{-1})[a]
Atenolol	0.8	0.18 ± 0.26
Caffeine	1.3	0.32 ± 0.16
Desipramine	12	7.02 ± 0.38
Enoxacin	0.9	1.65 ± 0.11
Hydrocortisone	1.9	2.36 ± 0.29
Ofloxacine	0.8	1.46 ± 0.19
Piroxicam	2.5	3.43 ± 0.38
Promazine	8.8	9.71 ± 1.10
Testosterone	17	14.87 ± 0.62
Verapamil	16	18.77 ± 0.09

[a] Data are the mean ± SD of 2 independent experiments. CNS+ >3.9, CNS - < 2.1.

Figure 40. Linear correlation between experimental and reported permeability of commercial drugs using the PAMPA-BBB assay.

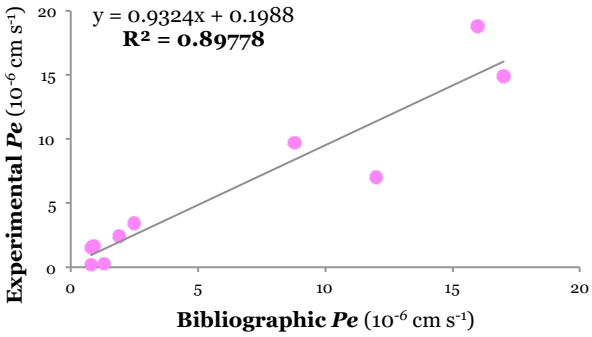

4.4.3 Docking studies on CK-1δ

These studies were performed by the research group of Professor Stefano Moro, University of Padua, Padua (Italy).

All CK-1δ inhibitors were built and their partial charges calculated after semi-empirical (PM6) energy minimization[247] using the MOE2015.[248] The crystallographic structure selected to perform docking studies was the human CK-1δ in complex with the inhibitor PF4800567 (PDB ID: 4HNF). All water molecules present in the pdb file were retained and the protein was subjected to the structure preparation tool of MOE2015.[248] Finally, protonate 3D tool was used to assign the protomeric state.[248] To identify the more appropriate protocol for the selected complexes we performed a self-docking benchmark using DockBench 1.01,[249] which compared the performance of 17 different posing/scoring protocols. The active site was

defined using a radius of 12 Å from the centre of mass of the co-crystallized ligand. Each ligand was docked 10 times, using GOLD[250] (ChemPLP[251] and Goldscore[252] were used as scoring functions for 4HNF) and the virtual screening tool of DockBench, adopting the parameters used in the benchmark study. Finally, the obtained conformations with 4HNF from the docking were rescored with ChemPLP.

5 Synthesis and Characterization of dual GSK-3/CK-1 Inhibitors

5.1 INTRODUCTION

As previously introduced, both GSK-3β and CK-1δ are involved in the neuroinflammatory process, mainly due to their role in Wnt and Hedgehog pathways,[76,100,253,254] and also in the formation of hyperphosphorylated protein *tau*, one of the major hallmark of the large family of neurodegenerative disorders classified as tauopathies, which include Alzheimer's disease (AD).[106,109] All these observations suggested that dual GSK-3β/CK-1δ inhibitors could be interesting for the treatment of neuroinflammation-related and neurodegenerative diseases. In particular, we describe here the design, synthesis and characterization of a dual GSK-3β/CK-1δ inhibitor with different inhibitory mechanisms towards the two kinases.

We decided to use the versatile adenine-like [1,2,4]triazolo[1,5-*a*][1,3,5]triazine (TT) nucleus as scaffold for the development of compounds with inhibitory activity towards both GSK-3β and CK-1δ. First of all, with the aim of elucidating the role of the substitutions on the TT scaffold on the affinity of this class of compounds towards GSK-3β and CK-1δ, preliminary series of TT derivatives were synthetized. Then, we supposed that a focused substitution at the 2-position of the TT nucleus could target the non-catalytic cysteine 199 (Cys199), hence offering the opportunity to obtain a covalent inhibition of GSK-3β (**Figure 41**). As already discussed in Chapter 1.5, in recent years, in fact, there has been a resurgence of interest in covalent inhibitors driven by a number of factors, including a general improved selectivity and potency compared with ATP-competitive kinase inhibitors and the realization that different of latest irreversible kinase inhibitors are exhibiting clinical efficacy and safety (e.g. afatinib, an irreversible EGFR inhibitor approved by the FDA in 2013 for the treatment of metastatic non small cell lung cancer).[131]

To our purpose, we decided to introduce on the TT scaffold at the 2-position the 2-cyanoacrylamide group, a Micheal acceptor moiety which presents a peculiar reactivity.[255] In fact, the presence of a nitrile group converts an irreversible Michael acceptor (for example, acrylate or acrylamide) into an electrophile that reacts with cysteine thiols under physiological conditions in a manner that is energetically favourable but reversible, thus minimizing the chance of irreversible modifications of off-target peptides (e.g. glutathione).[255]

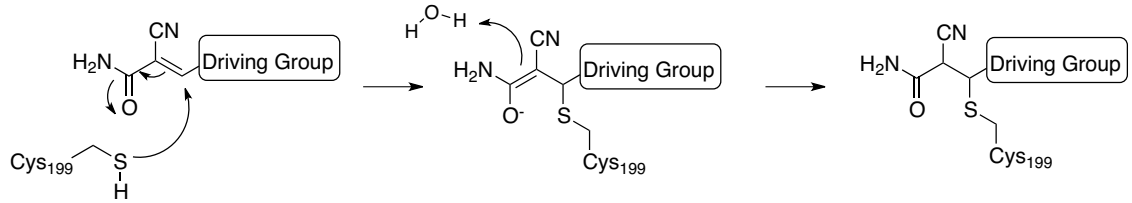

Figure 41. Reaction mechanism of 2-cyanoacrilamides towards Cys199 of GSK-3β.[256]

Regarding CK-1δ, we find the amido moiety in the potent ATP competitive CK-1δ inhibitor D4476 (**74**), which possesses an IC_{50} value of 0.3 μM, thus rendering the cyanoacrylamido group suitable to obtain a dual GSK-3β/CK-1δ inhibitor (**Figure 42**).[257] For the most potent compound of the series (**335**), the binding mode with both kinases, through computational and experimental studies, was elucidated and then its reactivity towards thiols was characterized by HPLC and UV-spectroscopy methods. Finally, PAMPA-BBB was performed to predict CNS permeability and *in vitro* assays on neuroinflammation models provided preliminary indications on dual CK-1/GSK-3β inhibition effectiveness.

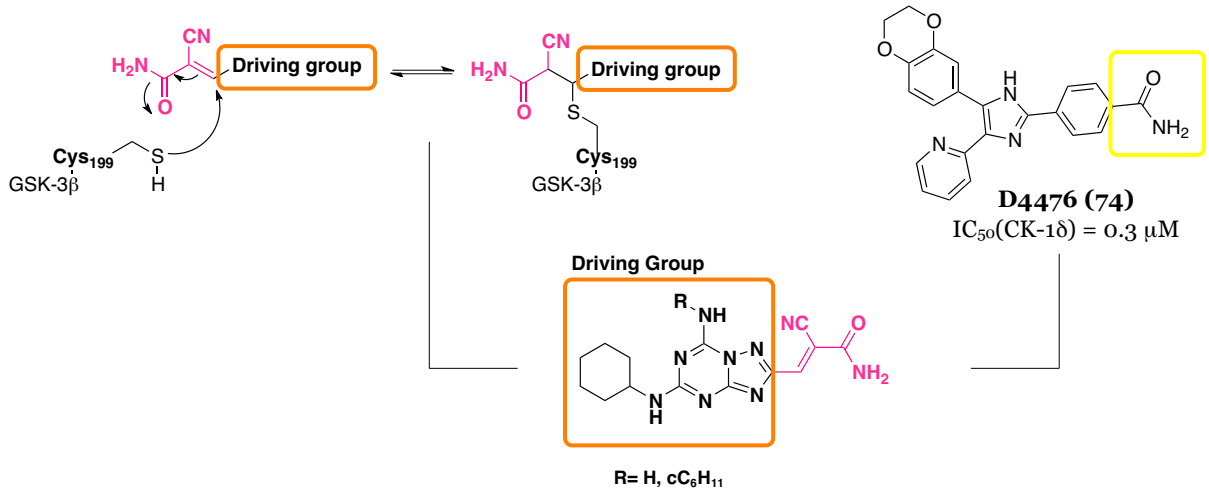

Figure 42. Rationale for the design of novel GSK-3β/CK-1δ inhibitors.

5.2 RESULTS AND DISCUSSION

5.2.1 Chemistry

5.2.1.1 Synthesis of 5,7-disubstituted[1,2,4]triazolo[1,5-*a*][1,3,5]triazines

The 2-unsubstituted compounds presenting the same substituents at both 7- and 5-positions of the TT scaffold (**302-303**) were obtained by reacting directly **165** (Chapter 3.2.1, **Scheme 1**) with a large excess of methanolic ammonia or cyclohexylamine, while the nucleophilic substitution at the 5-position of compounds **167** and **171** (Chapter 3.2.1, **Scheme 2**) was conducted in presence of a less amount of the required amine (3 equivalents) for a longer time of reaction (**304-306**) [**Scheme 12**].

Scheme 12. Synthesis of compounds **302-306**[a]

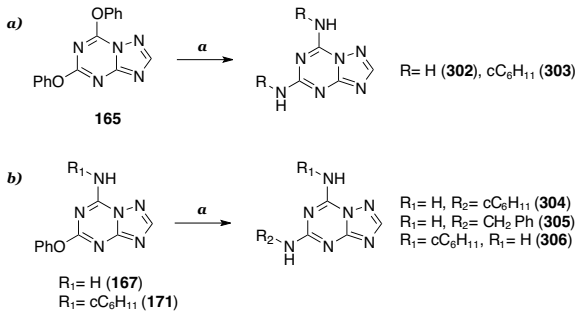

[a]Panel a) ***a:*** ammonia 7N in methanol or cyclohexylamine, methanol or ethanol, sealed tube, 75-95°C, 12 h.
Panel b) ***a:*** ammonia 7N in methanol, cyclohexylamine or benzylamine, ethanol, 95°C, sealed tube, 24-72 h.

The nucleophilic displacement of phenoxy group at the 5-position with aniline did not occur due to the lower reactivity of aniline. Therefore, we decided to apply another procedure reported in literature which started from the 7-amino-5-methylsulfanyl[1,2,4]triazolo[1,5-*a*][1,3,5]triazine (**309**), obtained by thermal reaction of 3-amino-1,2,4-triazole (**307**) with dimethyl *N*-cyanodithioiminocarbonate (**308**), where the reactivity of 5-methylsulfanyl group could be enhanced oxidizing it to the sulfoxide **310**.[214,258] This successfully allowed the introduction of the aminophenyl group on the TT scaffold, leading to compound **311** [**Scheme 13**].

Scheme 13. Synthesis of compound **311**[a]

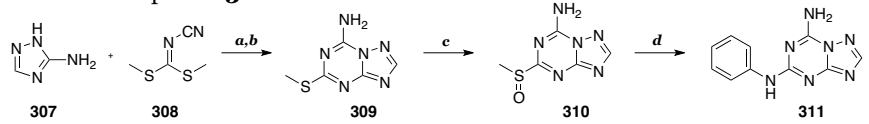

[a] ***a:*** neat, 170°C, 1 h; ***b:*** DCM-methanol, reflux, 1 h; ***c:*** *m*-CPBA, DCM, r.t., 12 h; ***d:*** aniline, acetonitrile, sealed tube, 80°C, 48 h.

5.2.1.2 Synthesis of 2,5,7-trisubstituted[1,2,4]triazolo[1,5-*a*][1,3,5]triazines

The 4,6-diphenoxy-1,3,5-triazin-2-yl hydrazides, from which after intramolecular cyclization will give rise to the TT nucleus, could be obtained in two different ways: the first one, reported in **Scheme 14**, implies the reaction of the desired hydrazide (in this case 3-cyanobenzohydrazide **314**, to obtain the final compounds **329** and **330**) with the triphenoxy-triazine **159** (Chapter 3.2.1, **Scheme 1**) in presence of DBU; the second one, used for the synthesis of derivatives **335-338**, implies the reaction of 2-hydrazinyl-4,6-diphenoxy-1,3,5-triazine (**160,** Chapter 3.2.1, **Scheme 1**) with the chloride of 2-(benzyloxy)acetic acid (**319**), obtained by Williamson reaction between chloroacetic acid (**317**) and benzyl alcohol (**316**) [**Scheme 15**]. Even in this case, the benzyl was used as protecting group of the hydroxyl group.

Scheme 14. Synthesis of compound **315** [a]

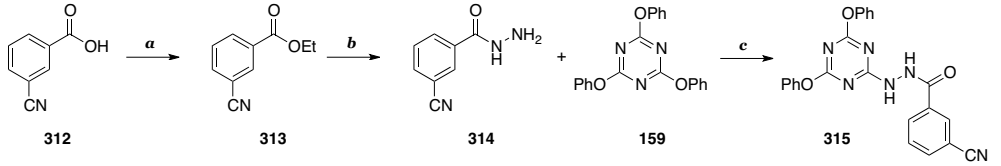

[a] ***a:*** H_2SO_4 cat., ethanol, reflux, 48 h; ***b:*** $NH_2NH_2 \cdot H_2O$, ethanol, reflux, 48 h; ***c:*** DBU, dry THF, r.t., 12 h.

Scheme 15. Synthesis of compound **320**[a]

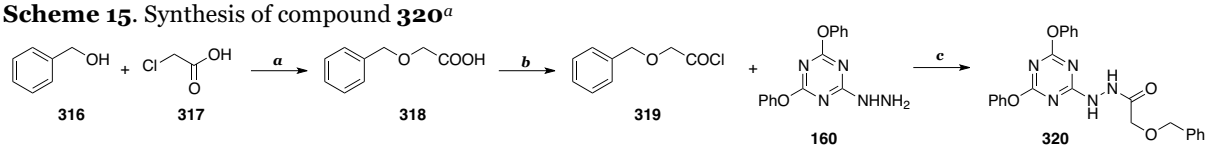

[a] ***a:*** NaH, dry toluene, r.t. for 1 h, then 80°C for 2 h; ***b:*** oxalyl chloride, DCM, reflux, 4 h; ***c:*** TEA, DCM, r.t., 12h.

The 2-substituted 5,7-diphenoxy-[1,2,4]triazolo[1,5-*a*][1,3,5]triazine derivatives **321** and **322** were obtained by intramolecular cyclization under dehydrative conditions, as previously described in Chapter 3.2.1, and subsequently converted into the 7-amino derivatives **323-324** with methanolic ammonia at room temperature. The further substitution at the 5-position (**325-327**), or at both 7- and 5- positions (**328**), required heating the mixture of compounds **323-324** and their desired amines in a sealed tube [**Scheme 16**].

Scheme 16. Synthesis of compounds **325-328**[a]

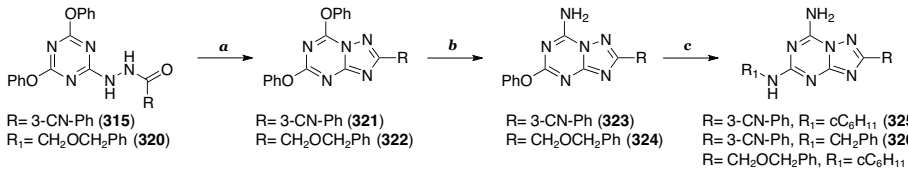

R= 3-CN-Ph (**315**)
R_1= CH_2OCH_2Ph (**320**)

R= 3-CN-Ph (**321**)
R= CH_2OCH_2Ph (**322**)

R= 3-CN-Ph (**323**)
R= CH_2OCH_2Ph (**324**)

R= 3-CN-Ph, R_1= cC_6H_{11} (**325**)
R= 3-CN-Ph, R_1= CH_2Ph (**326**)
R= CH_2OCH_2Ph, R_1= cC_6H_{11} (**327**)

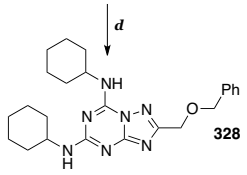

[a] ***a:*** P_2O_5, HMDSO, xylene, from r.t. to 90°C, 2.5 h, reflux, 4 h; ***b:*** ammonia 7N in methanol, methanol, r.t., 2 h; ***c:*** cyclohexylamine or benzylamine, EtOH, 100°C sealed tube, 12-48h; ***d:*** cyclohexylamine (large excess), EtOH, 95°C sealed tube, 24h.

The amido derivatives **329-330** were obtained after conversion of the nitriles via acid-catalysed hydration using a TFA-H_2SO_4 mixture [**Scheme 17**].[259]

Scheme 17. Synthesis of compounds **329-330**[a]

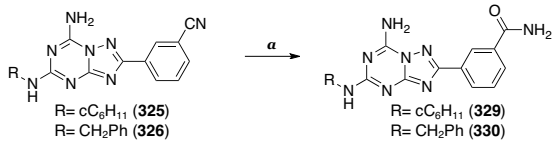

a: TFA-H_2SO_4 (4:1), 70°C, 3 h.

5.2.1.2.1 Introduction of a Micheal-acceptor moiety at 2-position of the [1,2,4]triazolo[1,5-*a*][1,3,5]triazine scaffold

In order to insert the Micheal-acceptor warhead at the 2-position, deprotection of hydroxyl group was performed with palladium on carbon as catalyst and heated ammonium formate as hydrogen source, delivering the alcohol derivatives **331-332**, which were in turn oxidized to aldehyde with Dess-Martin periodinane (**333-334**). The cyanoacrilamide derivatives **335-336** were obtained by Knoevenagel condensation between **333-334** and cyanoacetamide, in presence of DBU, while cyanoacrilates **337** and **338** derive from Wittig reaction of **333** and (triphenylphosphoranylidine)acetonitrile in a E/Z ratio of 50:50 [**Scheme 18**].[255]

Scheme 18. Synthesis of compounds **335-338**[a]

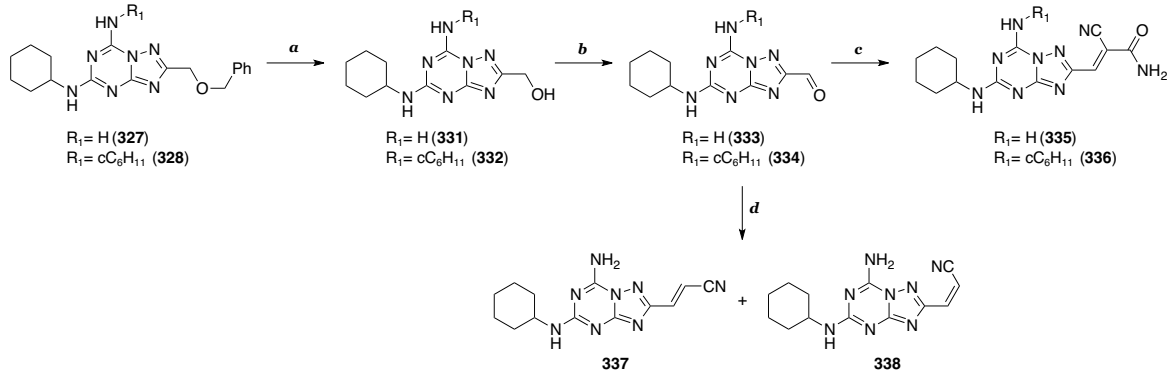

[a]***a:*** $HCOONH_4$, Pd/C, MeOH, reflux, 3 h; ***b***: Dess-Martin periodinane, DCM, r.t., 3h; ***c***: cyanoacetamide, DBU, DCM, r.t., 2h; ***d***: (triphenylphosphoranylidine)acetonitrile, DBU, DCM, r.t., 2h.

5.2.2 Enzymatic evaluation and CNS permeation prediction

All the newly synthesized derivatives were evaluated towards CK-1δ with the KinaseGlo® luminescence assay as described in Chapter 4.4.2.1. Compounds **335-338** were assayed with the KinaseGlo® luminescence assay in the group of Prof. Martinez (CIB, Madrid, ES) also towards GSK-3β. Prediction of the brain penetration of promising compounds was assessed using PAMPA-BBB assay, as previously described in Chapter 3.2.4.

Data about a preliminary series of triazolo-triazines (compounds **302-306** and **311**) were reported in **Table 14**. These compounds were synthesized with the aim of elucidating the role of the substitutions at the 5- and 7- positions of the TT scaffold on their affinity for GSK-3β. In particular we decided to maintain the 2-position free (R=H) and to modify the 7- (R_1= -H, cyclohexyl) and 5- (R_2= -H, cyclohexyl, phenyl, benzyl) positions. A certain activity towards GSK-3β was found only with the 5,7-disubstituted derivative **303** [IC_{50}(GSK-3β)=

3.1 μM], thus rendering it the scaffold to work on to further improve the affinity for GSK-3β (**Table 14**).

Table 14. TTs derivatives **302-306** and **311**

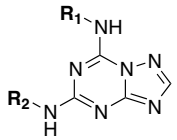

cmpd	R_1	R_2	IC_{50} μM (GSK-3β)[a]	IC_{50} μM (CK-1δ)[b]
302[c]	H	H	> 20	>40
304[d]	H	cC_6H_{11}	> 10	>40
306	cC_6H_{11}	H	> 20	>40
303[c]	cC_6H_{11}	cC_6H_{11}	3.1	>40
305[d]	H	CH_2Ph	> 20	>40
311	H	Ph	> 20	>40

[a]GSK-3β inhibition data obtained with LANCE® *Ultra* kinase assay; [b]CK-1δ inhibition data obtained with KinaseGlo® kinase assay; [c]**302** reported by Valbusa *et al.*[260] and Dolzhenko *et al.*[261]; **303** reported by Akaoshi *et al.*[262]; [d]synthesis and characterization were already performed in our research group.

Hypothesizing a similar pose between ATP and **303** in the ATP binding pocket of GSK-3β, we supposed that a focused substitution at the 2-position of the TT nucleus could target the non-catalytic cysteine 199 (Cys199), hence offering the opportunity to obtain a covalent inhibition of GSK-3β, which in general lead to improved selectivity and potency towards the target. In particular, the 2-cyanoacrylamide group is able to give a reversible thiol-Michael reaction with the thiol of Cys199: in this way, the ligand is able to make a covalent bond with the target but the reversibility feature of this reaction minimizes the chance of irreversible modifications of off-target peptides (e.g. glutathione).[255] In addition, the amido group can be also found in the CK-1δ inhibitor D4476 [**74,** IC_{50}(CK-1δ)= 0.3 μM], thus suggesting that the 2-cyanoacrilamido group could be suitable to obtain the inhibition of CK-1δ, too. [257] First of all, we tried to validate the efficacy of the amido group on CK-1δ by introducing the 3-amidophenyl moiety at the 2-position of the TT ring in compounds **329** and **330**. The choice of the 3-substituted phenyl ring is due to results previously obtained (Chapter 4) which showed that *meta* substitutions on the phenyl ring with groups able to make hydrogen bonding are better than *para* substitutions. As supposed, **329** and **330** showed good IC_{50} values towards CK-1δ [**329**, IC_{50}(CK-1δ)= 2.59 μM; **330**, IC_{50}(CK-1δ)= 4.28 μM] (**Table 15**).

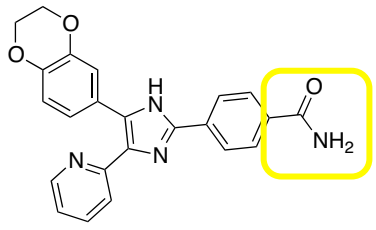

D4476 (74)
IC_{50}(CK-1δ) = 0.3 μM

Table 15. TTs derivatives **325-326, 329-330**

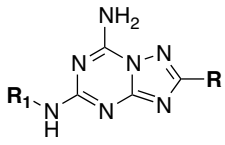

cmpd	R	R_1	IC_{50} (CK-1δ)
325	3-CN-Ph	cC_6H_{11}	>40
329	3-$CONH_2$-Ph	cC_6H_{11}	2.59 ±0.76
326	3-CN-Ph	CH_2Ph	>40
330	3-$CONH_2$-Ph	CH_2Ph	4.28 ±1.21

[b]CK-1δ inhibition data obtained with KinaseGlo® kinase assay; data are expressed ± SD (n=3).

Then, taking into account all these observation, we decided to synthetize new [1,2,4]triazolo[1,5-*a*][1,3,5]triazine derivatives bearing at the 2-position the 2-cyanoacrylamide moiety, that should confer potency towards both GSK-3β, through a

covalent bond with Cys199, and CK-1δ. Concerning the other positions, we maintained the double substitution with the cyclohexyl group (**336**), as present in compound **303**, and we decided to synthetize also the not-substituted derivative in 7-position (**335**), since the substitution at this position seems to affect negatively the affinity towards CK-1δ [**303**, IC_{50}(CK-1δ)= >40 μM *vs* **329**, IC_{50}(CK-1δ)= 2.59 μM]. Then, to further investigate the role of the 2-cyanoacrylamide moiety we decided to synthetize also the corresponding acrylonitrile (**337-338**) derivatives. Data are reported in **Table 16**.

Table 16. Kinase assay and PAMPA-BBB data of derivatives **335-338**

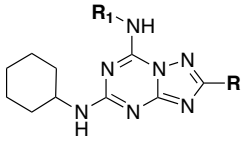

cmpd	R	R_1	IC_{50} (GSK-3β)[a]	IC_{50} (CK-1δ)[a]	*Pe* (10^{-6} cm s^{-1})[b] and CNS-prediction
335	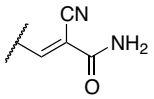	H	0.17 ± 0.02	0.68 ± 0.03	1.34 ±0.23 (CNS+/-)
336	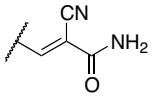	cC_6H_{11}	>10	>10	
337	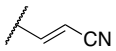	H	5.75 ± 0.21	>10	2.35 ±0.52 (CNS+/-)
338		H	>10	>10	

[a]Inhibition data obtained with KinaseGlo® kinase assay; data are expressed ± SD (n=3). [b]Permeability (*Pe* 10^{-6} cm s^{-1}) in the PAMPA-BBB assay of selected compounds with their predictive penetration in the CNS. Data are the mean ± SD of 2 independent experiments. Experiment validation with 10 commercial drugs was performed and gave the following correlation parameters: *Pe*(exp)= 1.0.664(bibl) - 0.8419 (R^2= 0.9655). Calculated limits: CNS + > 3.42, CNS - < 1.29.

As depicted in **Table 16**, the introduction of the cyanoacrylamide moiety at the 2-position of TT scaffold led to a substantial improvement of affinity towards both GSK-3β and CK-1δ, leading to IC_{50} values for compound **335** in the sub-micromolar range [**335**, IC_{50}(GSK-3β)= 0.17 μM; IC_{50}(CK-1δ)= 0.68 μM;]. The well-balanced GSK-3β/CK-1δ inhibitory activities allowed us to consider derivative **335** a dual inhibitor, thus confirming the validity of the rationale of the work. Notably, regarding the GSK-3β inhibitory profile, the cyanoacrilamide warhead introduced in the TT scaffold converted the inactive compound **304** [IC_{50}(GSK-3β) >10 μM] into a GSK-3β inhibitor with a good potency [**335**, IC_{50}(GSK-3β)= 0.17 μM], while the same modification on the promising **303** scaffold [IC_{50}(GSK-3β)= 3.1 μM] resulted detrimental in terms of inhibitory activity [**336**, IC_{50}(GSK-3β) >10 μM]. The replacement of the electrophilic warhead of **335** with the acrylonitrile moiety led to more than 30-fold less potent derivatives (**337-338**), which resulted inactive also towards CK-1δ. Concerning PAMPA-BBB results, we cannot consider compounds **335** and **337** clearly able to cross the BBB by passive permeation.

Based on these considerations, compound **335** was selected for additional studies aimed to elucidate its inhibitory mechanism and binding mode towards GSK-3β and CK-1δ, its reactivity towards thiol nucleophiles and also its effects on neuro-protection, despite the uncertain result of CNS-permeation.

5.2.3 Reactivity studies

We supposed that the GSK-3β inhibitory activity of derivative **335** is enhanced by covalent interaction of the Michael-acceptor group at the 2-position of the triazolo-triazine nucleus with the thiol unit of Cys199, located in the GSK-3β ATP binding site. So it was therefore necessary to characterize the reactivity of this compound in front of thiol groups. For this purpose, we have analysed by UV-spectroscopy and then HPLC-MS the reaction of compound **335** with the model thiol β-mercaptoethanol (βME) at room temperature (**Figure 43**).

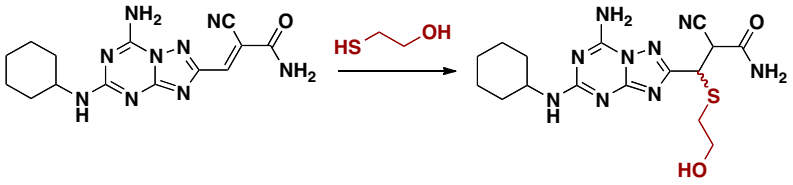

Figure 43. Reaction of compound **335** with βME.

In the first experiment, derivative **335** (0.85 mM) in PBS/DMSO 70:30 (pH 7.4) was treated with increasing concentrations of βME (from 0 to 100 mM) and monitored by UV-visible absorption spectroscopy. As depicted in **Figure 44**, we can observe a stepwise decrease in the UV-visible absorption band of the double-bond of cyanoacrylamide moiety of compound **335** (λ_{max}=350 nm, highlighted in orange) after addition of increasing amounts of βME.

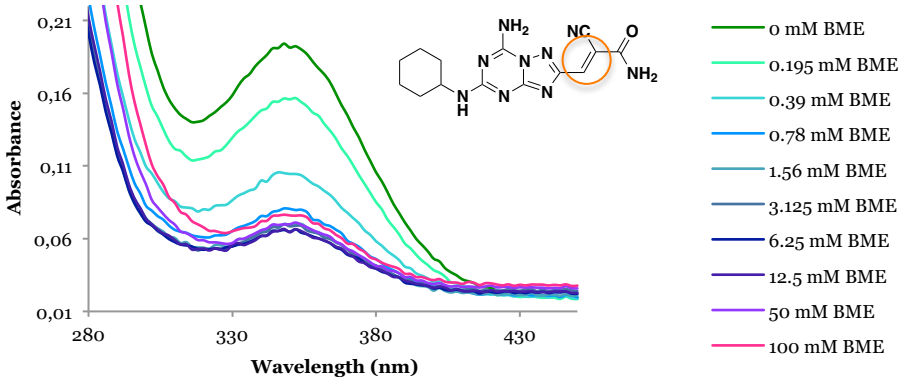

Figure 44. Reaction of compound **335** with βME is accompanied by a decrease in the 350 nm absorption band.

To further confirm the reactivity of derivative **335** in front of thiols we followed the reaction with βME by HPLC-MS (**Figure 45**). The reaction afforded 42% of the S-alkylated product for **335** in a compound-βME-triethylamine 1:1:1 mix ratio after 1 h, which increased to 53% after 2 hours. Despite the reactivity showed in the first hours, the total S-alkylation of compound **335** did not occur and the percentage remained nearly constant even after 24 hours (47%). A potential explanation for these results could be the reversible nature of the Michael-reaction between the cyanoacrylamide warhead and nucleophiles, as previously described in literature. In fact, the presence of two electron-withdrawing groups (EWGs) attached to the α-carbon of the Michael-acceptor group increases the susceptibility of the β-carbon to nucleophilic attack by thiols, but also increases the carbon acidity of the cyanoacrylamide adduct, thus enhancing the elimination rate and rendering the reaction reversible.[255]

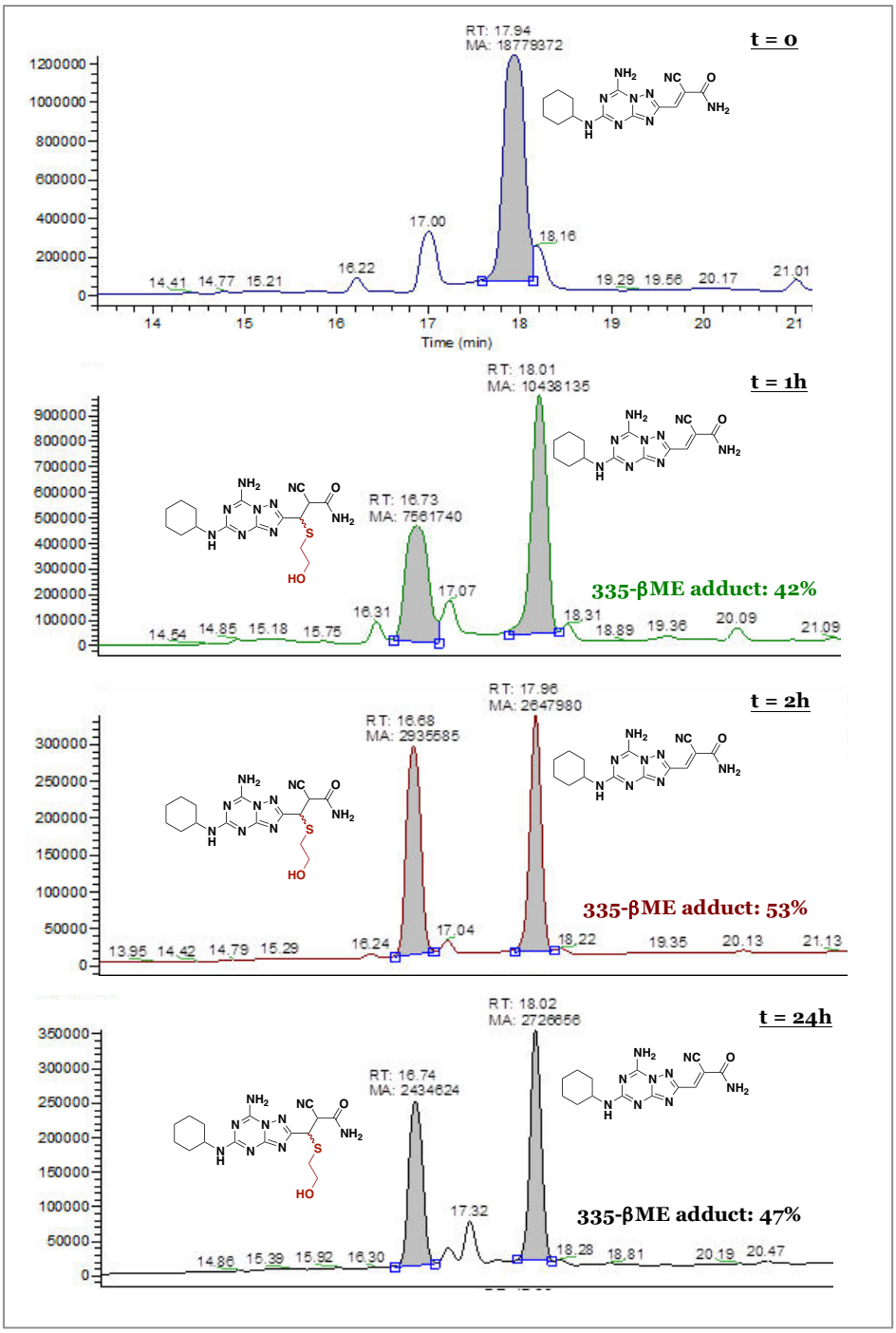

Figure 45. HPLC-MS chromatograms of compound **335** incubated with βME and TEA registered after different times (0, 1, 2 and 24h). Unmodified derivative **335** [m/z = 328.33 $(M+H)^+$] presented a retention time (t_R) of 17.9-18.0 min, while for the **335-βME** conjugate [m/z= 406.31 $(M+H)^+$] t_R was 16.7 min.

5.2.4 Binding-mode studies on GSK-3β and CK-1δ

5.2.4.1 Computer-assisted studies

Aimed to explore structural reasons for derivative **335** inhibitory activities towards GSK-3β and CK-1δ, molecular docking studies were performed.

Docking studies at the binding site of GSK-3β allowed gaining insight in effective interactions that led compound **335** to inhibit this kinase with an IC_{50} of 0.17 μM. This value likely resulted from a complex inhibition mechanism, including reversible competition with ATP and covalent interaction with GSK-3β through a thia-Michael reaction. As depicted in **Figure 46** (panel A), compound **335**, being an adenine-like derivative, lies in the hinge region, reproducing the typical binding fingerprints of protein kinases ATP-competitive inhibitors: it establishes two H-bonds, one between primary amino group at the 7-position and carbonyl of Asp133 and the other between secondary amino group at the 5-position and Val135. Moreover, derivative **335** was able to establish a hydrogen bond interaction also between its carbonyl of the amido group at the 2-position and amino group of the lateral chain of Lys85. Subsequently a covalent docking study was carried out where a thia-Michael reaction occurred by nucleophilic attack of GSK-3β Cys199 residue on the reactive cyanoacrilamide warhead at the 2-position of the TT scaffold (**Figure 46**, panel B).

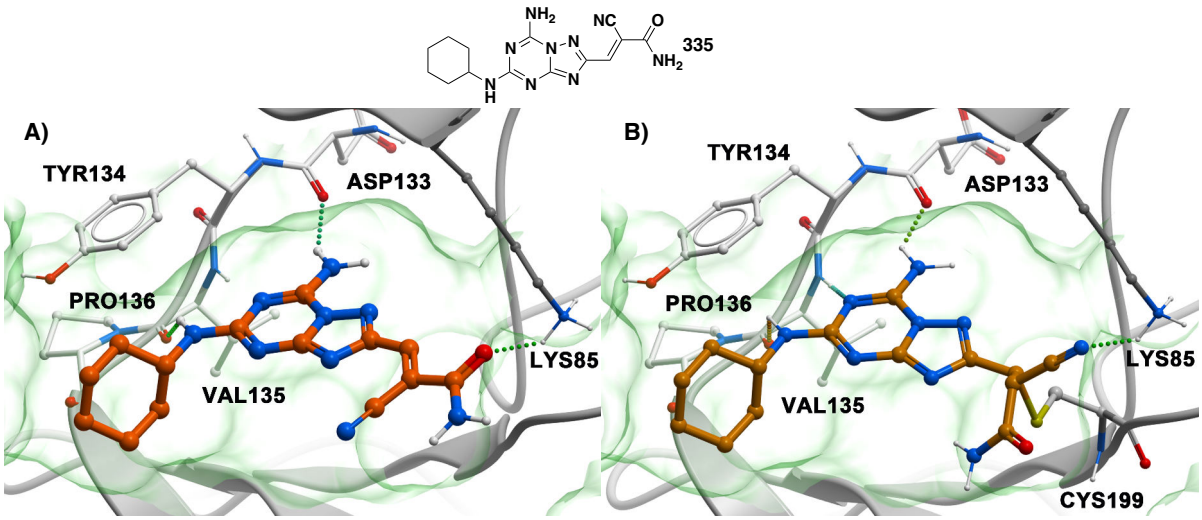

Figure 46. Panel A) Bound conformation of compound **335** at the binding site of GSK-3β (PDB code: 1Q5K) before the thia-Michael reaction occurred as predicted by ligand docking simulations. The ligand is reported in orange x-sticks. The key residues of the hinge region, Cys199 and Lys85 are reported in light grey x-sticks and labelled explicitly. A transparent green mesh describes the boundaries of the binding pocket. Hydrogen bond interactions are highlighted by dotted lines. Panel B) Covalently bound conformation of compound **335** at the binding site of GSK-3β predicted by docking simulations. The covalently bound ligand is reported in orange x-sticks. The key residues of the hinge region, Cys199 and Lys85 are reported in light grey x-sticks and labelled explicitly. A transparent green mesh describes the boundaries of the binding pocket. Hydrogen bond interactions are highlighted by dotted lines.

We can assume that non-covalent interactions of the molecule with the binding pocket of GSK-3β (Asp133, Val135, Lys85) are critical for the optimal orientation of the electrophile moiety towards a specific protein nucleophile residue (driving group), thus increasing the speed and selectivity of the covalent bond, and are ultimately responsible for the high potency of derivative **335**. In fact, the different binding pose of compound **303** (**Figure 47**) could provide an explanation for the inactivity of the di-substituted derivative **336**. In particular, the two cyclohexyl groups lie in the hydrophobic region II, the triazolo part of the ring interacts with the hinge residue Val135, while the 2-position of the TT is oriented towards Asp133 of the hinge region, so on the opposite site respect to Cys199.

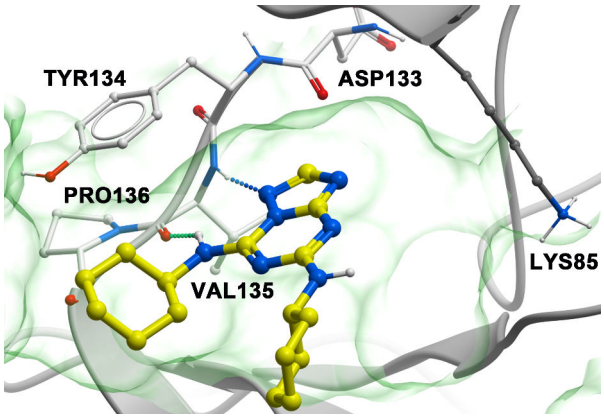

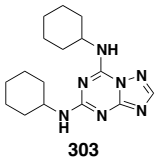

Figure 47. Bound conformation of compound **303** at the binding site of GSK-3β (PDB code: 1Q5K) as predicted by ligand docking simulations. The ligand is reported in yellow x-sticks. The key residues of the hinge region are reported in light grey x-sticks and labelled explicitly. A transparent green mesh describes the boundaries of the binding pocket. Hydrogen bond interactions are highlighted by dotted lines.

Concerning CK-1δ, a molecular docking investigation on derivative **335** showed interactions both with the hinge region and the phosphate-binding region of the ATP-binding cavity. In fact, derivative **335** makes a stabilizing interaction between its amino group at the 7-position and the sulfur of lateral chain of Met82 in the hinge region, while other hydrogen-bonding interactions have been detected between the carbonyl and amino group of the cyanoacrilamide moiety at the 2-position and the amino group of Lys38 and the carbonyl group of Asp149, respectively.

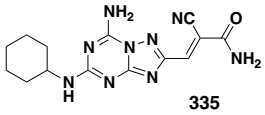

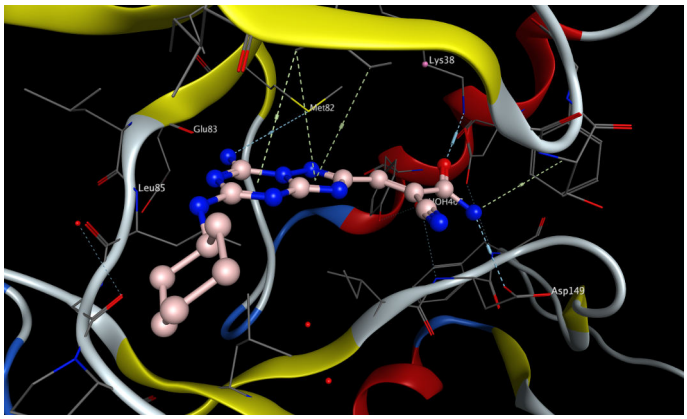

Figure 48. Compound **335** docked in the ATP-binding pocket of CK1-δ (PDB code: 4HNF). The hydrogen bonds formed between the ligand and the kinase cavity are depicted as light-blue dotted lines, while hydrophobic interactions as yellow dotted lines.

Moreover, hydrophobic interactions contribute to stabilize compound **335** in complex with CK-1δ. In particular, as reported in **Figure 48**, the two heteroaromatic cores and the amino group at the 2-position are involved in these kind of interactions.

It is worth noting how the orientation of compound **335** in the ATP-binding pocket is highly similar in both GSK-3β (**Figure 46**) and CK-1δ (Figure **48**).

5.2.4.2 Experimental kinetic studies

To experimentally confirm the binding-mode of compound **335** with GSK-3β and CK-1δ, kinetic experiments were performed on both kinases varying ATP and compound **335** concentrations, while the concentration of the substrates used in the phosphorylation reaction was kept constant. Each point is the mean of two different experiments, each one analysed in duplicate, using the ADP-Glo Kinase Assay.

Regarding CK-1δ, the intercept of the plot in the vertical axis ($1/V$) does not change, meaning that compound **335** acts as a competitive inhibitor of ATP binding towards CK-1δ (**Figure 49**).

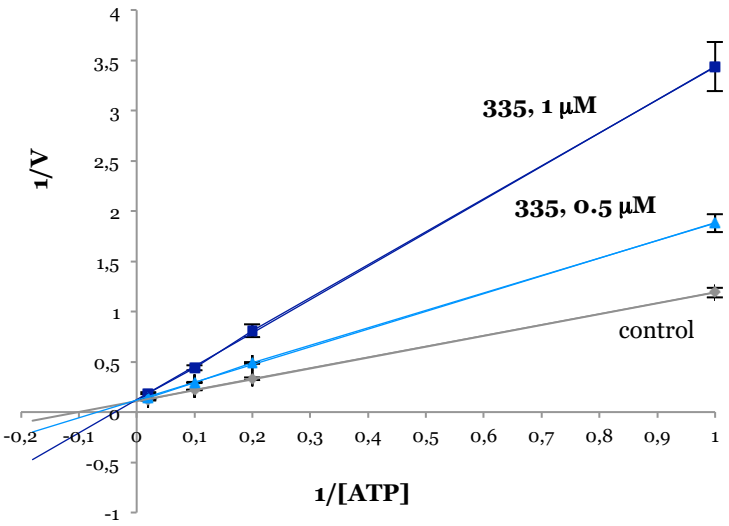

Figure 49.
ATP-competitivity study of compound **335** on CK-1δ.

On the other hand, double-reciprocal plotting of experimental data on GSK-3β, depicted in **Figure 50**, showed a mixed ATP-competitive/non-ATP-competitive behavior of **335**, in accordance to rationale underlying the design of this compound, which includes covalent interactions with GSK-3β. This could also provide an explanation for the discrete but not dramatic (as expected for a fully irreversible inhibitor) improvement of potency towards GSK-3β, and also reflects the attenuated reactivity showed in the HPLC-MS study with βME (Chapter 5.2.3).

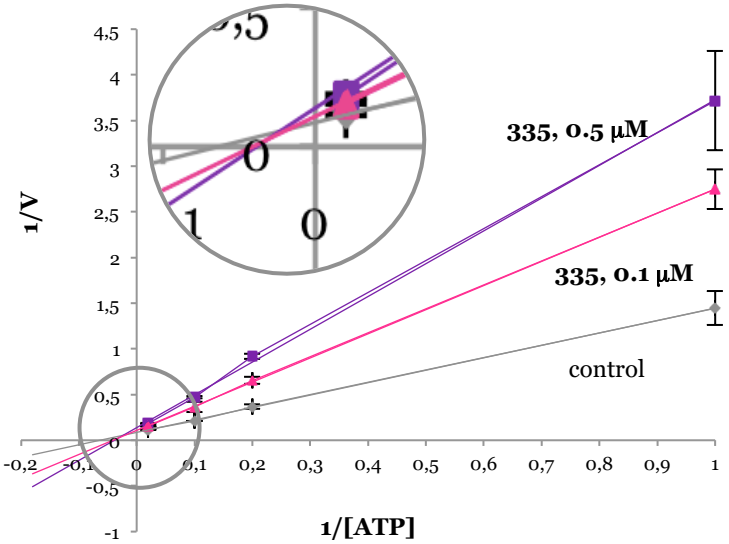

Figure 50.
ATP-competitivity study of compound **335** on GSK-3β.

Moreover, in order to study the binding reversibility of derivative **335** in respect to GSK-3β, kinetic assays were performed by determining the activity of the kinase after different times of incubation of the enzyme with the inhibitor. A covalent inhibitor is expected to show a time-dependent inhibition of the enzyme, with enzyme activity decreasing as a function of the time of exposure of the enzyme to the inhibitor. Hence, GSK-3β was pre-incubated for zero, five and ten minutes with derivative **335** at concentrations near to its IC_{50} value, and then enzymatic activity was evaluated. The results showed that the percentage of inhibition slightly increased with the inhibitor exposure time, confirming that a covalent but not fully irreversible interaction between compound **335** and GSK-3β took place (**Table 17**, **Figure 51**).

Table 17 and Figure 51. Time-dependent GSK-3β inhibition of derivative **335**.

Incubation time	% inhibition (GSK-3β)	% inhibition (GSK-3β)
	[335] = 0.5 μM	[335] = 0.1 μM
0	83.07 ±3.71	48.54 ±3.91
5	88.23 ±3.40	64.74 ±3.73
10	95.04 ±5.36	71.80 ±2.10

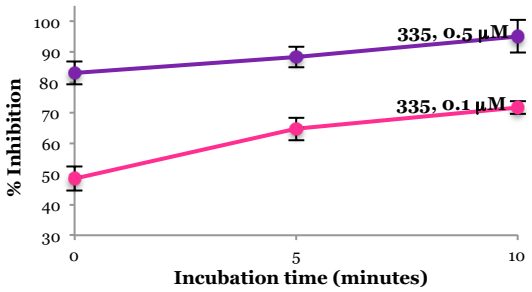

5.2.5 Biological evaluation in *in vitro* models of neurodegeneration

Since an abnormal increase in GSK-3β activity leads to an activation of the microglia followed by an increase in inflammation and neuronal death[263] and, similarly, CK-1δ contributes to exacerbate neurodegenerative disease progression,[58] we decided to study in different *in vitro* models the neuroprotective potential of GSK-3β/CK-1δ inhibition by **335** in collaboration with Dr. Teresa De Vita at Istituto Italiano di Tecnologia (Genova, IT).

These first evaluations were assessed in Parkinson's disease (PD) *in vitro* models, in presence of different neurotoxins (**Figure 52**), such as 4-phenyl-1-methyl-1,2,3,6-tetrahydropyridine (MPTP, **339**)[264] or 6-hydroxydopamine (6-OHDA, **341**).[265]

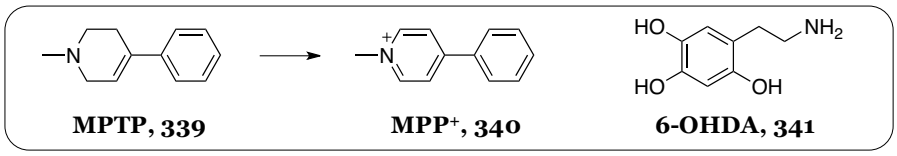

Figure 52. Neurotoxins commonly used in *in vitro* models of PD.

Both MPP+ (**340**), the toxic metabolite of MTPT (**339**), and 6-OHDA (**341**), hydroxylated analogue of dopamine, are thought to induce dopaminergic toxicity, and consequent parkinsonism by intra- and extracellular oxidation, hydrogen peroxide formation, and direct inhibition of the mitochondrial respiratory chain.[266,267] In the MPTP or 6-OHDA injury models, cell viability was measured in the presence of these neurotoxins, with or without treatment with lithium (as reference compound) and derivative **335**, using rat PC12 pheochromocytoma cells, an immortalized cell line with neuronal phenotypes. Before, compound **335** was proved not to be cytotoxic in this cell line after CellTiter-Glo® luminescent cell-viability assay (**Figure 53**), a method to determine the number of viable cells in culture based on quantitation of the ATP, a valid marker of metabolically active cells, by luciferase. On the contrary, in the same assay, MPP+ produced a significant and concentration-dependent neurotoxic effect in PC12 cell line (data not shown). The dose of 1.5 mM, which caused a 50% of cell death, was chosen for the subsequent neuroprotection studies. As depicted in **Figure 54**, two different assays were used to evaluate compound **335** in MPTP-model: the CellTiter-Glo® assay (panel A) and 3-(4,5-dimethythiazol-2-yl)-2,5-diphenyl tetrazolium bromide (MTT) methodology (panel B). This is a colorimetric assay that measures the reduction by mitochondrial succinate

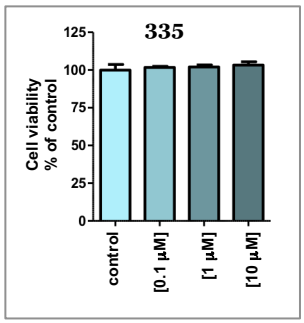

Figure 53. Cytotoxicity assay of compound **335**.

dehydrogenase of MTT (yellow) into formazan (dark purple). Since reduction of MTT can only occur in metabolically active cells, the level of mitochondrial activity is a measure of the viability of the cells.

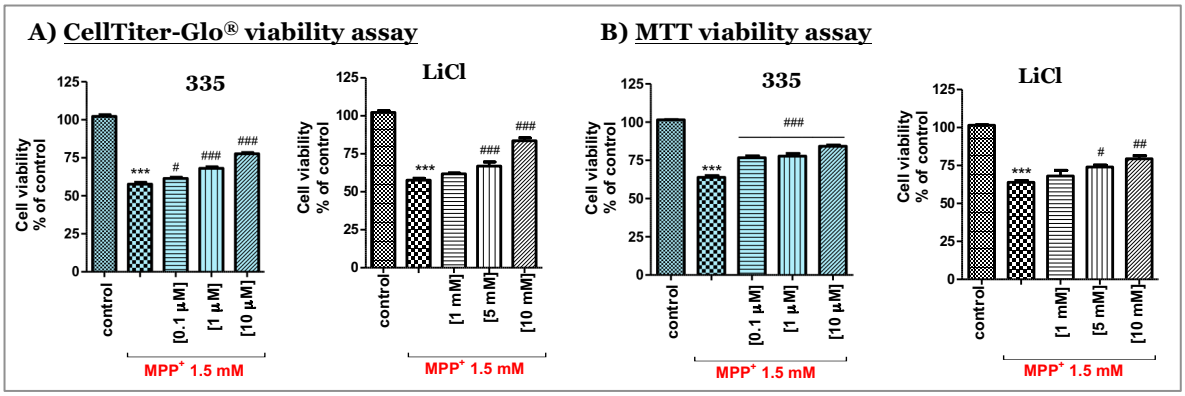

Figure 54. Neurotoxicity studies performed with compound **335** and LiCl (reference) in PC12 cells with [MPP+]=1.5 mM (***p<0.001 *vs* CTRL; #p<0.05 *vs* MPP+ 1.5 mM; ##p<0.01 *vs* MPP+ 1.5 mM; ###p<0.001 *vs* MPP+ 1.5 mM. Data were analyzed using one-way ANOVA followed by Turkey's Test).

In both assays, cells were pre-treated with increasing concentrations of compound **335** (0.1, 1, 10 µM) for 2 hours and then incubated with 1.5 mM of MPP+ for 24 hours. As we can observe, cell survival is diminished after treatment with MPP+ (second column of histograms); however, cells treated with the same dose of MPP+ and derivative **335** showed a dose-dependent increase in cell viability. These results are comparable to those obtained after treatment with lithium chloride (1, 5, 10 mM), a well-established neuroprotective agent, whose mechanisms of action also include GSK-3β inhibition.[268] Similarly, it was found that both compound **335** and lithium chloride prevent 6-OHDA-induced cell death in a concentration dependent manner (**Figure 55**).

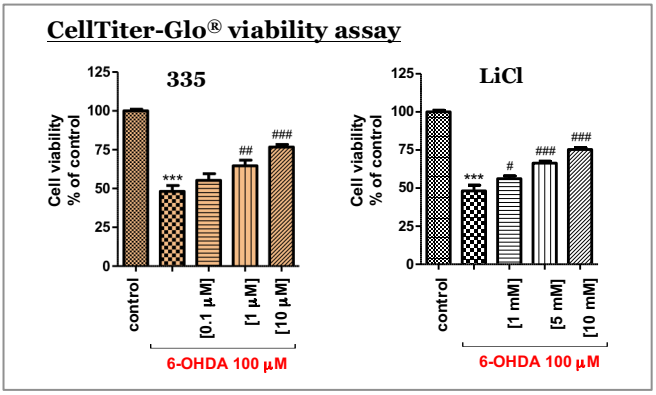

Figure 55. Neurotoxicity studies performed with compound **335** and LiCl (reference) in PC12 cells with [6-OHDA]=100 µM (5h-treatment; ***p<0.001 *vs* CTRL; #p<0.05 *vs* 6-OHDA 100µM; ##p<0.01 *vs* 6-OHDA 100µM; ###p<0.01 *vs* 6-OHDA 100 µM. Data were analyzed using one-way ANOVA followed by Turkey's Test).

Recent studies reported compelling evidences for a linkage between Wnt/β-catenin signalling and inflammatory events during PD progression.[254] In particular, β-catenin pathway is considered a pro-survival signalling cascade, since stabilized β-catenin regulates the expression of genes responsible of dopamine neurons survival/protection. It is widely recognized that kinase upregulation, including GSK-3β, leads to β-catenin degradation and increased neurons vulnerability, degeneration and death.[254,269] Therefore, we examined the effect in β-catenin expression of compound **335** in 6-OHDA-PD-model, using lithium chloride as reference compound as well. From these results, reported in **Figure 56**, we can infer that derivative **335**, albeit weakly in comparison to lithium, promotes β-catenin stabilization, thus restoring its neuroprotective potential in a PD-model.

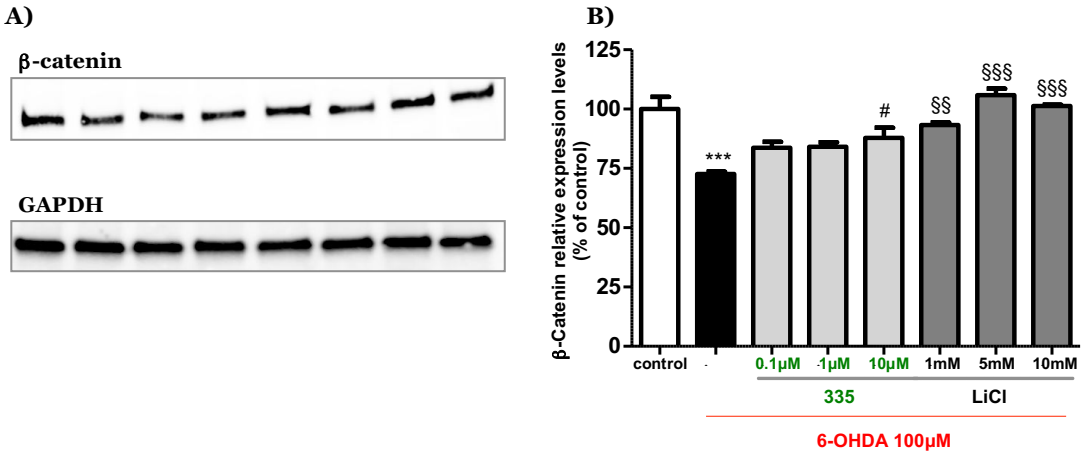

Figure 56. Effect of compound **335** and LiCl on expression of β-catenin. β-Catenin expression was analyzed (panel A) by Western Blotting. The relative intensity (panel B) of protein band was normalized to GAPDH by ImageJ Software. (***p<0.001 *vs* control; #p<0.05 *vs* 6-OHDA 100 μM; §§p<0.01 *vs* 6-OHDA 100 μM; §§§p<0.01 *vs* 6-OHDA 100 μM. Data were analyzed using one-way ANOVA followed by Turkey's Test).

In conclusion, all these experiments demonstrated that compound **335** is quite effective in protecting neuronal-like cells from the oxidative damage produced by MPTP/MPP^+ and 6-OHDA, therefore confirming that inhibition of GSK-3β and CK-1δ could be a valid therapeutic target for the treatment of neurodegenerative diseases, such as PD, and neuroinflammation-related disorders.

5.3 CONCLUSIONS

In the present part of the work, it was reported the synthesis and characterization of a new [1,2,4]triazolo[1,5-*a*][1,3,5]triazine derivative (**335**), designed to pursue a dual GSK-3β/CK-1δ inhibition. In particular, it presents at the 2-position of the TT scaffold an electrophile Michael-acceptor group aimed to covalently thus reversibly target the noncatalytic Cys199 residue of GSK-3β and, at the same time, to be able to establish noncovalent interactions within CK-1δ ATP-binding pocket. Specifically, the cyanoacrylamide group was chosen for its advantageous features, which include an increased yet intrinsically reversible reactivity in front of nucleophiles, a safer toxicity profile compared to disulfides, for example, and the presence of the amide group, a useful tool for optimizing the kinase affinity.[270]

Compound **335** showed a promising dual GSK-3β/CK-1δ inhibitory profile (IC_{50} values of 0.17 μM and 0.68 μM on GSK- 3β and CK-1δ, respectively), validating the rationale underlying this work. On the contrary, the dicyclohexyl derivative **336** and acrylonitriles derivatives (**337-338**) resulted nearly inactive towards both kinases.

The studies performed using HPLC-MS or UV-visible spectroscopy methodologies, in the presence of β-mercaptoethanol, provided a preliminary characterization of the behaviour of compound **335** in thiol addition reactions, confirming a moderate reactivity compatible with a covalent but reversible interaction. Furthermore, computer-aided and experimental studies helped in elucidating the binding modes of compound **335** to the kinases: in particular, it showed a mixed ATP-competitive/non-ATP-competitive behavior towards GSK-3β, also supported by a reversibility study that confirmed a time-dependent covalent inhibition of the kinase. Also molecular docking simulations validated the hypothesis of cooperation between covalent and noncovalent interactions within the kinase pocket, resulting in a high-affinity binding. In regard to CK-1δ, derivative **335** presents an ATP-competitive inhibitory mechanism, as easily conceivable due to its adenine-like structure.

Notably, we have also demonstrated neuroprotective effects of compound **335** in an *in vitro* model of dopaminergic cell death using rat PC12 cells, despite a borderline profile of CNS permeability. In fact, we showed that it attenuated MPTP/MPP^+- and 6-OHDA-induced neuronal cell death as measured by cell viability assays (MTT and CellTiter-Glo), also through Wnt/β-catenin pathway stabilization.

Considering all these findings, compound **335** could represent a valuable tool to further investigate the effects of a dual GSK-3β/CK-1δ inhibition as a neurodegenerative disease-modifying drug candidate.

5.4 EXPERIMENTAL SECTION

5.4.1 Chemistry

General material and methods used in the synthetic process are reported in Chapter 3.4.1.1.

5.4.1.1 Synthesis of compounds 302-306

5.4.1.1.1 Synthesis of [1,2,4]triazolo[1,5-*a*][1,3,5]triazine-5,7-diamine (302)

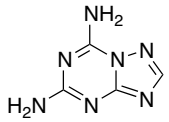

5,7-diphenoxy-[1,2,4]triazolo[1,5-*a*][1,3,5]triazine **165** (0.120 g, 0.39 mmol) was dissolved in methanol (3 mL) and 1.68 mL of methanolic ammonia 7 N (3.9 mmol) were added. The mixture was heated at 75°C in sealed tube for 12h. When the reaction was terminated, the white precipitate was filtered and washed with methanol. Yield 48.5% (29 mg); white solid; mp >300°C (EtOEt-light petroleum). ^{1}H NMR (400 MHz; DMSO-d_6): δ 8.29-7.89 (m, 3H), 6.91-6.78 (bs, 2H). ^{13}C NMR (101 MHz; DMSO-d_6): δ 163.1, 159.3, 154.6, 151.1. ES-MS (methanol/water) m/z: 151.9 $[M+H]^+$, 173.9 $[M+Na]^+$.

5.4.1.1.2 Synthesis of N^5-N^7-dicyclohexyl-[1,2,4]triazolo[1,5-*a*][1,3,5]triazine-5,7-amine (303)

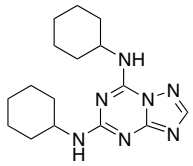

A mixture of of 5,7-diphenoxy-[1,2,4]triazolo[1,5-*a*][1,3,5]triazine **165** (0.120 g, 0.39 mmol) and cyclohexylamine (0.450 mL, 3.9 mmol) in absolute ethanol (3 mL) was poured into a sealed tube and heated at 95 °C for 12h. The solvent was removed in vacuo, and the crude product was purified by flash chromatography (EtOAc–light petroleum 6.5:3.5) to afford the final compound. Yield 64.5% (79 mg); white solid; mp 201-203°C (EtOEt-light petroleum); ^{1}H NMR (400 MHz; DMSO-d_6): δ 8.40 + 8.19 (d, J = 8.7 Hz, 1H), 8.03 + 8.01 (s, 1H), 7.37-7.31 (m, 1H), 4.00-3.79 (m, 1H), 3.79-3.60 (m, 1H), 2.01-1.39 (m, 12H), 1.38-1.00 (m, 8H). ^{13}C NMR (101 MHz; DMSO-d_6): δ 160.5, 159.2, 154.2, 148.3, 51.0+49.7, 32.9+32.7, 32.3, 25.7+25.49, 25.39+25.34. ES-MS (methanol) m/z: 316.1 $[M+H]^+$, 338.0 $[M+Na]^+$, 354.0 $[M+K]^+$.

5.4.1.1.3 Synthesis of compounds 304-306

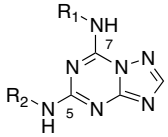

Compounds **304-306** were obtained according to **General Procedure (VI)** (Chapter 3.4.1.2.6).

R_1 = H (**304-305**), cC_6H_{11} (**306**)
R_2 = H (**306**), cC_6H_{11} (**304**), CH_2Ph (**305**)

N^5-cyclohexyl-[1,2,4]triazolo[1,5-*a*][1,3,5]triazin-5,7-diamine (**304**)

Flash chromatography eluent: EtOAc-light petroleum 5.5:4.5. Yield 34% (24 mg); white solid; mp 223°C (EtOEt-light petroleum); ^{1}H NMR (400 MHz, DMSO-d_6) δ: 8.33-7.99 (m, 3H), 7.27 + 7.20 (d, J = 8.0 Hz, 1H), 3.76-3.65 (m, 1H), 1.83-1.55 (m, 5H), 1.31-1.06 (m, 5H). ^{13}C NMR (101 MHz; DMSO-d_6): δ 160.7, 159.3, 154.5, 150.5, 49.7, 32.7, 25.3. ES-MS (acetonitrile) m/z: 234.5 $[M+H]^{+,}$ 256.5 $[M+Na]^+$, 272.4 $[M+K]^+$.

*N*5-benzyl-[1,2,4]triazolo[1,5-*a*][1,3,5]triazin-5,7-diamine (**305**)

Flash chromatography eluent: EtOAc-light petroleum 6:4. Yield 46% (33 mg); white solid; mp 263-267°C (EtOEt-light petroleum); ^{1}H NMR (400 MHz, DMSO-d_6) δ: 8.53-7.98 (m, 3H), 7.93-7.82 (m, 1H), 7.44-7.07 (m, 5H), 4.54-4.43 (m, 2H). ^{13}C NMR (101 MHz; DMSO-d_6): δ 161.7, 159.2, 154.5, 150.7, 140.4, 128.6, 127.4, 127.0, 44.2. ES-MS (methanol) m/z: 242.5 $[M+H]^+$, 264.4 $[M+Na]^+$.

*N*7-cyclohexyl-[1,2,4]triazolo[1,5-*a*][1,3,5]triazine-5,7-diamine (**306**)

Flash chromatography eluent: EtOAc-light petroleum 7:3. Yield 40% (28 mg); white solid; mp 225°C (EtOEt-light petroleum); ^{1}H NMR (400 MHz; DMSO-d_6): δ 8.23 (d, J = 8.5 Hz, 1H), 8.01 (s, 1H), 6.89 (s, 2H), 3.91-3.87 (m, 1H), 1.81-1.69 (m, 3H), 1.59-1.38 (m, 3H), 1.28-1.03 (m, 4H). ^{13}C NMR (101 MHz; DMSO-d_6): δ 163.0, 159.1, 154.2, 148.7, 49.9, 32.2, 25.36, 25.29. ES-MS (methanol) m/z: 234.0 $[M+H]^+$, 255.9 $[M+Na]^+$, 271.9 $[M+K]^+$.

5.4.1.2 Synthesis of compound 311

5.4.1.2.1 Synthesis of 5-(methylthio)-[1,2,4]triazolo[1,5-*a*][1,3,5]triazin-7-amine (309)[214]

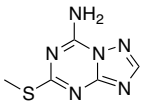

3-Amino-1,2,4-triazole **307** (1.0 g, 11.89 mmol) and dimethyl-*N*-cyanodithioiminocarbonate **308** (1.913 g, 13.08 mol) were mixed in a three-neck round bottom flask and stirred at 170°C in a stream of argon until the two powders melted (1h). The reaction mixture was then cooled and refluxed in a mixture of DCM and methanol for 1 hour. The solvent was removed under reduced pressure and the resulting solid was dissolved in ethyl ether (500 mL) and washed with water (5x150 mL). Yield 21% (0.455 g); white solid; mp 261-263°C (EtOEt); ^{1}H NMR (270 MHz; DMF-d_7): δ 9.06 (s, 1H), 8.81 (s, 1H), 8.40 (s, 1H), 2.55 (s, 3H). ^{13}C NMR (101 MHz; DMSO-d_6): δ 173.5, 157.2, 155.0, 150.2, 14.0. ES-MS (methanol/water) m/z: 182.9 $[M+H]^+$, 204.8 $[M+Na]^+$, 220.8 $[M+K]^+$.

5.4.1.2.2 Synthesis of 5-methylsulfinyl-[1,2,4]triazolo[1,5-*a*][1,3,5]triazin-7-amine (310)[214]

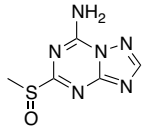

A solution of *meta*-chloroperoxybenzoic acid (*m*-CPBA)(1.1562 g, 6.6 mmol) in 10 ml of DCM was added dropwise to a cooled suspension of **309** (0.4 g, 2.2 mmol) in 15 ml of DCM. The resulting mixture was stirred overnight, the solvent was evaporated and ethanol was added to the residue. The solid was collected by filtration, washed with cool ethanol, and dried. Yield 58% (0.253 g); white solid; mp 232-235°C (lit. 238-240°C); ^{1}H NMR (270 MHz; DMSO-d_6): δ 9.59 + 9.23 (bs, 2H), 8.60 (s, 1H), 2.87 (s, 3H). ES-MS (methanol/acetonitrile) m/z: 220.8 $[M+Na]^+$, 236.8 $[M+K]^+$.

5.4.1.2.3 Synthesis of *N*5-phenyl-[1,2,4]triazolo[1,5-*a*][1,3,5]triazin-5,7-diamine (311)[271]

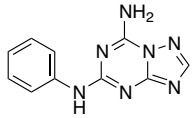

To 0.260 g (1.31 mmol) of compound **310** suspended in acetonitrile, aniline (0.884 mL, 10.48 mmol) was added. The mixture was heated in a sealed tube at 80°C overnight for 48h. The solvent was then removed under reduced pressure and the residue was purified by flash chromatography (DCM-MeOH 95:5). Yield 47% (140 mg); white solid; mp 286°C (EtOEt-light petroleum). ^{1}H

NMR (400 MHz; DMSO-d_6): δ 9.60 (s, 1H), 8.35 (bs, 2H), 8.17 (s, 1H), 7.76 (d, J = 7.7 Hz, 2H), 7.28 (t, J = 8.0 Hz, 2H), 7.00-6.96 (m, 1H). ^{13}C NMR (101 MHz; DMSO-d_6): δ 159.5, 158.7, 155.0, 151.0, 140.2, 128.8, 122.7, 120.4. ES-MS (methanol/acetonitrile) m/z: 228.0 $[M+H]^+$, 249.9 $[M+Na]^+$, 265.9 $[M+K]^+$.

5.4.1.3 Synthesis of compounds 325-326, 329-330

5.4.1.3.1 Synthesis of ethyl 3-cyano-benzoate (313)

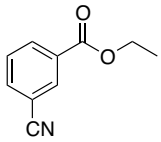

Concentrated H_2SO_4 (0.5 mL) was added dropwise to a solution of 3-cyanobenzoic acid **312** (10 g, 68 mmol) in absolute ethanol (500 mL), and the reaction mixture was refluxed for 12 h. Solvent was removed and the residue dissolved in EtOAc (300 mL) and washed with saturated $NaHCO_3$ solution and water 1:1 (3 x 100 mL). The reunited organic phases were anhydrified upon anhydrous Na_2SO_4, filtered, the solvent removed and the resulting ethyl ester derivative used without any further purification. Quantitative yield (11.7 g); white solid; mp 55-56°C (EtOEt-light petroleum); ^{1}H NMR (400 MHz, $CDCl_3$): δ 8.33-8.32 (m, 1H), 8.27 (dt, J = 7.8, 1.4 Hz, 1H), 7.83 (dt, J = 7.8, 1.4 Hz, 1H), 7.58 (t, J = 7.8 Hz, 1H), 4.41 (q, J = 7.1 Hz, 2H), 1.41 (t, J = 7.1 Hz, 3H). ES-MS (methanol) m/z: 148.0 $[M+H-(CH_2CH_3)]^+$ 176.0 $[M+H]^+$, 198.0 $[M+Na]^+$.

5.4.1.3.2 Synthesis of 3-cyano-benzohydrazide (314)

Compound **314** was prepared following the **General procedure (I)** (Chapter 3.4.1.2.1).

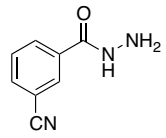

Flash chromatography eluent: EtOAc. Yield 60% (9.7 g); pale pink solid; mp 171-174°C (EtOEt-light petroleum); ^{1}H NMR (400 MHz, DMSO-d_6) δ: 9.96 (s, 1H), 8.19-8.09 (m, 2H), 7.97 (dt, J = 7.8, 1.4 Hz, 1H), 7.67 (t, J = 7.8 Hz, 1H), 4.56 (s, 2H). ES-MS (methanol) m/z: 162.0 $[M+H]^+$.

5.4.1.3.3 Synthesis of 3-cyano-*N*'-(4,6-diphenoxy-1,3,5-triazin-2-yl)benzohydrazide (315)

Compound **315** was prepared following the **General procedure (II)** (Chapter 3.4.1.2.2).

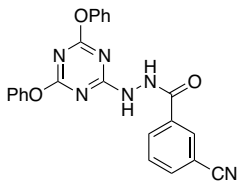

Flash chromatography eluent: DCM-MeOH 99:1. Yield 56.5% (6.7 g); white solid; mp 213-215°C (EtOEt-light petroleum); ^{1}H NMR (400 MHz, DMSO-d_6) δ: 10.57 (bs, 1H), 10.15 (bs, 1H), 8.05-7.96 (m, 3H), 7.69 (m, 1H), 7.45-7.41 (m, 2H), 7.28-7.08 (m, 8H). ES-MS (methanol) m/z: 425.1 $[M+H]^+$, 447.1 $[M+Na]^+$.

5.4.1.3.4 Synthesis of 3-(5,7-diphenoxy-[1,2,4]triazolo[1,5-*a*][1,3,5]triazin-2-yl)benzonitrile (323)

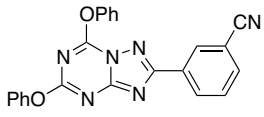

321

Compound **321** was prepared following the **General procedure (III$_b$)** (Chapter 3.4.1.2.3), but readily used in the next step without purification due to stability problems.

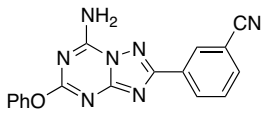

323

Compound **323** was prepared following the **General procedure (IV)** (Chapter 3.4.1.2.3).

Overall yield 19% (125 mg); white solid; mp 295-297°C (EtOEt-light

petroleum); ^{1}H NMR (400 MHz, DMSO-d_6) δ: 9.18 + 8.80 (bs, 2H), 8.41-8.37 (m, 2H), 8.01-7.96 (m, 1H), 7.76 (t, J = 7.8 Hz, 1H), 7.45 (t, J = 7.8 Hz, 2H), 7.29-7.23 (m, 3H). ^{13}C NMR (101 MHz; DMSO-d_6): δ 165.4, 162.4, 159.7, 152.8, 152.5, 134.4, 131.9, 131.5, 130.9, 130.4, 130.0, 125.9, 122.2, 118.7, 112.6. ES-MS (methanol) m/z: 330.1 $[M+H]^+$, 352.1 $[M+Na]^+$.

5.4.1.3.5 Synthesis of compounds 325 and 326

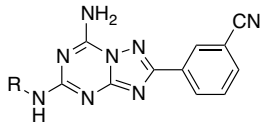

R = cC_6H_{11} (**325**), CH_2Ph (**326**)

Compounds **325-326** were obtained according to **General Procedure (VI)** (Chapter 3.4.1.2.6).

3-(7-amino-5-(cyclohexylamino)-[1,2,4]triazolo[1,5-*a*][1,3,5]triazin-2-yl)benzonitrile (**325**)

Flash chromatography eluent: DCM-MeOH 98:2. Yield 47.5% (0.476 g); white solid; mp 297-299°C (EtOEt-light petroleum); ^{1}H NMR (400 MHz, DMSO-d_6) δ: 8.62-8.29 (m, 2H), 8.29-7.85 (m, 3H), 7.82-7.65 (m, 1H), 7.48-7.29 (m, 1H), 3.82-3.63 (m, 1H), 1.96-1.50 (m, 5H), 1.37-1.01 (m, 5H). ^{13}C NMR (101 MHz; DMSO-d_6): δ 161.2, 160.7, 160.1, 150.4, 133.9, 132.6, 131.3, 130.7, 130.2, 118.8, 112.4, 49.9, 32.7, 25.3. ES-MS (methanol) m/z: 335.2 $[M+H]^+$, 357.2 $[M+Na]^+$.

3-(7-amino-5-(benzylamino)-[1,2,4]triazolo[1,5-*a*][1,3,5]triazin-2-yl)benzonitrile (**326**)

Flash chromatography eluent: DCM-MeOH 98:2. Yield 54% (0.555 g); white solid; mp 288-289°C (EtOEt-light petroleum); ^{1}H NMR (400 MHz, DMSO-d_6) δ: 8.62-7.87 (m, 6H), 7.77-7.70 (m, 1H), 7.36-7.26 (m, 4H), 7.26-7.18 (m, 1H), 4.56-4.45 (m, 2H). ^{13}C NMR (101 MHz; DMSO-d_6): δ 161.7, 161.3, 160.0, 150.6, 140.3, 133.9, 132.5, 131.4, 130.7, 130.3, 128.6, 127.5, 127.0, 118.8, 112.4, 44.3. ES-MS (methanol) m/z: 341.0 $[M-H]^-$.

5.4.1.3.6 Synthesis of compounds 329 and 330

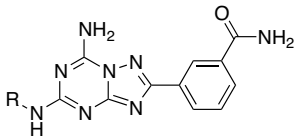

R = cC_6H_{11} (**329**)
CH_2Ph (**330**)

A solution of 0.2 mmol of nitrile derivatives (**325-326**) in 375 μL mixture of TFA-H_2SO_4 (4:1, v/v) was stirred at 70°C for three hours. Once completed, the reaction was quenched with 2 mL of ice-cold water. The precipitate was filtered and washed with cold water and methanol.

3-(7-amino-5-(cyclohexylamino)-[1,2,4]triazolo[1,5-*a*][1,3,5]triazin-2-yl)benzamide (**329**)

Yield 59% (41 mg); white solid; mp 266-268°C; ^{1}H NMR (400 MHz, DMSO-d_6) δ: 8.72-8.57 (m, 1H), 8.45-7.94 (m, 5H), 7.79-7.41 (m, 3H), 3.81-3.67 (m, 1H), 1.92-1.54 (m, 5H), 1.36-1.04 (m, 5H). ^{13}C NMR (101 MHz; DMSO-d_6): δ 184.7, 167.8, 165.6, 164.2, 160.5, 160.1, 158.4, 136.8, 135.5, 129.3, 126.7, 50.3+50.1, 32.8+32.6, 25.5+25.3. ES-MS (methanol) m/z: 353.2 $[M+H]^+$.

3-(7-amino-5-(benzylamino)-[1,2,4]triazolo[1,5-*a*][1,3,5]triazin-2-yl)benzamide (**330**)

Yield 59% (42 mg); white solid; mp 249-252°C; ^{1}H NMR (400 MHz, DMSO-d_6) δ: 8.81-7.87 (m, 7H), 7.64-7.13 (m, 7H), 4.58-4.45 (m, 2H). ^{13}C NMR (101 MHz; DMSO-d_6): δ 186.7, 167.9, 167.1, 161.7, 150.5, 140.1, 138.5, 135.5, 129.77, 129.62, 129.2, 128.7, 127.5, 127.1, 126.7, 44.3. ES-MS (methanol) m/z: 361.2 $[M+H]^+$.

5.4.1.4 Synthesis of compounds 335-338

5.4.1.4.1 Synthesis of benzyloxy acetic acid (318) [272]

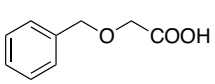

A solution of benzyl alcohol (21.6 g, 0.2 mol) in dry toluene (40 mL) was added at 0 °C to a stirred suspension of NaH (16.0 g, 60% dispersion in mineral oil, 0.4 mol) in dry toluene (100 mL). After mixing for 1 hour at room temperature, a solution of chloroacetic acid (27.8 g, 0.2 mol) in dry toluene (100 mL) was added. The resulting slurry was stirred at room temperature for 1 hour and then at 80°C for 2 hours. After cooling at room temperature, 300 mL of water were added and the mixture was washed with diethyl ether (3 x 100 mL). The aqueous layer was acidified with concentrated HCl (23 mL) to pH 2 and extracted repeatedly with DCM (3 x 100 mL). The combined organic extracts were dried over anhydrous sodium sulphate, the solvent was evaporated to give the crude product as pale yellow oil (yield 65%, 24.6 g). ^{1}H NMR (270 MHz; $CDCl_3$): δ 10.17 (bs, 1H), 7.31-7.18 (m, 5H), 4.53 (s, 2H), 4.02 (s, 2H). MS (methanol) m/z: 189.0 $[M+Na]^+$.

5.4.1.4.2 Synthesis of benzyloxyacetyl chloride (319)

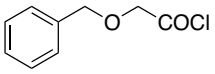

Benzyloxyacetic acid (5.19 g, 30.8 mmol) was dissolved in DCM (50 mL) and oxalyl chloride (3.39 mL, 40.0 mmol) was added at room temperature. The solution was stirred for 4 h under reflux then the solvent was removed by evaporation under reduced pressure to give the desired product, which was weighted and readily used in the next step without purification.

5.4.1.4.3 Synthesis of 2-(benzyloxy)-*N*'-(4,6-diphenoxy-1,3,5-triazin-2-yl)acetohydrazide (320)

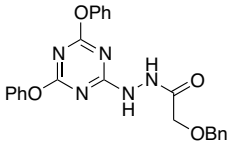

To a solution of (4,6-diphenoxy-[1,3,5]triazin-2-yl)-hydrazine (**160**, 7.0 g, 23.7 mmol) and triethylamine (23.7 mmol) in dry DCM (80 mL), benzyloxyacetyl chloride was added dropwise (30.8 mmol) and the mixture was stirred for 12h at room temperature. The solvent was removed under vacuum and the crude residue purified by flash chromatography (light petroleum-EtOAc 6.5:3.5) to afford the desired compound. Yeld 55% (5.8 g); white solid; mp 147°C (EtOEt-light petroleum); ^{1}H NMR (270 MHz, DMSO-d_6) δ: 9.94-9.87 (m, 2H), 7.48-7.15 (m, 15H), 4.48 (s, 2H), 3.92 (s, 2H). ES-MS (methanol) m/z: 444.0 $[M+H]^+$, 465.9 $[M+Na]^+$, 481.9 $[M+K]^+$.

5.4.1.4.4 Synthesis of 2-((benzyloxy)methyl)-5,7-diphenoxy-[1,2,4]triazolo[1,5-*a*][1,3,5]triazine (322)

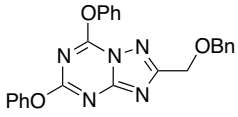

Compound **322** was prepared from compound **320** following the **General procedure (III_a)** (Chapter 3.4.1.2.3). Due to stability problems, the crude was roughly purified on silica plug (3-4 cm length) in light petroleum-EtOAc 7:3 and readily used in the next step.

5.4.1.4.5 Synthesis of 2-((benzyloxy)methyl)-5-phenoxy-[1,2,4]triazolo[1,5-*a*][1,3,5]triazin-7-amine (324)

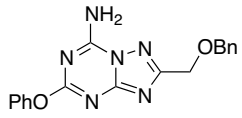

Compound **324** was obtained from compound **322** according to **General Procedure (IV)** (Chapter 3.4.1.2.4).

Flash chromatography eluent: EtOAc-light petroleum 7:3. Overall yield 30% (1.57 g); white solid; mp 113-114°C (EtOEt-light petroleum); ^{1}H NMR (400 MHz, DMSO-d_6): δ 9.09 (bs, 1H), 8.85 (bs, 1H), 7.45 (t, J = 7.9 Hz, 2H), 7.36 (d, J = 4.2 Hz, 4H), 7.33-7.21 (m, 4H), 4.60 (s, 4H). ^{13}C NMR (101 MHz, DMSO-d_6): δ 165.3, 164.7, 159.3, 152.9, 152.4, 138.3, 130.0, 128.7, 128.22, 128.03, 125.8, 122.2, 72.2, 65.5. ES-MS (methanol) m/z: 348.9 $[M+H]^+$, 370.8 $[M+Na]^+$, 386.8 $[M+K]^+$.

5.4.1.4.6 Synthesis of 2-((benzyloxy)methyl)-*N*^{5}-cyclohexyl-[1,2,4]triazolo[1,5-*a*][1,3,5]triazine-5,7-diamine (327)

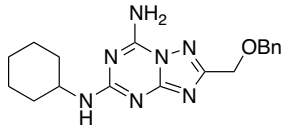

Compound **327** was obtained from compound **324** according to **General Procedure (VI)** (Chapter 3.4.1.2.6).

Flash chromatography eluent: EtOAc-light petroleum 1:1. Yield 49% (52 mg); mp 96-98°C. ^{1}H NMR (400 MHz, DMSO-d_6): δ 8.32-7.91 (m, 2H), 7.36-7.19 (m, 6H), 4.56 (s, 2H), 4.47 (s, 2H), 3.76-3.65 (m, 1H), 1.87-1.52 (m, 5H), 1.33-1.03 (m, 5H). ^{13}C NMR (101 MHz, DMSO-d_6): δ 178.2, 163.4, 159.7, 150.4, 138.4, 128.7, 128.2, 128.0, 72.1, 65.7, 49.7, 32.7, 25.8, 25.3. ES-MS (methanol) m/z: 354.2 $[M+H]^+$, 376.2 $[M+Na]^+$.

5.4.1.4.7 Synthesis of 2-((benzyloxy)methyl)-*N*^{5}-*N*^{7}-dicyclohexyl-[1,2,4]triazolo[1,5-*a*][1,3,5]triazine-5,7-amine (328)

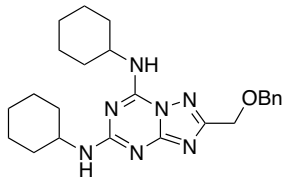

A mixture of 2-((benzyloxy)methyl)-5,7-diphenoxy-[1,2,4]triazolo[1,5-*a*][1,3,5]triazine (**322**) and a large excess of cyclohexylamine (5 mL) in absolute ethanol (40 mL) was poured into a sealed tube and heated at 95 °C for 24 h. The solvent was removed under vacuum, and the crude product was purified by flash chromatography (EtOAc–light petroleum 4:6) to afford the final compound as sticky foam. Overall yield 12.5% (82 mg). ^{1}H NMR (400 MHz): δ 8.49 + 8.26 (d, J = 8.7 Hz, 1H), 7.46-7.28 (m, 6H), 4.59 (s, 2H), 4.51 (s, 2H), 3.96-3.65 (m, 2H), 1.90-1.42 (m, 12H), 1.35-1.04 (m, 8H). ^{13}C NMR (101 MHz, DMSO-d_6): δ 160.0, 159.2, 153.6, 151.6, 147.7, 128.2, 127.70, 127.52, 71.6, 65.2, 49.3, 32.9, 31.8, 25.7+25.6, 25.3. ES-MS (methanol) m/z: 436.2 $[M+H]^+$, 458.3 $[M+Na]^+$.

5.4.1.4.8 Synthesis of compounds 331-332

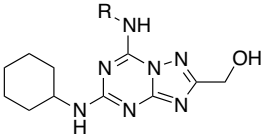

R = H (**331**), cC_6H_{11} (**332**)

Compounds **331-332** were obtained from compounds **327-328** according to **General Procedure (XIII)** (Chapter 4.4.4.1.5).

(7-amino-5-(cyclohexylamino)-[1,2,4]triazolo[1,5-*a*][1,3,5]triazin-2-yl)methanol (**331**)

Yield 72% (38 mg); white solid; mp 177-180°C (EtOEt-light petroleum); ^{1}H NMR (400 MHz, DMSO-d_6): δ 8.39-7.83 (m, 2H), 7.37-7.17 (m, 1H), 5.36-5.29 (m, 1H), 4.53-4.39 (m, 2H), 3.77-3.66 (m, 1H), 1.95-1.52 (m, 5H), 1.39-1.03 (m, 5H). ^{13}C NMR (101 MHz, DMSO-d_6): δ 166.5, 160.6, 159.7, 150.4, 58.0, 49.7+49.0, 33.1+32.7, 25.7+25.3. ES-MS (methanol) m/z: 264.1 $[M+H]^+$, 286.1 $[M+Na]^+$, 302.0 $[M+K]^+$.

(5,7-bis(cyclohexylamino)-[1,2,4]triazolo[1,5-*a*][1,3,5]triazin-2-yl)methanol (**332**)

Flash chromatography eluent: DCM-MeOH 95:5. Yeld 62% (43 mg); white solid; 165-167°C (EtOEt-light petroleum). ^{1}H NMR (400 MHz): δ 8.42 + 8.19 (d, J = 8.4 Hz, 1H), 7.44 + 7.34 (d, J = 7.7 Hz, 1H), 5.39-5.28 (m, 1H), 4.44 (d, J = 4.6 Hz, 2H), 3.97-3.79 (m, 1H), 3.76-3.61 (m, 1H), 1.95-1.36 (m, 12H), 1.36-1.00 (m, 8H). ^{13}C NMR (101 MHz, DMSO-d_6): δ 166.3, 163.3, 160.4, 148.2, 58.0, 49.76, 49.68, 32.9+32.7, 32.3+32.0, 25.7+25.51, 25.38+25.33. ES-MS (methanol) m/z: 346.5 $[M+H]^+$, 368.4 $[M+Na]^+$.

5.4.1.4.9 Synthesis of compounds 333-334[273]

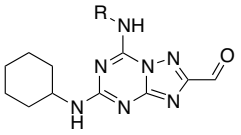

R = H (**333**), cC_6H_{11} (**334**)

A solution of 1 mmol of alcohol **331-332** in 15 mL of DCM at 0°C was oxidised at room temperature with 1.5 mmol of Dess-Martin reagent. After 3 hours of stirring, the reaction mixture was diluted with DCM (20 mL) and washed with a 1:1 solution of saturated sodium thiosulfate and saturated sodium bicarbonate to destroy the excess of Dess-Martin periodinane (3 x 10 mL). The organic phase was then dried over anhydrous sodium sulfate, the solvents removed under reduced pressure and the residue purified by flash chromatography.

7-amino-5-(cyclohexylamino)-[1,2,4]triazolo[1,5-*a*][1,3,5]triazine-2-carbaldehyde (**333**)

Flash chromatography eluent: EtOAc- MeOH 95:5. Yeld 68% (0.178 g); white solid; mp 153-156°C (EtOEt-light petroleum); ^{1}H NMR (500 MHz, DMSO-d_6): δ 9.91 (s, 1H), 8.68-8.22 (m, 2H), 7.63 + 7.51 (d, J = 8.0 Hz, 1H), 3.82-3.63 (m, 1H), 2.03-1.42 (m, 5H), 1.41-1.04 (m, 5H). ES-MS (methanol) m/z: 262.1 $[M+H]^+$, 284.0 $[M+Na]^+$.

5,7-bis(cyclohexylamino)-[1,2,4]triazolo[1,5-*a*][1,3,5]triazine-2-carbaldehyde (**334**)

Flash chromatography eluent: DCM-MeOH 95:5. Yeld 73% (0.251 g); white solid; mp 133-135°C (EtOEt-light petroleum); ^{1}H NMR (400 MHz, DMSO-d_6): δ 9.92 (s, 1H), 8.92 + 8.68 (d, J = 8.0 Hz, 1H), 7.74 + 7.66 (d, J = 7.8 Hz, 1H), 4.01-3.83 (m, 1H), 3.78-3.64 (m, 1H), 1.92-1.45 (m, 12H), 1.36-1.06 (m, 8H). ES-MS (methanol) m/z: 376.5 $[M+Na]^+$.

5.4.1.4.10 Synthesis of compounds 335-336[255]

R = H (**335**), cC_6H_{11} (**336**)

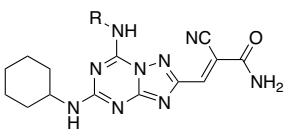

To a solution of aldehyde **333-334** (0.4 mmol) in DCM (5 ml), DBU (4.8 mmol) and 2-cyanoacetamide (4.8 mmol) were added. The reaction was stirred at room temperature until all the starting material had been consumed. Then the organic phase was dried over anhydrous sodium sulphate, the solvent was removed under reduced pressure and the residue was purified by flash column chromatography to give the desired products.

3-(7-amino-5-(cyclohexylamino)-[1,2,4]triazolo[1,5-*a*][1,3,5]triazin-2-yl)-2-cyanoacrylamide (**335**)

Flash chromatography eluent: DCM-MeOH 96:4. Yeld 14% (18 mg); yellow solid; mp 218-221°C (EtOEt-light petroleum); ^{1}H NMR (400 MHz, DMSO-d_6): δ 8.64-7.87 (m, 4H), 7.86-7.79 (m, 1H), 7.55-7.48 (m, 1H), 3.82-3.72 (m, 1H), 1.96-1.53 (m, 5H), 1.44-1.04 (m, 5H). ^{13}C NMR (68 MHz, DMSO-d_6): δ 162.4, 160.6, 159.5, 158.3, 150.1, 138.9, 115.1, 112.8, 50.1+49.4, 32.6+32.3, 25.3+24.9. ES-MS (methanol) m/z: 328.1 $[M+H]^+$, 350.1 $[M+Na]^+$, 366.0 $[M+K]^+$.

3-(5,7-bis(cyclohexylamino)-[1,2,4]triazolo[1,5-*a*][1,3,5]triazin-2-yl)-2-cyanoacrylamide (**336**)

Flash chromatography eluent: DCM-MeOH 99:1. Yield 8% (13 mg); pale yellow solid; mp 199-204°C (EtOEt-light petroleum); ^{1}H NMR (400 MHz, DMSO-d_6): δ 8.65-8.40 (m, 1H), 8.10-7.89 (m, 2H), 7.84-7.77 (m, 1H), 7.67-7.59 (m, 1H), 4.00-3.84 (m, 1H), 3.84-3.67 (m, 1H), 1.99-1.42 (m, 12H), 1.41-1.04 (m, 8H). ^{13}C NMR (68 MHz, DMSO-d_6): δ 161.9, 160.1, 159.1, 157.9, 147.5, 138.5, 114.8, 112.3, 49.59, 49.49, 32.4+32.3, 31.7, 25.3+25.04, 24.87. ES-MS (methanol) m/z: 410.3 $[M+H]^+$, 432.3 $[M+Na]^+$.

5.4.1.4.11 Synthesis of (cyanomethylene)triphenylphosphorane (342) [274]

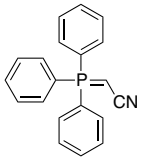

Triphenylphosphine (6.55 g, 0.025 mol) and chloroacetonitrile (1.9 g, 0.025 mol) were dissolved in ethyl acetate (5 mL) and the mixture was heated under reflux for 90 min. The resulting precipitate was filtered off and washed with diethyl ether to afford (cyanomethyl)triphenylphosphonium chloride as colorless crystals, that were suspended in DCM (40 mL) and stirred while triethylamine (2.5 equiv) was added over 15 min. The mixture was stirred for further 30 minutes and then washed thoroughly with water (3 x 10 mL), dried, and evaporated to give the ylide **342** as a white solid. Yield 10% (0.753 g); mp 195-196°C (EtOEt-light petroleum); ^{1}H NMR (400 MHz, DMSO-d_6): δ 7.74-7.56 (m, 15H), 1.73-1.71 (m, 1H). ES-MS (methanol) m/z: 302.1 $[M+H]^+$.

5.4.1.4.12 Synthesis of 3-(7-amino-5-(cyclohexylamino)-[1,2,4]triazolo[1,5-*a*][1,3,5]triazin-2-yl)acrylonitrile derivatives (337-338)

To a solution of aldehyde **333** (0.100 mg, 0.38 mmol) in DCM (10 mL) 0.458 g of (triphenylphosphoranylidine)acetonitrile **342** (1.52 mmol) were added and the reaction mixture was stirred at room temperature. After 5 hours the reaction was complete and the crude mixture, after concentration, was adsorbed on silica and purified by flash chromatography to yield the two isomers of the acrylonitrile derivative.

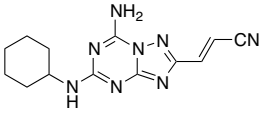

Isomer E (**337**) - Flash chromatography eluent: EtOAc-light petroleum 1:1. Yeld 27.5% (30 mg); white solid; mp 247-249°C (EtOEt-light petroleum). ^{1}H NMR (400 MHz; DMSO-d_6): δ 8.52-8.05 (m, 2H), 7.57-7.42 (m, 2H), 6.62 (d, J = 16.2 Hz, 1H), 3.79-3.61 (m, 1H), 1.91-1.55 (m, 5H), 1.35-1.05 (m, 5H). ^{13}C NMR (68 MHz, DMSO-d_6): δ 160.2, 159.3, 158.9, 149.9, 140.01, 117.7, 104.1, 49.7+49.5, 32.5+32.2, 25.3+24.8. ES-MS (methanol) m/z: 285.1 [M+H]+, 307.1 [M+Na]+.

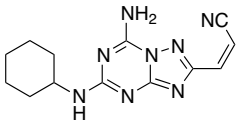

Isomer Z (**338**) - Flash chromatography eluent: EtOAc-light petroleum 1:1 to 7:3. Yeld 27% (30 mg); white solid; mp 197-200°C (EtOEt-light petroleum). ^{1}H NMR (400 MHz; DMSO-d_6): δ 8.58-7.96 (m, 2H), 7.52-7.41 (m, 1H), 7.21 (d, J = 12.0 Hz, 1H), 6.17 (d, J = 12.0 Hz, 1H), 3.82-3.71 (m, 1H), 1.93-1.53 (m, 5H), 1.43-1.04 (m, 5H). ^{13}C NMR (68 MHz, DMSO-d_6): δ 160.1, 159.1, 158.8, 149.9, 137.5, 116.4, 102.6, 49.4, 32.4+32.3, 25.3+24.9. ES-MS (methanol) m/z: 285.1 $[M+H]^+$, 307.1 $[M+Na]^+$, 323.1 $[M+K]^+$.

5.4.2 Biological Procedures

5.4.2.1 GSK-3β Kinase Assay – LANCE® *Ultra* TR-FRET kit

These studies were performed by Dr. Alessandra Feoli, in the research group of Professor Sabrina Castellano, University of Salerno, Fisciano (Italy), following the procedure described in Chapter 3.4.2.1

5.4.2.2 GSK-3β Kinase Assays and Reversibility Studies – Kinase-Glo® kit

These studies were performed by Dr. Concepcioń Perez, in the research group of Professor Ana Martinez, Instituto de Quimica Medica-CSIC, Madrid (Spain).

Kinase-Glo® assays were performed, following the procedure of Baki et al.,[238] in assay buffer using black 96-well plates. In a typical assay, 10 μL (10 μM) of test compound, dissolved in DMSO at 1 mM concentration and diluted in advance in assay buffer [50 mM HEPES (pH 7.5), 1 mM EDTA, 1 mM EGTA and 15 mM magnesium acetate] to the desired concentration, and 10 μL (20 ng) of human recombinant GSK-3β were added to each well followed by 20 μL of assay buffer containing 25 μM of GS-2 substrate and 1 μM ATP. The final DMSO concentration in the reaction mixture did not exceed 1%. After 30 min of incubation at 30 °C, the enzymatic reaction was stopped with 40 μL of Kinase-Glo reagent. Glow-type luminescence was recorded after 10 min using a FLUOstar Optima multimode reader. The activity is proportional to the difference of the total and consumed ATP. The inhibitory activities were calculated on the basis of maximal activities measured in the absence of inhibitor. The IC_{50} was defined as the concentration of each compound that reduces 50% the enzymatic activity with respect to that without inhibitors.
In the reversibility studies, the activity of the enzyme was determined after different times of incubation (0, 5, 10 min) of the enzyme with the inhibitor.

5.4.2.3 GSK-3β Kinetic Assays– ADP-Glo kit

These studies were performed by Dr. Concepcioń Perez, in the research group of Professor Ana Martinez, Instituto de Quimica Medica-CSIC, Madrid (Spain), following the procedure described in Chapter 3.4.2.2

5.4.2.4 CK-1δ Kinase Assays and Kinetic Assay – Kinase-Glo® kit/ADP-Glo kit

Kinase assays were performed following the procedure described in Chapter 4.4.2.1; *kinetic assays were performed by Dr. Concepcioń Perez, in the research group of Professor Ana Martinez, Instituto de Quimica Medica-CSIC, Madrid (Spain), following the procedure described in Chapter 3.4.2.2, adapted to CK-1δ.*

5.4.2.5 Prediction of CNS permeation: PAMPA-BBB Assay

Prediction of the brain penetration was assessed using a parallel artificial membrane permeability assay (PAMPA), following the procedure described in Chapter 3.4.2.3.[229] Results obtained and assay validation were reported in **Table 18** and in **Figure 57**:

Table 18. Permeability (*Pe* 10^{-6} cm s^{-1}) in the PAMPA-BBB assay for 10 commercial drugs (used in the experiment validation) and the newly synthetized compounds with their predictive penetration in the CNS.

Compound	Bibl.[229]	*Pe* (10^{-6} cm s^{-1})[a]	Prediction[b]
Atenolol	0.8	0.54 ± 0.70	
Caffeine	1.3	0.10 ± 0.21	
Desipramine	12	11.45 ± 1.48	
Enoxacin	0.9	0.10 ± 0.78	
Hydrocortisone	1.9	0.37 ± 0.01	
Ofloxacine	0.8	0.83 ± 0.57	
Piroxicam	2.5	0.1 ± 0.01	
Promazine	8.8	11.85 ± 1.24	
Testosterone	17	16.84 ± 2.89	
Verapamil	16	15.69 ± 3.89	
335		**1.34 ± 0.23**	**CNS -/+**
337		**2.35 ± 0.52**	**CNS -/+**

[a] Data are the mean ± SD of 2 independent experiments.
[b] Calculated limits: CNS + > 3.42, CNS - < 1.29.

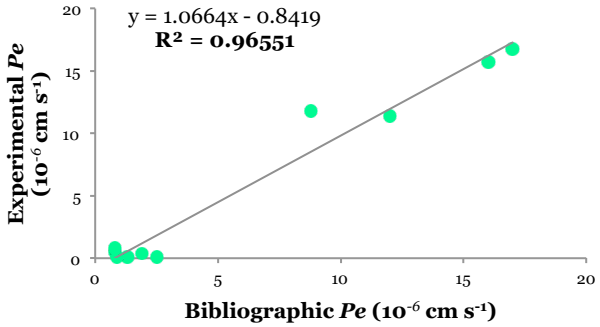

Figure 57. Linear correlation between experimental and reported permeability of commercial drugs using the PAMPA-BBB assay.

5.4.2.6 *In vitro* Assays on Neurodegeneration Models

These studies were performed by Dr. Teresa De Vita, in the research group of Professor Andrea Cavalli, Istituto Italiano di Tecnologia, Genoa (Italy)

The neuroprotective effects of the compound **335** were evaluated in PC12 cells following induction of cell death by two different dopamine neurotoxins: MPP+ (1-methyl-4-phenylpyridinium) or 6-OHDA (6-hydroxydopamine).

Cell culture. Rat pheochromocytoma cell line (PC12) was obtained from American Type Culture Collection (ATCC) and grown in RPMI 1640 medium supplemented with heat-inactivated 10% horse serum (HS), 5% fetal bovine serum (FBS) and 1% penicillin and streptomycin. Cells were grown in 10 cm^2 tissue culture dishes and cultured to a confluence of 80–90% and then subcultured with 0.25% trypsin. Cells were maintained in a humidified atmosphere of 5% carbon dioxide (CO_2) at 37°C. The cell culture medium was replaced every 2 days. All the experiments were conducted at least three times.

Cell treatments. PC12 cells were seeded in 96-well plates at 8×10^4 cells in a final volume of 100 µl/well and incubated in a humidified atmosphere of 5% carbon dioxide (CO_2) at 37°C. Twenty-four hours after plating, cells were used for treatments. Cells were incubated for 24h in the presence of MPP+ at different concentrations ranging from 100 µM to 1.5 mM and incubated for 5h with gradually increased concentrations of 6-OHDA (50-300 µM). For both of toxins, the dose that produces a significant neurotoxic effect was determined and used in the following neuroprotection experiments. For neuroprotection experiments, cells were treated for 24h with MPP+ in the presence of different concentrations of compound **335** (0.1-10 µM). In parallel, cells were treated with MPP+ with LiCl (1-10 mM). At the end of the cell treatments, cells were processed in various ways. For the experiments with 6-OHDA, cells were pretreated with gradually increased concentrations of compound **335** (0.1-10 µM), LiCl (1-10 mM) for 2h and then treated with 100 µM 6-OHDA for another 5h. To investigate Wnt/β-catenin signaling pathway, PC12 cells were seeded in 6-well plates at a density of 5×10^5 for 24h. Cells were pretreated with gradually increased concentrations of compound **335** (0.1-10 µM), LiCl (1-10 mM) for 2h and then treated with 100 µM 6-OHDA for another 2h.

Cell viability assay by CellTiter-Glo Luminescent. The CellTiter-Glo® Luminescent Cell Viability Assay (Promega) is a homogeneous method to determine the number of viable cells in culture based on quantitation of the ATP present, which signals the presence of metabolically active cells. The addition of solution consisting of two reagents results in cell lysis and generation of a luminescent signal proportional to the amount of ATP present. The plates were equilibrated at room temperature for approximately 30 minutes. 100 µL of reagents were added to 100 µl of medium containing cells and incubated at room temperature for 10 minutes to stabilize luminescent signal. The luminescence is recorded with a luminometer.

MTT assay. The MTT (3-[4,5-dimethylthiazol-2-yl]-2,5 diphenyl tetrazolium bromide) assay is based on the conversion of MTT into formazan crystals by living cells, which determines mitochondrial activity. Cells were grown in a 96-well tissue culture plate and incubated with 10µl of 5mg/ml MTT solution for approximately 4 hours in a humidified incubator. After this incubation period, a water-insoluble formazan dye is formed. After solubilization, with 10 µL of DMSO 100%, the formazan dye is quantified using a scanning multi-well spectrophotometer (ELISA reader). The measured absorbance at a wavelength of 570 nm with 655 nm as a reference wavelength is directly correlates to the number of viable cells.

Western Blotting. Cells were washed with cold PBS and homogenized 5 minutes with ice-cold lysis buffer (10 mM Hepes, 10 mM KCl, 0.1 mM EDTA, 1 mM DTT, 0.5% Nonidet, 0.5 mM PMSF) containing protease inhibitor cocktail. Tubes are centrifuged at 12.000 g at 4°C for 15 minutes. BCA protein assay kit was used to measure protein concentration. 25 µg of protein samples were boiled for 5 min with loading buffer and separated onto 4-15% Mini-PROTEAN TGX Precast Protein Gel. Proteins were transferred onto nitrocellulose membranes. Membranes were subsequently blocked for 1h at room temperature in blocking buffer (5% skim milk, 0.05% Tween 20 and Tris-buffered saline (TBS)). Then, the membranes were incubated overnight at 4 °C on an orbital shaker with primary antibodies: rabbit polyclonal anti-β-catenin (1:500 dilution) and mouse monoclonal anti-GAPDH (1:2000). After washed three times with TBST (15 min each), membranes were incubated with secondary antibodies: peroxidase-labeled goat anti-rabbit IgG (1:5000), goat anti mouse IgG/IgM HRP (1:5000) at room temperature for 1h and washed with TBST for three times.

The bands were visualized using enhanced chemiluminescences (ECL) method. Membranes probed for GAPDH used as an internal control. The protein bands were quantified using image analysis software (ImageJ, V1.42, National Institute of Health, Bethesda, MD) and protein levels were expressed as percent (%) of control.

5.4.3 Chemical Reactivity

HPLC-MS methodology.[173] Hundred microliters of a methanol solution of compound **335** (25 mM), 100 μL of methanol solution of 2-mercaptoethanol (25 mM) and 100 μL of methanol solution of triethylamine (25 mM) were added to 700 mL of methanol and stirred for 1, 2 or 24 h. The reaction progress was followed by HPLC-MS (HPLC Finningan Surveyor with *Waters* 2996 PDA Detector, coupled to ESI mass spectrometer Pump Plus; column SunFire™ C18, 3.5 μm, 4.6 mm x 50 mm), in a gradient from water-acetonitrile 90:10 to acetonitrile (100%), with both solvents containing 0.1% formic acid, over 25 minutes. Peaks corresponding to derivative **335** and βME adduct were identified by their masses and the percentage in each sample was determined by measuring the area under the curve for these peaks in the full scan PDA trace. Compound **335** (MW = 327) showed a retention time of 18.0 min, while retention time for the S-alkylated derivative (MW = 405) presented a retention time of 16.7 min.

UV-visible spectrometry methodology.[255] Reactions of compound **335** with βME were monitored with a multimode plate reader Tecan Infinite M1000, using Greiner UV Star® flat-bottom clear 96-well plates. Reactions were initiated by mixing 25 μL of derivative **335** (1.7 mM in PBS/DMSO 70:30, pH 7.4) with 25 μL of 2-mercaptoethanol (0–200 mM in PBS/DMSO 70:30, pH 7.4, two-fold dilution series). Final solutions, containing 0.85 mM of compound **335** and increasing concentrations of βME, were incubated for 10 min at room temperature before acquiring absorption spectra (250–500 nm). Formation of the thiol adduct was monitored by the disappearance of the absorbance peak (λ_{max}= 350 nm) relative to the no-βME control sample.

5.4.4 Computational procedures

5.4.4.1 Docking studies on GSK-3β

These studies were performed by Dr. Giovanni Bottegoni, in the research group of Professor Andrea Cavalli, Istituto Italiano di Tecnologia, Genoa (Italy).

A standard docking procedure was applied to generate the bound pose of compound **303** and the non-covalently bound pose of compound **335** at the binding site of GSK-3β (PDB: 1Q5K). This specific crystal structure was selected in light of the suitable results obtained in previous exploratory docking studies.[184] Hydrogen atoms were added. Polar hydrogen atoms and the positions of asparagine and glutamine side chain amidic groups were optimized and assigned the lowest energy conformation. After optimization, histidines were automatically assigned the tautomerization state that improved the hydrogen-bonding pattern. Finally, the original ligand was deleted. All the residues with at least one side chain non-hydrogen atom in the range of 3.5 Å from the co-crystallized ligand were considered part of the pocket. The binding site was represented by pre-calculated 0.5 Å spacing potential grid maps,

representing van der Waals potentials for hydrogens and heavy atoms, electrostatics, hydrophobicity, and hydrogen bonding, respectively. The van der Waals interactions were described by a smoother form of the Lennard Jones potential, capping the repulsive contribution to 4 kcal/mol. Each ligand was assigned the MMFF force field atom types and charges.[275] The docking engine used was the Biased Probability Monte Carlo (BPMC) stochastic optimizer as implemented in ICM.[276] Given the number of rotatable bonds in the ligand, the basic number of BPMC steps to be carried out was calculated by an adaptive algorithm (thoroughness 3.0). The binding energy was assessed with the ICM empirical scoring function.[277] For each ligand, the best scoring pose was selected as representative of the ligand bound conformation.

The covalently bound pose of compound **335** was obtained by means of the covalent docking procedure as implemented in ICM3.8, providing the general reaction scheme reported in **Figure 58** and identifying Cys199 as the activated nucleophile residue.

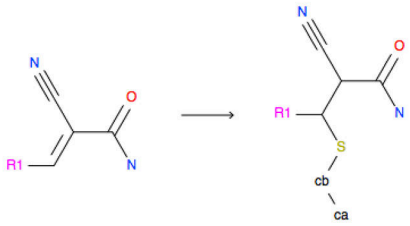

Figure 58. Covalent reaction in .rxn format provided as input for ICM3.8 covalent docking protocol.

5.4.4.2 Docking studies on CK-1δ

These studies were performed by the research group of Prof. Stefano Moro, Molecular Modeling section, University of Padua, Padua (Italy), according to procedure described in Chapter 4.4.3.

6 Conclusions

The aim of this thesis has been the synthesis of novel small-molecule inhibitors of GSK-3β and CK-1δ. Since GSK-3β and CK-1δ have been implicated in a variety of biological functions and their deregulation has been described in several diseases, developing effective inhibitors for both kinases is a central issue in these years. In particular, we focused on the design and decoration of two adenine-like systems, [1,2,4]triazolo[1,5-*a*][1,3,5]triazines (TT) and [1,2,4]triazolo[1,5-*c*]pyrimidines (TP), and the main outcomes can be summarized as follows (**Figure 59**):

- **GSK-3β inhibitors:** a small library of TT derivatives, presenting inhibitory activities towards GSK-3β in the low micromolar range, was obtained, confirming the suitability of this versatile scaffold to develop new kinase inhibitors. The most interesting results were achieved when 2-position of the scaffold was not substituted, while substitutions at both 5- (e.g. 3-pyridylmethylamino) and 7- (e.g. 2-aminobutan-1-ol) positions were required to create positive interactions with GSK-3β kinase pocket. Kinetic experiments confirmed an ATP-competitive inhibitory mechanism of TT derivatives towards the kinase. Moreover, some of the most active derivatives resulted to be able to pass the blood-brain barrier (BBB) according to the PAMPA assay, an essential feature for all those drugs that target CNS diseases.
- **CK-1δ inhibitors:** with the aim of obtaining novel CK-1δ inhibitors, both TT and TP scaffolds were exploited and substitutions at all positions of the bicyclic cores were investigated. This led to several compounds that showed inhibitory activities in the sub-micromolar range, and few of them resulted also CNS permeable at the PAMPA-BBB assay. The SAR studies on these compounds, supported by molecular docking simulations, highlighted the *m*-hydroxyphenyl or *m,m*-dihydroxyphenyl moieties at the 2-position and a free amino group at the 5 (TP) or 7 (TT) positions as key features to confer affinity to the kinase, while other positions should be further exploited to improve the inhibitory activity on this kinase and the pharmacokinetic profile of these compounds.

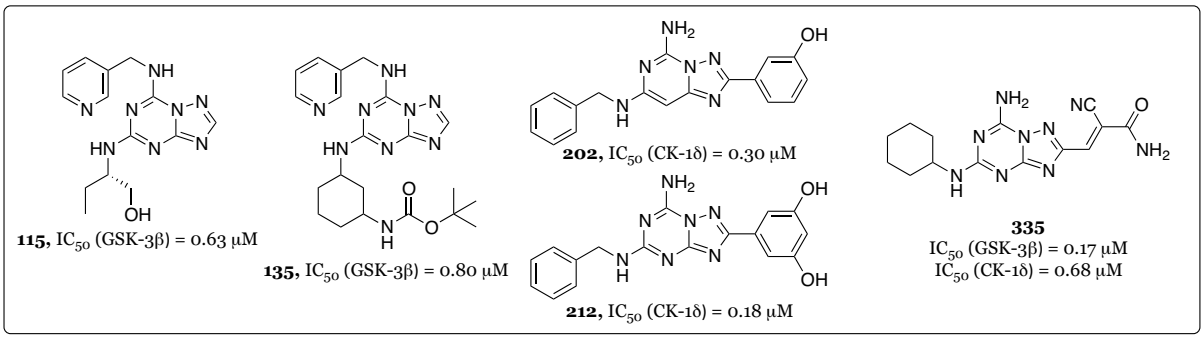

Figure 59. Representative novel kinase inhibitors.

- **Dual GSK-3β/CK-1δ inhibitor:** since the multi-targeted approach has emerged as a new paradigm for novel kinase inhibitors, we focused in the last chapter of this work on the design and synthesis of a dual GSK-3β/CK-1δ inhibitor. In particular, compound **335** displayed an encouraging balanced dual low-micromolar inhibition profile towards both GSK-3β and CK-1δ. Its peculiarity is found in the inhibitory mechanism: ATP-competitive towards CK-1δ and mixed ATP-competitive/non-ATP-competitive for GSK-3β, due to the presence of a Michael-acceptor moiety (cyanoacrylamide) that could covalently yet reversibly target non-catalytic Cys199 of the latter kinase. Notably, these

findings translate into a neuroprotective effect of compound **335** showed in preliminary studies in *in vitro* models of PD, thus confirming the potential of this kinase inhibitor.

In conclusion, we have obtained new GSK-3β and/or CK-1δ inhibitors with IC_{50} values in the submicromolar range, thus confirming that TT and TP nuclei are suitable scaffolds for the synthesis of new entities as protein kinase inhibitors. Future perspectives consist in the further development of adenine-like derivatives, with optimized neuroprotective and pharmacokinetic properties, in order to study their potential in neurodegenerative and neuroinflammation disease models. Moreover, deeper studies on compound **335** will be performed to highlight the effectiveness of the simultaneous inhibition of GSK-3β and CK-1δ.

7 References

1. Manning G. The Protein Kinase Complement of the Human Genome. *Science*. **2002;** 298(5600):1912–34.
2. Roskoski R. A Historical Overview of Protein Kinases and Their Targeted Small Molecule Inhibitors. *Pharmacol Res*. **2015;** 100:1–23.
3. Marks F, Klingmuller U, Muller-Deker K. Cellular Signal Processing: an Introduction to the Molecular Mechanisms of Signal Transduction. *Garland Science*, New York NY. **2009;** 656 pages.
4. Johnson LN, Barford D. The Effects of Phosphorylation on the Structure and Function of Proteins. *Annu Rev Biophys Biomol Struct*. **1993;** 22:199–232.
5. Duong-Ly K, Peterson JR. The Human Kinome and Kinase Inhibition as a Therapeutic Strategy. *Curr Protoc Pharmacol*. **2013;** 2:1–21.
6. Noble ME, Endicott JA, Johnson LN. Protein Kinase Inhibitors: Insights into Drug Design from Structure. *Science*. **2004;** 303(March):1800–5.
7. Zhang J, Yang PL, Gray NS. Targeting Cancer with Small Molecule Kinase Inhibitors. *Nat Rev Cancer*. **2009;** 9(1):28–39.
8. Cohen P. The Origins of Protein Phosphorylation. *Nat Cell Biol*. **2002;** 4(5):127–30.
9. Cohen P. Protein Kinases-the Major Drug Targets of the Twenty-First Century? *Nat Rev Drug Discov*. **2002;** 1(4):309–15.
10. Wu P, Nielsen TE, Clausen MH. Small-Molecule Kinase Inhibitors: an Analysis of FDA-Approved Drugs. *Drug Discov Today*. **2016;** 21(1):5–10.
11. Hunter T. Protein Kinase Classification. *Methods Enzymol*. **1991;** 200:3–37.
12. Johnson LN, Lewis RJ. Structural Basis for Control by Phosphorylation. *Chem Rev*. **2001;** 101(8):2209–42.
13. Taylor SS, Kornev AP. Protein Kinases: Evolution of Dynamic Regulatory Proteins. *Trends Biochem Sci*. **2011;** 36(2):65–77.
14. Ojo KK, Arakaki TL, Napuli AJ, Inampudi KK, Keyloun KR, Zhang L, Hol WG, Verlinde CL, Ethan A, Van Voorhis WC. Structure Determination of Glycogen Synthase Kinase-3 from Leishmania Major and Comparative Inhibitor Structure-Activity Relationships with Trypanosoma Brucei GSK-3. *Mol Biochem Parasitol*. **2012;** 176(2):98–108.
15. Knippschild U, Krüger M, Richter J, Xu P, García-Reyes B, Peifer C, Halekotte J, Bakulev V, Bischof J. The CK1 Family: Contribution to Cellular Stress Response and Its Role in Carcinogenesis. *Front Oncol*. **2014;** 4(May):96.
16. Ryves WJ, Dajani R, Pearl L, Harwood A. Glycogen Synthase Kinase-3 Inhibition by Lithium and Beryllium Suggests the Presence of Two Magnesium Binding Sites. *Biochem Biophys Res Commun*. **2002;** 290(3):967–72.
17. Bertrand JA, Thieffine S, Vulpetti A, Cristiani C, Valsasina B, Knapp S, Kalisz HM, Flocco M. Structural Characterization of the GSK-3β Active Site Using Selective and Non-Selective ATP-Mimetic Inhibitors. *J Mol Biol*. **2003;** 333(2):393–407.
18. Hanks SK, Hunter T. Protein Kinases 6. The Eukaryotic Protein Kinase Superfamily: Kinase (Catalytic) Domain Structure and Classification. *FASEB J*. **1995;** 9(8):576–96.
19. Ombrato R, Cazzolla N, Mancini F, Mangano G. Structure-Based Discovery of 1H-Indazole-3-Carboxamides as a Novel Structural Class of Human GSK-3 Inhibitors. *J Chem Inf Model*. **2015;** 55(12):2540–51.
20. Xu RM, Carmel G, Sweet RM, Kuret J, Cheng X. Crystal Structure of Casein Kinase-1, a Phosphate-Directed Protein Kinase. *EMBO J*. **1995;** 14(5):1015–23.
21. Buch I, Fishelovitch D, London N, Raveh B, Wolfson HJ, Nussinov R. Allosteric Regulation of Glycogen Synthase Kinase 3β: A Theoretical Study. *Biochemistry*. **2010;** 49(51):10890–901.
22. Longenecker KL, Roach PJ, Hurley TD. Three-Dimensional Structure of Mammalian Casein

Kinase I : Molecular Basis for Phosphate Recognition. **1996;** 618–31.
23. Steichen JM, Iyer GH, Li S, Saldanha A, Deal MS, Woods VL, Taylor SS. Global Consequences of Activation Loop Phosphorylation on Protein Kinase A. *J Biol Chem*. **2010;** 285(6):3825–32.
24. Hari SB, Merritt EA, Maly DJ. Sequence Determinants of a Specific Inactive Protein Kinase Conformation. *Chem Biol*. **2013;** 20(6):806–15.
25. Hughes K, Nikolakaki E, Plyte SE, Totty NF, Woodgett JR. Modulation of the Glycogen Synthase Kinase-3 Family by Tyrosine Phosphorylation. *EMBO J*. **1993;** 12(2):803–8.
26. ter Haar E, Coll J, Austen D, Hsiao H, Swenson L, Jain J. Structure of GSK3 Reveals a Primed Phosphorylation Mechanism. *Nat Struct Biol*. **2001;** 8:593–6.
27. Lochhead PA, Kinstrie R, Sibbet G, Rawjee T, Morrice N, Cleghon V. A Chaperone-Dependent GSK3β Transitional Intermediate Mediates Activation-Loop Autophosphorylation. *Mol Cell*. **2006;** 24(4):627–33.
28. Knippschild U, Gocht A, Wolff S, Huber N, Löhler J, Stöter M. The Casein Kinase 1 Family: Participation in Multiple Cellular Processes in Eukaryotes. *Cell Signal*. **2005;** 17(6):675–89.
29. Dajani R, Fraser E, Roe S, Young N, Good V, Dale T., Pearl L. Crystal Structure of Glycogen Synthase Kinase 3 Beta: Structural Basis for Phosphate-Primed Substrate Specificity and Autoinhibition. *Cell*. **2001;** 105:721–32.
30. Grimes CA, Jope RS. The Multifaceted Roles of Glycogen Synthase Kinase 3β in Cellular Signaling. *Prog Neurobiol*. **2001;** 65(4):391–426.
31. Longenecker KL, Roach PJ, Hurley TD. Crystallographic Studies of Casein Kinase I Delta toward a Structural Understanding of Auto-Inhibition. *Acta Crystallogr D Biol Crystrallogr*. **1998;** 54(3):473–5.
32. Embi N, Rylatt DB, Cohen P. Glycogen Synthase Kinase-3 from Rabbit Skeletal Muscle. Separation from Cyclic-AMP-Dependent Protein Kinase and Phosphorylase Kinase. *Eur J Biochem*. **1980;** 107(2):519–27.
33. Lu KP, Liou Y, Zhou XZ, Liou Y. Pinning Down Phosphorylation Signaling. *Trends Cell Biol*. **2002;** 12(4):164–72.
34. Woodgett J. Glycogen Synthase Kinase-3. *Encycl Biol Chem*. **2004;** 2:255–60.
35. Doble B, Woodgett J. GSK-3: Tricks of The Trade for a Multi-Tasking Kinase. *J Cell Sci*. **2003;** 116(7):1175–1166.
36. Jacobs KM, Bhave SR, Ferraro DJ, Jaboin JJ, Hallahan DE, Thotala D. GSK-3β: A Bifunctional Role in Cell Death Pathways. *Int J Cell Biol*. **2012;** 2012, 11 pages.
37. Mukai F, Ishiguro K, Sano Y, Fujita SC. Alternative Splicing Isoform of Tau Protein Kinase I/Glycogen Synthase Kinase 3β. *J Neurochem*. **2002;** 81:1073–83.
38. Hoeflich KP, Luo J, Rubie E a, Tsao MS, Jin O, Woodgett JR. Requirement for Glycogen Synthase Kinase-3beta in Cell Survival and NF-kappaB Activation. *Nature*. **2000;** 406(July):86–90.
39. Lau KF, Miller CC, Anderton BH, Shaw PC. Expression Analysis of Glycogen Synthase Kinase-3 in Human Tissues. *J Pept Res*. **1999;** 54(1):85–91.
40. Fiol CJ, Mahrenholz AM, Wang Y, Roeske RW, Roach PJ. Formation of Protein Kinase Recognition Sites by Covalent Modification of the Substrate. Molecular Mechanism for the Synergistic Action of Casein Kinase II and Glycogen Synthase Kinase 3. *J Biol Chem*. **1987;** 262(29):14042–8.
41. Jho E, Lomvardas S, Costantini F. A GSK3β Phosphorylation Site in Axin Modulates Interaction with β-Catenin and Tcf-Mediated Gene Expression. *Biochem Biophys Res Commun*. **1999;** 266(1):28–35.
42. Cross D, Alessi DR, Cohen P, Andjelkovich M, Hemmings B. Inhibition of Glycogen

Synthase Kinase-3 by Insulin Mediated by Protein Kinase B. *Nature*. **1995;** 378(6559):785–9.
43. Saito Y, Vandenheedet JR, Cohen P. The Mechanism by Which Epidermal Growth Factor Inhibits Glycogen Synthase Kinase 3 in A431 Cells. **1994;** 31:27–31.
44. Ding V, Chen R-H, McCormick F. Differential Regulation of Glycogen Synthase Kinase 3 by Insulin and Wnt Signaling. *J Biol Chem*. **2000;** 275(42):32475–81.
45. Miller JR. The Wnts. *Genome Biol*. **2002;** 3(1):3001.1–3001.15.
46. Amit S, Hatzubai A, Birman Y, Andersen JS, Ben-Shushan E, Mann M, Ben-Neriah Y, Alkalay I. Axin-Mediated CKI Phorphorylation of β-Catenin at Ser 45: A Molecular Switch for the Wnt Pathway. *Genes Dev*. **2002;** 16:1066–76.
47. Liu C, Li Y, Semenov M, Han C, Baeg GH, Tan Y, Zhang Z, Lin X, He X. Control of B-Catenin Phosphorylation/Degradation by a Dual-Kinase Mechanism. *Cell*. **2002;** 108(6):837–47.
48. Cohen P, Goedert M. GSK3 Inhibitors: Development and Therapeutic Potential. *Nat Rev*. **2004;** 3:479–87.
49. He T-C, Sparks AB, Rago C, Hermeking H, Zawel L, da Costa LT, Morin PJ, Vogelstein B, Kinzler KW. Identification of c-MYC as a Target of the APC Pathway. *Science*. **1998;** 281(5382):1509–12.
50. Goñi-Oliver P, Lucas JJ, Avila J, Hernández F. N-Terminal Cleavage of GSK-3 by Calpain: A New Form of GSK-3 Regulation. *J Biol Chem*. **2007;** 282(31):22406–13.
51. Meijer L, Flajolet M, Greengard P. Pharmacological Inhibitors of Glycogen Synthase Kinase 3. *TRENDS Pharmacol Sci*. **2004;** 25(9).
52. Franca-Koh J, Yeo M, Fraser E, Young N, Dale TC. The Regulation of Glycogen Synthase Kinase-3 Nuclear Export by Frat/GBP. *J Biol Chem*. **2002;** 277(46):43844–8.
53. Burnett G, Kennedy EP. The Enzymatic Phosphorylation of Proteins. *Cancer*. **1954;** 969–80.
54. Venerando A, Ruzzene M, Pinna LA. Casein Kinase: The Triple Meaning of a Misnomer. *Biochem J*. **2014;** 460(2):141–56.
55. Lasa-Benito M, Marin O, Meggio F, Pinna LA. Golgi Apparatus Mammary Gland Casein Kinase: Monitoring by a Specific Peptide Substrate and Definition of Specificity Determinants. *FEBS Lett*. **1996;** 382(1–2):149–52.
56. Price MA. CKI, There's More than One: Casein Kinase I Family Members in Wnt and Hedgehog Signaling. **2006;** 399–410.
57. Flotow H, Graves PR, Wang A, Fiol CJ, Roeske RW, Roach PJ. Phosphate Groups as Substrate Determinants for Casein Kinase I Action. *J Biol Chem*. **1990;** 265(24):14264–9.
58. Perez DI, Gil C, Martínez A. Protein Kinases CK1 and CK2 as New Targets for Neurodegenerative Diseases. *Med Res Rev*. **2011;** 31(6):924–54.
59. Graves PR, Roach PJ. Role of COOH-Terminal Phosphorylation in the Regulation of Casein Kinase Iδ. *J Biol Chem*. **1995;** 270(37):21689–94.
60. Marin O, Bustos VH, Cesaro L, Meggio F, Pagano MA, Antonelli M, Allende CC, Pinna LA, Allende JE. A Noncanonical Sequence Phosphorylated by Casein Kinase 1 in Beta-Catenin May Play a Role in Casein Kinase 1 Targeting of Important Signaling Proteins. *Proc Natl Acad Sci U S A*. **2003;** 100(18):10193–200.
61. Flotow H, Roach PJ. Role of Acidic Residues as Substrate Determinants for Casein Kinase I. *J Biol Chem*. **1991;** 266(6):3724–7.
62. Stöter M, Krüger M, Banting G, Henne-Bruns D, Knippschild U. Microtubules Depolymerization Caused by the CK1 Inhibitor IC261 May Be Not Mediated by CK1 Blockage. *PLoS One*. **2014;** 9(6):1–13.
63. Milne DM, Looby P, Meek DW. Catalytic Activity of Protein Kinase CK1 Delta (Casein

Kinase 1delta) Is Essential for its Normal Subcellular Localization. *Exp Cell Res*. **2001;** 263(1):43–54.

64. Cheong JK, Virshup DM. Casein Kinase 1: Complexity in the Family. *Int J Biochem Cell Biol*. **2011;** 43(4):465–9.
65. Sillibourne JE, Milne DM, Takahashi M, Ono Y, Meek DW. Centrosomal Anchoring of the Protein Kinase CK1δ Mediated by Attachment to the Large, Coiled-Coil Scaffolding Protein CG-NAP/AKAP450. *J Mol Biol*. **2002;** 322(4):785–97.
66. Buller C, Loberg R, Fan M. A GSK-3/TSC2/mTOR Pathway Regulates Glucose Uptake and GLUT1 Glucose Transporter Expression. *Am J Physiol Cell Physiol*. **2008;** 680:836–43.
67. Shen W, Taylor B, Jin Q, Nguyen-Tran V, Meeusen S, Zhang Y-Q, Kamireddy A, Swafford A, Powers AF, Walker J, Lamb J, Bursalaya B, Di Donato M, Harb G, Qiu M, Filippi CM, Deaton L, Turk CN, Suarez-Pinzon WL et al. Inhibition of DYRK1A and GSK3β Induces Human β-Cell Proliferation. *Nat Commun*. **2015;** 6:8372.
68. Flotow H, Roach PJ. Synergistic Phosphorylation of Rabbit Muscle Glycogen Synthase by Cyclic AMP-Dependent Protein Kinase and Casein Kinase I. *J Biol Chem*. **1989;** 264(16):9126–8.
69. Palm DC, Rohwer JM, Hofmeyr JHS. Regulation of Glycogen Synthase from Mammalian Skeletal Muscle - A Unifying View of Allosteric and Covalent Regulation. *FEBS J*. **2013;** 280(1):2–27.
70. Polakis P. Wnt Signaling and Cancer Wnt Signaling and Cancer. **2000;** (650):1837–51.
71. Alves dos Santos MT, Smidt MP. En1 and Wnt Signaling in Midbrain Dopaminergic Neuronal Development. *Neural Dev*. **2011;** 6(1):23.
72. Marchetti B, Pluchino S. Wnt Your Brain Be Inflamed? Yes, It Wnt! *Trends Mol Med*. **2013;** 19(3):144–56.
73. Wu D, Pan Q. GSK3: A Multifaceted Kinase in Wnt Signaling. *Trends Biochem Sci*. **2010;** 35(3):161–8.
74. Ferrarese A, Marin O, Bustos VH, Venerando A, Antonelli M, Allende JE, Pinna LA. Chemical Dissection of the APC Repeat 3 Multistep Phosphorylation by the Concerted Action of Protein Kinases CK1 and GSK3. *Biochemistry*. **2007;** 46(42):11902–10.
75. Scales SJ, de Sauvage FJ. Mechanisms of Hedgehog Pathway Activation in Cancer and Implications for Therapy. *Trends Pharmacol Sci*. **2009;** 30(6):303–12.
76. Dellovade T, Romer JT, Curran T, Rubin LL. The Hedgehog Pathway and Neurological Disorders. *Annu Rev Neurosci*. **2006;** 29(1):539–63.
77. Ruat M, Hoch L, Faure H, Rognan D. Targeting of Smoothened for Therapeutic Gain. *Trends Pharmacol Sci*. **2014;** 35(5):237–46.
78. Price MA, Kalderon D. Proteolysis of the Hedgehog Signaling Effector Cubitus Interruptus Requires Phosphorylation by Glycogen Synthase Kinase 3 and Casein Kinase 1. *Cell*. **2002;** 108(6):823–35.
79. Zhao B, Li L, Tumaneng K, Wang CY, Guan KL. A Coordinated Phosphorylation by Lats and CK1 Regulates YAP Stability through SCFβ-TRCP. *Genes Dev*. **2010;** 24(1):72–85.
80. Huang W, Lv X, Liu C, Zha Z, Zhang H, Jiang Y, Xiong Y, Lei QY, Guan KL. The N-Terminal Phosphodegron Targets TAZ/WWTR1 Protein for SCFβ-TrCP-Dependent Degradation in Response to Phosphatidylinositol 3-Kinase Inhibition. *J Biol Chem*. **2012;** 287(31):26245–53.
81. Azzolin L, Zanconato F, Bresolin S, Forcato M, Basso G, Bicciato S. Role of TAZ as Mediator of Wnt Signaling. *Cell*. **2012;** 151(7):1443–56.
82. Beurel E, Jope RS. The Paradoxical Pro- and Anti-Apoptotic Actions of GSK3 in the Intrinsic and Extrinsic Apoptosis Signaling Pathways. *Prog Neurobiol*. **2006;** 79(4):173–89.

83. Turenne GA, Price BD. Glycogen Synthase kinase3 Beta Phosphorylates Serine 33 of p53 and Activates p53's Transcriptional Activity. *BMC Cell Biol*. **2001;** 2:12.
84. Schittek B, Sinnberg T. Biological Functions of Casein Kinase 1 Isoforms and Putative Roles in Tumorigenesis. *Mol Cancer*. **2014;** 13(1):231.
85. Warrington R, Watson W, Kim HL, Antonetti FR. An Introduction to Immunology and Immunopathology. *Allergy, Asthma Clin Immunol*. **2011;** 7 Suppl 1:s1.
86. Glass CK, Saijo K, Winner B, Marchetto MC, Gage H. Mechanisms Underlying Inflammation in Neurodegeneration. *Cell*. **2010;** 140(6):918–34.
87. Frank-Cannon TC, Alto LT, McAlpine FE, Tansey MG. Does Neuroinflammation Fan the Flame in Neurodegenerative Diseases? *Mol Neurodegener*. **2009;** 4:47.
88. Karin M. Inflammation-Activated Protein Kinases as Targets for Drug Development. *Proc Am Thorac Soc*. **2005;** 2(4):385–6.
89. Jope RS, Cheng Y, Lowell JA, Worthen RJ, Sitbon YH, Beurel E. Stressed and Inflamed, Can GSK3 Be Blamed? *Trends Biochem Sci*. **2016;** 1–13.
90. Richmond A. Nf-Kappa B, Chemokine Gene Transcription and Tumour Growth. *Nat Rev Immunol*. **2002;** 2:664–74.
91. Steinbrecher KA, Wilson III W, Cogswell PC, Baldwin AS. Glycogen Synthase Kinase 3b Functions to Specify Gene-Specific, NF-kB-Dependent Transcription. *Mol Cell Biol*. **2005;** 25(19):8444–55.
92. Jope R, Yuskaitis CJ, Beurel E. Glycogen Synthase Kinase-3 (GSK3): Inflammation, Diseases, and Therapeutics. *Neurochem Res*. **2007;** 32:577–95.
93. Martin M, Rehani K, Jope RS, Michalek SM. Toll-like Receptor-Mediated Cytokine Production Is Differentially Regulated by Glycogen Synthase Kinase 3. *Nat Immunol*. **2005;** 6(8):777–84.
94. Ramesh G, MacLean AG, Philip MT. Cytokines and Chemokines at the Crossroads of Neuroinflammation, Neurdegeneration and Neuropathic Pain. *Mediators Inflamm*. **2013;** 2013:1–20.
95. Green H, Nolan Y. GSK-3 Mediates the Release of IL-1beta, TNF-Alfa and IL-10 from Cortical Glia. *Neurochem Int*. **2012;** 61:666–71.
96. Martinez A, Castro A, Dorronsoro I, Alonso M. Glycogen Synthase Kinase 3 (GSK-3) Inhibitors as New Promising Drugs for Diabetes, Neurodegeneration, Cancer, and Inflammation. *Med Res Rev*. **2002;** 22(4):373–84.
97. Beyaert R, Vanhaesebroeck B, Declercq W, Vanlint J, Vandenabeele P, Agostinis P, Vandenheede JR, Fiers W. Casein Kinase-1 Phosphorylates the P75 Tumor-Necrosis-Factor Receptor and Negatively Regulates Tumor-Necrosis-Factor Signaling for Apoptosis. *J Biol Chem*. **1995;** 270(40):23293–9.
98. Jope RS, Roh M-S. Glycogen Synthase Kinase-3 (GSK3) in Psychiatric Diseases and Therapeutic Interventions. *Curr Drug Targets*. **2006;** 7(11):1421–34.
99. Klein P, Melton DA. A Molecular Mechanism for the Effect of Lithium on Development. *Proc Natl Acad Sci USA*. **1996;** 93:8455–9.
100. Beurel E, Grieco SF, Jope RS. Glycogen Synthase Kinase-3 (GSK3): Regulation, Actions, and Diseases. *Pharmacol Ther*. **2014;** 148:114–31.
101. Martinez A. Preclinical Efficacy on GSK-3 Inhibitors: Towards a Future Generation of Powerful Drugs. *Med Res Rev*. **2008;** 28(5):773–96.
102. Matsunaga S, Ikeda M, Kishi T, Fukuo Y, Aleksic B, Yoshimura R, Okochi T, Yamanouchi Y, Kinoshita Y, Kawashima K, Umene-Nakano W, Inada T, Kunugi H, Kato T, Yoshikawa T, Ujike H, Nakamura J, Ozaki N, Kitajima T et al. An Evaluation of Polymorphisms in Casein Kinase 1 Delta and Epsilon Genes in Major Psychiatric Disorders. *Neurosci Lett*. **2012;** 529(1):66–9.

103. McClung CA. Circadian Genes, Rhythms and the Biology of Mood Disorders Colleen. *Pharmacol Ther*. **2007;** 114(2):222–32.
104. Reischl S, Kramer A. Kinases and Phosphatases in the Mammalian Circadian Clock. *FEBS Lett*. **2011;** 585(10):1393–9.
105. Avila J, Hernàndez F. GSK-3 Inhibitors for Alzheimer's Disease. *Expert Rev Neurother*. **2007;** 7(11):1527-33.
106. Hanger DP, Byers HL, Wray S, Leung KY, Saxton MJ, Seereeram A, Reynolds CH, Ward MA, Anderton BH. Novel Phosphorylation Sites in Tau from Alzheimer Brain Support a Role for Casein Kinase 1 in Disease Pathogenesis. *J Biol Chem*. **2007;** 282(32):23645–54.
107. Singh TJ, Haque N, Grundke-Iqbal I, Iqbal K. Rapid Alzheimer-like Phosphorylation of Tau by the Synergistic Actions of Non-Proline-Dependent Protein Kinases and GSK-3. *FEBS Lett*. **1995;** 358(3):267–72.
108. Llorens-Marítin M, Jurado J, Hernández F, Avila J. GSK-3β, a Pivotal Kinase in Alzheimer Disease. *Front Mol Neurosci*. **2014;** 7(May):1–46.
109. Hanger DP, Anderton BH, Noble W. Tau Phosphorylation: The Therapeutic Challenge for Neurodegenerative Disease. *Trends Mol Med*. **2009;** 15(3):112–9.
110. Hooper C, Killick R, Lovestone R. The GSK3 Hypothesis of Alzheimer's Disease. *J Neurochem*. **2008;** 104:1433–9.
111. Dickson DW. Parkinson's Disease and Parkinsonism: Neuropathology. *Cold Spring Harb Perspect Med*. **2012;** 2: a009258.
112. Morales-Garcia J, Susin C, Alonso-Gil S, Perez D., Palomo V, Perez C, Conde S, Santos A, Gil C, Martinez A, Perez-Castillo A. Glycogen Synthase Kinase-3 Inhibitors as Potent Therapeutic Agents for the Treatment of Parkinson Disease. *ACS Chem Neurosci*. **2013;** 4:350–60.
113. Wang W, Yang Y, Ying C, Li W, Ruan H, Zhu X, You Y, Han Y, Chen R, Wang Y, Li M. Inhibition of Glycogen Synthase Kinase-3β Protects Dopaminergic Neurons from MPTP Toxicity. *Neuropharmacology*. **2007;** 52(8):1678–84.
114. Kozikowski AP, Gaisina IN, Petukhov PA, Sridhar J, King LT, Blond SY, Duka T, Rusnak M, Sidhu A. Highly Potent and Specific GSK-3beta Inhibitors that Block Tau Phosphorylation and Decrease Alpha-Synuclein Protein Expression in a Cellular Model of Parkinson's Disease 16. *ChemMedChem*. **2006;** 1(2):256–66.
115. L'Episcopo F, Tirolo C, Testa N, Caniglia S, Morale MC, Deleidi M, Serapide MF, Pluchino S, Marchetti B. Plasticity of Subventricular Zone Neuroprogenitors in MPTP (1-Methyl-4-Phenyl-1,2,3,6-Tetrahydropyridine) Mouse Model of Parkinson's Disease Involves Cross Talk between Inflammatory and Wnt/β-Catenin Signaling Pathways: Functional Consequences for Neuropr. *J Neurosci*. **2012;** 32(6):2062–85.
116. Lei P, Ayton S, Bush A., Adlard P. GSK-3 in Neurodegenerative Diseases. *Int J Alzheimers Dis*. **2011;** 2011:18246.
117. Salado IG, Redondo M, Bello ML, Liachko NF, Kraemer BC, Miguel L, Lecourtois M, Gil C, Martinez A, Perez DI. Protein Kinase CK-1 Inhibitors As New Potential Drugs for Amyotrophic Lateral Sclerosis. *J Med Chem*. **2014;** 57(6):2755-72.
118. Higashi S, Tsuchiya Y, Araki T, Wada K, Kabuta T. TDP-43 Physically Interacts with Amyotrophic Lateral Sclerosis-Linked Mutant CuZn Superoxide Dismutase. *Neurochem Int*. **2010;** 57(8):906–13.
119. Koh S-H, Baek W, Kim SH. Brief Review of the Role of Glycogen Synthase Kinase-3β in Amyotrophic Lateral Sclerosis. *Neurol Res Int*. **2011;** 2011:205761.
120. Moujalled D, James JL, Parker SJ, Lidgerwood GE, Duncan C, Meyerowitz J, Nonaka T, Hasegawa M, Kanninen KM, Grubman A, Liddell JR, Crouch PJ, White AR. Kinase Inhibitor Screening Identifies Cyclin-Dependent Kinases and Glycogen Synthase Kinase 3

as Potential Modulators of TDP-43 Cytosolic Accumulation during Cell Stress. *PLoS One*. **2013;** 8(6).

121. Zuccotto F, Ardini E, Casale E, Angiolini M. Through The "Gatekeeper Door": Exploiting the Active Kinase Conformation. *J Med Chem*. **2010;** 53(7):2681–94.
122. Traxler P, Furet P. Strategies toward the Design of Novel and Selective Protein Tyrosine Kinase Inhibitors. *Pharmacol Ther*. **1999;** 82:195–206.
123. Smyth LA, Collins I. Measuring and Interpreting the Selectivity of Protein Kinase Inhibitors. *J Chem Biol*. **2009;** 2(3):131–51.
124. Garuti L, Roberti M, Bottegoni G. Non-ATP Competitive Protein Kinase Inhibitors. *Curr Med Chem*. **2010;** 17(25):2804–21.
125. Müller S, Chaikuad A, Gray NS, Knapp S. The Ins and Outs of Selective Kinase Inhibitor Development. *Nat Chem Biol*. **2015;** 11(11):818–21.
126. Lamba V, Ghosh I. New Directions in Targeting Protein Kinases: Focusing Upon True Allosteric and Bivalent Inhibitors. *Curr Pharm Des*. **2012;** 18:2936–45.
127. Roskoski R. Classification of Small Molecule Protein Kinase Inhibitors Based upon the Structures of Their Drug-Enzyme Complexes. *Pharmacol Res*. **2016;** 103:26–48.
128. Barf T, Kaptein A. Irreversible Protein Kinase Inhibitors: Balancing the Benefits and Risks. *J Med Chem*. **2012;** 55(14):6243–62.
129. Singh J, Petter RC, Baillie TA, Whitty A. The Resurgence of Covalent Drugs. *Nat Rev Discov*. **2011;** 10(4):307–17.
130. Liu Q, Sabnis Y, Zhao Z, Zhang T, Buhrlage SJ, Jones H, Gray NS. Developing Irreversible Inhibitors of the Protein Kinase Cysteinome. *Chem Biol*. **2013;** 20(2):146–59.
131. Yu HA, Pao W. TARGETED THERAPIES: Afatinib—new Therapy Option for EGFR-Mutant Lung Cance. *Nat Rev Clin Oncol*. **2013;** 10(10):551–2.
132. Ponader S, Chen S, Buggy JJ, Balakrishnan K, Gandhi V, Wierda G, Keating MJ, Brien SO, Chiorazzi N, Burger J a, Wierda WG. Lymphocytic Leukemia Cell Survival and Tissue Homing in Vitro and in The Bruton Tyrosine Kinase Inhibitor PCI-32765 Thwarts Chronic Lymphocytic Leukemia Cell Survival and Tissue Homing in Vitro and in Vivo. **2014;** 119(5):1182–9.
133. Kwiatkowski N, Zhang T, Rahl PB, Abraham BJ, Reddy J, Ficarro SB, Dastur A, Amzallag A, Ramaswamy S, Tesar B, Jenkins CE, Hannett NM, McMillin D, Sanda T, Sim T, Kim ND, Look T, Mitsiades CS, Weng AP et al. Targeting Transcription Regulation in Cancer with a Covalent CDK7 Inhibitor. *Nature*. **2014;** 511(7511):616–20.
134. Palomo V, Martinez A. Glycogen Synthase Kinase 3 (GSK-3) Inhibitors: A Patent Update (2014-2015). *Expert Opin Ther Pat*. **2016;** 3776:1–10.
135. Georgievska B, Sandin J, Doherty J, Mörtberg A, Neelissen J, Andersson A, Gruber S, Nilsson Y, Schött P, Arvidsson PI, Hellberg S, Osswald G, Berg S, Fälting J, Bhat R V. AZD1080, a Novel GSK3 Inhibitor, Rescues Synaptic Plasticity Deficits in Rodent Brain and Exhibits Peripheral Target Engagement in Humans. *J Neurochem*. **2013;** 125(3):446–56.
136. Eldar-Finkelman H, Martinez A. GSK-3 Inhibitors: Preclinical and Clinical Focus on CNS. *Front Mol Neurosci*. **2011;** 4(32).
137. Dominguez J, Fuertes A, Orozco L, Del Monte-Millan M, Delgado E, Medina M. Evidence for Irreversible Inhibition of Glycogen Synthase Kinase-3β by Tideglusib. *J Biol Chem*. **2012;** 287:893–904.
138. Luna-Medina R, Cortes-Canteli M, Sanchez-Galiano S, Morales-Garcia J, Martinez A, Santos A, Perez-Castillo A. NP031112, a Thiadiazolidinone Compound, Prevents Inflammation and Neurodegeneration under Excitotoxic Conditions: Potential Therapeutic Role in Brain Disorders. *J Neurosci*. **2007;** 27(21):5766–76.
139. Zamek-Gliszczynski MJ, Abraham TL, Alberts JJ, Kulanthaivel P, Jackson KA, Chow KH,

Mccann DJ, Hu H, Anderson S, Furr NA, Barbuch RJ, Cassidy KC. Pharmacokinetics, Metabolism, and Excretion of the Glycogen Synthase Kinase-3 Inhibitor LY2090314 in Rats, Dogs, and Humans: A Case Study in Rapid Clearance by Extensive Metabolism with Low Circulating Metabolite Exposure. *Drug Metab Dispos*. **2013;** 41(4):714–26.

140. Gray JE, Infante JR, Brail LH, Simon GR, Cooksey JF, Jones SF, Farrington DL, Yeo A, Jackson KA, Chow KH, Zamek-Gliszczynski MJ, Burris HA. A First-in-Human Phase I Dose-Escalation, Pharmacokinetic, and Pharmacodynamic Evaluation of Intravenous LY2090314, a Glycogen Synthase Kinase 3 Inhibitor, Administered in Combination with Pemetrexed and Carboplatin. *Invest New Drugs*. **2015;** 33(6):1187–96.
141. Rizzieri DA, Cooley S, Odenike O, Moonan L, Chow KH, Jackson K, Wang X, Brail L, Borthakur G. An Open-Label Phase 2 Study of Glycogen Synthase Kinase-3 Inhibitor LY2090314 in Patients with Acute Leukemia. *Leuk Lymphoma*. **2016;** 8194:1–7.
142. Martinez A, Castro A, Medina M. Glycogen Synthase Kinase 3 (GSK-3) and Its Inhibitors: Drug Discovery and Development. Wiley. **2006.**
143. Meijer L, Thunnissen AMWH, White AW, Garnier M, Nikolic M, Tsai LH, Walter J, Cleverley KE, Salinas PC, Wu YZ, Biernat J, Mandelkow EM, Kim SH, Pettit GR. Inhibition of Cyclin-Dependent Kinases, GSK-3β and CK1 by Hymenialdisine, a Marine Sponge Constituent. *Chem Biol*. **2000;** 7(1):51–63.
144. Wan Y, Hur W, Cho C, Liu Y, Adrian F, Lozach O, Bach S, Mayer T, Fabbro D, Meijer L, Gray NS. Synthesis and Target Identification of Hymenialdisine Analogs. *Chem Biol*. **2004;** 11(2):247–59.
145. Kramer T, Schmidt B, Lo Monte F. Small-Molecule Inhibitors of GSK-3: Structural Insights and Their Application to Alzheimer's Disease Models. *Int J Alzheimer's Dis*. **2012;** 2012.
146. Johnson JL, Rupasinghe SG, Stefani F, Schuler MA, Gonzalez de Mejia E. Citrus Flavonoids Luteolin, Apigenin, and Quercetin Inhibit Glycogen Synthase Kinase-3β Enzymatic Activity by Lowering the Interaction Energy within the Binding Cavity. *J Med Food*. **2011;** 14(4):325–33.
147. Knockaert M, Wieking K, Schmitt S, Leost M, Grant KM, Mottram J, Kunick C, Meijer L. Intracellular Targets of Paullones. *J Biol Chem*. **2002;** 277(28):25493–2550.
148. Fukunaga K, Sakai D, Watanabe K, Nakayama K, Kohara T, Tanaka H, Sunada S, Nabeno M, Okamoto M, Saito KI, Eguchi JI, Mori A, Tanaka S, Inazawa K, Horikawa T. Discovery of Novel 2-(alkylmorpholin-4-yl)-6-(3-fluoropyridin-4-yl)-pyrimidin-4(3H)-ones as Orally-Active GSK-3β Inhibitors for Alzheimer's Disease. *Bioorganic Med Chem Lett*. **2015;** 25(5):1086–91.
149. Fukunaga K, Uehara F, Aritomo K, Shoda a, Hiki S, Okuyama M, Usui Y, Watanabe K, Yamakoshi K, Kohara T, Hanano T, Tanaka H, Tsuchiya S, Sunada S, Saito K, Eguchi J, Yuki S, Asano S, Tanaka S et al. 2-(2-Phenylmorpholin-4-yl)pyrimidin-4(3H)-ones: a New Class of Potent, Selective and Orally Active Glycogen Synthase Kinase-3beta Inhibitors. *Bioorg Med Chem Lett*. **2013;** 23(24):6933–7.
150. Engler TA, Malhotra S, Burkholder TP, Henry JR, Mendel D, Porter WJ, Furness K, Diefenbacher C, Marquart A, Reel JK, Li Y, Clayton J, Cunningham B, McLean J, O'Toole JC, Brozinick J, Hawkins E, Misener E, Briere D et al. The Development of Potent and Selective Bisarylmaleimide GSK3 Inhibitors. *Bioorganic Med Chem Lett*. **2005;** 15(4):899–903.
151. Engler TA, Henry JR, Malhotra S, Cunningham B, Furness K, Brozinick J, Burkholder TP, Clay MP, Clayton J, Diefenbacher C, Hawkins E, Iversen PW, Li Y, Lindstrom TD, Marquart AL, McLean J, Mendel D, Misener E, Briere D et al. Substituted 3-imidazo[1,2-*a*]pyridin-3-yl-4-(1,2,3,4-tetrahydro-[1,4]diazepino-[6,7,1-hi]indol-7-yl)pyrrole-2,5-diones as Highly Selective and Potent Inhibitors of Glycogen Synthase Kinase-3. *J Med Chem*. **2004;**

47(16):3934–7.
152. Bone HK, Damiano T, Bartlett S, Perry A, Letchford J, Ripoll YS, Nelson AS, Welham MJ. Involvement of GSK-3 in Regulation of Murine Embryonic Stem Cell Self-Renewal Revealed by a Series of Bisindolylmaleimides. *Chem Biol*. **2009;** 16(1):15–27.
153. Ye Q, Shen Y, Zhou Y, Lv D, Gao J, Li J, Hu Y. Design, Synthesis and Evaluation of 7-Azaindazolyl-Indolyl-Maleimides as Glycogen Synthase Kinase-3β (GSK-3β) Inhibitors. *Eur J Med Chem*. **2013;** 68:361–71.
154. Ye Q, Mao W, Zhou Y, Xu L, Li Q, Gao Y, Wang J, Li C, Xu Y, Xu Y, Liao H, Zhang L, Gao J, Li J, Pang T. Synthesis and Biological Evaluation of 3-([1,2,4]triazolo[4,3-*a*]pyridin-3-yl)-4-(indol-3-l)-maleimides as Potent, Selective GSK-3β Inhibitors and Neuroprotective Agents. *Bioorganic Med Chem*. **2015;** 23(5):1179–88.
155. Lo Monte F, Kramer T, Bolander A, Plotkin B, Eldar-Finkelman H, Fuertes A, Dominguez J, Schmidt B. Synthesis and Biological Evaluation of Glycogen Synthase Kinase 3 (GSK-3) Inhibitors: An Fast and Atom Efficient Access to 1-aryl-3-benzylureas. *Bioorg Med Chem Lett*. **2011;** (21):5610–5.
156. Saitoh M, Kunitomo J, Kimura E, Iwashita H, Uno Y, Onishi T, Uchiyama N, Kawamoto T, Tanaka T, Mol C, Dougan D, Textor G, Snell G, Takizawa M, Itoh F, Kori M. 2-{3-[4-(Alkylsulfinyl)phenyl]-1-benzofuran-5-yl}-5-methyl-1,3,4-oxadiazole Derivatives as Novel Inhibitors of Glycogen Synthase Kinase-3beta with Good Brain Permeability. *J Med Chem*. **2009;** 52(20):6270–86.
157. Onishi T, Iwashita H, Uno Y, Kunitomo J, Saitoh M, Kimura E, Fujita H, Uchiyama N, Kori M, Takizawa M. A Novel Glycogen Synthase Kinase-3 Inhibitor 2-Methyl-5-(3-{4-[(S)-Methylsulfinyl]phenyl}-1-benzofuran-5-yl)-1,3,4-Oxadiazole Decreases Tau Phosphorylation and Ameliorates Cognitive Deficits in a Transgenic Model of Alzheimer's Disease. *J Neurochem*. **2011;** 119(6):1330–40.
158. Hu S, Ueda M, Stetson L, Ignatz-Hoover J, Moreton S, Chakrabarti A, Xia Z, Karan G, De Lima M, Agrawal MK, Wald DN. Small Molecule Therapeutics A Novel Glycogen Synthase Kinase-3 Inhibitor Optimized for Acute Myeloid Leukemia Differentiation Activity. *Mol Cancer Ther*. **2016;** 15(7):1–10.
159. Chun K, Park JS, Lee HC, Kim YH, Ye IH, Kim KJ, Ku IW, Noh MY, Cho GW, Kim H, Kim SH, Kim J. Synthesis and Evaluation of 8-Amino-[1,2,4]triazolo[4,3-*a*]pyridin-3(2H)-one Derivatives as Glycogen Synthase Kinase-3 (GSK-3) Inhibitors. *Bioorganic Med Chem Lett*. **2013;** 23(13):3983–7.
160. Miyazaki Y, Maeda Y, Sato H, Nakano M, Mellor G. Rational Design of 4-Amino-5,6-Diaryl-furo[2,3-*d*]pyrimidines as Potent Glycogen Synthase Kinase-3 Inhibitors. *Bioorg Med Chem Lett*. **2008;** 18:1967–71.
161. Pandey MK, DeGrado TR. Glycogen Synthase Kinase-3 (GSK-3)-Targeted Therapy and Imaging. *Theranostics*. **2016;** 6(4):571–93.
162. Ibrahim N, Mouawad L, Legraverend M. Novel 8-Arylated Purines as Inhibitors of Glycogen Synthase Kinase. *Eur J Med Chem*. **2010;** 45(8):3389–93.
163. Furlotti G, Alisi MA, Cazzolla N, Dragone P, Durando L, Magarò G, Mancini F, Mangano G, Ombrato R, Vitiello M, Armirotti A, Capurro V, Lanfranco M, Ottonello G, Summa M, Reggiani A. Hit Optimization of 5-Substituted-N-(piperidin-4-ylmethyl)-1H-indazole-3-carboxamides: Potent Glycogen Synthase Kinase-3 (GSK-3) Inhibitors with *in vivo* Activity in Model of Mood Disorders. *J Med Chem*. **2015;** 58:8920–37.
164. Khan I, Tantray MA, Hamid H, Alam MS, Kalam A, Hussain F, Dhulap A. Synthesis of Benzimidazole Based Thiadiazole and Carbohydrazide Conjugates as Glycogen Synthase Kinase-3β Inhibitors with Anti-Depressant Activity. *Bioorg Med Chem Lett*. **2016;** 26:4020–4.

165. Park H, Shin Y, Kim J, Hong S. Application of Fragment-Based de Novo Design to the Discovery of Selective Picomolar Inhibitors of Glycogen Synthase Kinase-3 Beta. *J Med Chem*. **2016;** 59(19):9018-34.
166. Cociorva OM, Li B, Nomanbhoy T, Li Q, Nakamura A, Nakamura K, Nomura M, Okada K, Seto S, Yumoto K, Liyanage M, Zhang MC, Aban A, Leen B, Szardenings AK, Rosenblum JS, Kozarich JW, Kohno Y, Shreder KR. Synthesis and Structure-Activity Relationship of 4-Quinolone-3-Carboxylic Acid Based Inhibitors of Glycogen Synthase Kinase-3β. *Bioorg Med Chem Lett*. **2011;** 21(19):5948–51.
167. Luo G, Chen L, Burton CR, Xiao H, Sivaprakasam P, Krause CM, Cao Y, Liu N, Lippy J, Clarke WJ, Snow K, Raybon J, Arora V, Pokross M, Kish K, Lewis HA, Langley DR, Macor JE, Dubowchik GM. Discovery of Isonicotinamides as Highly Selective, Brain Penetrable, and Orally Active Glycogen Synthase Kinase-3 Inhibitors. *J Med Chem*. **2016;** 59(3):1041–51.
168. Sivaprakasam P, Han X, Civiello RL, Jacutin-Porte S, Kish K, Pokross M, Lewis HA, Ahmed N, Szapiel N, Newitt JA, Baldwin ET, Xiao H, Krause CM, Park H, Nophsker M, Lippy JS, Burton CR, Langley DR, Macor JE et al. Discovery of New Acylaminopyridines as GSK-3 Inhibitors by a Structure Guided in-Depth Exploration of Chemical Space around a Pyrrolopyridinone Core. *Bioorganic Med Chem Lett*. **2015;** 25(9):1856–63.
169. Wagner FF, Bishop JA, Gale JP, Shi X, Walk M, Ketterman J, Patnaik D, Barker D, Walpita D, Campbell AJ, Nguyen S, Lewis M, Ross L, Weïwer M, An WF, Germain AR, Nag PP, Metkar S, Kaya T et al. Inhibitors of Glycogen Synthase Kinase 3 with Exquisite Kinome-Wide Selectivity and Their Functional Effects. *ACS Chem Biol*. **2016;** 11(7):1952–63.
170. Eldar-Finkelman H, Licht-Murava A, Pietrokovski S, Eisenstein M. Substrate Competitive GSK-3 Inhibitors-Strategy and Implications. *Biochim Biophys Acta*. **2010;** 1804:598–603.
171. Martinez A, Alonso M, Castro A, Perez C, Moreno F. First Non-ATP Competitive Glycogen Synthase Kinase 3β (GSK-3β) Inhibitors: Thiadiazolidinones (TDZD) as Potential Drugs for the Treatment of Alzheimer's Disease. *J Med Chem*. **2002;** 45:1292–9.
172. Martinez A, Alonso M, Fuertes A, Navarro ML, Perez-Puerto M, Castro A. Neuropharma, S.A. GSK-3 INHIBITORS. US8686042. **2014.**
173. Perez DI, Conde S, Pérez C, Gil C, Simon D, Wandosell F, Moreno FJ, Gelpí JL, Luque FJ, Martínez A. Thienylhalomethylketones: Irreversible Glycogen Synthase Kinase 3 Inhibitors as Useful Pharmacological Tools. *Bioorganic Med Chem*. **2009;** 17(19):6914–25.
174. Perez DI, Palomo V, Pérez C, Gil C, Dans PD, Luque FJ, Conde S, Martínez A. Switching Reversibility to Irreversibility in Glycogen Synthase Kinase 3 Inhibitors: Clues for Specific Design of New Compounds. *J Med Chem*. **2011;** 54(12):4042–56.
175. Hamman M, Alonso D, Martin Aparicio E, Fuertes A, Perez-Puerto M, Castro A, Morales S, Navarro M, Del Monte-Millan M, Medina M, Pennaka H, Balaiah A, Peng J, Cook J, Wahyuono S, Martinez A. Glycogen Synthase Kinase-3 (GSK-3) Inhibitory Activity and Structure-Activity Relationship (SAR) Studies of the Manzamine Alkaloids. Potential for Alzheimer's Disease. *J Nat Prod*. **2007;** 70:1397–405.
176. Bidon-Chanal A, Fuertes A, Alonso D, Perez D, Martinez A, Luque F, Medina M. Evidence for a New Binding Mode to GSK-3: Allosteric Regulation by the Marine Compound Palinurin. *Eur J Med Chem*. **2013;** 60:479–89.
177. Licht-Murava A, Paz R, Vaks L, Avrahami L, Plotkin B, Eisenstein M, Eldar-Finkelman H. A Unique Type of GSK-3 Inhibitor Brings New Opportunities to the Clinic. *Sci Signal*. **2016;** 9(454).
178. Pérez DI, Pistolozzi M, Palomo V, Redondo M, Fortugno C, Gil C, Felix G, Martinez A, Bertucci C. 5-Imino-1,2-4-Thiadiazoles and Quinazolines Derivatives as Glycogen Synthase Kinase 3β (GSK-3β) and Phosphodiesterase 7 (PDE7) Inhibitors: Determination of Blood-

Brain Barrier Penetration and Binding to Human Serum Albumin. *Eur J Pharm Sci*. **2012;** 45(5):677–84.

179. Palomo V, Perez D, Perez C, Soteras I, Encinas A, Castro A, Campillo N, Gil C, Perez-Castillo A, Martinez A. 5-Imino-1,2,4-Thiadiazoles: First Small Molecules as Substrate Competitive Inhibitors of Glycogen Synthase Kinase 3. *J Med Chem*. **2012;** 55(4):1645–61.
180. Palomo V, Soteras I, Perez DI, Perez C, Gil C, Campillo NE, Martinez A. Exploring the Binding Sites of Glycogen Synthase Kinase 3. Identification and Characterization of Allosteric Modulation Cavities. *J Med Chem*. **2011;** 54(24):8461–70.
181. Zhang P, Li S, Gao Y, Lu W, Huang K, Ye D, Li X, Chu Y. Novel Benzothiazinones (BTOs) as Allosteric Modulator or Substrate Competitive Inhibitor of Glycogen Synthase Kinase 3β (GSK-3β) With Cellular Activity of Promoting Glucose Uptake. *Bioorganic Med Chem Lett*. **2014;** 24(24):5639–43.
182. Prati F, De Simone A, Armirotti A, Summa M, Pizzirani D, Scarpelli R, Bertozzi SM, Perez DI, Andrisano V, Perez-Castillo A, Monti B, Massenzio F, Polito L, Racchi M, Sabatino P, Bottegoni G, Martinez A, Cavalli A, Bolognesi ML. 3,4-Dihydro-1,3,5-triazin-2(1H)-ones as the First Dual BACE-1/GSK-3β Fragment Hits against Alzheimer's Disease. *ACS Chem Neurosci*. **2015;** 6(10):1665–82.
183. Prati F, De Simone A, Bisignano P, Armirotti A, Summa M, Pizzirani D, Scarpelli R, Perez DI, Andrisano V, Perez-Castillo A, Monti B, Massenzio F, Polito L, Racchi M, Favia AD, Bottegoni G, Martinez A, Bolognesi ML, Cavalli A. Multitarget Drug Discovery for Alzheimer's Disease: Triazinones as BACE-1 and GSK-3β Inhibitors. *Angew Chemie Int Ed*. **2015;** 54(5):1578–82.
184. Di Martino RMC, De Simone A, Andrisano V, Bisignano P, Bisi A, Gobbi S, Rampa A, Fato R, Bergamini C, Perez DI, Martinez A, Bottegoni G, Cavalli A, Belluti F. Versatility of the Curcumin Scaffold: Discovery of Potent and Balanced Dual BACE-1 and GSK-3β Inhibitors. *J Med Chem*. **2016;** 59(2):531–44.
185. Boulahjar R, Ouach A, Bourg S, Bonnet P, Lozach O, Meijer L, Guguen-Guillouzo C, Le Guevel R, Lazar S, Akssira M, Troin Y, Guillaumet G, Routier S. Advances in tetrahydropyrido[1,2-*a*]isoindolone (Valmerins) Series: Potent Glycogen Synthase Kinase 3 and Cyclin Dependent Kinase 5 Inhibitors. *Eur J Med Chem*. **2015;** 101:274–87.
186. Hédou D, Godeau J, Loaëc N, Meijer L, Fruit C, Besson T. Synthesis of thiazolo[5,4-*f*]quinazolin-9(8H)-ones as Multi-Target Directed Ligands of Ser/Thr Kinases. *Molecules*. **2016;** 21(5).
187. Lipina TV, Palomo V, Gil C, Martinez A, Roder JC. Dual Inhibitor of PDE7 and GSK-3 - VP1.15 Acts as Antipsychotic and Cognitive Enhancer in C57BL/6J Mice. *Neuropharmacology*. **2013;** 64:205–14.
188. Gompel M, Leost M, Bal De Kier Joffe E, Puricelli L, Hernandez Franco L, Palermo J, Meijer L. Meridianins, a New Family of Protein Kinase Inhibitors Isolated from the Ascidian Aplidium Meridianum. *Bioorganic Med Chem Lett*. **2004;** 14(7):1703–7.
189. Zhu C, Jing L, Yu N, Yang X, Zhao Y. A New Lignan and Active Compounds Inhibiting NF-κB Signaling Pathway from Caulis Trachelospermi. *Acta Pharm Sin B*. **2013;** 3(2):109–12.
190. Baunbæk D, Trinkler N, Ferandin Y, Lozach O, Ploypradith P, Rucirawat S, Ishibashi F, Iwao M, Meijer L. Anticancer Alkaloid Lamellarins Inhibit Protein Kinases. *Mar Drugs*. **2008;** 6(4):514–27.
191. Bain J, Plater L, Elliott M, Shpiro N, Hastie CJ, Mclauchlan H, Klevernic I, Arthur JSC, Alessi DR, Cohen P. The Selectivity of Protein Kinase Inhibitors: A Further Update. *Biochem J*. **2007;** 408(3):297–315.
192. Esposito G, Bourguet-Kondracki M-L, Mai LH, Longeon A, Teta R, Meijer L, Van Soest R, Mangoni A, Costantino V. Chloromethylhalicyclamine B, a Marine-Derived Protein Kinase

CK1δ/ε Inhibitor. *J Nat Prod*. **2016;** 79(11):2953-60.
193. Cozza G, Pinna LA. Casein Kinases as Potential Therapeutic Targets. *Expert Opin Ther Targets*. **2015;** 8222(2):1–22.
194. Cheong JK, Nguyen TH, Wang H, Tan P, Voorhoeve PM, Lee SH, Virshup DM. IC261 Induces Cell Cycle Arrest and Apoptosis of Human Cancer Cells via CK1δ/ε and Wnt/β-Catenin Independent Inhibition of Mitotic Spindle Formation. *Oncogene*. **2011;** 30(22):2558–69.
195. Cozza G, Gianoncelli A, Montopoli M, Caparrotta L, Venerando A, Meggio F, Pinna L a, Zagotto G, Moro S. Identification of Novel Protein Kinase CK1 Delta (CK1delta) Inhibitors through Structure-Based Virtual Screening. *Bioorg Med Chem Lett*. **2008;** 18(20):5672–5.
196. Kurihara T, Sakurai E, Toyomoto M, Kii I, Kawamoto D, Asada T, Tanabe T, Yoshimura M, Hagiwara M, Miyata A. Alleviation of Behavioral Hypersensitivity in Mouse Models of Inflammatory Pain with Two Structurally Different Casein Kinase 1 (CK1) Inhibitors. *Mol Pain*. **2014;** 10(1):17.
197. Wager TT, Chandrasekaran RY, Bradley J, Rubitski D, Berke H, Mente S, Butler T, Doran A, Chang C, Fisher K, Knafels J, Liu S, Ohren J, Marconi M, Demarco G, Sneed B, Walton K, Horton D, Rosado A et al. Casein Kinase 1 δ/ε Inhibitor PF-5006739 Attenuates Opioid Drug-Seeking Behavior. *ACS Chem Neurosci*. **2014**; 5(12):1253–1265.
198. Yang LL, Li GB, Yan HX, Sun QZ, Ma S, Ji P, Wang ZR, Feng S, Zou J, Yang SY. Discovery of N^6-Phenyl-1H-pyrazolo[3,4-*d*]pyrimidine-3,6-diamine Derivatives as Novel CK1 Inhibitors Using Common-Feature Pharmacophore Model Based Virtual Screening and Hit-to-Lead Optimization. *Eur J Med Chem*. **2012;** 56:30–8.
199. Meijer L, Nelson DJ, Riazanski V, Gabdoulkhakova AG, Hery-Arnaud G, Le Berre R, Loaëc N, Oumata N, Galons H, Nowak E, Gueganton L, Dorothée G, Prochazkova M, Hall B, Kulkarni AB, Gray RD, Rossi AG, Witko-Sarsat V, Norez C, Becq F, Ravel D, Mottier D, Rault G. Modulating Innate and Adaptive Immunity by (R)-Roscovitine: Potential Therapeutic Opportunity in Cystic Fibrosis. *J Innate Immun*. **2016;** 8(4):330–49.
200. Oumata N, Bettayeb K, Ferandin Y, Demange L, Lopez-Giral A, Goddard ML, Myrianthopoulos V, Mikros E, Flajolet M, Greengard P, Meijer L, Galons H. Roscovitine-Derived, Dual-Specificity Inhibitors of Cyclin-Dependent Kinases and Casein Kinases 1. *J Med Chem*. **2008;** 51(17):5229–42.
201. Bibian M, Rahaim RJ, Choi JY, Noguchi Y, Schürer S, Chen W, Nakanishi S, Licht K, Rosenberg LH, Li L, Feng Y, Cameron MD, Duckett DR, Cleveland JL, Roush WR. Development of Highly Selective Casein Kinase 1δ/1ε (CK1δ/ε) Inhibitors with Potent Antiproliferative Properties. *Bioorganic Med Chem Lett*. **2013;** 23(15):4374–80.
202. Rosenberg LH, Lafitte M, Quereda V, Grant W, Chen W, Bibian M, Noguchi Y, Fallahi M, Yang C, Chang JC, Roush WR, Cleveland JL, Duckett DR. Therapeutic Targeting of Casein Kinase 1 D in Breast Cancer. **2015;** 7(318):1–13.
203. Richter J, Bischof J, Zaja M, Kohlhof H, Othersen O, Vitt D, Alscher V, Pospiech I, García-Reyes B, Berg S, Leban J, Knippschild U. Difluoro-dioxolo-benzoimidazol-benzamides as Potent Inhibitors of CK1δ and ε with Nanomolar Inhibitory Activity on Cancer Cell Proliferation. *J Med Chem*. **2014;** 57(19):7933–46.
204. Lee JW, Hirota T, Peters EC, Garcia M, Gonzalez R, Cho CY, Wu X, Schultz PG, Kay SA. A Small Molecule Modulates Circadian Rhythms through Phosphorylation of the Period Protein. *Angew Chemie - Int Ed*. **2011;** 50(45):10608–11.
205. Pike I., Kuhn K, Kienle S, Hamilton WDO, Heal JR, Sheridan JM. Electrophoretics Limited. A Casein Kinase I Delta Inhibitor. WO2016180981A1, **2016.**
206. Pike IH, Ward MA, Russel CL, Mitra V. Electrophoretics Limited. Biomolecules Involved in Alzheimer's Disease. WO2016189163A1, **2016.**

207. Velaparthi U, Kumaravel S, Karuppiah AMSS, Maheshwarappa SH, Rachamreddy CR, Wittman MD. Imidazo-Pyridazine Derivatives as Casein Kinase 1 Delta/Epsilon Inhibitors. Bristol-Myers Squibb Company. WO2015195880A1, **2015.**
208. Laco F, Low JL, Oh S, Chai CL, Zhong Q. Agency for Science, Technology and Research - National University of Singapore. 2,4,5-Tri-substituted Azole-Based Casein Kinase 1 Inhibitors as Inducers for Cardiomyogenesis. WO2015119579A1, **2015.**
209. Peifer C, Abadleh M, Bischof J, Hauser D, Schattel V, Hirner H, Knippschild U, Laufer S. 3,4-Diaryl-Isoxazoles and -Imidazoles as Potent Dual Inhibitors of p38a Mitogen Activated Protein Kinase and Casein Kinase 1δ. *J Med Chem*. **2009;** 52(23):7618–30.
210. Shanware NP, Williams LM, Bowler MJ, Tibbetts R. Non-Specific in Vivo Inhibition of CK1 by the Pyridinyl Imidazole p38 Inhibitors SB 203580 and SB 202190. *BMB Rep*. **2009;** 42(3):142–7.
211. Verkaar F, Van Der Doelen AA, Smits JFM, Blankesteijn WM, Zaman GJR. Inhibition of Wnt/beta-Catenin Signaling by p38 MAP Kinase Inhibitors is Explained by Cross-Reactivity with Casein Kinase 1δ/1ε. *Chem Biol*. **2011;** 18(4):485–94.
212. Huart AS, Saxty B, Merritt A, Nekulova M, Lewis S, Huang Y, Vojtesek B, Kettleborough C, Hupp TR. A Casein Kinase 1/Checkpoint Kinase 1 Pyrazolo-Pyridine Protein Kinase Inhibitor as Novel Activator of the p53 Pathway. *Bioorganic Med Chem Lett*. **2013;** 23(20):5578–85.
213. Esvan YJ, Zeinyeh W, Boibessot T, Nauton L, Théry V, Knapp S, Chaikuad A, Loaëc N, Meijer L, Anizon F, Giraud F, Moreau P. Discovery of pyrido[3,4-*g*]quinazoline Derivatives as CMGC Family Protein Kinase Inhibitors: Design, Synthesis, Inhibitory Potency and X-Ray Co-Crystal Structure. *Eur J Med Chem*. **2016;** 118:170–7.
214. Caulkett PW, Jones G, McPartlin M, Renshaw N, Stewart S, Wright B. Adenine Isosteres with Bridgehead Nitrogen. Part 1. Two Indipendent Syntheses of the [1,2,4]triazolo[1,5-*a*]triazine Ring System Leading to a Range of Substituents in the 2,5 and 7 Positions. *J Chem Soc Perkin Trans*. **1995;** 1:801–8.
215. Dolzhenko AV, Dolzhenko AV, Chui WK. 1,2,4-Triazolo[1,5-*a*][1,3,5]Triazines (5-Azapurines): Synthesis and Biological Activity. *Heterocycles*. **2006;** 68(8):1723–59.
216. Federico S, Paoletta S, Cheong SL, Pastorin G, Cacciari B, Stragliotto S, Klotz KN, Siegel J, Gao Z-G, Jacobson KA, Moro S, Spalluto G. Synthesis and Biological Evaluation of a New Series of 1,2,4-triazolo[1,5-*a*]-1,3,5-triazines as Human A(2A) Adenosine Receptor Antagonists with Improved Water Solubility. *J Med Chem*. **2011;** 54(3):877–89.
217. Federico S, Ciancetta A, Porta N, Redenti S, Pastorin G, Cacciari B, Klotz KN, Moro S, Spalluto G. 5,7-Disubstituted-[1,2,4]triazolo[1,5-*a*][1,3,5]triazines as Pharmacological Tools to Explore the Antagonist Selectivity Profiles toward Adenosine Receptors. *Eur J Med Chem*. **2016;** 108:529–41.
218. Tsumoki H, Shimada J, Imma H, Nakamura A, Nonaka H, Shiozaki S, Ichikawa S, Kanda T, Kuwana Y, Ichimura M, Suzuki F. [1,2,4]Triazolo[1,5-*c*]Pyrimidine Derivatives. Kyowa Hakko Kogyo Co., Ltd. EP0976753A1, **1998.**
219. Federico S, Ciancetta A, Porta N, Redenti S, Pastorin G, Cacciari B, Klotz KN, Moro S, Spalluto G. Scaffold Decoration at Positions 5 and 8 of 1,2,4-triazolo[1,5-*c*]pyrimidines to Explore the Antagonist Profiling on Adenosine Receptors: A Preliminary Structure–Activity Relationship Study. *J Med Chem*. **2014;** 57:6210–25.
220. Redenti S, Ciancetta A, Pastorin G, Cacciari B, Moro S, Spalluto G, Federico S. Pyrazolo[4,3-e][1,2,4]triazolo[1,5-*c*]pyrimidines and Structurally Simplified Analogs. Chemistry and SAR Profile as Adenosine Receptor Antagonists. *Curr Top Med Chem*. **2016;** 16(28):3224–57.
221. Jorda R, Paruch K, Krystof V. Cyclin-Dependent Kinase Inhibitors Inspired by Roscovitine: Purine Bioisosteres. *Curr Pharm Des*. **2012;** 18(20):2974–80.

222. Miyazaki Y, Maeda Y, Sato H, Nakano M, Mellor GW. Rational Design of 4-amino-5,6-diaryl-furo[2,3-*d*]pyrimidines as Potent Glycogen Synthase Kinase-3 Inhibitors. *Bioorganic Med Chem Lett*. **2008;** 18(6):1967–71.
223. Pastorin G, Federico S, Paoletta S, Corradino M, Cateni F, Cacciari B, Klotz KN, Gao ZG, Jacobson KA, Spalluto G, Moro S. Synthesis and Pharmacological Characterization of a New Series of 5,7-Disubstituted-[1,2,4]triazolo[1,5-*a*][1,3,5]triazine Derivatives as Adenosine Receptor Antagonists: A Preliminary Inspection of Ligand-Receptor Recognition Process. *Bioorganic Med Chem*. **2010;** 18(7):2524–36.
224. Rayasam GV, Tulasi VK, Sodhi R, Davis JA, Ray A. Glycogen Synthase Kinase 3: More than a Namesake. *Br J Pharmacol*. **2009;** 156(6):885–98.
225. Henderson JT, Piquette-Miller M. Blood-Brain Barrier: An Impediment to Neuropharmaceuticals. *Clin Pharmacol Ther*. **2015;** 97(4):308–13.
226. Cardoso FL, Brites D, Brito MA. Looking at the Blood-Brain Barrier: Molecular Anatomy and Possible Investigation Approaches. *Brain Res Rev*. **2010;** 64(2):328–63.
227. Van Asperen J, Mayer U, Van Tellingen O, Beijnen JH. The Functional Role of P-Glycoprotein in the Blood-Brain Barrier. *J Pharm Sci*. **1997;**86(8):881–4.
228. Mikitsh JL, Chacko A. Pathways for Small Molecule Delivery to the Central Nervous System Across the Blood-Brain Barrier. *Perspect Med Chem*. **2014;** 6:11–24.
229. Di L, Kerns EH, Fan K, McConnell OJ, Carter GT. High Throughput Artificial Membrane Permeability Assay for Blood-Brain Barrier. *Eur J Med Chem*. **2003;** 38(3):223–32.
230. Bakhite E, Abdel-Rahman A, Al-Taifi E. Fluorine-Containing Heterocycles: Part I. Synthesis of New 7-(2-thienyl)-9-trifluoromethylpyrido[3,2:4,5]thieno[3,2-*d*]pyrimidines and Related Fused Tetracyclic Systems. *J Chem Res*. **2005;** 3:147–54.
231. de Keczer SA, Masjedizadeh MR, Wu S-Y, Lara-Jaime T, Comstock K, Dvorak C, Liu Y-Y, Berger W. M+4 stable Isotope Labeling of Levovirin and M+7 and Carbon-14 Labeling of Levovirin Valinate pro-Drug. *J Label Compd Radiopharm*. **2006;** 49:1223–36.
232. Hutton J. Chemical Process. Imperial Chemical Industries, Plc. US5326869, **1994.**
233. Ogata S, Mochizuki A, Kakimoto M, Imai Y. Synthesis of Amides and Amidines by Reaction of Carboxylic Acids and Amines in the Presence of Polyphosphoric Acid Trimethylsilyl Ester (PPSE). *Bulletin of the Chemical Society of Japan*. **1986.** 59: 2171–7.
234. El Ashry ESH, Nadeem S, Shah MR, Kilany YE. Recent Advances in the Dimroth Rearrangement. *Adv Heterocycl Chem*. **2010;** 101(10):161–228.
235. Crivori P, Cruciani G, Carrupt PA, Testa B. Predicting Blood-Brain Barrier Permeation from Three-Dimensional Molecular Structure. *J Med Chem*. **2000;** 43(11):2204–16.
236. Hirabayashi A, Mukaiyama H, Kobayashi H, Shiohara H, Nakayama S, Ozawa M, Miyazawa K, Misawa K, Ohnota H, Isaji M. Bioorganic & Medicinal Chemistry A Novel Syk Family Kinase Inhibitor : Design, Synthesis, and Structure–Activity 1, 2,4-Triazolo [1,5-c]pyrimidine Derivatives. **2008;** 16:7347–57.
237. Pave GA, Firth JD, Stewart L, Rigoreau LJM, Wynne EL. Cancer Research Technology Limited. [1,2,4]triazolo[1,5-a]pyridine and [1,2,4]triazolo[1,5-c]pyrimidine compounds and their use. WO2009047514A1, **2009.**
238. Baki A, Bielik A, Molnár L, Szendrei G, Keserü GM. A High Throughput Luminescent Assay for Glycogen Synthase Kinase-3beta Inhibitors. *Assay Drug Dev Technol*. **2007;** 5(1):75–83.
239. Slobutsey C, Audrieth L, Campbell R. Acid Catalysis in Liquid Ammonia in Ammonolysis of Diethylmalonate. *Proc Natl Acad Sci USA*. **1937;** 23:611–5.
240. Jacquemard U, Dias N, Lansiaux A, Bailly C, Logé C, Robert JM, Lozach O, Meijer L, Mérour JY, Routier S. Synthesis of 3,5-bis(2-indolyl)pyridine and 3-[(2-indolyl)-5-phenyl]pyridine Derivatives as CDK Inhibitors and Cytotoxic Agents. *Bioorganic Med*

Chem. **2008;** 16(9):4932–53.
241. Kulkarni PP, Kadam a. J, Mane RB, Desai UV, Wadgaonkar PP. Demethylation of Methyl Aryl Ethers Using Pyridine Hydrochloride in Solvent-Free Conditions under Microwave Irradiation. *J Chem Res*. **1999;** (6):394–5.
242. Matasi J, Caldwell J, Tulshian D, Silverman L, Neustadt B. Schering Corporation. Adenosine A2a Receptor Antagonists. EP1453835, **2006.**
243. Píša O, Rádl S. Synthesis of 4-Quinolones: *N*,*O*-Bis-(trimethylsilyl)acetamide-Mediated Cyclization with Cleavage of Aromatic C-O Bond. *Eur J Org Chem*. **2016;** 2016(13):2336–50.
244. Van der Vijgh WJF, Bast A, Van Acker FAA, Menge WMP, Haenen GRM. Vrije Universiteit Medisch Centrum (Vumc). Novel Flavonoids. WO200121608, **2001.**
245. Illig CR, Subasinghe NL, Hoffman JB, Wilson KJ, Rudolph JM, Bone RF, Klein SL, Randle TL. 3-Dimensional Pharmaceuticals, Inc. Compounds and Compositons for Treating C1s-Mediated Diseases and Conditions. US20020037915, **2002.**
246. Maxwell BD, Boyé OG, Ohta K. The 14C, 13C and 15N Syntheses of MON 37500, a Sulfonylurea Wheat Herbicide. *J Label Compd Radiopharm*. **2005;** 48(6):397–406.
247. Stewart JJP. Optimization of Parameters for Semiempirical Methods V: Modification of NDDO Approximations and Application to 70 Elements. *J Mol Model*. **2007;** 13(12):1173–213.
248. Chemical Computing Group (CCG) Inc. Molecular Operating Environment (MOE), Version 2014.09. Available from: http://www.chemcomp.com.
249. Cuzzolin A, Sturlese M, Malvacio I, Ciancetta A, Moro S. DockBench: An Integrated Informatic Platform Bridging the Gap between the Robust Validation of Docking Protocols and Virtual Screening Simulations. *Molecules*. **2015;** 20(6):9977–93.
250. Cambridge Crystallographic Data Centre: 12 Union Road, Cambridge U. GOLD Suite, Version 5.2.
251. Korb O, Stützle T, Exner TE. Empirical Scoring Functions for Advanced Protein-Ligand Docking with PLANTS. *J Chem Inf Model*. **2009;** 49(1):84–96.
252. Jones G, Willett P, Glen R, Leach A, Taylor R. Development and Validation of a Genetic Algorithm for Flexible Docking. *J Mol Biol*. **1997;** 267:727–48.
253. Cruciat C-M. Casein Kinase 1 and Wnt/β-Catenin Signaling. *Curr Opin Cell Biol*. **2014;** 31:46–55.
254. Episcopo FL, Tirolo C, Caniglia S, Testa N, Morale MC, Serapide MF, Pluchino S, Marchetti B. Targeting Wnt Signaling at the Neuroimmune Interface for Dopaminergic Neuroprotection/Repair in Parkinson's Disease. *J Mol Cell Biol*. **2014;** 6:13–26.
255. Serafimova IM, Pufall M a, Krishnan S, Duda K, Cohen MS, Maglathlin RL, McFarland JM, Miller RM, Frödin M, Taunton J. Reversible Targeting of Noncatalytic Cysteines with Chemically Tuned Electrophiles. *Nat Chem Biol*. **2012;** 8(5):471–6.
256. Carmi C, Mor M, Petronini PG, Alfieri RR. Clinical Perspectives for Irreversible Tyrosine Kinase Inhibitors in Cancer. *Biochem Pharmacol*. **2012;** 84(11):1388–99.
257. Rena G, Bain J, Elliott M, Cohen P. D4476, a Cell-Permeant Inhibitor of CK1, Suppresses the Site-Specific Phosphorylation and Nuclear Exclusion of FOXO1a. *EMBO Rep*. **2004;** 5(1):60–5.
258. Caulkett PWR, Jones G, Collis, Michael George Poucher SM. Zeneca Limited. Preparation of (amino)heteroaryl[1,2,4]triazolo[1,5-*a*]triazines and Related Compounds as Adenosine A2 Receptor Antagonists. EP0459702, **1991.**
259. Moorthy JN, Singhal N. Facile and Highly Selective Conversion of Nitriles to Amides via Indirect Acid-Catalyzed Hydration Using TFA or AcOH-H_2SO_4. *J Org Chem*. **2005;** 70(5):1926–9.

260. Valbusa L, Coraluppi E, Quaglia A, Tavella M. M3 Company. Forming Direct Positive Images with Direct Positive Silver Halide Elements. EP0168730B1, **1986.**
261. Dolzhenko AV, Dolzhenko AV, Chui WK. Synthesis of 5,7-Diamino[1,2,4]triazolo[1,2-*a*][1,3,5]triazines via Annulation of 1,3,5-Triazine Ring onto 3(5)-Amino-1,2,4-Trizoles. *Heterocycles*. **2007;** 71(2):429–36.
262. Akahoshi F, Takeda S, Okada T, Kajii M, Nishimura H, Sugiura M, Inoue Y, Fukaya C, Naito Y, Imagawa T, Nakamura N. Synthesis and Pharmacological Activity of triazolo[1,5-a]triazine Derivatives Inhibiting Eosinophilia. *J Med Chem*. **1998;** 41(16):2985–93.
263. Yuskaitis CJ, Jope RS. Glycogen Synthase Kinase-3 Regulates Microglial Migration, Inflammation, and Inflammation-Induced Neurotoxicity. *Cell Signal*. **2009;** 21(2):264–73.
264. Arraf Z, Amit T, Youdim MBH, Farah R. Lithium and Oxidative Stress Lessons from the MPTP Model of Parkinson's Disease. *Neurosci Lett*. **2012;** 516(1):57–61.
265. Schober A. Classic Toxin-Induced Animal Models of Parkinson's Disease: 6-OHDA and MPTP. *Cell Tissue Res*. **2004;** 318(1):215–24.
266. Smeyne RJ, Jackson-Lewis V. The MPTP Model of Parkinson's Disease. *Mol Brain Res*. **2005;** 134(1):57–66.
267. Blandini F, Armentero MT, Martignoni E. The 6-Hydroxydopamine Model: News from the Past. *Park Relat Disord*. **2008;** 14:124–9 (SUPPL.2).
268. Lazzara CA, Kim YH. Potential Application of Lithium in Parkinson's and Other Neurodegenerative Diseases. *Front Neurosci*. **2015;** 9:1–10.
269. L'Episcopo F, Serapide MF, Tirolo C, Testa N, Caniglia S, Morale MC, Pluchino S, Marchetti B. A Wnt1 Regulated Frizzled-1/β-Catenin Signaling Pathway as a Candidate Regulatory Circuit Controlling Mesencephalic Dopaminergic Neuron-Astrocyte Crosstalk: Therapeutical Relevance for Neuron Survival and Neuroprotection. *Mol Neurodegener*. **2011;** 6(1):49.
270. Miller RM, Taunton J. Targeting Protein Kinases with Selective and Semipromiscuous Covalent Inhibitors. *Methods Enzymol*. **2014;** 548:93–116.
271. Caulkett PW, Jones G, Collis M, Pouche S. Zeneca Limited. Azole Derivatives. EP0459702 A1**, 1991.**
272. Pintér Á, Haberhauer G. Oxazole Cyclopeptides for Chirality Transfer in C3-Symmetric Octahedral Metal Complexes. *Eur J Org Chem*. **2008;** (14):2375–87.
273. Baloglu E, Ghosh S, Lobera M, Schmidt DR. Tempero Pharmaceuticals, Inc. Compounds and Methods. WO2013019621A1, **2013.**
274. Wasserman HH, Petersen AK. A Convergent Synthesis of Poststatin: Application of the Acyl Cyanophosphorane Coupling Procedure in the Formation of a Peptidic α-Keto Amide. *Tetrahedron Lett*. **1997;** 38(6):953–6.
275. Halgren TA. Merck Molecular Force Field. *J Comput Chem*. **1996;** 17(5–6):490–519.
276. Totrov M, Abagyan R. Protein-Ligand Docking as an Energy Optimization Problem. In Drug Receptor Thermodynamics : Introduction and Applications. Raffa RB, editor. **2011.** 603-624 p.
277. Totrov M, Abagyan R. Derivation of Sensitive Discrimination Potential for Virtual Ligand Screening. *Proc Third Annu Int Conf Comput Mol Biol - RECOMB '99*. **1999;** 312–20.

Acknowledgements

First and foremost, I would like to thank my advisor, Prof. Giampiero Spalluto, for his support over these years, for all of the opportunities I have been afforded and for having believed in me.

I am deeply grateful to Dr. Stephanie Federico, for her constant guidance, patience and support during roller coasters of these years and, most important of all, for her invaluable friendship.

I would also thank Prof. Ana Martinez, for welcoming me in her research group, for her flawless generous advices, support and helpfulness during the internship and in the last part of my PhD. I am also grateful to Dr. Daniel Perez for his advices, help and expertise during my stay in Madrid, and to all the research group of Prof. Martinez.

I am thankful to all our collaborators on these projects: Prof. Stefano Moro, Prof. Andrea Cavalli, Dr. Giovanni Bottegoni and Dr. Teresa De Vita, Prof. Sabrina Castellano and Dr. Alessandra Feoli, Dr. Giorgio Cozza.

Over the past three years, I also have had the pleasure of working with many awesome people whom I would like to thank:

Giuly, for making me your faithful assistant and your partner-in-crime for unofficial experiments, for your hugs and for being such an awesome friend. Davide, Sara, Giulia, Edoardo and Veronica, for your valuable work and for your enjoyable company. Ana and Talita, for our true friendship, born in a lab and bloomed outside, stronger than all distances. My amazing PAMPA-team and all the Chemfinders for making my time in Madrid an unforgettable experience.

Finally, from the bottom of my heart, I would like to thank Mum and Dad, for their unconditional love, support and encouragement, and all my beloved family. My friends Stefania, Federica and Irene, for being like sisters. And of course Paolo, for holding my hand and making everything easier.